

FTD-MT- 64-61

AD61473

TT 65-62083

COPY	2	OF	3	287
HARD COPY			\$.	6.00
MICROFICHE			\$.	1.50

277P

# TRANSLATION

JOURNAL OF APPLIED MECHANICS AND TECHNICAL PHYSICS  
(COLLECTION OF ARTICLES)

No. 5

1963

## FOREIGN TECHNOLOGY DIVISION

AIR FORCE SYSTEMS COMMAND

WRIGHT-PATTERSON AIR FORCE BASE

OHIO



DDC  
MAY 12 1965

1151A B

ARCHIVE COPY

CLEARINGHOUSE FOR FEDERAL SCIENTIFIC AND TECHNICAL INFORMATION, CFSTI  
INPUT SECTION 410.11

LIMITATIONS IN REPRODUCTION QUALITY OF TECHNICAL ABSTRACT BULLETIN  
DOCUMENTS, DEFENSE DOCUMENTATION CENTER (DDC)

AD 614773

TT 65-62093

1. AVAILABLE ONLY FOR REFERENCE USE AT DDC FIELD SERVICES.  
COPY IS NOT AVAILABLE FOR PUBLIC SALE.
2. AVAILABLE COPY WILL NOT PERMIT FULLY LEGIBLE REPRODUCTION.  
REPRODUCTION WILL BE MADE IF REQUESTED BY USERS OF DDC.
- A. COPY IS AVAILABLE FOR PUBLIC SALE.
- B. COPY IS NOT AVAILABLE FOR PUBLIC SALE.
3. LIMITED NUMBER OF COPIES CONTAINING COLOR OTHER THAN BLACK  
AND WHITE ARE AVAILABLE UNTIL STOCK IS EXHAUSTED. REPRODUCTIONS  
WILL BE MADE IN BLACK AND WHITE ONLY.

TSL-121-2/65

DATE PROCESSED: 14 May 65

PROCESSOR: E. D. Jaeger

# EDITED MACHINE TRANSLATION

JOURNAL OF APPLIED MECHANICS AND TECHNICAL PHYSICS  
(COLLECTION OF ARTICLES)

English Pages: 273

S/0207-063-000-005

THIS TRANSLATION IS A RENDITION OF THE ORIGINAL FOREIGN TEXT WITHOUT ANY ANALYTICAL OR EDITORIAL COMMENT. STATEMENTS OR THEORIES ADVOCATED OR IMPLIED ARE THOSE OF THE SOURCE AND DO NOT NECESSARILY REFLECT THE POSITION OR OPINION OF THE FOREIGN TECHNOLOGY DIVISION.

PREPARED BY:  
TRANSLATION DIVISION  
FOREIGN TECHNOLOGY DIVISION  
WP-AFB, OHIO.

Akademiya Nauk SSSR - Sibirskoye Otdeleniye

PMTF

ZHURNAL PRIKLADNOY MEKHANIKI I TEKHNICHESKOY FIZIKI

No 5

1963  
Sentyabr' - Oktyabr'

Izdatel'stvo Akademii Nauk SSSR

Pages 1-160

## TABLE OF CONTENTS

Calculation of Volt-Ampere Characteristics of Thermionic Converter in Diffusion Conditions, by V. P. Karmazin and I. P. Stakhanov.....	1
Transfer Equations for Nonisothermistic Multitype Plasma, by M. Ya. Aliyevskiy and V. M. Zhdanov.....	14
On Theory of Weak Diffusion Waves, by G. S. Leonov and V. A. Pogosyan.....	24
Change of Electric Potential Near Wall of Channel During Motion of Ionized Gas in Magnetic Field, by G. A. Lyubimov.....	33
Rotational Relaxation in Plane-Parallel Rarefaction Wave, by V. N. Arkhipov and L. I. Severinov.....	52
Theory of Differential Ejector, by B. A. Uryukov.....	61
On Calculation of Thermal Diffusion in Laminar Flow of Viscous Liquid at Moderate Values of Thermal and Diffusion Prandtl Numbers, by A. M. Suponitskiy.....	72
On Flows of Liquid with Formation of Closed Cavitation Cavities, by A. Ye. Khoperskov.....	81
On Cracks Spreading Between Flat Plates on Rectilinear Boundary of Gluing, by R. V. Gol'dstein and R. L. Salganik.....	91
Equilibrium Cracks in Strip of Finite Width, by I. A. Markuzon.....	102
Equilibrium of a Twin for Plane Surface of Siotropic Medium, by A. M. Kosevich and L. A. Pasmur.....	113
On Strain Waves in Durable Rocks, by Ye. I. Shenyakin.....	122
Approximate Equation of State of Solid Bodies, by V. M. Gogolev, V. G. Myrkin, and G. I. Yablokov.....	139
Experimental Investigation of Dynamic Stressfield in Soft Earth, During Contact Explosion, by V. D. Alekseyenko.....	149
Forming of Shock Wave and Scattering of Products of Explosion in Air, by V. V. Adushkin.....	164
Course of Reaction in Detonation Wave of Explosive Mixtures, by A. Ya. Apin, I. M. Voskoboynikov, and G. S. Sosnova.....	179
Influence of Pressure on Disturbance of Stability of Combustion of Porous Explosives, by A. F. Belyayev, A. I. Korotkov, and A. A. Sulimov.....	185
On Influence of Pressure on Combustion Rate of Ammonium Perchlorate, by A. P. Glazkova.....	193

On Heat Exchange of Microthermocouples Under Conditions of Combustion of Condensed Substances, by A. A. Zenin.....	203
Dispersion and Accidental Error of Measurement of Temperature of Locally Isotropic Turbulent Flow, by Yu. L. Rozenshmok.....	216
On One Nonlinear Problem of Thermal Conduction, by S. I. Anisimov and T. L. Perel'man.....	223
On Heat Exchange at Critical Point of a Blunt Body at Small Reynolds Numbers, by I. N. Murzinov.....	229
Determination of Average Section of Collisions of Electrons with Neutral Atoms of Weakly-Ionized Gas Mixture, by E. P. Zimin and V. A. Popov.....	235
Flow Between Parallel Walls in Periodic Magnetic Field, by I. B. Chakmarev.....	239
About Modeling of Magnetohydrodynamic Flow in Channel in Electrolytic Bath, by V. V. Nazarenko.....	242
Variational Methods of Solution of Problems of Deformation and Stability of Plates and Shells Under Conditions of Creep, by G. V. Ivanov.....	247
Approximate Method of Calculation for Creep Buckling, by S. A. Shesterikov..	252
Torsion of Prismatic Rods of Ideally Plastic Material with Calculation of Microstresses, by I. A. Berezhnoy and D. D. Ivlev.....	258
Theory of Straight Lines of Discontinuity of Stresses for True Plane Flow of a Rigidly-Plastic Body, by O. D. Grigor'yev.....	266
Relaxation of Stresses in Thin-Walled Pipe, by V. S. Namestnikov.....	269

MT-54-61.

Journal of Applied Mechanics and Technical Physics, No. 5, Sept. - Oct. 1963.

Pages cover - 160.

## CALCULATION OF VOLT-AMPERE CHARACTERISTICS OF THERMIONIC CONVERTER IN DIFFUSION CONDITIONS

V. P. Karmazin and I. P. Stakhanov

(Moscow)

1. Formulation of problem and boundary conditions. Considered is a flat thermionic energy converter (TEP) filled with cesium under conditions when length of free path of electrons  $l_e$  is significantly less than distance between electrodes  $L$ . Degree of ionization is assumed so little that electron scattering and ionization occurs basically on atoms of Cs. This assumption is justified, if  $n/n_a \leq 0.001$  ( $n, n_a$  — concentration of electrons and atoms). If concentration of electrons can be calculated from condition of thermodynamic equilibrium, the degree of ionization corresponds temperature  $\sim 2000^\circ\text{K}$ .

Ions and atoms are freely exchanged by energy, therefore their temperatures coincide:  $T_i = T_a$ . At sufficiently high pressures (when  $l_e/L \ll 1$ ) temperature  $T_i$  linearly changes from cathode to anode. In region of pressures interesting us, due to weak exchange by energy between electrons and ions, temperature of electrons  $T_e \neq T_i$ . If temperature is established mainly under the influence of Coulomb collisions, then characteristic distance, at which "Maxwellization" of spectrum of electrons occurs, is of order  $(\frac{1}{3}l_e l_c)^{1/2}$ , where  $l_c$  — "Coulomb" length of free path of electrons.

If one were to assume that near the cathode local thermodynamic equilibrium takes place, then concentration and level of chemical potential of electrons at the cathode do not depend on material of the cathode, in particular on its work function. Therefore, in order to receive dependence of volt-ampere (VI) characteristics from work functions of cathode, it is necessary to consider deviation from thermodynamic equilibrium on cathode, appearing due to passage of current through TEP.

For obtaining boundary conditions on cathode, let us consider region between planes one of which is conducted at distance  $x_1 \geq d$  from cathode and other - at distance  $x_2 \geq l_c$  (here Debye radius  $d \ll l_c$ ). Since the space charge is concentrated in region between cathode and plane  $x_1$ , we will consider that between planes  $x_1$  and  $x_2$  potential in practice does not change.

Electrons and ions, emitted by the cathode (ions appear owing to surface ionization), have Maxwellian distribution with temperature of cathode.

We will assume that electrons, moving from plasma to cathode, have Maxwellian distribution with temperature different than temperature of cathode and ions - Maxwellian distribution with temperature coinciding with temperature of cathode. Since  $d \ll l_c$ , then in layer of space charge particles move without collisions and distribution functions on surface  $x_1$  have following form:

$$f_e = \begin{cases} \frac{m^3 I_{e0}}{2\pi (kT')^3} \exp\left(\frac{e\Delta\varphi'}{kT'} - \frac{mv^2}{2kT'}\right) & \left( \begin{array}{l} \Delta\varphi' > 0, \sqrt{2e\Delta\varphi'/m} < v_x < \infty \\ \Delta\varphi' < 0, 0 < v_x < \infty \end{array} \right) \\ n' \left(\frac{m}{2\pi kT'_e}\right)^{3/2} \exp\left(-\frac{mv^2}{2kT'_e}\right) & \left( \begin{array}{l} \Delta\varphi' > 0, -\infty < v_x < \sqrt{2e\Delta\varphi'/m} \\ \Delta\varphi' < 0, -\infty < v_x < 0 \end{array} \right) \end{cases} \quad (1.1)$$

$$f_i = \begin{cases} \frac{M^3 I_{i0}}{2\pi (kT')^3} \exp\left(-\frac{e\Delta\varphi'}{kT'} - \frac{Mv^2}{2kT'}\right) & \left( \begin{array}{l} \Delta\varphi' > 0, 0 < v_x < \infty \\ \Delta\varphi' < 0, \sqrt{-2e\Delta\varphi'/M} < v_x < \infty \end{array} \right) \\ n' \left(\frac{M}{2\pi kT'}\right)^{3/2} \exp\left(-\frac{Mv^2}{2kT'}\right) & \left( \begin{array}{l} \Delta\varphi' > 0, -\infty < v_x < 0 \\ \Delta\varphi' < 0, -\infty < v_x < \sqrt{-2e\Delta\varphi'/M} \end{array} \right) \end{cases} \quad (1.2)$$

Here  $\Delta\varphi'$  - difference of potentials between surface  $x_1$  and cathode (potential of surface  $x_1$  is taken at zero),  $m$ ,  $M$  - masses of electron and ion,  $T'$  - temperature of cathode,  $T'_e$  - temperature of electrons at cathode,  $n'$  - density of

plasma at cathode,  $I_{e0}$ ,  $I_{i0}$  - flows of emission of electrons and ions from cathode. During derivation (1.1), (1.2) it was assumed that potential in layer of space charge changes smoothly.

We will further assume that distribution function on surface  $x_1$  coincides with locally Maxwellian function, with diffusion corrections, which determine flows of heat and particles different than zero. Desired boundary conditions are easily received, calculating balance of number of particles and energy in volume included between surfaces  $x_1$  and  $x_2$ :

at  $\Delta\varphi' > 0$

$$I_{e0} - \frac{n'_e v'_e}{4} \exp\left(-\frac{e\Delta\varphi'}{kT'_e}\right) = I_e, \quad \frac{n'_i v'_i}{4} = I_{i0} \exp\left(-\frac{e\Delta\varphi'}{kT'_i}\right) \quad (1.3)$$

$$T'_e = T' + \frac{\lambda'_e}{2kI_{e0}} \frac{dT'_e}{dx} + \frac{I_e}{I_{e0}} \frac{e\Delta\varphi'}{2k} \quad \left( v'_e = \sqrt{\frac{8kT'_e}{\pi m}}, \quad v'_i = \sqrt{\frac{8kT'_i}{\pi M}} \right) \quad (1.4)$$

at  $\Delta\varphi' < 0$

$$I_{e0} \exp\left(\frac{e\Delta\varphi'}{kT'_e}\right) = \frac{n'_e v'_e}{4}, \quad I_{i0} - \frac{n'_i v'_i}{4} \exp\left(\frac{e\Delta\varphi'}{kT'_i}\right) = I_i, \quad T'_e = T' \quad (1.5)$$

Here  $I_e$ ,  $I_i$  - electronic and ionic flows through TEP, prime quantities relative to cathode or to region near cathode. During derivation of these relationships in second equation (1.3) and first and third equations (1.5) members of order  $\frac{1}{L}$ , are rejected, since

$$\frac{4I_{e,i}}{n'_e v'_{e,i}}, \quad \frac{2\lambda'_e}{kn'_e v'_e} \frac{dT'_e}{dx} \sim \frac{l}{L} \ll 1$$

However, relation

$$\frac{4I_{e,i}}{n'_e v'_{e,i}} \exp\left(\frac{|e\Delta\varphi'|}{kT'_e}\right)$$

in general, is not assumed small. In case, when  $|e\Delta\varphi'| \sim kT'$ , in (1.3) and (1.5) it is possible to disregard  $I_e$  and  $I_i$  and in (1.4) to put  $T'_e = T'$ . Here (1.3) - (1.5) correspond to equilibrium boundary conditions.

We will introduce parameter

$$\omega = (I_{i0}/I_{e0}) \sqrt{M/m} \quad (1.6)$$

It is easy to see that during equilibrium boundary conditions

$$\Delta\varphi' = (KT'/e)\frac{1}{2}\ln\omega \quad (1.7)$$

If  $\omega < 1$ , which corresponds to condition  $\Delta\varphi' < 0$ , then condition in near cathode region can be called undercompensated (ionic emission current is small as compared with electronic). If  $\omega > 1$  ( $\Delta\varphi' > 0$ ), then condition will be called overcompensated (electronic emission current is small as compared with ionic). It is necessary, certainly, to keep in mind that under the conditions of diffusion operating regime of TEP, as much as desired strong over or under compensation cannot lead to appearance of space charge anywhere but in a thin layer near the surface of cathode.

We will estimate approximately the boundaries of  $\omega$ , at which significant deflections from equilibrium conditions on cathode occur. At  $\omega > 1$  this takes place if

$$1/4n'v_e' \exp(-e\Delta\varphi'/kT') \sim I_e$$

or, proceeding from (1.7), if

$$1/4n'v_e' \sim I_e V \bar{\omega}$$

Similarly, for  $\omega < 1$  deflections appear when

$$1/4n'v_i' V \bar{\omega} \sim I_i$$

Since  $4I_{e,i}/n'v_{e,i}' \sim l_e/L$ , then equilibrium boundary conditions on cathode, and consequently, independence of VI characteristics of work function of cathode take place when

$$(l_e/L)^2 \ll \omega \ll (L/l_e)^2 \quad (1.8)$$

Actually, when  $\omega < 1$  deflections from equilibrium conditions on cathode occur later than when  $\omega > 1$ . Indeed, from (1.5) we obtain

$$n' = \left[ \frac{16I_{e0}}{v_e'v_i'} (I_{i0} - I_i) \right]^{1/2}$$

and since in regime of saturation current  $I_i \rightarrow 0$ , hence equilibrium value is obtained.

Similarly boundary conditions on anode can be obtained. It is necessary only to consider that emission of electrons and ions from anode is absent due to its low temperature. Taking distribution function of electrons and ions near anode in the form of Maxwellian functions with temperatures  $T_e''$  and  $T''$  (two primes mean that quantity is that on anode or in region near anode) and calculating balance of number of particles and energy, we receive:

$$I_e = \frac{n'' v_e''}{4}, \quad I_i = -\frac{n'' v_i''}{4} \exp\left(-\frac{e\Delta\varphi''}{kT_e''}\right) \quad \text{when } \Delta\varphi'' > 0 \quad (1.9)$$

$$I_e = \frac{n'' v_e''}{4} \exp\left(\frac{e\Delta\varphi''}{kT_e''}\right), \quad I_i = \frac{n'' v_i''}{4} \quad \text{when } \Delta\varphi'' < 0 \quad (1.10)$$

$$Q_e = I_e (2kT_e'' - e\varphi'' - e\Phi), \quad \Phi = \begin{cases} \Delta\varphi'' & (\Delta\varphi'' < 0) \\ 0 & (\Delta\varphi'' > 0) \end{cases} \quad (1.11)$$

Here  $\Delta\varphi''$  - difference of potentials between anode and plasma at anode,  $Q_e$  - flow of total energy of electrons from plasma to anode.

2. System of fundamental equations and its solution. Equations of diffusion in three-component mixture, with regard for small degree of ionization and great difference of masses of electron and ion, have form

$$I_e = nu_e \frac{d\varphi}{dx} - D_e \frac{dn}{dx} - D_e^T \frac{n}{T_e} \frac{dT_e}{dx} \quad (2.1)$$

$$I_i = -nu_i \frac{d\varphi}{dx} - D_i \frac{dn}{dx} - D_i^T \frac{n}{T_i} \frac{dT_i}{dx} \quad (2.2)$$

$$Q_e = -\lambda \frac{dT_e}{dx} + I_e (2kT_e - e\varphi) \quad (2.3)$$

Here  $u_{e,i}$  --- mobility,  $D_{e,i}$  - coefficients of diffusion,  $n$  - concentration of plasma,  $\varphi$  - is potential, counted from plane  $x_1$ . Coefficients  $D_e^T$  and  $D_i^T$ , in general, differ somewhat from usual coefficients of thermal diffusion. Flows  $I_e$ ,  $I_i$ , and  $Q_e$  are constant in volume, i.e., volume of ionization and recombination will be disregarded.

Due to complexity of boundary conditions and dependence of coefficients on unknown functions ( $n$ ,  $T_e$ ,  $\varphi$ ) themselves the considered system of equations can

be solved only numerically. Approximation method of solution with equilibrium boundary conditions on cathode based on disregard in (2.1) and (2.2) of members proportional to  $dT_{e,i}/dx$ , and approximation of  $n(x)$  and  $\varphi(x)$  linear functions is given in [1].

Below, for obtaining solution of equations of diffusion a different character of behavior of  $n$  and  $T_e, T_i$  in interelectrode space is used. At the time when  $n(x)$  decreases from cathode to anode approximately by order of two,  $T_e(x)$  and  $T_i(x)$  change by 1.5 - 3 times. Therefore, taking as  $T_e(x)$  and  $T_i(x)$  certain constant mean values  $\langle T_e \rangle$ , and  $\langle T_i \rangle$ , it is possible from (2.1) and (2.2) to find  $n(x)$  and  $\varphi(x)$ . Putting these  $n$  and  $\varphi$  in (2.3), we find  $T_e(x)$ . Further, with the help of this value of  $T_e(x)$ , we receive new  $n(x)$  and  $\varphi(x)$  which we again put in (2.3), etc. Just this method was applied during programming of diffusion problem on electronic computer. In given work for obtaining of more simple, approximate solution the same method is used, but instead of  $T_e(x)$  and  $T_i(x)$  in equations (2.1) and (2.2) are put each time quantities  $\langle T_e \rangle$  and  $\langle T_i \rangle$ , (constants in interelectrode space). Here  $\langle T_e \rangle$  is found from solution of (2.3), where as  $n(x)$  and  $\varphi(x)$  are put in solutions of (2.1) and (2.2) at preceding value of  $\langle T_e \rangle$ . Since  $T_i$  is determined only by temperatures of cathode and anode, then

$$\langle T_i \rangle = \frac{1}{2} [T' + T''] \quad (2.4)$$

Similarly

$$\langle T_e \rangle = \frac{1}{2} [T_e'(I_c) + T_e''(I_a)] \quad (2.5)$$

Thus, a system of differential equations with boundary conditions reduces to a system of algebraic equations solved by consecutive approximations.

Setting Richardson current in the form

$$I_{rc} = \frac{A}{e} (T')^2 \exp\left(-\frac{eV'}{kT'}\right) \equiv \frac{1}{4} n_{ek} v_{ek} \quad \left(v_{ek} = \left[\frac{8kT'}{\pi m}\right]^{1/2}\right)$$

Let us turn to dimensionless variables

$$\xi = \frac{x}{L}, j_0 = \frac{I_0}{I_{c0}}, j_1 = \frac{I_1}{I_{c1}}, j_{10} = \frac{I_{10}}{I_{c10}} = \omega, v = \frac{n}{n_{c1}}, \theta = \frac{T^*}{T'},$$

$$\tau_{e,1} = \frac{T_{e,1}}{T'}, \psi = \frac{e\phi}{kT'}, \Psi = \frac{e\Phi}{kT'}, \zeta_0 = \frac{4D_0}{v_{ek}L}, \zeta_1 = \frac{4D_1}{v_1L}, s = \frac{kn_{ek}v_{ek}L}{2\lambda_0} \quad (2.6)$$

Assuming that all particles interact as elastic spheres and that  $\lambda_0$  is determined by expression for thermal conduction of Lorentz gas  $\lambda_0 = 2/3 knv_e \frac{1}{e}$ , we obtain

$$\zeta_0 = \gamma_e \sqrt{\tau_e \tau_i}, \quad \zeta_1 = \gamma_i \tau_i'^{1/2}, \quad s = \gamma_e v \sqrt{\tau_e \tau_i} \quad (2.7)$$

where

$$\gamma_e = \frac{4}{3} \frac{l_e'}{L} = 5.90 \cdot 10^{-6} \frac{T'}{\rho L}, \quad \gamma_i = \frac{4}{3} \frac{l_i'}{L} = \gamma_e \frac{\sigma_e}{\sqrt{2\sigma_i}} \quad (2.8)$$

Here  $\sigma_e, \sigma_i$  - scattering cross section of electrons and ions on atoms of Cs,  $l_e', l_i'$  - length of free path of electrons and ions near cathode. Pressure  $p$  in (2.8) is expressed in mm of mercury,  $L$  - in cm,  $T'$  - in °K. Numerical constant in (2.8) corresponds [2] to value  $\sigma_e = 2 \times 10^{-14} \text{ cm}^2$ .

Solving equations (2.1) - (2.2) relative to derivatives and using (1.16) we obtain

$$\frac{dv}{d\xi} = -\frac{1}{\tau_i(\tau_e - \tau_i)} \left( \sqrt{\tau_e} \frac{j_e}{\tau_e} + \sqrt{\tau_i} \frac{j_i}{\tau_i} \right) \quad (2.9)$$

$$\frac{d\psi}{d\xi} = \frac{1}{v} \frac{\tau_e}{\tau_e + \tau_i} \left( \frac{j_e}{\tau_e \sqrt{\tau_e}} - \frac{j_i}{\tau_i \sqrt{\tau_i}} \right) \quad (2.10)$$

$$\frac{d\tau_e}{d\xi} = \frac{j_e}{2\tau_e \tau_i v \sqrt{\tau_e}} [2(\tau_e - \tau_e') + \psi' + \Psi - \psi] \quad (2.11)$$

Boundary conditions (1.3) - (1.4) on cathode ( $\xi = 0$ ) in overcompensated regime take form

$$v' \sqrt{\tau_e'} \exp\left(-\frac{\Delta\psi'}{\tau_e'}\right) = 1 - j_c, \quad v' = \omega e^{-\Delta\psi'} \quad (2.12)$$

$$2(1 - j_c)(\tau_e' - 1) = j_c [\psi' + \Psi + \Delta\psi' - 2(\tau_e' - 1)] \quad (2.13)$$

and in undercompensated regime

$$e^{-\Delta\psi'} = v', \quad v' e^{-\Delta\psi'} = \omega - j_c, \quad \tau_e' = 1 \quad (2.14)$$

Let us remember that

$$\begin{aligned} v(0) &\equiv v', & \tau_e(0) &\equiv \tau_e', & \psi(0) &= 0, & v(1) &\equiv v''; \\ \psi(1) &\equiv \psi'', & \tau_e(1) &\equiv \tau_e'' \end{aligned}$$

Boundary conditions (1.9) - (1.10) on anode ( $\xi = 1$ ) take form

$$j_e = v'' \sqrt{\tau_e''} \exp(\Delta\psi'' / \tau_e'') \quad j_i' = v' \sqrt{\theta} \quad \text{when} \quad \Delta\psi'' < 0 \quad (2.15)$$

$$j_e = v' \sqrt{\tau_e'}, \quad j_i = v'' \sqrt{\theta} \exp(-\Delta\psi'' / \theta) \quad \text{when} \quad \Delta\psi'' > 0 \quad (2.16)$$

From (2.9) - (2.11) and boundary conditions it is easy to see that  $v(\xi)$ ,  $\psi(\xi)$ ,  $\tau_e(\xi)$  and values of these quantities in regions adjacent to electrodes,  $v'$ ,  $\tau_e'$ ,  $\Delta\psi'$ ,  $v''$ ,  $\psi''$ ,  $\Delta\psi''$ ,  $\tau_e''$  as current functions  $j_e$  can be determine defining four dimensionless parameters  $l_e' / L \sim T' / pL$ ,  $\sigma_i$ ,  $\tau_e$ ,  $\theta = T'' / T$ ,  $\omega$ . Work of output of cathode enters only into parameter  $\omega$ . Thus, calculation of dimensionless volt-ampere characteristics, i.e., dependence of  $j_e$  on quantity  $-(\psi'' + \Delta\psi'' + \Delta\psi')$ , reduces only to assignment of these four parameters and does not depend on concrete values of scattering cross sections  $\sigma_e$  and  $\sigma_i$ , and also work function of surface of cathode in pairs of Cs.

Since in equations (2.9) and (2.10), according to (2.4) and (2.5),

$$\tau_i = 1/2(1 + \theta) = \text{const}, \quad \tau_e = 1/2(\tau_e'(j_e) + \tau_e''(j_e)) = \text{const}$$

then

$$v(\xi) = v' - \alpha\xi \quad (2.17)$$

$$\psi(\xi) = (\beta / \alpha) \ln [v' / v(\xi)] \quad (2.18)$$

where through  $\alpha$  and  $\beta$  are designated constants in right sides of (2.9) and (2.10). Logarithmic movement of potential is easy to understand if one considers that concentration of electrons near anode is very small, and thus, a large part of voltage falls near anode.

We proceed further in the following manner. During fixed  $j_e$  we arbitrarily assign zero approximations  $\tau_e'$  and  $\tau_e''$ . When  $\omega > 1$  from (2.12) we find  $v_e'$  and  $\Delta\psi_e'$ . In case  $\Delta\psi'' < 0$ , assuming in (2.17)  $\xi = 1$  and using the second of equations

(2.15), from  $\alpha$  and  $\beta$  we exclude  $j_i$  and find  $v_0', \Delta\psi_0'$  from (2.18) -  $\psi_0'$ . In case  $\Delta\psi' > 0$ , ion current can be determined from expression for  $\alpha$ , of first equation

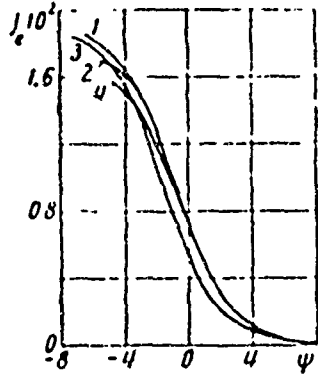


Fig. 1

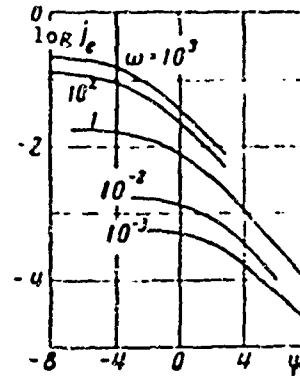


Fig. 2

of (2.16) and equation (2.17) when  $\xi = 1$ . Then  $\psi_0''$  and  $\Delta\psi_0''$  are found. For determination of subsequent approximations of electron temperature we write (2.11) in the form ( $k$  - number of approximation,  $k = 0, 1, 2, \dots$ )

$$\frac{d\tau_{e(k+1)}}{d\xi} = \frac{j_e}{\tau_e \tau_i \sqrt{\tau_{ek}}} \left[ \frac{\tau_{e(k+1)}(\xi) - \tau_{e(k+1)}'}{v_k(\xi)} + \frac{\psi_k'' - \psi_k - \psi_k(\xi)}{2v_k(\xi)} \right] \quad (2.19)$$

After substitution of (2.17) and (2.18) this equation is easily integrated

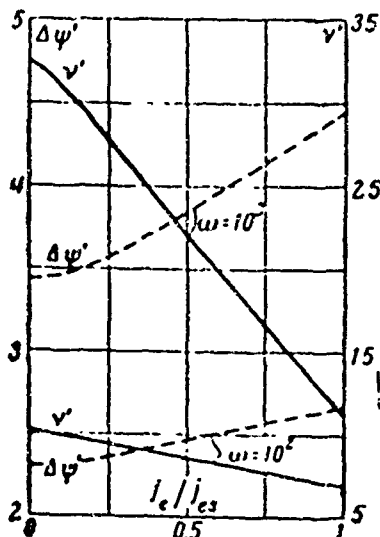


Fig. 3.

Considering in received equation  $\xi = 0$  (or  $\xi = 1$ ), jointly with (2.13) we obtain linear system of two equations for determination of  $\tau_{e(k+1)}$  and  $\tau_{e(k+1)}$ . Found  $\tau_{e(k+1)}$  and  $\tau_{e(k+1)}$  are used for obtaining  $v_{k+1}, v_{k+1}'$  etc. Thus, for every value of  $j_e$  by method of successive approximations we find  $v', \Delta\psi', v(\xi), \Delta\psi'', \psi(\xi), \tau_e(\xi)$  corresponding to it.

When  $\omega < 1$  from (2.14) for  $v_k'$  we obtain equation

$$\omega - j_{ik} = (v_k')^2 \quad (2.20)$$

Excluding hence ionic current, just as in case of  $\omega > 1$ , we receive for determination of  $v_k'$  a quadratic equation. Further we easily find  $v_k'$ ,  $\Delta\psi_k'$ ,  $v_k(\xi)$  etc. Calculation showed that for achievement of accuracy to 3%, 3-4 iterations were sufficient with suitable choice of  $\tau_0'$  and  $\tau_0''$ .

3. Results of Calculation. Results of calculation of dimensionless VI characteristics by above-stated method are represented in Figs. 1 - 6.

In Fig. 1 is given dependence of current intensity  $j_e$  on voltage drop between electrodes  $\psi = -(\psi' + \Delta\psi')$  during equilibrium boundary conditions on cathode ( $\omega = 1$ ).

Curves in Fig. 1 correspond to following values of parameters:

Curve	1	2	3	4
$l_e'/L =$	0.01	0.05	0.01	0.01
$\sigma_1/\sigma_2 =$	5	5	25	5
$\theta =$	0.5	0.5	0.5	0.667

(In Fig. 1 values of ordinates for curve 2 should be increased by 5 times.)

Saturation current  $j_{es}$  during increase of  $l_e'/L$  5 times, increases approximately by 5 times in accordance with [1]. Increase of  $\sigma_1$  by 5 does not change  $j_{es}$ , but shifts VI characteristic to the left by quantity of order  $kT'/e$ , which is coupled with growth by approximately that quantity of the near anode barrier  $\Delta\psi'$ . Decrease of relation  $T''/T'$  from 1/2 to 1/3 decreases  $j_{es}$  by approximately 15%. When  $T' = \text{const}$  this is caused by increase of concentration

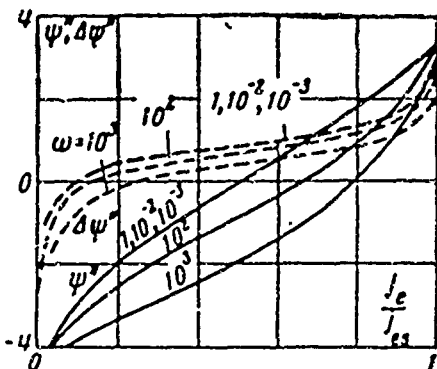


Fig. 4.

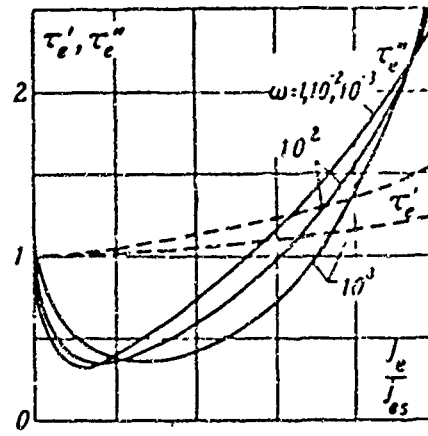


Fig. 5.

of atoms near anode which leads to increase of resistance to current through

TEP. Let us note that during equilibrium boundary conditions on cathode, distinction of VI characteristics calculated by such method from characteristic received during solution of equations (2.1) - (2.3) on electronic computer is near 15%.

Figs. 2 - 5 show influence of degree of compensation of  $\omega$  on VI characteristics and on quantity of density, temperature and potential at electrodes (when  $i_e'/L = 10^{-2}$ ,  $\sigma_1/\sigma_2 = 5$ ,  $\theta = 0.5$ ). Values  $v'$  and  $\Delta\psi'$  (Fig. 3) coincide with equilibrium values for overcompensated regime at  $j_e = 0$ , and for undercompensated regime - at  $j_e = j_{es}$  ( $j_i = 0$ ). It is necessary to note that at value selected in calculation of  $i_e'/L = 0.01$  the range of changes of  $\omega$  is rather great in order to include strongly over or undercompensation conditions. As was noted above, deviations from equilibrium regime at  $\omega > 1$  occur earlier than at  $\omega < 1$ . In connection with this, results of calculation with  $\omega = 10^2, 10^3$  noticeably differ from equilibrium whereas at  $\omega = 1, 10^{-2}, 10^{-3}$  they practically coincide. In particular, in the last case  $v' = \sqrt{\omega}$  and  $\Delta\psi' = \frac{1}{2} \ln \omega$ . Near anode, jump of potential  $\Delta\psi'$  (Fig. 4) changes sign at significantly smaller currents ( $i_e'/i_{es} \approx 0.1$ ), than voltage drop in volume  $\psi'$  ( $i_e'/i_{es} \approx 0.55$ ). Quantity  $\Delta\psi'$  at  $0.1 \leq i_e'/i_{es} \leq 0.9$  of order  $kT'/e$ , sharply changes only at  $i_e'/i_{es} < 0.1$  and  $i_e'/i_{es} > 0.9$ . At  $\omega > 10^2$  deflection of movement of  $\psi'$  ( $j_e$ ) is already noticeable from linear (Fig. 4). Heating of electrons at anode can be very strong and can exceed temperature of cathode by 1.7 - 2.8 times (Fig. 5). Under these conditions volume ionization appears and TEP starts to work in regime of low-voltage arc. At those currents when  $\Delta\psi' = 0$ , quantity  $v'$  attains minimum. At these same currents,  $v'$  also has minimum which follows from boundary conditions on anode. (Let us note that, as calculations showed,  $v'/v \leq 10^{-2} - 10^{-3}$ .)

In Fig. 6 are presented measured VI characteristics of TEP calculated at various values of work function of cathode  $W'$ . These characteristics were obtained from curves in Fig. 2. Here it was assumed that

$$\sigma_2 = 2 \cdot 10^{-11} \text{ cm}^2, \sigma_1 = 10 \cdot 10^{-11} \text{ cm}^2, A = 120 \text{ s/cm}^2, V_1 = 3.86 \text{ V } W' = 1.7 \text{ V}$$

Determining  $W'$  from expression

$$\omega = 3.18 \cdot 10^{-6} \frac{p}{(T')^{3/2}} \exp\left(23.2 \frac{W' - 1.93}{T'}\right), \quad T' = \frac{T}{10^3} \quad (3.1)$$

we find voltage on load  $V$

$$V = W' - W'' - \Delta\varphi' - \Delta\varphi'' - \varphi'' \quad (3.2)$$

(In expression (3.1),  $p$  and  $T'$  correspond to condition  $l_0/L = 10^{-2}$ ). From Fig. 6 we see that in interval  $2.25 < W'' < 2.80$  v VI characteristics do not depend on work function of cathode. However, at  $W' = 3.5$  v, saturation current decreases almost by 1.5 times.

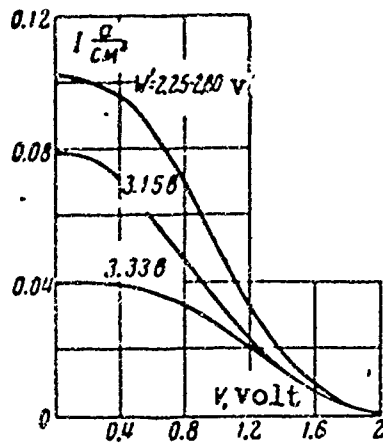


Fig. 6.

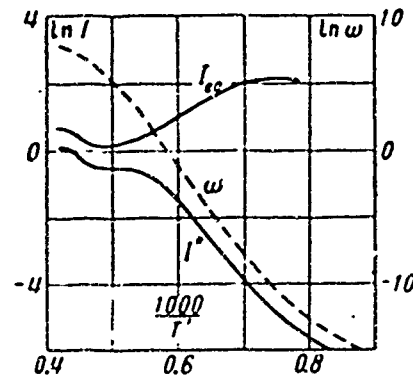


Fig. 7.

From equation (3.2), assuming  $V = 0$ , one can determine dependence of current of short circuit  $I^*$  on temperature of cathode  $T'$  (S-shaped curve). Tungsten was taken as cathode material, work function of which in pairs of Cs was found from data of Langmuir [3]. Pressure, interelectrode distance, and parameters of anode were taken as equal to:

$$p = 1 \text{ mm Hg} \quad L = 1 \text{ mm} \\ T'' = 800^\circ \text{K}, \quad W'' = 1.7 \text{ v}$$

Values of  $W'$  and  $\omega$  calculated for certain  $T$  are presented in table. Qualitatively, form of S-shaped curve (Fig. 7) agrees with experimental results. For obtaining of quantitative agreement, more precise definition of size of section  $\sigma_0$  is required and also calculation of Coulomb collisions. If

$$\frac{dT_{el}}{dx} = 0, \quad \frac{dn}{dx} \approx \frac{n'' - n'}{L} = -\frac{n'}{L}$$

Table

T, °K	W, e	$\omega$
1170	1.72	$3.33 \cdot 10^{-7}$
1270	1.86	$4.87 \cdot 10^{-6}$
1370	2.02	$6.65 \cdot 10^{-5}$
1470	2.22	$1.18 \cdot 10^{-3}$
1570	2.46	$2.61 \cdot 10^{-2}$
1670	2.70	$3.94 \cdot 10^{-1}$
1770	2.92	3.33
1870	3.14	$2.23 \cdot 10^1$
1970	3.36	$1.22 \cdot 10^2$
2070	3.55	$4.02 \cdot 10^2$
2170	3.73	$1.06 \cdot 10^3$
2270	3.86	$1.53 \cdot 10^3$
2370	4.02	$2.88 \cdot 10^3$

then from qualitative analysis of equations (1.6), (1.7), and (2.1) it follows that slopes of S-shaped curve at  $\omega < (i_0/L)^2$  is determined by quantity of work function of anode  $W^a$ , and at  $1 \gg \omega \gg (i_0/L)^2$  -ionizing energy of cesium.

Submitted  
26 May 1963

#### Literature

1. B. Ya. Moyzhes and G. Ye. Pikus, On theory of plasma thermoelement. Phys. of the solid body, 1960, Vol. 2, 756.
2. D. N. Mirlin, G. Ye. Pikus, and V. G. Yur'yev, Determination of sections of electron scattering by electro-conductance of weakly ionized gas, Journal of Tech. Phys., 1962, Vol. 32, No 6, 766.
3. J. B. Taylor and G. Langmuir. The Evaporation [of] atoms, Ions and Electrons from Cesium Films on Tungsten.

## TRANSFER EQUATIONS FOR NONISOTHERMISTIC MULTITYPE PLASMA

M. Ya. Aliyevskiy and V. M. Zhdanov

(Sverdlovsk)

In present work a system of transport equations following from kinetic equation for particles of  $\alpha$ -type, leads to closed form by use of approximation of Grad's "13-moments" to distribution function [2]. Besides usual equations of continuity, conservation of momentum and energy conservation for each of the components of plasma, the obtained system contains equations for nondiagonal part of stress tensor and heat flow of particles. Temperatures of components are considered different.

Relationships for known properties of transfer in plasma follow from general transport equations on the assumption that parameters of plasma change little on mean free paths and for times of the order of time of collisions. It is shown, in particular, that expressions for tensor of viscosity of heat flow and of conductance current in two-temperature partially ionized gas ( $T_e \geq T_i = T_a$ ) have, with certain limitations, the same form as in [7] if series of quantities entering into them is determined at electronic temperature  $T_e$ .

1. Transport equations in approximation of "13-moments." Transport equation for certain quantity  $\psi_\alpha(c_\alpha, r, t)$ , referred to system of coordinates moving with average mass velocity of gas  $u$  can be obtained by multiplication of left and right sides of kinetic equation by  $\psi_\alpha$  with subsequent integration according to space of velocity of particles [1]. (Here  $c_\alpha$  - relative velocity of a particle,  $r$  - its position,  $t$  - time). Considering, in particular,  $\psi_\alpha^{(0)} = m_\alpha$ ,  $\psi_\alpha^{(1)} = m_\alpha c_\alpha$  and  $\psi_\alpha^{(2)} = (m_\alpha/2) c_\alpha^2$ , where  $m_\alpha$  - mass of  $\alpha$ -particle, we arrive at equations of continuity, conservation of momentum, and energy conservation for

$\alpha$ - component of plasma which in the presence of electric and magnetic fields take form:

$$\frac{\partial \rho_\alpha}{\partial t} + \nabla \rho_\alpha u_\alpha = 0 \quad (1.1)$$

$$\rho_\alpha \frac{d_\alpha u_\alpha}{dt} + \nabla P_\alpha^* - n_\alpha e_\alpha (E + u_\alpha \times B) = R_\alpha^{(1)} \quad (1.2)$$

$$\frac{3}{2} \frac{d p_\alpha}{dt} + \frac{3}{2} p_\alpha \nabla u + \nabla q_\alpha + P_{\alpha ik} \frac{\partial u_i}{\partial x_k} - \rho_\alpha w_\alpha F_\alpha = R_\alpha^{(2)} \quad (1.3)$$

(by repeated Latin indices summation is implied).

Here  $e_\alpha, n_\alpha, u_\alpha, q_\alpha$  - are respectively charge, density, average velocity and heat flow of  $\alpha$ - particles; introduced, furthermore, are mass density  $\rho_\alpha = m_\alpha n_\alpha$  and average relative velocity  $w_\alpha = u_\alpha - u$  particles of  $\alpha$ - type. Components of tensor  $P_\alpha^*$  are coupled with usual stress tensor  $P_\alpha$  by relationship

$$P_{\alpha ik}^* = P_{\alpha ik} - \rho_\alpha w_{\alpha i} w_{\alpha k} \quad (1.4)$$

In turn,  $P_\alpha$  is divided into two parts

$$P_{\alpha ik} = p_\alpha \delta_{ik} + \pi_{\alpha ik} \quad (1.5)$$

where  $p_\alpha$  - partial pressure of  $\alpha$ -component of plasma, and  $\pi_\alpha$  can be conditionally called tensor of viscous stresses of  $\alpha$ - particles.

During writing of (1.2) and (1.3) the following abbreviations were used

$$\frac{d_\alpha}{dt} = \frac{\partial}{\partial t} + (u_\alpha \nabla), \quad \frac{d}{dt} = \frac{\partial}{\partial t} + (u \nabla), \quad F_\alpha = \frac{e_\alpha}{m_\alpha} (E + u \times B) - \frac{du}{dt} \quad (1.6)$$

here  $E$  - electric field strength,  $B$  - vector of magnetic induction.

Quantities  $R_\alpha^{(1)}$  and  $R_\alpha^{(2)}$ , appearing in right sides of equations (1.2) and (1.3), represent respectively average change of momentum and  $\alpha$ - particle energy during collisions. Calculation of them requires knowledge of dynamics of collisions of form of distribution function of particles in plasma.\*

Equations (1.1) - (1.3) will not form, in general, closed system since besides usual hydrodynamic variables  $\rho_\alpha, u_\alpha, p_\alpha$  present in them are moments of

---

\*For particles, interacting according to law  $\sim r^{-1}$ , these quantities can be calculated without knowledge of concrete form of distribution function.

a higher order: stress tensor  $P_\alpha$  (more accurately, its nondiagonal part -  $\pi_\alpha$ ) and vector of flow of heat  $q_\alpha$ . For these quantities their own transport equations can be obtained, however in them, in turn, will appear two moments of a high order. Reduction of these moments to those variables for which transport equations were already formed is possible only during use of determined approximation and distribution function. Below, to this aim is used approximation of Grad's "13-moments" [2]. Application of this approximation to a multicomponent gas mixture and to completely ionized two-component plasma was discussed in works [3,4], in the same place are given corresponding closed systems of transport equations for these cases.

Expression for  $f_\alpha(c_\alpha, r, t)$  in approximation of 13-moments has form [3]:

$$f_\alpha = f_\alpha^{(0)} \left[ 1 + \gamma_\alpha w_\alpha c_\alpha + \frac{\gamma_\alpha}{2p_\alpha} \pi_{\alpha ik} c_{\alpha i} c_{\alpha k} + \frac{\gamma_\alpha}{5p_\alpha} (\gamma_\alpha c_\alpha^2 - 5) h_\alpha c_\alpha \right] \quad (1.7)$$

where

$$f_\alpha^{(0)} = n_\alpha \left( \frac{\gamma_\alpha}{2\pi} \right)^{3/2} \exp \left( -\frac{\gamma_\alpha c_\alpha^2}{2} \right), \quad h_\alpha = q_\alpha - \frac{5}{2} p_\alpha w_\alpha, \quad \gamma_\alpha = \frac{m_\alpha}{kT_\alpha} \quad (1.8)$$

Here  $k$  - Boltzmann constant,  $T_\alpha$  - temperature of  $\alpha$ - particles (relative to average mass velocity  $u$ ).

Multiplying kinetic equation for  $\alpha$ - particles by

$$\psi_{\alpha ik}^{(2)} = m_\alpha \left( c_{\alpha i} c_{\alpha k} - \frac{1}{3} \delta_{ik} c_\alpha^2 \right), \quad \psi_{\alpha i}^{(3)} = \frac{1}{2} m_\alpha (c_\alpha^2 - 5 / \gamma_\alpha) c_{\alpha i} \quad (1.9)$$

we arrive in approximation of 13-moments at following equations for quantities  $\pi_{\alpha ik}$  and  $h_\alpha$  (or  $q_\alpha$ )

$$\begin{aligned} \frac{d\pi_{\alpha ik}}{dt} + \pi_{\alpha ik} \frac{\partial u_l}{\partial x_l} + 2 \left\{ \pi_{\alpha il} \frac{\partial u_k}{\partial x_l} \right\} + \frac{4}{5} \left\{ \frac{\partial q_{\alpha i}}{\partial x_k} \right\} + 2p_\alpha e_{ik} - \\ - 2 \{ p_\alpha w_{\alpha i} F_{\alpha k} \} - 2 \frac{e_\alpha}{m_\alpha} \{ (\pi_\alpha \times B)_{ik} \} = R_{\alpha ik}^{(2)} \end{aligned} \quad (1.10)$$

$$\begin{aligned} \frac{dh_{\alpha i}}{dt} + \frac{7}{5} h_{\alpha i} \frac{\partial u_l}{\partial x_l} + \frac{2}{5} h_{\alpha l} \frac{\partial u_l}{\partial x_i} + \frac{7}{5} h_{\alpha l} \frac{\partial u_l}{\partial x_i} + \frac{5}{3} p_\alpha w_{\alpha i} \frac{\partial u_l}{\partial x_l} + \\ + 2p_\alpha w_{\alpha i} e_{ii} + \frac{1}{\gamma_\alpha} \frac{\partial \pi_{\alpha ll}}{\partial x_i} + \frac{7}{2\gamma_\alpha} \pi_{\alpha ll} \frac{1}{T_\alpha} \frac{\partial T_\alpha}{\partial x_i} + \frac{5}{2\gamma_\alpha} \frac{p_\alpha}{T_\alpha} \frac{\partial T_\alpha}{\partial x_i} + \\ + \frac{5}{2} n_\alpha k w_{\alpha i} \frac{dT_\alpha}{dt} - F_{\alpha i} \pi_{\alpha ll} - \frac{e_\alpha}{m_\alpha} (h_\alpha \times B)_i = R_{\alpha i}^{(3)} \end{aligned} \quad (1.11)$$

where designations used are

$$(K_i L_k) = \frac{1}{2} (K_i L_k + K_k L_i) - \frac{1}{3} K_i L_i \delta_{ik}$$

$$e_{ik} = \left\{ \frac{\partial u_i}{\partial x_k} \right\}. \quad (\pi_a \times B)_{ik} = \pi_{a11} \sigma_{iklm} B_m$$

( $\sigma_{iklm}$  - commutation tensor).

Right sides of equations (1.2), (1.3), (1.10), and (1.11), the linear combinations of moments relative to integral of collisions, are written in general form as

$$R_a^{(n)} = \sum_{\beta} \int (\psi_a^{(n)'} - \psi_a^{(n)}) f_a f_{\beta} g_{a\beta} b db d\epsilon d\sigma_a d\sigma_{\beta} \quad (1.12)$$

Here  $g_{a\beta} = |c_a - c_{\beta}|$ ,  $b$  - impact parameter of  $\alpha$ - and  $\beta$ - particles,  $\epsilon$  - azimuthal angle, by prime (mark) is designated value of quantity  $\psi^{(n)}$  after collision.

Using expressions for  $f_a, f_{\beta}$  in the form of (1.7) and disregarding during calculation  $R_a^{(n)}$  (1.12) quadratic members on  $w_a, w_{\beta}$  and  $h_a$ , we arrive at following general expressions

$$R_{a1}^{(1)} = \sum_{\beta} G_{a\beta}^{(1)} (w_{a1} - w_{\beta 1}) + \sum_{\beta} G_{a\beta}^{(2)} \gamma_{c\beta} \left( \frac{h_{a1}}{\gamma_a p_a} - \frac{h_{\beta 1}}{\gamma_{\beta} p_{\beta}} \right)$$

$$R_{a2}^{(2)} = \sum_{\beta} G_{a\beta}^{(1)} \frac{3k}{m_a + m_{\beta}} (T_a - T_{\beta})$$

$$R_{a1k}^{(2)} = \sum_{\beta} \frac{1}{\gamma_a + \gamma_{\beta}} \left[ G_{a\beta}^{(3)} \frac{h_{a1k}}{p_a} + G_{a\beta}^{(4)} \frac{h_{\beta 1k}}{p_{\beta}} \right]$$

$$R_{a1}^{(3)} = \frac{1}{\gamma_a} \sum_{\beta} \left[ G_{a\beta}^{(5)} \frac{h_{a1}}{p_a} + G_{a\beta}^{(6)} \frac{h_{\beta 1}}{p_{\beta}} + \frac{5\gamma_{a\beta}}{2\gamma_a} G_{a\beta}^{(7)} (w_{a1} - w_{\beta 1}) + 5\lambda_{a\beta} G_{a\beta}^{(11)} w_{a1} \right] \quad (1.13)$$

Knowledge of dynamics of collisions of particles allows to calculate values of  $G_{a\beta}^{(n)}$ . If only elastic interactions of particles are considered then coefficients  $G_{a\beta}^{(n)}$  turn out to be linear combinations of quantities  $\Omega_{a\beta}^{(n)}$ , which are generalizations of known Chapman-Cowling integrals [1] in case of different temperatures of components. For identical temperatures these coefficients are found in [2]. In case considered by us, calculations are complicated and lead to following values of coefficients.

$$\begin{aligned}
G_{\alpha\beta}^{(1)} &= B_{\alpha\beta}^{(1)}, & G_{\alpha\beta}^{(2)} &= B_{\alpha\beta}^{(2)} \\
G_{\alpha\beta}^{(3)} &= B_{\alpha\beta}^{(3)} - (\gamma_\beta/\gamma_\alpha) \lambda_{\alpha\beta} B_{\alpha\beta}^{(7)}, & G_{\alpha\beta}^{(4)} &= B_{\alpha\beta}^{(4)} - \lambda_{\alpha\beta} B_{\alpha\beta}^{(7)} \\
G_{\alpha\beta}^{(5)} &= B_{\alpha\beta}^{(5)} + \frac{1}{2} (\gamma_\beta/\gamma_\alpha) \lambda_{\alpha\beta} [B_{\alpha\beta}^{(8)} - B_{\alpha\beta}^{(9)} - 2(\gamma_\alpha/\gamma_\beta) B_{\alpha\beta}^{(10)}] - \\
& & & - (\gamma_\beta/\gamma_\alpha) \lambda_{\alpha\beta}^2 (B_{\alpha\beta}^{(8)} - \frac{1}{2} B_{\alpha\beta}^{(9)}) \\
G_{\alpha\beta}^{(6)} &= B_{\alpha\beta}^{(6)} - \frac{1}{2} \lambda_{\alpha\beta} (B_{\alpha\beta}^{(8)} - B_{\alpha\beta}^{(9)} + 2B_{\alpha\beta}^{(10)}) + \lambda_{\alpha\beta}^2 (B_{\alpha\beta}^{(8)} - \frac{1}{2} B_{\alpha\beta}^{(9)}) \\
G_{\alpha\beta}^{(7)} &= B_{\alpha\beta}^{(7)} + \lambda_{\alpha\beta} B_{\alpha\beta}^{(11)} - \lambda_{\alpha\beta}^2 B_{\alpha\beta}^{(12)}
\end{aligned} \tag{1.14}$$

where

$$\begin{aligned}
B_{\alpha\beta}^{(1)} &= -\frac{16}{3} \mu_{\alpha\beta} n_\alpha n_\beta \Omega_{\alpha\beta}^{11}, & B_{\alpha\beta}^{(2)} &= -\frac{16}{3} \mu_{\alpha\beta} n_\alpha n_\beta \left( \frac{2}{3} \Omega_{\alpha\beta}^{12} - \Omega_{\alpha\beta}^{11} \right) \\
B_{\alpha\beta}^{(3)} &= -\frac{16}{3} \mu_{\alpha\beta} n_\alpha n_\beta \left[ (\gamma_\beta/\gamma_\alpha) \Omega_{\alpha\beta}^{22} + \frac{10}{3} \Omega_{\alpha\beta}^{11} \right] \\
B_{\alpha\beta}^{(4)} &= -\frac{16}{3} \mu_{\alpha\beta} n_\alpha n_\beta \left( \Omega_{\alpha\beta}^{22} - \frac{10}{3} \Omega_{\alpha\beta}^{11} \right) \\
B_{\alpha\beta}^{(5)} &= -\frac{64}{15} \mu_{\alpha\beta} \kappa_{\alpha\beta} n_\alpha n_\beta \left[ \Omega_{\alpha\beta}^{22} + \left( \frac{15}{4} \gamma_\alpha/\gamma_\beta + \frac{25}{8} \gamma_\beta/\gamma_\alpha \right) \Omega_{\alpha\beta}^{11} - \right. \\
& & & \left. - \frac{1}{2} \gamma_\beta/\gamma_\alpha (5\Omega_{\alpha\beta}^{12} - \Omega_{\alpha\beta}^{13}) \right] \\
B_{\alpha\beta}^{(6)} &= -\frac{64}{15} \mu_{\alpha\beta} \kappa_{\alpha\beta} n_\alpha n_\beta \left[ \Omega_{\alpha\beta}^{22} - \frac{55}{3} \Omega_{\alpha\beta}^{11} + \frac{1}{2} (5\Omega_{\alpha\beta}^{12} - \Omega_{\alpha\beta}^{13}) \right] \\
B_{\alpha\beta}^{(7)} &= -\frac{16}{3} \mu_{\alpha\beta} n_\alpha n_\beta \left[ \Omega_{\alpha\beta}^{22} - \frac{4}{3} \Omega_{\alpha\beta}^{12} \right] \\
B_{\alpha\beta}^{(8)} &= -\frac{64}{15} \mu_{\alpha\beta} \kappa_{\alpha\beta} n_\alpha n_\beta \left[ 5\Omega_{\alpha\beta}^{12} - 2\Omega_{\alpha\beta}^{13} \right] \\
B_{\alpha\beta}^{(9)} &= -\frac{64}{15} \mu_{\alpha\beta} \kappa_{\alpha\beta} n_\alpha n_\beta \left[ 5\Omega_{\alpha\beta}^{22} - 2\Omega_{\alpha\beta}^{23} \right] \\
B_{\alpha\beta}^{(10)} &= -\frac{64}{15} \mu_{\alpha\beta} \kappa_{\alpha\beta} n_\alpha n_\beta \left[ \Omega_{\alpha\beta}^{22} - \frac{11}{2} \Omega_{\alpha\beta}^{12} + \frac{25}{4} \Omega_{\alpha\beta}^{11} \right] \\
B_{\alpha\beta}^{(11)} &= -\frac{64}{15} \mu_{\alpha\beta} n_\alpha n_\beta \left[ \Omega_{\alpha\beta}^{22} - \Omega_{\alpha\beta}^{12} - \frac{5}{2} \Omega_{\alpha\beta}^{11} \right] \\
B_{\alpha\beta}^{(12)} &= -\frac{64}{15} \mu_{\alpha\beta} n_\alpha n_\beta \left[ \Omega_{\alpha\beta}^{22} - 2\Omega_{\alpha\beta}^{12} \right]
\end{aligned} \tag{1.15}$$

Here

$$\Omega_{\alpha\beta}^{lr} = \sqrt{\pi} \int_0^\infty \int_0^\infty \zeta^{2r+2} e^{-\zeta^2} g_{\alpha\beta} (1 - \cos^l \chi_{\alpha\beta}) b db d\zeta \quad \left( \zeta = \kappa_{\alpha\beta} (\gamma_{\alpha\beta}/2)^{1/2} \right)$$

where  $\chi_{\alpha\beta}$  - scattering angle in system of center of masses of colliding molecules.

Quantities  $\mu_{\alpha\beta}$ ,  $\kappa_{\alpha\beta}$ ,  $\gamma_{\alpha\beta}$  and  $\lambda_{\alpha\beta}$  are determined by expressions:

$$\mu_{\alpha\beta} = \frac{m_\alpha m_\beta}{m_\alpha + m_\beta}, \quad \kappa_{\alpha\beta} = \frac{\gamma_{\alpha\beta}}{\gamma_\alpha + \gamma_\beta}, \quad \gamma_{\alpha\beta} = \frac{\gamma_\alpha \gamma_\beta}{\gamma_\alpha + \gamma_\beta}, \quad \lambda_{\alpha\beta} = \frac{1 - T_\beta/T_\alpha}{1 + m_\beta/m_\alpha}$$

For case of identical temperatures ( $T_\alpha = T_\beta = T$ )

$$\gamma_{\alpha\beta} = \frac{\mu_{\alpha\beta}}{kT}, \quad \kappa_{\alpha\beta} = \frac{\mu_{\alpha\beta}}{m_\alpha + m_\beta}, \quad \lambda_{\alpha\beta} = 0$$

and coefficients (1.14), (1.15) coincide with those found in work [3].

2. Relationships for properties of transfer in plasma. Equations (1.1 - 1.3) and (1.10 - 1.11) together with expression found above for  $R_i^{(n)}$  will form closed system of quasi-linear, differential equations relative to variables  $\rho_\alpha$ ,  $u_\alpha$ ,  $p_\alpha$ ,  $\pi_{\alpha ik}$  and  $h_\alpha$ . Summation of first three of them according to  $\alpha$  leads to usual equations of continuity, motion, and energy for plasma as a whole

$$\frac{\partial \rho}{\partial t} + \operatorname{div} \rho u = 0, \quad \rho \frac{du}{dt} + \nabla p + \operatorname{div} \pi = j \times B \quad (2.1)$$

$$\frac{3}{2} \frac{dp}{dt} + \frac{5}{2} p \operatorname{div} u + \operatorname{div} q + \pi_{ik} \frac{\partial u_i}{\partial x_k} = j E' \quad (2.2)$$

$$E' = E + u \times B$$

Here,  $\rho$  - mass density,  $p$  - pressure,  $\pi$  - tensor of viscous stresses,  $q$  - heat flow for plasma on the whole obtained by simple summation of corresponding quantities for components; in addition are used condition of quasi-neutrality of plasma and expression for current density of conductance

$$\sum_\alpha n_\alpha e_\alpha = 0, \quad j = \sum_\alpha n_\alpha e_\alpha w_\alpha \quad (2.3)$$

For determination of quantities  $w_\alpha$ ,  $\pi_\alpha$  and  $h_\alpha$  (or  $q_\alpha$ ) it is possible to use equations (1.2), (1.10), and (1.11). The latter are markedly simplified if one assumes that macroscopic parameters of plasma change slightly at distances of order of effective length of free path and for a time of order of the time of collisions of particles in plasma. It is easy to show [3 - 4] that during observance of these conditions it is possible to disregard derivatives  $dw_\alpha / dt$ ,  $dn_{\alpha ik} / dt$ ,  $dh_{\alpha i} / dt$  and nonlinear members in left parts of equations (1.2) and

(1.10) - (1.11) thanks to which expression for vector and tensor properties of transfer in plasma will be determined by solution of systems of linear algebraic equations. Here  $du/dt$  in left part of (1.2) should be replaced from equation of motion (2.1). Then equation of conservation of momentum for the  $\alpha$ -component of plasma takes form:

$$n_\alpha \sum_{\beta} \mu_{\alpha\beta} \tau_{\alpha\beta}^{-1} \left[ \mathbf{w}_\alpha - \mathbf{w}_\beta + \frac{\gamma_\beta}{\gamma_\alpha + \gamma_\beta} A_{\alpha\beta}^{(2)} \left( \frac{\mathbf{h}_\alpha}{p_\alpha} - \frac{\gamma_\alpha}{\gamma_\beta} \frac{\mathbf{h}_\beta}{p_\beta} \right) \right] = - \left( \Delta p_\alpha - \frac{p_\alpha}{\rho} \Delta p \right) - \left( \operatorname{div} \pi_\alpha - \frac{p_\alpha}{\rho} \operatorname{div} \pi \right) + n_\alpha e_\alpha (\mathbf{E}' + \mathbf{w}_c \times \mathbf{B}) - \frac{p_\alpha}{\rho} (\mathbf{j} \times \mathbf{B}) \quad (2.4)$$

Equations for tensors  $\pi_\gamma$  and vectors  $\mathbf{h}_\gamma$  obtained in considered approximation can be conveniently presented in the form

$$\pi_{\alpha ik} + \sum_{\beta \neq \alpha} a_{\alpha\beta} \pi_{\beta ik} = - 2\eta_\alpha \varepsilon_{\alpha ik} + \frac{4}{3} (\pi_{\alpha l i} \sigma_{\alpha l m} \theta_{\alpha m} \tau_\alpha) \quad (2.5)$$

$$\mathbf{h}_\alpha + \sum_{\beta \neq \alpha} b_{\alpha\beta} \mathbf{h}_\beta = - \lambda_\alpha \mathbf{R}_\alpha + (\mathbf{h}_\alpha \times \boldsymbol{\omega}_\alpha \tau_\alpha^*) \quad (2.6)$$

Here

$$\eta_\alpha = \frac{2}{3} p_\alpha \tau_\alpha, \quad \lambda_\alpha = \frac{5k}{2n_\alpha} p_\alpha \tau_\alpha^*, \quad \boldsymbol{\omega}_\alpha = \frac{e_\alpha}{m_\alpha} \mathbf{B} \quad (2.7)$$

$$a_{\alpha\beta} = \frac{2}{3} \frac{m_\beta}{m_\alpha + m_\beta} \left( 1 + \frac{\gamma_\beta}{\gamma_\alpha} \right)^{-1} \frac{p_\alpha}{p_\beta} \tau_\alpha \tau_{\alpha\beta}^{-1} A_{\alpha\beta}^{(4)}, \quad b_{\alpha\beta} = \frac{m_\beta}{m_\alpha + m_\beta} \frac{p_\alpha}{p_\beta} \tau_\alpha^* \tau_{\alpha\beta}^{-1} A_{\alpha\beta}^{(6)}$$

$$\tau_\alpha^{-1} = \frac{1}{8} (A_{\alpha\alpha}^{(3)} + A_{\alpha\alpha}^{(4)}) \tau_{\alpha\alpha}^{-1} + \frac{2}{3} \sum_{\beta \neq \alpha} \frac{m_\beta}{m_\alpha + m_\beta} \left( 1 + \frac{\gamma_\beta}{\gamma_\alpha} \right)^{-1} A_{\alpha\beta}^{(3)} \tau_{\alpha\beta}^{-1}$$

$$(\tau_\alpha^*)^{-1} = \frac{1}{2} (A_{\alpha\alpha}^{(5)} + A_{\alpha\alpha}^{(6)}) \tau_{\alpha\alpha}^{-1} + \sum_{\beta \neq \alpha} \frac{m_\beta}{m_\alpha + m_\beta} A_{\alpha\beta}^{(5)} \tau_{\alpha\beta}^{-1} \quad (2.8)$$

Finally,

$$\varepsilon_{\alpha ik} = \varepsilon_{ik} - \frac{e_\alpha}{kT_\alpha} (\omega_{\alpha i} E_k') \quad (2.9)$$

$$\mathbf{R}_{\alpha i} = \frac{\partial T_\alpha}{\partial x_i} + \frac{2}{5} \frac{T_\alpha}{p_\alpha} \frac{\partial \pi_{\alpha ik}}{\partial x_k} - \frac{2}{5} \frac{e_\alpha}{k p_\alpha} \pi_{\alpha i l} E_l' + \frac{1}{k} \sum_{\beta} \mu_{\alpha\beta} \tau_{\alpha\beta}^{-1} \left[ \frac{\gamma_\beta}{\gamma_\alpha + \gamma_\beta} A_{\alpha\beta}^{(7)} (\mathbf{w}_{\alpha i} - \mathbf{w}_{\beta i}) + 2\lambda_{\alpha\beta} \mathbf{v}_{\alpha i} \right] \quad (2.10)$$

$$\tau_{\alpha\beta}^{-1} = \frac{16}{3} n_\beta \Omega_{\alpha\beta}^{(11)}, \quad A_{\alpha\beta}^{(n)} = G_{\alpha\beta}^{(n)} / G_{\alpha\beta}^{(1)} \quad (2.11)$$

Here,  $\tau_{\alpha\beta}$  has order of magnitude of time of collisions of  $\alpha$ - and  $\beta$ - particles

and  $A_{\alpha\beta}^{(n)}$  depends on mass ratios and temperatures of particles and also on ratios of various types of cross sections for given form of collisions. For electron-neutron collisions, if  $\gamma_e \ll \gamma_n$ ,  $\tau_{\alpha\beta}^{-1}$  actually coincides with effective frequency of collisions of electron normally utilized in kinetics of plasma [5].

$$\tau_{\alpha\beta}^{-1} = \nu_{\alpha\beta} = \frac{4}{3} \left( \frac{2}{\pi} \right)^{1/2} \gamma_e^{1/2} \int_0^{\infty} v(v) v^4 \exp\left(-\frac{\gamma_e v^2}{2}\right) dv$$

$$v(v) = n_a v \int q(v, \chi) (1 - \cos \chi) d\Omega, \quad d\Omega = \sin \chi d\chi d\epsilon \quad (2.12)$$

Here  $\nu$  — frequency of collisions with momentum transfer,  $q(v, \chi)$  — differential cross section of elastic scattering of electron (indices  $e$  and  $a$  relate respectively to electron and neutral).

For collisions of heavy particles in plasma (ions with neutrals and neutrals among themselves) it is possible to connect  $\tau_{\alpha\beta}$  with binary coefficient of diffusion  $[D_{\alpha\beta}]_1$  (first approximation of Chapman - Cowling [1])

$$\gamma_{\alpha\beta} \tau_{\alpha\beta}^{-1} = n_\beta / n [D_{\alpha\beta}]_1 \quad (2.13)$$

In case of Coulomb interactions in expressions for  $\Omega_{\alpha\beta}^{(r)}$  appears, in general, a divergence which can be formally eliminated by cutting of collision parameter at distances of the order of Debye screening length  $\lambda_D$ . Then

$$\tau_{\alpha\beta}^{-1} = \frac{16 \sqrt{\pi}}{3} n_\beta \left( \frac{\gamma_{\alpha\beta}}{2} \right)^{1/2} \left( \frac{e_\alpha e_\beta}{\mu_{\alpha\beta}} \right)^2 \ln \Lambda_{\alpha\beta} \quad \left( \Lambda_{\alpha\beta} = \frac{\mu_{\alpha\beta}}{\gamma_{\alpha\beta}} \frac{3\lambda_D}{|e_\alpha e_\beta|} \right) \quad (2.14)$$

Changing to analysis of system of equations (2.4) - (2.6) we note preliminarily that members depending on electric field  $E$  in (2.9) and (2.10) turn out to be essential only in very strong fields\* (see [4, 6]) and therefore in the future can be omitted. When structure of expressions for tensor of viscosity and heat flow of particles in multi-type plasma during absence of magnetic field differs little from corresponding expressions in the case of multicomponent gas mixture

---

\*By the term "strong electrical field" here is understood a field in which charged particles, during the time between collisions, are accelerated to energies comparable to energy of their thermal random motion.

[3], it specifically is due to presence of Coulomb interactions of particles and the fact that every component of mixture can correspond its own kinetic temperature  $T_i$ . Presence of magnetic field noticeable complicates results. However, even in this case, the system of equations permits solution in the most general form. Here equations of diffusion (2.3) can be used for derivation of a generalized Ohm's law in multi-type plasma, connecting current density of conductance  $j$  with voltages of electric and magnetic fields and also with pressure and temperature gradients.

Solution of equations (2.4) - (2.6) can be somewhat simplified thanks to presence in them of a small parameter - mass ratio of electron  $m_e$  to mass of heavy particles in plasma  $m_\beta$  ( $\beta \neq e$ ).

In particular, if condition  $\gamma_e \ll \gamma_\beta$  is fulfilled on

$$\frac{m_e T_\beta}{m_\beta T_e} \ll 1 \quad (2.15)$$

then in equation of diffusion (2.4) written for electron component of plasma ( $\alpha = e$ ), it is possible to disregard members with heat flow of heavy components  $h_\beta$ . Estimating under those same conditions the order of magnitude of coefficients  $a_{e\beta}$  and  $b_{e\beta}$  in equations (2.5), (2.6), we find

$$a_{e\beta} \sim \frac{n_\beta m_e}{n_e m_\beta} \frac{\gamma_e}{\gamma_{e\beta}} \ll 1, \quad b_{e\beta} \sim \frac{n_e m_e}{n_\beta c_{1\beta}} \frac{\gamma_e}{\gamma_{e\beta}} \ll 1 \quad (\beta \neq e)$$

Thus, tensor of viscosity and heat flow of electrons can be determined independently of equations for other components. In turn, in equations for ions and atoms it is possible by the same considerations to disregard quantities  $\pi_e$  and  $h_e$ . Approximate solutions correspond to fulfillment of conditions

$$\frac{m_e}{m_\beta} T_e \ll T_\beta \ll T_e \quad (\beta \neq e) \quad (2.16)$$

Let us note that expressions obtained here for tensor of viscosity and heat flow of electrons have the same form as in work [7] where the case of three-component plasma with identical temperatures of components was considered.

Distinction is that all quantities depending on temperature must be determined during electron temperature  $T_e$  and summation for  $\beta$  in expressions for  $\tau^{-1}$ ,  $(\tau^*)^{-1}$  and  $\tau$  is extended to all components of multi-type plasma.

Solution of system of equations for tensors of viscosity and heat flow of heavy components in general case can be written in form of determinants; in the particular case of three-component plasma with  $T_i = T_a$  corresponding expressions can be taken from work [7].

Analogous remarks can be made and with respect to derivation of generalized Ohm's law in three-component plasma with temperature of electrons different than temperatures of ions and atoms. During fulfillment of conditions (2.16) relationship (4.10) in work [7] remains correct for it where all quantities, with the exception of  $\tau_{\alpha}$ , are determined at electron temperature  $T_e$ .

Submitted  
9 March 1963

#### Literature

1. S. Chapman and T. Cowling. Mathematical theory of nonuniform gases, II, 1960.
2. H. Grad. On the kinetic theory of rarefied gases, *Comm. Pure and Appl. Math.*, 1949, vol. 2 p. 331. (Russian trans. in coll. "Mechanics," 1952, 4 (14), page 71 and 5 (15), page 61).
3. V. Zhdanov, Yu. Kagan, and A. Sazykin. Influence of viscous transfer of momentum on diffusion in gas mixtures, *Journal of Experm. and Theor. Phys.*, 1962, vol. 42, issue. 3.
4. R. Herdan and B. S. Liley. Dynamic equations and transport relationships for a thermal plasma, *Rev. Mod. Phys.*, 1960, vol. 32, p. 731.
5. V. L. Ginzburg. Propagation of electromagnetic waves in plasma, *Fizmatgiz*, 1960.
6. V. M. Yeleonskiy and V. M. Zhdanov. On hydrodynamic approximation for ionized gas in strong electric field, "Applied Mechanic and Technical Physics" 1963, No. 1.
7. V. M. Zhdanov. Transfer phenomenon in partially ionized gas, "Applied Math. and Mechanics," 1962, vol 26, issue 2.

## ON THEORY OF WEAK DIFFUSION WAVES

G. S. Leonov and V. A. Pogosyan

(Moscow)

In work [1] on the basis of analysis of solution of system hydrodynamic and electrodynamic equations for electron and ionic gases during absence of external magnetic field, it was shown that in cylindrical symmetric discharge two types of traveling waves along axis of discharge pipe can exist; electronic and ionic. It was also shown that electron waves fade quickly, and that ion waves can fade as well as be strengthened. At present it is clear that striae (layers) do not have direct relation to longitudinal electric oscillations of electrons and ions in plasma. Druyvesteyn [2] examined mobile striae as waves of density of charged particles in plasma of positive column depending on processes of appearance and disappearance of particles. Possibility of existence of waves of such type ensures from joint solution of diffusion equations for electrons and positive ions and Poisson equation. To further development [2] is devoted a series of works [3 - 6] in which initial equations were determined and expanded. In these investigations is applied method of small perturbations. Resultant dispersion relationships are suitable for description of only moving or only standing striae. On the basis of experimental data in [7] a conclusion is made about unique nature of striae. To theoretical proof of this conclusion is devoted work [8]. In contrast to [3 - 6, 8] below is considered a more complete system of equations in which thermal diffusion and dependence of parameters of equations on electron temperature is considered.

Obtained dispersion relationship is useful for description both of mobile and motionless striae. It can be extended also to the case of a positive column in a longitudinal magnetic field.

1. General equations. As is known, in a positive column with moving striae the density of electrons  $N_e$ , density of ions  $N_p$ , electron temperature  $T$ , and also longitudinal gradient of potential  $E$  are functions of coordinate  $x$ , taken along

axis of pipe and time  $t$ . Carrier densities change, furthermore, with change of distance of considered point from axis of pipe, as and in case of uniform positive column.

Let us consider a cylindrical positive column. It is assumed that following conditions are satisfied:

- 1) electrons and ions have Maxwellian distribution by velocities at constant by section of column temperatures  $T_e$  and  $T_p$ ;
- 2) recombination occurs only on walls of vessel;
- 3) mean free path of electrons and ions is small as compared with radius of column;
- 4) ionization occurs only during single collision between electron and atom in the basic state, and consequently, rate of ionization does not depend on concentration of electrons.

For laminar positive column with these assumptions we have:

a) Equations of balance of carriers

$$\frac{\partial N_e}{\partial t} + \operatorname{div}(N_e W_e) - ZN_e = 0, \quad \frac{\partial N_p}{\partial t} + \operatorname{div}(N_p W_p) - ZN_p = 0 \quad (1.1)$$

Here  $W_e$  and  $W_p$  are vectors of drift velocities of electrons and ions having constituents  $w_{ez}, w_{er}$  and  $w_{pz}, w_{pr}$  along axis  $z$  and radius  $r$ ; accordingly,  $Z$  - number of ion pairs formed by one electron in one second.

For  $Z$  we write following simplified expression:

$$Z(U_e) = A \sqrt{U_e} \exp\left(-\frac{U_e}{U_0}\right) \quad (1.2)$$

In the future we will be limited to consideration of only central region of positive column, which allows to simplify problem by means of its reduction to a one-dimension problem. In equations of (1.1) it is possible to separate variables. Considering, as usual, that in a laminar positive column, for the same reasons as in quasi-neutral plasma of uniform column, radial motion of carriers is regulated by ambipolar diffusion, we obtain (under Schottky boundary conditions)

$$N_e = n_e(x, t) J_0\left(\frac{2.4r}{R}\right), \quad N_p = n_p(x, t) J_0\left(\frac{2.4r}{R}\right)$$

where  $n_e(x, t)$  and  $n_p(x, t)$  - density of electrons and ions on axis of discharge,  $J_0(\mu r)$  - Bessel function of zero order, 2.4 - first root of equation  $J_0(\mu r) = 0$ . Using these relationships for  $N_e$  and  $N_p$ , taking into account that we now consider points near axis of pipe, we will receive a one-dimensional variant of equations of (1.1) in the form

$$\begin{aligned} \frac{\partial n_e}{\partial t} + \frac{\partial}{\partial x} (n_e w_{ex}) + \frac{n_e}{\tau_D} - Zn_e = 0, \quad \tau_D = \left(\frac{R}{2.4}\right)^2 \frac{1}{D_a}, \quad D_a = b_p U_e \\ \frac{\partial n_p}{\partial t} + \frac{\partial}{\partial x} (n_p w_{px}) + \frac{n_p}{\tau_D} - Zn_e = 0 \end{aligned} \quad (1.3)$$

Here

$$w_{ex} = -be \left[ E + \frac{U_e}{n_e} \frac{\partial n_e}{\partial x} + \left( \delta - \frac{3}{2} \right) \frac{\partial U_e}{\partial x} \right], \quad w_{px} = b_p \left[ E - \frac{U_p}{n_p} \frac{\partial n_p}{\partial x} \right] \quad (1.4)$$

Quantity  $\tau_D$  represents diffusion life of carriers,  $R$  - radius of pipe,  $D_a$  - ambipolar diffusion coefficient,  $b_p$  - mobility of ions,  $b_e$  - mobility of electrons,  $U_e$  - electron temperature, expressed in electron volts,  $k$  - Boltzmann constant,  $e$  - charge of electron. In uniform positive column diffusion in axial direction is completely compensated. In every cross section of such a column the number of ions appearing in volume is balanced by losses of particles on walls due to radial diffusion. Condition of balance of particles in this case [9] will be

$$Z\tau_D = 1 \quad (1.5)$$

In the presence of striae, together with radial diffusion one should consider axial diffusion along the positive column.

b) Poisson equation

$$\partial E / \partial x = 4\pi e (n_p - n_e) \quad (1.6)$$

c) Equation of energy conservation electron gas

$$\frac{\partial}{\partial t} \left( n_e \frac{3}{2} U_e \right) + \frac{\partial}{\partial x} \left( n_e u_{ex} \frac{3}{2} U_e \right) = - n_e u_{ex} E - n_e H(U_e) \quad (1.7)$$

First member on the right in (1.7) gives energy obtained by electrons from electric field per unit volume in unit of time; the second member gives loss of energy by these electrons during collision. Second member on the left expresses flow of energy through considered volume

$$w_{ex} = - \frac{2}{3} \delta b_e \left[ E + \frac{U_e}{n_e} \frac{\partial n_e}{\partial x} + \left( \delta^* - \frac{3}{2} \right) \frac{\partial U_e}{\partial x} \right] \quad (1.8)$$

Through distribution function  $f_0$  quantities  $\delta$  and  $\delta^*$ , entering in (1.3) and (1.8) are expressed respectively [10]

$$\delta = \int_0^{\infty} w^2 \lambda f_0 dw \bigg/ \int_0^{\infty} w^3 \lambda f_0 dw, \quad \delta^* = \int_0^{\infty} w^4 \lambda f_0 dw \bigg/ \int_0^{\infty} w^3 \lambda f_0 dw$$

Values  $\delta$  and  $\delta^*$  for various gases are unequal, which is caused by dependence of cross section for electron-atom collisions on velocity of electrons in actual gases.

Here on the right are given calculated values of  $\delta$  and  $\delta^*$  for He, Ne, and Ar; here dependence of cross section  $\theta$  on velocity was approximated in the form of a step function

$\theta = C \theta_0 \theta^q$	He	Ne	Ar
	$q = -1$	1	?
	$\delta \approx 1/2$	$1/2$	1
	$\delta^* = 1/2$	$1/2$	2

Equations (1.3), (1.6), and (1.7) will be initial for problem. Analogous equations were used for description of mobile striae in works [5,6]. In [5] in equations (1.3) and (1.7) are omitted members containing product  $U_e$  on  $x$ . In [6] in equation (1.3) the member containing product  $U_p$  by  $\partial \ln n_p / \partial x$  is absent and furthermore, only small rates are considered.

2. Equations describing perturbed state. System of initial equations allows

solution corresponding to stationary (uniform) state of positive column. Changes appearing in striae  $n_e$  and  $n_p$ ,  $E$  and  $U_e$  will be presented in following form:

$$\begin{aligned} n_e &= n [1 + v_e(x, t)], & n_p &= n [1 + v_p(x, t)] \\ E &= E_0 [1 + \eta(x, t)], & U_e &= U_{e0} [1 + v(x, t)] \end{aligned} \quad (2.1)$$

where  $n$ ,  $E_0$ ,  $U_{e0}$  characterize positive column in steady state, and  $v_e$ ,  $v_p$ ,  $\eta$ , and  $v$  describe perturbation. Put (2.1) in equations (1.3), (1.6) and (1.7) and limit to case when deviation from steady state is so small that products  $v_e$ ,  $v_p$ ,  $\eta$ ,  $v$  and squares of these quantities can be disregarded; we assume that perturbations are subordinated to spatial-time dependence of form

$$v_e, v_p, \eta, v \sim e^{i(kx - \omega t)} \quad (2.2)$$

In result we obtain

$$-i\omega v_e/b_e - iE_0 k v_e - iE_0 k^2 \eta + U_{e0} k^2 v_e + (\delta - 3/2) - U_{e0} k^2 v - U_{e0} Z' (U_{e0}) v/b_e = 0 \quad (2.3)$$

$$-i\omega v_p/b_p + iE_0 k v_p + iE_0 k \eta + U_p k^2 v_p + \tau^{-1} v_p/b_p - Z' (U_{e0}) U_{e0} v/b_p - Z (U_{e0}) v_e/b_p = 0 \quad (2.4)$$

$$iE_0 k \eta = 4\pi n (v_p - v_e) \quad (2.5)$$

$$\begin{aligned} -3/2 iU_{e0} \omega v_e - 3/2 iU_{e0} \omega v_e - i\delta b_e E_0 U_{e0} k v_e - i\delta b_e U_{e0} E_0 k \eta - \\ - i\delta b_e E_0 U_{e0} k v + \delta b_e U_{e0}^2 v_e k^2 + \delta^2 \delta (\delta - 3/2) U_{e0}^2 k^2 v - \\ - 2b_e E_0^2 \eta - i b_e E_0 U_{e0} k v_e - i b_e (\delta - 3/2) E_0 U_{e0} k v = 0 \end{aligned} \quad (2.6)$$

Here, as and in work [5] was not taken into account change of quantity coupled with change of  $T_e$ . We multiply (2.6) by  $ik/2E_0 b_e$  and reject members which contain  $b_e$  in denominator due to their smallness. Putting (2.5) in (2.3), (2.4), and (2.6), we obtain

$$(-iE_0 k + 4\pi n + U_{e0} k^2) v_e - 4\pi n v_p + \delta_1 U_{e0} k^2 v = 0 \quad (2.7)$$

$$\left(4\pi n + \frac{1}{\tau_D b_p}\right) v_e + \left(\frac{i\omega}{b_p} - iE_0 k - \frac{1}{\tau_D b_p} - U_p k^2 - 4\pi n\right) v_p - \frac{Z' (U_{e0}) U_{e0}}{b_p} v = 0 \quad (2.8)$$

$$\begin{aligned} \left(\frac{\delta U_{e0}}{2} k^2 + 4\pi n + \frac{4i\pi n \delta U_{e0}}{2E_0} k + \frac{i\delta U_{e0}^2 k^2}{2E_0} + \frac{U_{e0} k^2}{2}\right) v_e - \\ - \left(\frac{4i\pi n \delta U_{e0} k}{2E_0} + 4\pi n\right) v_p + \left(\frac{\delta U_{e0} k^2}{2} + \frac{i\delta_0 U_{e0}^2 k^2}{2E_0} + \frac{\delta_1 U_{e0} k^2}{2}\right) v = 0 \end{aligned} \quad (2.9)$$

Here

$$\delta_1 = \delta - \frac{1}{2}, \quad \delta_0 = \delta (\delta^* - \frac{1}{2})$$

Conducted linearization of equations means that only small amplitudes of waves are permissible. For comparison of results of present calculations with experiment it is possible to turn to data of measurements of length and frequency of very weak mobile striae. Experience shows that generally in mobile striae, spread of change of electric potential can attain several volts, and electron temperature and density of carriers can change by more than twice (strong striae). Experimental investigation of discharge in helium showed that influence of sharpness of striae on their length and frequency is weakly manifested. Therefore, it is possible to assume that the given formulas can be applied for appraisal of shown quantities also in the case of sufficiently sharp striae,

3. Dispersion relationship. Equations (2.7), (2.8), and (2.9) represent linear uniform algebraic equations relative to  $v_e$ ,  $v_p$  and  $v$ . From condition of existence of non-trivial solution of these equations and considering also that for striae condition as that shown in [5] is satisfied

$$\frac{1}{4\pi en} \left| \frac{i\omega}{b_p} - iE_0 k - \frac{1}{\tau_D b_p} - U_p k^2 \right| \ll 1$$

after certain simple conversions, we find

$$\begin{aligned} \frac{iU_{e0}^2}{2E_0} \gamma k^4 + \frac{U_{e0}^2 \delta k^3}{2} - i\delta_1 U_{e0} k^2 + \frac{\gamma U_{e0}^2 \omega}{2E_0 \delta_p} k^2 - \\ - \frac{3iU_{e0}^2 \omega}{4\delta_p} k - \frac{U_{e0}^2 z'}{2b_p} k + \frac{iU_{e0} E_0 z'}{b_p} = 0 \end{aligned} \quad (3.1)$$

where  $\gamma = \delta (\delta^* - \delta)$ . Let us assume now  $k = \kappa + i\theta$ , i.e.,

$$v_e, v_p, \eta, v \sim e^{-\theta x} e^{i(\kappa x - \omega t)}$$

If  $\theta > 0$ , then wave is weakened in positive direction (in direction from anode to cathode).

It is easy to see that after substitution,  $k = \kappa + i\theta$  equation of (3.1) breaks up into two equations which can be obtained by means of equating of real

and imaginary parts to zero.

On the assumption that  $|\theta/x| \ll 1$ , disregarding members above first degree, we obtain

$$\left[ \frac{3U_{\infty}^2 \delta x^2}{2} + \frac{\gamma U_{\infty}^2 \omega x}{E_0 b_p} - \frac{U_{\infty}^2 Z'}{2b_p} \right] \theta + \frac{\gamma U_{\infty}^2 x^4}{2E_0} - \delta_1 U_{\infty} E_0 x^2 - \frac{3U_{\infty} \omega x}{4b_p} + \frac{U_{\infty} E_0 Z'}{b_p} = 0 \quad (3.2)$$

$$\left[ -\frac{2\gamma U_{\infty}^2 x^2}{E_0} + 2\delta_1 U_{\infty} x E_0 + \frac{3U_{\infty} \omega}{4b_p} \right] \theta + \frac{U_{\infty}^2 \delta x^2}{2} + \frac{\gamma U_{\infty}^2 \omega}{2E_0 b_p} x^2 + \frac{U_{\infty}^2 Z' (U_{\infty})}{2b_p} x = 0 \quad (3.3)$$

From (3.3) we find

$$x = \left[ \left( \frac{\gamma \omega}{2\delta b_p E_0} \right)^2 + \frac{Z' (U_{\infty})}{b_p \delta} \right]^{1/2} - \frac{\gamma \omega}{2\delta b_p E_0} \quad (3.4)$$

Expanding expression under the square root sign in (3.4) in series, we have

$$x = \frac{Z' (U_{\infty}) E_0}{\gamma \omega} - \frac{1}{8} \left( \frac{2\delta b_p E_0}{\gamma \omega} \right)^{1/2} \left( \frac{Z' (U_{\infty})}{b_p \delta} \right)^2 + \dots \quad (3.5)$$

So that for large  $\omega$

$$x \approx \frac{Z' E_0}{\gamma \omega} = \frac{U_1^* E_0}{\gamma U_{\infty} \tau_D \omega} \quad (3.6)$$

From (1.2) follows relationship

$$\frac{dZ}{dU_{\infty}} = \frac{U_1^*}{U_{\infty}^2} Z(U_{\infty}) = \frac{U_1^*}{U_{\infty}^2} \frac{1}{\tau_D}, \quad U_1^* = U_1 + 0,5 U_{\infty} \quad (3.7)$$

Putting in (3.6) expression (1.3) for  $\tau_D$  and considering (3.7), we finally find

$$x \approx \frac{\lambda^2 b_p U_1^* E_0}{\gamma H^2 U_{\infty}^2 \omega} \quad (3.8)$$

Assuming here  $\gamma = 2\delta$ , are obtain for  $\kappa$  Wojaczek's expression [5].

Action of magnetic fields on plasma decreases ambipolar diffusion in direction perpendicular to it in ratio

$$\frac{1}{(1 + \omega_p \omega_p \tau_c \tau_p)} \quad \left( \omega = \frac{eB}{mc} \right)$$

Here  $\omega$  - gyromagnetic frequency,  $\tau$  - average time of free path of carriers.

Thus, in the presence of magnetic field parallel to axis of positive column quantity  $\tau_D$  differs from its own value in absence of field by factor  $1 + \omega_p \omega_p \tau_c \tau_p$ . Noting this, we finally obtain for  $\kappa$

$$\kappa = \left[ \left( \frac{\gamma_{01}}{2\delta b_p E_0} \right)^2 + \frac{\lambda^2 U_i^*}{\delta U_{e0} R^2 (1 + b_p b_e B^2 / c^2)} \right]^{1/2} - \frac{\gamma \omega}{2\delta b_p E_0} \quad (3.9)$$

Assuming here  $\omega = 0$ , we obtain dispersion relationship for motionless striae

$$\kappa = \frac{\lambda}{R} \left[ \frac{U_i^*}{\delta U_{e0} (1 + b_p b_e B^2 / c^2)} \right]^{1/2} \quad (3.10)$$

Hence when  $B=0$  Chapnik's formula is obtained [4]. For  $\theta$  from (3.2) we have

$$\theta = \frac{-\gamma U_{e0}^2 \kappa^4 / 2E_0 + \delta U_{e0} E_0 \kappa^2 + 3U_{e0}^2 \omega \kappa / (b_p - U_{e0} E_0 / b_p)}{\gamma U_{e0}^2 \delta \kappa^2 + \gamma U_{e0}^2 \omega \kappa / b_p E_0 - U_{e0}^2 E_0 / 2b_p} \quad (3.11)$$

If in (3.11) instead of  $\kappa$  we substitute its expression from (3.4), we receive bond between  $\theta$  and  $\omega$ . General analysis of this bond is difficult. However it is easy to see that in two extreme cases corresponding to sufficiently large and small frequencies,  $\theta$  has negative value.

We will list results of comparison of lengths of striae  $\underline{l} = \underline{l}_2$  calculated by formula (3.9) with experimental data ( $\underline{l} = \underline{l}_1$ ) from [11]. Comparison was made for helium at pressure of 0.9 mm Hg and radius of pipe of 1 cm.

$B =$	0	400	600	1000	1200	(gs)
$(2\pi)^{-1}\omega =$	19800	18600	17100	14200	12900	(cps)
$E =$	4.2	3.8	3.3	3.2	3.0	(v/cm)
$\underline{l}_1 =$	5.8	6.1	6.2	6.9	7.8	(cm)
$\underline{l}_2 =$	2.9	3.2	3.6	4.7	5.6	(cm)

Character of function of length of motionless striae on size of magnetic field obtained by formula (3.10) corresponds to experimental data for  $H_2$ , given in [1].

The authors are grateful to A. A. Zaytsev for attention to the work.

Submitted  
3 June 1963

#### Literature

1. M. V. Konyukov, and Ya. P. Terletskiy. On electroacoustic waves in gas-discharge plasma. Zh. eksperim. and teor. fiz., 1954, vol. 27, No 5 (11), page 542.
2. M. I. Druyvesteyn. Versuch einer theorie der positiven säule mit laufenden Schichten, Physica, 1934. Vol. 1, No 4. S. 273.
3. A. B Stewart. Oscillating glow discharge plasma, J. Appl. Phys., 1956, vol, 27, No 8, p. 911.
4. P. M. Chapnik. On theory of laminar, positive column, Reports of Academy of Sciences of USSR, 1956, vol. 107, No 4, page 529.
5. K. Wojaczek. Vereinfachte Diffusionstheorie der Laufenden Schichten, Ann. phys., 1959, 7 Folge, Band 3, S. 37.
6. H. Rother. Theorie der Diffusionswellen (Laufende Schichten in Niederdruckentladungen, Ann. phys., 1959, 7 Folge, Band 4, S. 373.
7. B. N. Klyarfel'd. Formation of striae in gas discharge. Zh. eksperim. and teor. fiz., 1952 Vol. 22, No 1, page 66.
8. A. V. Nedospasov. The question of striae in inert gases, Zh. tekhn. fiz., 1958, XXVIII, No. 1, page 173
9. V. L. Granovskiy. Electric current in gas. M. - L. 1952, Vol. I.
10. S. Chapman and T. Cowling. Mathematical theory of nonuniform gases, IL, 1960.
11. A. A. Zaytsev, and M. Ya. Vasil'yev. Laminar, positive column of gas discharge in longitudinal magnetic field, Radio engineering and electronics, 1962, Vol. 7, No 3, page 557.

CHANGE OF ELECTRIC POTENTIAL NEAR WALL OF CHANNEL DURING  
MOTION OF IONIZED GAS IN MAGNETIC FIELD

G. A. Lyubimov

(Moscow)

Distribution of electric potential in channel with conducting walls through which gas moves in the presence of magnetic field is usually calculated on the basis of equations of magnetohydrodynamics. However, such calculation is correct only for nucleus of flow and viscous boundary layers.

Near the walls, as was shown in work [2], formation is possible of layers adjacent to electrode of thickness of order of several mean free paths of the electron in which sharp change of potential occurs due to emitting properties of wall. Therefore, a full description of electric processes in channel requires calculation of phenomena in layers adjacent to electrode.

In present work problem of change of potential in layer adjacent to electrodes is considered during more general (as compared with work [2]) assumptions which, apparently, are well suited to flow of dense gases and temperature of electrodes of order 2500°. Formulas are derived allowing to calculate voltampere characteristic of channel and examples of calculations are given.

1. Change of electrical potential in viscous boundary layers. Let an electroconductive liquid move in plane channel in transverse magnetic field (Fig. 1). Here, owing to separation of charges in region of flow, electric field will be formed and walls limiting channel turn out to be under various potential. If walls - conductors (electrodes) are united through external load  $R$ , then, owing to difference of potentials, induced by the motion of liquid electric currents

will flow in external circuit.\*

For simplicity let channel have constant cross section, speed of liquid  $U$  be unchanged along channel, magnetic field be constant ( $H = H_0 e_y, H_0 = \text{const}$ ), and electric conductance ( $\sigma$ ) be constant. In this case, if liquid is ideal ( $U = \text{const}$ ) electric field is constant in channel and is created by surface charges. Difference of potentials induced in flow, is found from Ohm's law and is equal to

$$jR = \Delta\varphi = \varphi_a - \varphi_{-a} = \left(\frac{UH_0}{c} - \frac{j}{\sigma}\right) 2a$$

$$\varphi = \left(\frac{UH_0}{c} - \frac{j}{\sigma}\right) z, \quad \frac{UH_0}{c} > \frac{j}{\sigma} \quad (1.1)$$

Here  $\mathcal{E} = 2aUH_0/c$  plays role of emf, and  $2a/\sigma$  — internal resistance of equivalent generator.

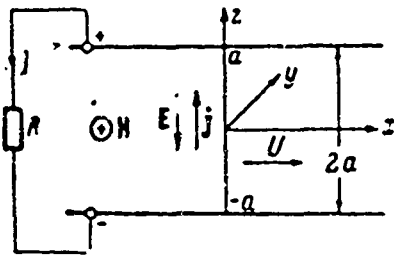


Fig. 1.

If liquid flowing in channel is viscous, then on walls of channel (electrodes) a viscous boundary layer will be formed. In the examined flow,

viscous boundary layer is a charged layer [1]. When  $R_m \ll 1$  density of charge in boundary layer is determined by relationship

$$4\pi\rho_s = -c^{-1}H \text{rot } v \quad (1.2)$$

Furthermore, if wall is cold, conductance of liquid in boundary layer can be lower than conductance in nucleus of flow, and in general,  $\sigma = \sigma(z)$ . Presence of spatial charge and changeability of conductance in boundary layer indicate that electric field changes inside boundary layer. General equations describing change of potential inside boundary layer in the considered formulation when  $\sigma = \sigma(z)$  and  $u = u(z)$ , were obtained by A. B. Vatazhin.

In order to graphically present a picture of change of potential in boundary layer and dependence of change of potential across the boundary layer on parameters

\*In the future  $R$  is understood as external resistance calculated at  $1 \text{ cm}^2$  of surface of electrode. If  $R^0$  — total external resistance, then  $R = SR^0$ , where  $S$  — area of electrode.

of the problem, let us consider a model problem. We consider that flow in channel consists of nucleus moving with constant speed, boundary layers of thickness  $\delta$  (Fig. 2), and linear distribution of speeds on  $z$  (Couette flow). It is known that Couette flow in many respects simulates well the boundary layer. Therefore the simple relationships obtained in such a schematization of the problem can be used for approximate appraisal of change of potential and other quantities in boundary layer.

From relationship (1.2) it follows that the viscous boundary layer near positive electrode is positively charged, and at negative electrode - negatively. For determination of potential inside boundary layer it is necessary to solve equation

$$\frac{d^2\varphi}{dz^2} = 4\pi\rho_e = \frac{H_0}{c} \frac{\partial u}{\partial z} = \frac{H_0 U}{c\delta} \quad (1.3)$$

As boundary conditions during solution of this equation it is necessary to

assign current density on wall and value of potential on external edge of boundary layer (at  $z = \mp a \pm \delta$ ), which is determined from solution of (1.1) for nucleus of flow. If  $\sigma = \text{const}$ , solution of (1.3) has form

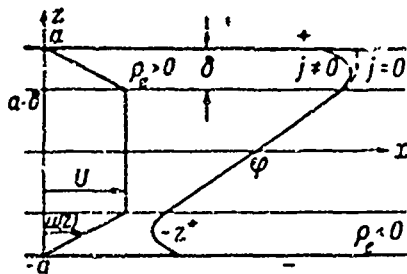


Fig. 2.

$$\begin{aligned} \varphi &= \varphi_{-a} + \left[ \frac{H_0 U}{c} \frac{z+a}{2\delta} - \frac{j}{\sigma} \right] (z+a) & \text{when} & \quad -a < z < -(a-\delta) \\ \varphi &= \varphi_a - \left[ \frac{H_0 U}{c} \frac{a-z}{2\delta} - \frac{j}{\sigma} \right] (a-z) & \text{when} & \quad a-\delta < z < a \end{aligned} \quad (1.4)$$

Qualitative picture of distribution of potential in channel is presented in Fig. 2.

From (1.1) and (1.4), equating difference of potentials ( $\varphi_a - \varphi_{-a}$ ) induced in flow to change of potential on external load  $iR$  following formulas can be obtained:

$$j = \frac{u^* H_0}{c} \frac{2a}{R+r}, \quad 2\varphi_a = \frac{u^* H_0}{c} 2a \frac{R}{R+r}, \quad r = \frac{2a}{\sigma}, \quad u^* = \frac{1}{2a} \int_{-a}^a u dz \quad (1.5)$$

As will be clear further, relationships of (1.5) are true, in general, small currents. At large currents first relationship of (1.5) must be replaced by relationship (6.4). Formulas (1.4) and (1.7) expressing change of potential in boundary layer depend on current density. Therefore they can be used at any currents, if current density is found from (6.4). It is natural that main characteristics of (1.5) depending only on flow rate decrease in the presence of boundary layer. Change of potential across boundary layer

$$\varphi_a - \varphi_{a-\delta} = \frac{H_0}{c} \left( u^{**} - u^* \frac{r}{R+r} \right) \delta, \quad u^{**} = \frac{i}{\delta} \int_{a-\delta}^a u dz = \frac{U}{2} \quad (1.6)$$

Relationship (1.6) shows that if conductance of gas inside boundary layer is high (such as in nucleus of flow), then change of potential across boundary layer has order of  $\delta$ , where at large  $R$  (small currents) potential in boundary layer increases in reference to nucleus, but small  $R$  (large currents) it diminishes ( $u^{**} < u^*$ ). Here if  $\delta/2a \sim 100$ , change of potential in boundary layer is of order of 1% in reference to emf. of nucleus.

Solution of (1.4) shows that inside boundary layer is point ( $z = \pm z^*$ ), in which electric field equals zero ( $\sigma\varphi/\partial z = 0$ ). At  $|z| > z^*$  we have  $E_z > 0$ ; at  $|z| < z^*$  takes place reverse inequality  $E_z < 0$ . This is intelligible, since near walls where speeds are small electric current must be directed with electric field ( $j \sim \sigma E$ ), and far from walls where  $|E| < UH/c$ , current is directed against electric field (this is possible since emf acts in the space).

If conductance of gas changes across boundary layer (for example, cooled wall and  $\sigma = \sigma(T)$ ), formulas giving solution of (1.3) can be written in the form ( $\sigma_0$  - conductance of nucleus of flow)

$$\begin{aligned} \varphi &= \varphi_a - \left[ \frac{H_0 U}{c} \frac{(a-z)}{2\delta} - j \frac{1}{c-z} \int_a^z \frac{dz}{\sigma(z)} \right] (a-z) \quad \text{when } a-\delta < z < a \\ \varphi &= \varphi_{-a} + \left[ \frac{H_0 U}{c} \frac{z+a}{2\delta} - j \frac{1}{a+z} \int_{-a}^z \frac{dz}{\sigma(z)} \right] (z+a) \quad \text{when } -a < z < -(a-\delta) \\ j &= \sigma_0 \left[ -\frac{\varphi_a}{a} + \frac{u^* H_0}{c} \right], \quad j = \frac{u^* H_0}{c} 2a \frac{i}{r^2 + R^2}, \quad \varphi_a = \frac{u^* H_0 a}{c} \frac{R}{R+r} \end{aligned}$$

$$\varphi_a - \varphi_{a-b} = \frac{H_0}{c} \left( u^{**} - u^* \frac{2a}{\delta} \frac{r^2}{R_1 r^2} \right) \delta, \quad r^0 = \int_a^{a-b} \frac{dz}{\sigma(z)}$$

$$\sigma^0 = \frac{a}{r^0 + (a-b)\beta_0}, \quad r^* = \frac{2a}{\sigma^0} \quad (1.7)$$

Relationships of (1.7) show that if resistance of cold boundary layers ( $r^0$ ) becomes comparable with resistance of nucleus, then potential drop in boundary layer can be very large (almost all emf is extinguished in these layers). On the other hand, increase of resistance of boundary layers can be considered as increase of effective external resistance if one were to calculate emf and difference of potentials by parameters of nucleus of flow.

2. Presence of change of potential in layer adjacent to electrode. Distribution of potential in channel described by relationships of (1.7) or by those analogous to them in case of more general formulation of problem takes place in region where usual relationship for current density

$$\mathbf{j} = \sigma (\mathbf{E} + c^{-1} \mathbf{v} \times \mathbf{H}) \quad (2.1)$$

As was shown in [2], this relationship can be used at distances of the order of several mean paths of electrons from boundary wall through which current is fed (or withdrawn). Therefore, near surface of electrode formation of narrow layers is possible in which potential sharply changes. The average speed of liquid in these layers is equal to zero. These narrow regions of variation of potential will be called layers adjacent to electrodes.

Formation of layers adjacent to electrodes is due to emitting properties of wall [2]. Indication of existence of such layers, and also certain considerations about dependence of potential drop in them on physical processes at the gas - solid interface, are contained in works [3, 4]. Possible connection between change of potential in layer adjacent to electrode with emitting properties of electrode and corresponding changes of boundary conditions for internal problem is indicated in [2].

In work [2] in expression of change of potential in layer adjacent to electrode through emitting properties of electrode and other parameters of problem, a series of assumptions is made. In present work this problem is considered under less rigid assumptions.

3. Forms of electron emission. We will assume everywhere in the future that parameters of the problem (pressure, temperature, degree of ionization, and others) are such that current density is determined only by electron component (ions do not have average speed across flow). Under these conditions current density flowing through liquid (gas) is determined to a significant degree by quantity of electrons emitted from surface of electrode. In considered problem (Fig. 1) electrons enter gas from positive electrode and depart from gas through negative electrode.

Current density of electrons emitted from surface in absence of external electric field depends on temperature of surface and work function of material of electrode [5]

$$j_e = AT^2 \exp\left\{-\frac{e\Phi}{kT}\right\} = AT^2 \exp\left\{-\frac{116000\Phi}{T}\right\} \quad (3.1)$$

Here T - temperature of surface of emitter, e - charge of electron, k - Boltzmann constant,  $\Phi$  - work function in volts, and A - constant, which for metals without calculation of thermal expansion is equal to 120 a/cm<sup>2</sup>.degree<sup>2</sup>. Generally this experimental constant, depending on material of emitter (value of A for various materials, can be found, for example, in table given in [5].

Presence of electric field accelerating electrons at surface of emitter leads to decrease of effective work function (Schottky effect). Current density of emission is determined with this relationship

$$j_e = AT^2 \exp\left\{-\frac{e\Phi}{kT} + \frac{e^2 E^{3/2}}{kT}\right\} = AT^2 \exp\left\{-\frac{116000\Phi}{T} + \frac{4.39}{T} \sqrt{E}\right\} \quad (3.2)$$

If near surface of emitter there is electric field braking electrons and potential of electric field is minimum near surface of emitter, then part of

electrons emitted by surface will be reflected from potential barrier to outside of emitter. Current density of electrons passing potential barrier will be determined by relationship [5]

$$j_s = j_0 \exp \left\{ -\frac{eW}{kT} \right\} = j_0 \exp \left\{ -\frac{11600W}{T} \right\}, \quad W > 0, \quad (3.3)$$

Here  $W$  - height of potential barrier outside surface of emitter in volts.

We will consider that space charge inside layer adjacent to electrode is absent. Then electric field inside this layer is constant, and distribution of potential on gas - electrode interface has form shown in Fig. 3. Here, electric field in (3.2) is determined as

$$E = \frac{\varphi_{\pm}}{d} \quad (3.4)$$

where  $d$  - thickness of layer, adjacent to electrodes  $\varphi_{\pm}$  - change of potential in layer adjacent to electrode.

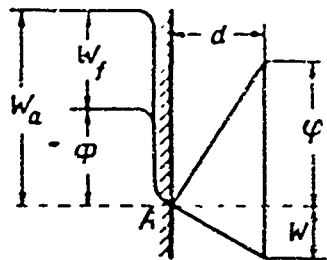


Fig. 3.

For thickness of layer adjacent to electrodes ( $d$ ) we will take Debye length in the future

$$d = \left( \frac{kT}{4\pi e^2 n} \right)^{1/2} \quad (3.5)$$

Assumptions (3.4) - (3.5) need,

in general, justification and more

precise definition. But it is possible to think that  $E$  determined by (3.4)

characterizes in a certain sense average electric field inside the layer.

Thickness of layer adjacent to electrodes coincides with Debye length (3.5)

during absence of current. Question of thickness of layer adjacent to electrode

in the presence of current is unanswered. Perhaps this thickness will be less

than Debye length. Certain considerations on this account are contained in [6].

Potential inside layer adjacent to electrodes will be measured from potential of surface of wall (point A on Fig. 3). Here,  $\varphi_{\pm}$  and  $W$  will give change of potential in layer adjacent to electrodes.

4. Gas - wall contact potentials during absence of current. Let ionized gas border on surface of a solid. If temperature of solid  $T \neq 0$  and solid is a conductor, then from surface of solid electrons are emitted according to law (3.1). On the other hand, if gas and solid are in state of thermodynamic equilibrium, then temperature of gas near solid is equal to temperature of solid, temperatures of components (electrons, ions, neutrals) coincide, and distribution of particles of gas, according to velocities inside components, is Maxwellian.

Here the number of charged particles ( $N_e, N_i$ ) coming to wall from gas is accordingly equal to

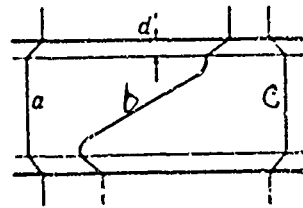


Fig. 4.

$$j_e = N_e e = n_e e \sqrt{\frac{kT}{2\pi m_e}}$$

$$j_i = N_i e = n_i e \sqrt{\frac{kT}{2\pi m_i}} \quad (4.1)$$

Here  $n_e, n_i$  - number of electrons and ions per unit of volume near solid. In the future we will disregard  $j_i$ , since  $m_i \gg m_e$  and  $n_e \sim n_i$ .

In general  $j \neq j_e$ . Here, since total current on gas - solid interface is equal to zero, near surface of solid layer of thickness  $d$ , will be formed inside which potential changes from value on solid to value in gas. Here, if  $j_e > j_i$ , distribution of potential is such that it brakes emitted electrons. Distribution of potential in channel represented in Fig. 1 in this case has form depicted in Fig. 4a at velocity of gas equal to zero, and form depicted in Fig. 4b at  $U \neq 0$ . Change of potential in layer adjacent to electrodes in this case ( $W_0$ ), as follows from (3.1), (3.3), and (4.1) is found from equation

$$AT^2 \exp \left\{ -\frac{11600}{T} (\Phi + W_0) \right\} = n_e e \sqrt{\frac{kT}{2\pi m_e}} \quad (4.2)$$

At  $j_e < j_i$  electrons coming to wall from gas are braked (distribution of potential in this case is represented in Fig. 4c). From (3.2) and (4.1) it

follows that

$$AT^2 \exp \left\{ -\frac{11600}{T} \Phi + \frac{4.79}{T} \sqrt{\frac{\Phi_0}{z}} \right\} = n_e e \sqrt{\frac{kT}{2\pi m_e}} \exp \left\{ -\frac{11600}{T} \Phi_0 \right\} \quad (4.3)$$

An analogous approach to calculation of difference of electrode - gas potentials is contained in [7].

Boundary between (4.2) and (4.3) is determined from equation

$$j_s = AT^2 \exp \left\{ -\frac{11600}{T} \Phi \right\} = n_e e \sqrt{\frac{kT}{2\pi m_e}} \quad (4.4)$$

In subsequent calculations, as working gas argon with addition of 0.1% potassium is examined. Density of electrons is calculated by the Saha formula at a temperature equal to temperature of wall. For this working mixture one can determine from (4.4) dependence of boundary value of pressure ( $p^*$ ) on temperature and material of wall (ionization potential of potassium  $U_1 = 4.34$  v).

When  $p < p^*$  case (4.2) applies; when  $p > p^*$  - case (4.3).

In order to obtain a presentation of orders of magnitudes, we list values of pressure  $p^*$ , mm. Hg column as functions of T for tungsten ( $A = 120$  a/cm<sup>2</sup>. degree<sup>2</sup>,  $\Phi = 4.52$  v) and graphite [8] ( $A = 5.93$  a/cm<sup>2</sup>. deg.<sup>2</sup>,  $\Phi = 3.93$  v).

T = 3000	2900	2800	2700	2600	2500	
$p^* = 1.52$	0.88	0.48	0.25	0.19	0.09	tungsten
$p^* = 6.64$	3.26	1.52	0.68	0.28	0.11	graphite

For the same materials, values of contact potentials of difference of gas - solid ( $\Phi_0$ ), calculated for working mixture + 0.1 % K) at pressure 0.1 mm are:

T = 3000	2900	2800	2700	2600	2500	
$\Phi_0 = 0.25$	0.33	0.41	0.49	0.57	0.65	tungsten
$\Phi_0 = 0.43$	0.48	0.54	0.60	0.65	0.72	graphite

Let us note that  $\Phi_0$  (or  $W_0$ ) represents potential of gas in reference to surface of solid. In order to find difference of potentials between gas and the mass of solid, it is necessary to  $\Phi_0 (W_0)$  to add height of potential barrier of

solid  $W_0 = \Phi + W$ , ( $W$  - the greatest value of energy of electrons in metal at absolute zero).

5. Change of potential in layers adjacent to electrodes in the presence of current. Let external resistance  $R$  be other than infinity. Then during motion of gas in channel in external circuit and in gas electric currents will flow. If through  $c_0$  is designated average velocity of electrons across channel, then

$$c_0 = \frac{j}{ne}, \quad n \equiv n_0 \quad (5.1)$$

It is clear that in situation depicted in Fig. 1 flow of electrons from gas to positive electrode will decrease, and to negative - will increase.

Difference of flows of electrons from surface of solid and from gas should equal current density  $j$  flowing in system. Thus, relationships\*

$$j_{s+} - j_{n+} = j, \quad j_{n-} - j_{s-} = j \quad (5.2)$$

Here  $j_{s+}$ ,  $j_{s-}$  - current density from positive and negative electrodes respectively, and

$$\begin{aligned} j_{s\pm} &= j_s(T_{\pm}) \exp\left\{\frac{11600}{T_{\pm}} \varphi_{\pm}\right\} & \text{when } \varphi_{\pm} < 0 \\ j_{s\pm} &= j_s(T_{\pm}) \exp\left\{\frac{4.39}{T} \sqrt{\frac{\varphi_{\pm}}{d}}\right\} & \text{when } \varphi_{\pm} > 0 \end{aligned} \quad (5.3)$$

where  $T_+$ ,  $T_-$  - temperature of positive and negative electrodes, and  $\varphi_+$ ,  $\varphi_-$  - change of potential in layers adjacent to electrodes in the presence of current. Change of potential in layers adjacent to electrodes ( $\varphi_+$ ,  $\varphi_-$ ) is considered negative if potential in layer diminishes in reference to potential of surface of wall, otherwise  $\varphi_+$ ,  $\varphi_-$  are positive.

If electrons have average velocity in direction from positive electrode to negative and have Maxwellian distribution according to velocities, then

---

\*Note that if flow of ions to wall is not disregarded, relationships of (5.2) take form  $j_{s+} - j_{n+} + j_i = j$ ,  $j_{n-} - j_{s-} - j_i = j$ , where  $j_i$  is determined by (4.1). It is evident that influence of ion current exists only at small current densities  $i \leq i_c$ .

number of electrons passing from gas to electrodes, if change of potential in

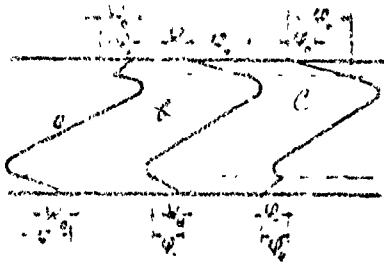


Fig. 5a.

both layers adjacent to electrodes is negative (electrons proceeding from gas do not encounter potential barrier; distribution of potential is qualitative as in Fig. 5a), is

$$n_{\pm}^* = \frac{n}{r_0 \sqrt{\pi}} \int_{\pm c_0}^{\infty} (u \mp c_0) \exp \left\{ -\frac{u^2}{r_0^2} \right\} du$$

$$v_0^2 = \frac{2kT}{m} \quad (m \equiv m_e) \quad (5.4)$$

Such a situation takes place at small currents when potential of gas in respect to solid at  $j = 0$  is negative (4.2). If in the same case large currents flow, then in layer adjacent to electrodes on positive electrode the change of potential becomes positive (Fig. 5b). Here electrons passing to positive electrode from gas encounter potential barrier  $\varphi_+$ . Electrons passing to negative electrode do not encounter barrier. Consequently,

$$n_{\pm}^{**} = \frac{n}{r_0 \sqrt{\pi}} \int_{\zeta}^{\infty} (u - c_0) \exp \left\{ -\frac{u^2}{v_0^2} \right\} du, \quad \zeta = c_0 + \sqrt{\frac{2e\varphi_+}{m}}, \quad \varphi_+ > 0$$

$$n_{-}^* = \frac{n}{r_0 \sqrt{\pi}} \int_{-\infty}^{\infty} (u + c_0) \exp \left\{ -\frac{u^2}{r_0^2} \right\} du, \quad \varphi_- < 0 \quad (5.5)$$

If during absence of current potential of gas relative to electrode is positive, then at  $j \neq 0$  distribution of potential has form as in Fig. 5c, and number of electrons passing from gas to electrodes is

$$n_{\pm}^{**} = \frac{n}{r_0 \sqrt{\pi}} \int_{\zeta}^{\infty} (u \pm c_0) \exp \left\{ -\frac{u^2}{r_0^2} \right\} du, \quad \zeta = \sqrt{\frac{2e\varphi_{\pm}}{m}} \pm c_0 \quad (5.6)$$

Using relationship (5.1) and (5.4) - (5.6), it is easy to obtain expression for  $j_{\pm}$  appearing in equations of (5.2)

$$j_{\pm}^* = j_c \exp \left\{ -\frac{j^2 m}{e^2 n^2 2kT} \right\} \mp \frac{j}{2} \left[ 1 \mp \psi \left( \frac{j}{en} \sqrt{\frac{m}{kT}} \right) \right]$$

$$j_{\pm}^{**} = j_c \exp \left\{ -\frac{m}{2kT} \left( \frac{j}{en} \pm \sqrt{\frac{2e\varphi_{\pm}}{m}} \right)^2 \right\} \pm \quad (5.7)$$

$$\mp \frac{j}{2} \left\{ 1 \mp \psi \left[ \frac{j}{en} \pm \sqrt{\frac{e\varphi_{\pm}}{ms}} \right] \sqrt{\frac{m}{kT}} \right\}, \quad \psi(x) = \sqrt{\frac{2}{\pi}} \int_0^x \exp\left(-\frac{t^2}{2}\right) dt \quad (5.8)$$

In these relationships  $j_0$  is determined by (4.1).

Relationships (5.2) after substitution in them of (5.3) and (5.7) - (5.9) can serve as expression of change of potential in layers adjacent to electrodes  $\varphi_+$ ,  $\varphi_-$  through current density  $j$ .

If  $(j/en)^2 \ll 2e\varphi_{\pm}/m$ , then in (5.8) it is possible to reject corresponding members in arguments of the functions.

Dependence of  $\varphi_+$  and  $\varphi_-$  on  $j$  for various temperatures, if electrodes are graphite [8], is represented in Figs. 6 and 7. (Working mixture is Ar. 0.1% K,  $p = 0.1$  atm.) For graphite electrodes at temperatures below  $3000^\circ$  in absence of current case (4.3) occurs.

In Fig. 6 curves for which  $\varphi < \varphi_0$  give change of potential in layer adjacent to electrodes on negative electrode, and curves for which  $\varphi > \varphi_0$  - on positive electrode (in Fig. 6 are depicted only initial sections of these curves). In Fig. 7 are presented curves of  $\varphi_+ = \varphi_+(j)$  for large  $j$ .

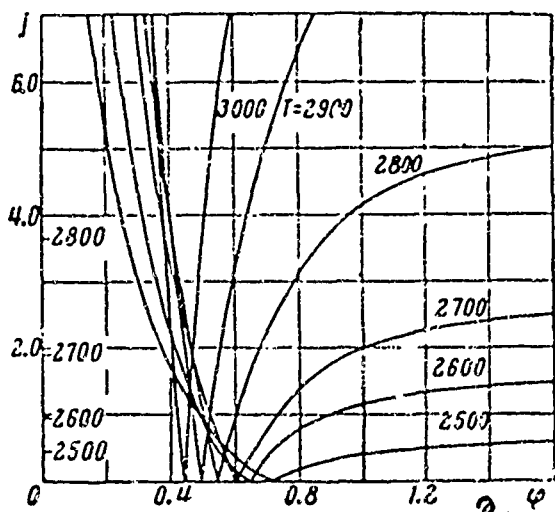


Fig. 6.

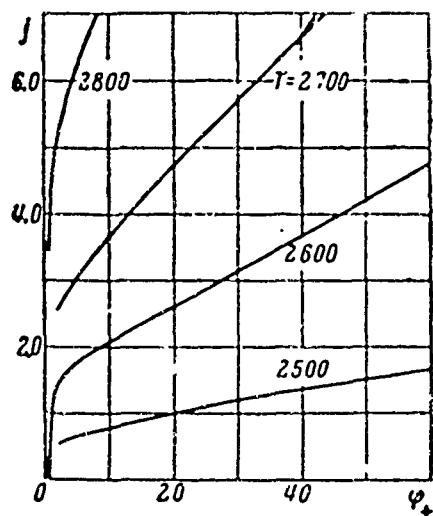


Fig. 7.

Figs. 6, 7 show that change of potential in layer adjacent to electrodes on negative electrode ( $\varphi_-$ ) weakly depends on amount of current  $j$ . Furthermore,

since this change has order of tenths of one volt, then it, in a number of cases, can be disregarded during determination of difference of potentials between electrodes. Change of potential in layer adjacent to electrodes on positive electrode ( $\varphi_+$ ) changes relatively little to currents  $i \sim i_0$ , where  $\varphi_+ \sim \varphi_0$  at  $i \leq i_0$ . At  $i > i_0$ , change of potential  $\varphi_+$  grows quickly with increase of current and this build-up is faster the lower the temperature of electrode. This is coupled with the fact that increase of current at  $i > i_0$  is related to Schottky effect and requires presence of large electric field near electrode.

In Fig. 6 on axis of ordinates points are not marked corresponding to emission current  $i_0 = 13.41 \text{ a/cm}^2$  for  $T = 3000^\circ$  and  $i_0 = 7.6 \text{ a/cm}^2$  for  $T = 2900^\circ$ .

6. Volt-ampere characteristic of channel. In formulas (1.1), (1.5), and (1.7), during expression of current ( $j$ ) through external resistance and emf, change of potential was not considered in layers adjacent to electrodes. Here volt-ampere characteristic of channel had form

$$(R + r)j = \mathcal{E} \quad (6.1)$$

Proceeding thus, they are deflected away from emitting layer of electrode. It is assumed that "necessary" current density determined by (6.1) is ensured by emission of electrode. In order to write expression for volt-ampere characteristic taking into account emitting layers of electrode, it is necessary to set up laws of emission of electrode and to determine change of potential in layers adjacent to electrode [2].

Distribution of potential in channel under the conditions with which (4.3) takes place in absence of current is presented in Fig. 8. (These conditions correspond to calculations of section 5 for graphite electrodes [8] and working mixture of Ar + 0.1% K at  $p = 0.1 \text{ atm}$ ).

Difference of potentials on external load, on the one hand, is equal to

$$\varphi_A - \varphi_B = jR \quad (6.2)$$

On the other to

$$\varphi_A - \varphi_B = \mathcal{E} - rj - \varphi_+ + \varphi_- + \Phi_+ - \Phi_- \quad (6.3)$$

From (6.2) and (6.3) we obtain volt-ampere characteristic of channel

$$(R + r)j = \mathcal{E} - \varphi_+(j, T_+) + \varphi_-(j, T_-) + \Phi_+ - \Phi_- \quad (6.4)$$

This relationship shows that calculation of emitting properties of electrodes

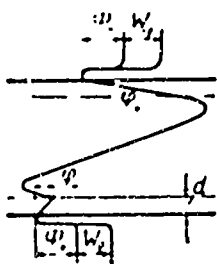


Fig. 8.

indicates that volt-ampere characteristic becomes nonlinear.

Relationship (6.4) shows that from the standpoint of obtaining large currents at the same emf  $\mathcal{E}$ , it is advantageous for the positive electrode

to have a larger work function than negative ( $\Phi_+ > \Phi_-$ ). Let us note that this conclusion refers to the case when  $\varphi_- > 0$ . At small work function of negative electrode  $\varphi_-$  can be less than zero for all  $j$  or at  $j$  larger than a certain value. Under these conditions it is more profitable to have negative electrode with low work function. Furthermore, since (see Figs. 6, 7)

$$\varphi_+(j, T_1) < \varphi_+(j, T_2), \quad \varphi_-(j, T_1) > \varphi_-(j, T_2) \quad \text{when} \quad T_1 > T_2$$

it is profitable to heat positive electrode, and to cool negative. But since work functions of various materials differ by amounts of order of several volts and change of potential  $\varphi_-$  has order of tenths of one volt in a wide range of temperatures changes then in a number of cases (when  $E$  larger or of the order of tens of volts) during calculations it is possible to consider  $\Phi_+ = \Phi_-$  and  $T_+ = T_-$ . Here

$$(R + r)j = \mathcal{E} - \varphi_+(j, T) + \varphi_-(j, T) \quad (6.5)$$

Here  $T$  - temperature of positive electrode. Relationship (6.5) will be accurate if  $T_+ = T_- = T$  and material of electrodes is identical. These conditions in the future will be assumed fulfilled.

In Figs. 9 and 10 are presented volt-ampere characteristics of channel

calculated by (6.5). During calculation it was assumed that velocity profile in channel has form

$$u/u_0 = [1 - |y|/a]^2$$

where  $u_0 = 1$  km/sec - velocity on axis of channel; profile of temperatures resembles velocity profile; working mixture is Ar + 0.1 % K, temperature on axis of channel  $T_0 = 3000^\circ$ ; electrode materials is graphite [8] ( $A = 5.93$  a/cm<sup>2</sup> · deg<sup>2</sup> ·  $\Phi = 3.93$  v); external resistance  $R = 0$ . Fig. 9 corresponds to channel of width  $2a = 40$  cm, Fig. 10 - channel  $2a = 400$  cm.

Fig. 9 shows that during calculation of influence of electric field of layer adjacent to electrodes on emission of electrons from electrodes, section of saturation current [2] is absent in volt-ampere characteristic. Volt-ampere characteristic has nearly rectilinear section (6.1) at currents  $i \sim i_s$ . At larger currents, volt-ampere characteristic is nearly straight, but angle of inclination is less than on initial section. This attests to fact that presence of layers adjacent to electrodes can be considered as increase of equivalent internal resistance of channel ( $r^* = \eta/j$ ). Thus,  $r^*$  is almost constant for small and large currents, with the exception of a narrow (by currents) transitional section of volt-ampere characteristic.

Since increase of resistance owing to layers adjacent to electrodes, roughly speaking, depends only on magnitude of current  $j$ , its contribution to  $r^*$  is less, the greater the internal resistance of the channel. This situation is illustrated in Fig. 10 (internal resistance of channel corresponding to this figure is ten times greater than channel corresponding to (Fig. 9)). Fig. 10 shows that volt-ampere characteristics for channel is 400 cm closer to rectilinear characteristics of (6.1) than to characteristic of channel  $2a = 40$  cm. (Volt-ampere characteristics of (6.1), for various temperatures, are tangential to corresponding curves in Figs. 9, 10 at origin of coordinates).

In Fig. 11 is shown dependence of volt-ampere characteristic on amount of

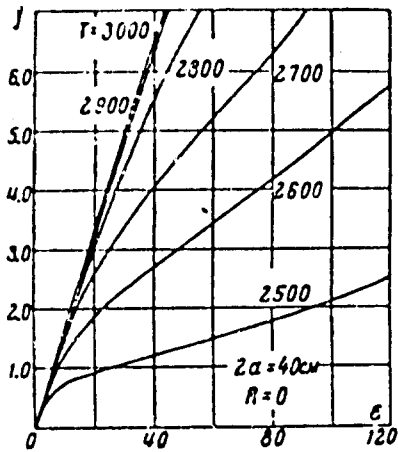


Fig. 9.

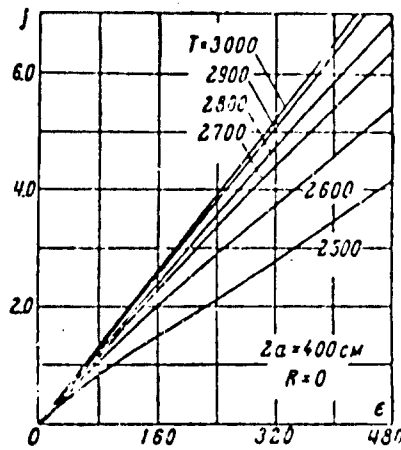


Fig. 10.

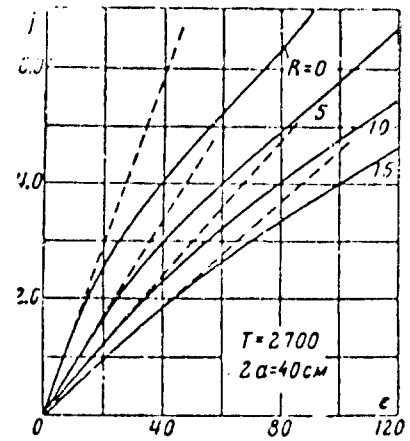


Fig. 11.

load ( $R$ , ohm) for  $T = 2700^\circ$ . Under these conditions,  $r = 6.923$  ohm. In this figure are given characteristics of (6.1) by dotted line. With growth of external resistance volt-ampere characteristic approaches rectilinear of (6.1).

7. Discussion of results. Motion of ionized gas in channel in transverse magnetic field is accompanied by appearance of electric field. Here walls of channel are under various electric potentials. If walls of channel (Fig. 1) are connected through external load, currents can flow in gas and in external circuit.

Flow of current in channel is due to the fact that electrons enter the gas space through one of walls (positive electrode) and leave the gas through the other wall (negative electrode), ensuring thereby, continuity of flow lines. It is natural therefore, that amount of current flowing in system and difference of potentials on external load depend not only on hydrodynamic and electric parameters of flow and external circuit, but also on mechanism of electrons transfer at the interface of gas and electrodes.

Quantity of electrons entering gas from surface of electrode depends on emitting properties of material of electrode, which one can determine by two constants  $\phi$  and  $A$ , from temperature of electrode, and from amount of electric field near surface of electrode). Electric field near surface of electrode is

determined by structure (distribution of charge, thickness etc.) of layer adjacent to electrodes.

Difference of potentials on external load is determined by change of potential in various regions of flow and is given by relationship (6.3). Amount of current flowing in system is given by (6.4).

Relationship (6.4) shows that for solution of problem it is necessary to know relationship between changes of potential in layers adjacent to electrodes ( $\varphi_+$ ,  $\varphi_-$ ) and other quantities determining the problem. It is clear that this relationship essentially must depend on emitting properties of electrode. Character of dependence of  $\varphi_+$  and  $\varphi_-$  on parameters determining problem (material of electrode, its temperature and pressure in gas flow, speed etc.) can be fixed either experimentally or theoretically.

In work [2] and in present work is shown how to establish similar relationship on basis of certain systems of assumptions regarding properties of the surface of electrode and flow of gas. Comparing results of these works, we see that final result depends essentially on character of assumptions made. It is necessary to say that assumptions made here are very close to conditions taking place during flow of gas in channels and apparently, are well observed during flow of dense gases and rather high temperatures of electrodes ( $T \geq 2500^\circ$ ). Absence of experimental data on gas flows under such conditions does not allow to compare results of theory with experiment.

Calculations show that at temperatures below  $2500^\circ$  and current densities of order of several amperes, potential drop in layers adjacent to electrodes becomes order of tens of volts. Electric fields active here in the layer adjacent to electrodes attain values of  $10^5 - 10^6$  v/cm. With such fields, assumptions made here will apparently not hold true.

At fields of order  $10^6$  v/cm considerable field emission is possible [9]. Although, theoretically, field emission occurs during fields of order  $10^7$  v/cm,

but experimental data show [5] that considerable field emission, especially with poor electrode surfaces, is possible during fields as small as  $10^6$  v/cm. Furthermore, during large accelerating fields, electrons in layer adjacent to electrodes are accelerated to energies higher than gas ionization potential and, consequently, can ionize gas by means of collision. Here, density of charged particles near electrode can differ considerably from density given by Saha formula and accepted in present work. Finally, ions accelerated in large electrical fields colliding with the surface of the electrode can knock out additional electrons and thereby increase density of emitting current [3]. Density of ionic current here can be small.

Given considerations indicate that at low temperatures of electrodes a more detailed examination of processes occurring in layers adjacent to electrodes is needed. At the same time, since theoretical description of above-mentioned processes cannot be done in an exhausting manner, during the study of these processes it is necessary, apparently, to use experimental data.

Submitted  
8 June 1963

#### Literature

1. G. A. Lyubimov. On formulation of problem of magnetohydrodynamic boundary layer, PMM, 1962, XXVI, issue 5.
2. G. A. Lyubimov. On boundary conditions on surface of interface of ionized gas - solid, PMTF, 1963, 4.
3. H. A. Pain and P. R. Smy. Experiments on power generation from a moving plasma, J. fluid mech., 1961, vol. 10, No 1 (Coll. trans. "Mechanics", IL, 1963, No 3).
4. D. W. George and H. K. Messerle. Electrode conduction processes in air plasma, J. fluid. mech., 1962, vol. 13, No 3 (Coll. trans. "Mechanics," IL, 1963, No 2).
5. V. I. Gaponov. Electronics, Fizmatgiz, 1960.
6. H. W. Lewis and I. R. Reitz. Thermoelectric properties of the plasma diode, J. Appl. Phys., 1959, vol. 30, No 9.
7. B. Ya. Moyzhes and G. E. Pikus. On theory of plasma thermoelement, Phys. of the solid, 1960, vol. 2, issue 4.

8. G. Y. Mullaney, P. H. Kydd, and N. R. Dibelius. Electrical conductivity in flame gases with large concentration of potassium, J. Appl. Phys., 1961, vol. 32, No 4. (Coll. trans. "Plasma in magnetic field," State Atomic Publishing House, 1962).

9. M. I. Elison and G. F. Vasil'yev. Field emission, Fizmatgiz, 1958.

## ROTATIONAL RELAXATION IN PLANE-PARALLEL RAREFACTION WAVE

V. N. Arkhipov and L. I. Severinov

(Moscow)

Influence of relaxation on flow parameters in plane-parallel rarefaction wave formed during supersonic flow around a blunt point was investigated in linear placement only for slight deviation from equilibrium [1] and for small deviation from frozen flow [2]. Generally, without these limitations it can be investigated only by nonlinear method. Here such investigation is conducted by method of characteristics.

Subject of investigation is rotary relaxation. Study of this form of relaxation in flow of gas is mathematically the most simple; here it is possible, comparatively easily, to obtain visible results illustrating influence of relaxation on flow. At the same time mathematical peculiarities of solution of the problem related to calculation of relaxation and also qualitative results have general character for all forms of relaxation.

During investigation of structure of shock waves, rotational relaxation is usually disregarded. However, in rarefaction waves it can play a large role, as was shown by Wood and Parker [3] in example of one-dimensional, non-stationary rarefaction wave. Furthermore, theoretical [4] and experimental [5] results recently were obtained allowing to think that time of rotational relaxation (and, consequently, its influence on flow) is increased with rise of temperature. In connection with this below is also investigated influence of amount of time of relaxation on character of flow in rarefaction wave.

1. Fundamental equations. We will take thermodynamic circuit used in [3].

We will introduce polar coordinates  $r, \varphi$  with beginning of reference at vertex of parallel to left side of the angle. We will make typical velocity angle. Angle  $\varphi$  will be reckoned from initial direction of velocity vector, frozen speed of

of sound  $a_f$ , in incident flow, and characteristic time of problem  $\tau_0$  (as  $\tau_0$  it is possible to select, for example, time for which sonic disturbance of high rate passes distance of 1 cm). We will introduce further dimensionless variables by formulas

$$\begin{aligned} r^x &= \frac{r}{a_{f_0} \tau_0}, & \tau^x &= \frac{\tau}{\tau_0}, & p^x &= \frac{P}{P_0}, & \rho^x &= \frac{\rho}{\rho_0}, & S^x &= \frac{S - S_0}{R} \\ T^x &= \frac{T}{T_0}, & u_r^x &= \frac{u_r}{a_{f_0}}, & u_\varphi^x &= \frac{u_\varphi}{a_{f_0}}, & V^x &= \frac{V}{a_{f_0}}, & c_i^x &= \frac{c_i}{R} \\ c_{pf}^x &= \frac{c_{pf}}{R}, & c_{vf}^x &= \frac{c_{vf}}{R}, & a_f^x &= \frac{a_f}{a_{f_0}}, & \theta^x &= \frac{\theta}{T_0}, & V^2 &= u_r^2 + u_\varphi^2 \end{aligned}$$

( $\tau \sim 1/p$ ,  $a_{f_0}^2 = \gamma_f P_0 / \rho_0$ ,  $\gamma_f = c_{pf} / c_{vf}$ ,  $c_p = c_{vf} + c_i$ ,  $c_{pf} = c_{vf} + R$ ).

Here  $f_0$  - parameters of incident flow;  $T$  - progressive temperature;  $\theta$  - internal temperature,  $\tau$  - relaxation time;  $c_{pf}$ ,  $c_{vf}$ ,  $c_i$  - specific heat capacities assumed constant;  $p$  - pressure;  $\rho$  - density;  $S$  - entropy;  $u_r$ ,  $u_\varphi$  - radial and transverse components of velocity;  $a_f$  - frozen speed of sound;  $R$  - gas constant.

In the future we will disregard viscosity, thermal conductivity, and diffusion.

Equations of motion of compressible liquid and equation of relaxation have form (index  $x$  is omitted)

$$\begin{aligned} \rho u_r + r \frac{\partial(\rho u_r)}{\partial r} + \frac{\partial(\rho u_\varphi)}{\partial \varphi} &= 0 \\ r \rho u_r \frac{\partial u_r}{\partial r} - \rho u_\varphi^2 + \rho u_\varphi \frac{\partial u_r}{\partial \varphi} + \frac{r}{\gamma_f} \frac{\partial p}{\partial r} &= 0 \\ \rho u_\varphi \frac{\partial u_\varphi}{\partial \varphi} + \rho u_r u_\varphi + r \rho u_r \frac{\partial u_\varphi}{\partial r} + \frac{1}{\gamma_f} \frac{\partial p}{\partial \varphi} &= 0 \\ r u_r \frac{\partial S}{\partial r} + u_\varphi \frac{\partial S}{\partial \varphi} &= \frac{r c_i (T - \theta)^2}{T \theta \tau} \\ r u_r \frac{\partial \theta}{\partial r} + u_\varphi \frac{\partial \theta}{\partial \varphi} &= \frac{r (T - \theta)}{\tau} \end{aligned} \tag{1.1}$$

These equations allow integral

$$\frac{\gamma_f}{\gamma_f - 1} \frac{P}{\rho} + c_i (\theta - 1) + \frac{\gamma_f V^2}{2} = \text{const} \tag{1.2}$$

System (1.1) is closed by equations

$$S = c_{p1} \ln T + c_1 \ln \theta - \ln p, \quad p = \rho T \quad (1.3)$$

2. Characteristics. Boundary conditions. Two families exist of characteristics of system (1.1), differential equations of which are

$$r \left( \frac{d\varphi}{dr} \right)_{\pm} = \operatorname{tg} (\beta - \varphi \pm \alpha_1) \quad (2.1)$$

Along characteristics are satisfied conditions

$$\pm \cot \alpha_1 \left( \frac{dp}{dr} \right)_{\pm} + \tau_1 \rho V^2 \left( \frac{d\beta}{dr} \right)_{\pm} = \mp \frac{\tau_1 c_1 a_1 \rho (T - \theta)}{c_{p1} \tau T \cos (\beta - \varphi \pm \alpha_1)} \quad (2.2)$$

Here  $\beta$  — angle of inclination of velocity vector to initial direction

$$\alpha_1 = \operatorname{arc} \sin \frac{a_1}{V}, \quad a_1^2 = \frac{p}{\rho} \quad (2.3)$$

Along lines of flow equations of which  $rd\varphi/dr = \tan (\varphi - \beta)$ , are satisfied conditions

$$\frac{dS}{dr} = \frac{c_1 (T - \theta)^2}{T \tau \theta V \cos (\beta - \varphi)}, \quad \frac{d\theta}{dr} = \frac{T - \theta}{V \tau \cos (\beta - \varphi)} \quad (2.4)$$

Flow of gas remains uniform to characteristic

$$\varphi = \varphi_0 = \operatorname{arc} \sin (a_1 / V_0)$$

Therefore boundary conditions at  $\varphi = \varphi_0$  can be written in the form

$$V = V_0, \quad \beta = S = 0, \quad p = \rho = T = \theta = a_1 = 1 \quad (2.5)$$

Let  $\varphi^*$  — angle of inclination of second side of angle ( $\varphi^* < 0$ ). Then

$$\beta (r, \varphi^*) = \varphi^* \quad (2.6)$$

Further in calculations everywhere is taken  $\tau = 1 / \Lambda p$ , where  $\Lambda$  — relation of characteristic time of problem to characteristic time of relaxation.

3. Maximum form of equations at  $r \rightarrow 0$ . In limit at  $r \rightarrow 0$  equations (1.1) will be turned into system of ordinary differential equations describing Prandtl - Mayer supersonic frozen flow. System has form

$$\begin{aligned}
\rho^\circ u_r^\circ + \frac{d(\rho^\circ u_r^\circ)}{d\varphi} &= 0, & -\rho^\circ u_\varphi^{\circ 2} + \rho^\circ u_\varphi^\circ \frac{du_r^\circ}{d\varphi} &= 0 \\
\rho^\circ u_\varphi^\circ \frac{du_\varphi^\circ}{d\varphi} + \rho^\circ u_r^\circ u_\varphi^\circ + \frac{1}{\gamma_f} \frac{d\rho^\circ}{d\varphi} &= 0 \\
u_\varphi^\circ \frac{dS^\circ}{d\varphi} &= 0, & u_\varphi^\circ \frac{d\theta^\circ}{d\varphi} &= 0
\end{aligned} \tag{3.1}$$

Here and in the future index  $^\circ$  designates function at  $r = 0$ . Solution of this system for  $\varphi_* \leq \varphi \leq \varphi_0$  has form

$$\begin{aligned}
u_\varphi^\circ &= -a_f^\circ, & \frac{2}{\gamma_f - 1} u_\varphi^{\circ 2} + V^{\circ 2} &= V_+^2 = \text{const}, & u_r^\circ &= V_+ \sin \alpha \\
u_\varphi^\circ &= -\lambda V_+ \cos \alpha, & \rho^\circ &= \frac{\cos^{2\omega} \alpha}{\cos^{2\omega} \alpha_0}, & \rho^{\circ 0} &= \frac{\cos^{2\omega+2} \alpha}{\cos^{2\omega+2} \alpha_0} \\
T^\circ &= \frac{\cos^2 \alpha}{\cos^2 \alpha_0}, & a_f^\circ &= \frac{\cos \alpha}{\cos \alpha_0}, & S^\circ &= 0, & \theta^\circ &= 1 \\
\alpha &= \lambda (\varphi_0 - \varphi) + \alpha_0, & \lambda &= \sqrt{\frac{\gamma_f - 1}{\gamma_f + 1}}, & \omega &= \frac{1}{\gamma_f - 1} \\
\tan \alpha_0 &= \lambda \sqrt{V_0^2 - 1}
\end{aligned} \tag{3.2}$$

In region  $\varphi^* \leq \varphi \leq \varphi_*$  parameters of state and motion of gas are constant:

$f(\varphi) = f(\varphi_*) = f_*$ . Angle  $\varphi_*$  is determined from equality  $\beta(\varphi_*) = \varphi^*$ .

4. Characteristic variables. We will introduce characteristic variables  $\xi$  and  $\eta$  ( $\xi$  is constant throughout characteristic of first family,  $\eta$  is constant throughout characteristic of second family). Let  $\eta = r$  at  $\varphi = \varphi_0$ , and  $\xi = \varphi$  at  $r = 0$ ; equations (2.1), (2.2), (2.4) will take form

$$r\varphi_\eta = \text{tg}(\beta - \varphi + \alpha_f) r_\eta, \quad r\varphi_\xi = \text{tg}(\beta - \varphi - \alpha_f) r_\xi \tag{4.1}$$

$$p_\eta \text{ctg} \alpha_f + \gamma_f \rho V^2 \beta_\eta = -\frac{\Lambda \gamma_f a_f c_f (T - \theta) p p r_\eta}{T c_{p_f} \cos(\beta - \varphi + \alpha_f)} \tag{4.2}$$

$$-p_\xi \text{ctg} \alpha_f + \gamma_f \rho V^2 \beta_\xi = \frac{\Lambda \gamma_f a_f c_f (T - \theta) p p r_\xi}{T c_{p_f} \cos(\beta - \varphi - \alpha_f)} \tag{4.3}$$

$$\begin{aligned}
VS_\xi r_\eta \cos(\beta - \varphi - \alpha_f) + VS_\eta r_\xi \cos(\beta - \varphi + \alpha_f) &= \\
= 2\Lambda \cos \alpha_f p (T - \theta)^2 r_\xi r_\eta
\end{aligned} \tag{4.4}$$

$$\begin{aligned}
V\theta_\xi r_\eta \cos(\beta - \varphi - \alpha_f) + V\theta_\eta r_\xi \cos(\beta - \varphi + \alpha_f) &= \\
= 2\Lambda \cos \alpha_f p (T - \theta) r_\xi r_\eta
\end{aligned} \tag{4.5}$$

Boundary conditions are:

$$\varphi = \xi, r = 0, \theta = 0 \text{ at } \eta = 0; \quad \varphi = \varphi_0, r = \eta, V = V_0, S = \beta = 0$$

$$a_f = \theta = p = \rho = T = 1 \text{ at } \xi = \varphi_0$$

5. Derivatives. For study of solution in environment of point  $r = 0$  it is important to know derivatives of this point. In region  $\varphi_* \leq \varphi \leq \varphi_0$  we will determine characteristic derivatives. We differentiate equations (4.1), (4.3) - (4.5) by  $\eta$ , equation (4.2) by  $\xi$ .

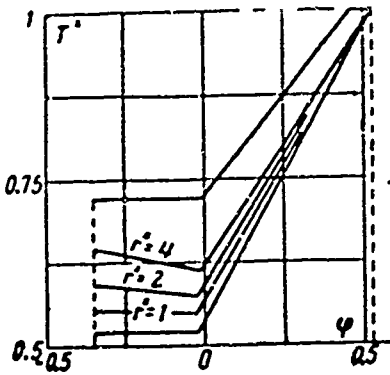


Fig. 1.

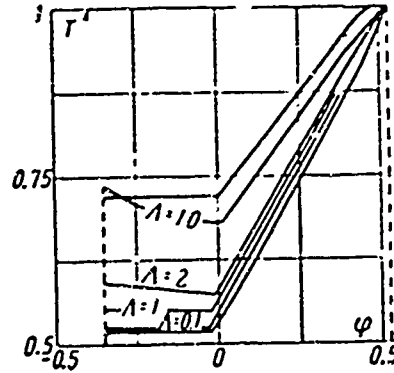


Fig. 2.

and let us turn to limit at  $\eta \rightarrow 0$  in received equations and in equation (4.2).

Designating  $f^{(1)}(\xi) = (\partial f / \partial \eta)_{r=0}$ , we receive

$$2\varphi^{(1)} = \beta^{(1)} + \alpha_f^{(1)}, \quad r^{(1)} = \operatorname{tg} 2(\beta^0 - \xi) r_{\xi}^{(1)}$$

$$p^{(1)} \operatorname{ctg} \alpha_f^0 + \gamma_f \rho^0 V^0 \beta^{(1)} = - \frac{c_f}{c_{pf}} \Lambda \gamma_f a_f^0 \rho^0 (T^0 - 1)$$

$$p_{\xi} \alpha_f^{(1)} \operatorname{csc}^2 \alpha_f^0 - p_{\xi}^{(1)} \operatorname{ctg} \alpha_f^0 + \gamma_f (\rho^{(1)} V^0 + 2\rho^0 V^0 V_{\xi}^{(1)}) \beta_{\xi} +$$

$$+ \gamma_f \rho^0 V^0 \beta_{\xi}^{(1)} = \frac{\gamma_f \Lambda c_f \rho^0 p^0 (T^0 - 1) a_f r_{\xi}^{(1)}}{c_{pf} T^0 \cos 2(\beta^0 - \xi)} \quad (5.1)$$

$$V^0 T^0 S_{\xi}^{(1)} r^{(1)} \cos 2(\beta^0 - \xi) + V^0 T^0 S^{(1)} r_{\xi}^{(1)} = 2\Lambda \cos \alpha_f^0 c_f \rho^0 (T^0 - 1)^2 r_{\xi}^{(1)} r^{(1)} \quad (5.2)$$

$$V^0 \beta_{\xi}^{(1)} r^{(1)} \cos 2(\beta^0 - \xi) + V^0 \theta^{(1)} r_{\xi}^{(1)} = 2\Lambda \cos \alpha_f^0 (T^0 - 1) r_{\xi}^{(1)} r^{(1)} \quad (5.3)$$

$$- p^{(1)} \alpha_{\xi}^0 \operatorname{cosec}^2 \alpha_f^0 + p_{\xi}^{(1)} \operatorname{ctg} \alpha_f^0 + \gamma_f (\rho_{\xi}^0 V^0 + 2\rho^0 V^0 V_{\xi}^0) \beta^{(1)} +$$

$$+ \gamma_f \rho^0 V^0 \beta_{\xi}^{(1)} = - \left[ \gamma_f a_f^0 \frac{c_f \Lambda \rho^0}{c_{pf} T^0} (T^0 - 1) p^0 \right] r^{(1)} - \gamma_f a_f^0 \frac{c_f}{c_{pf}} \frac{\rho^0}{T^0} (T^0 - 1) \Lambda p^0 r_{\xi}^{(1)} \quad (5.4)$$

Functions  $f^0$  are determined by the formulas of (3.2).

We will differentiate also equations (1.2), (1.3), (2.3) by  $\xi$  and let us turn to limit at  $\eta \rightarrow 0$ . These equations jointly with (5.1) - (5.4) allow

to determine function  $f^{(1)}$  in closed form for  $\gamma_1 = 5/3$ . Thus, for example, integration of second equation of (5.1) and equations of (5.2) and (5.3) gives

$$r^{(1)} = \frac{\cos^2 \alpha_0 \sin^{1/2} \alpha_0}{\cos^2 \alpha \sin^{1/2} \alpha} \quad (5.5)$$

$$S^{(1)} = \frac{2\Lambda c_1 \cos^2 \alpha \sin^{1/2} \alpha_0}{\cos^4 \alpha_0 \sin^{1/2} \alpha} \left[ \frac{1}{2} (\alpha_0 - \alpha) + \frac{1}{4} (\sin 2\alpha - \sin 2\alpha_0) - \right. \\ \left. - 2 \cos^2 \alpha_0 (\alpha - \alpha_0) + \cos^4 \alpha_0 (\tan \alpha - \tan \alpha_0) \alpha_0 \right] \quad (5.6)$$

$$\alpha^{(1)} = \frac{2\Lambda \cos^2 \alpha \sin^{1/2} \alpha_0}{\cos^4 \alpha_0 \sin^{1/2} \alpha} \left[ \frac{1}{2} (\alpha_0 - \alpha) + \frac{1}{4} (\sin 2\alpha - \sin 2\alpha_0) - \cos^2 \alpha_0 (\alpha - \alpha_0) \right] \quad (5.7)$$

In interval  $\varphi^* \leq \varphi \leq \varphi_*$  it is necessary to determine  $(\partial f / \partial r)_{r=0} = f_1(\varphi)$ .

Equations for functions of  $f_1$  can be obtained by differentiating system (1.1) - (1.3) by  $r$  and crossing to limit at  $r \rightarrow 0$ . System has form

$$\begin{aligned} u_*^\circ \frac{dp_1}{d\varphi} + p_*^\circ \frac{du_{\varphi_1}}{d\varphi} &= F_1, & \rho_*^\circ u_*^\circ \frac{du_{r_1}}{d\varphi} &= F_2, \\ \frac{1}{\gamma_1} \frac{dp_1}{d\varphi} &= \rho u_*^\circ \frac{du_{\varphi_1}}{d\varphi} = F_3, \\ u_*^\circ \frac{dS_1}{d\varphi} &= F_4, & u_*^\circ \frac{d\theta_1}{d\varphi} &= F_5 \end{aligned}$$

where  $F_1, F_2, F_3, F_4, F_5$  - functions of  $f^\circ, f_1$ . This system can be integrated for  $\gamma_1 = 5/3$  in closed form. The simplest expressions are obtained for  $S_1$  and  $\theta_1$ :

$$S_1 = \sec(\varphi - \beta_*) \left[ - \frac{\Lambda c_1 p_* (T_* - 1)^2}{V_* T_*} (\varphi - \beta_*) + \text{const} \right] \quad (5.8)$$

$$\theta_1 = \sec(\varphi - \beta_*) \left[ - \frac{\Lambda p_* (T_* - 1)}{V_*} (\varphi - \beta_*) + \text{const} \right] \quad (5.9)$$

Constants are determined from boundary conditions at  $\varphi = \varphi_*$ .

6. Gradients on straight line  $\varphi = \varphi_*$ . Let  $\Lambda = 1$ . We will designate

$f^\circ(\eta) = f_1(\varphi_*, \eta)$ . We will differentiate by  $\xi$  first equations of (4.1), (1.3),

(2.3) and equations (4.2) and (1.2) and let us assume in received equations,

in second equation (4.1) and in equations (4.3) - (4.5) that  $\xi = \varphi_*$ . We

obtain

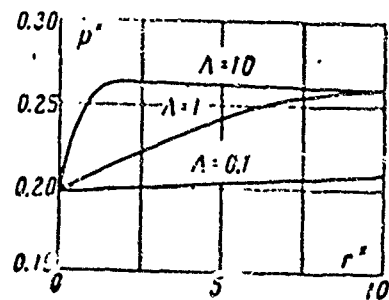


Fig. 3.

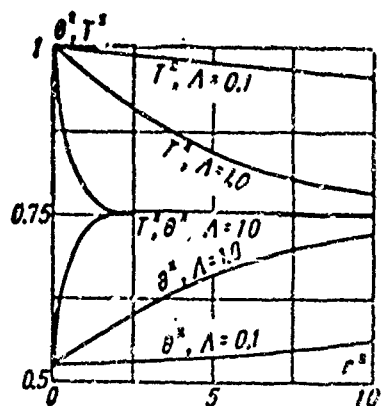


Fig. 4.

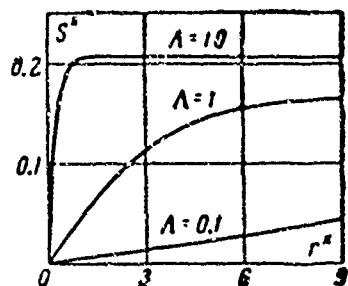


Fig. 5.

$$\begin{aligned} \eta \varphi^{\infty} + \operatorname{tg} 2\varphi_0 r^{\infty} &= 0 \\ -p^{\infty} \operatorname{ctg} \varphi_0 + \gamma_j V_0^2 \beta^{\infty} &= 0 \\ \theta^{\infty} = S^{\infty} &= 0 \\ \eta \varphi_n^{\infty} + \varphi^{\infty} &= \beta^{\infty} + \alpha_j^{\infty} \\ V_j^{\infty} &= -\frac{\gamma_j}{2(\gamma_j - 1)} T^{\infty} \end{aligned}$$

$$\alpha_j^{\infty} = \frac{\gamma_j}{2V_0^2 \sqrt{V_0^2 - 1}} \left( V_0^2 + \frac{1}{\gamma_j - 1} \right) T^{\infty}$$

$$T^{\infty} = \frac{\gamma_j - 1}{\gamma_j} p^{\infty}$$

$$p_n^{\infty} \operatorname{ctg} \alpha_{j0} \pm \gamma_j V_0^2 \beta_n^{\infty} = -\gamma_j \frac{c_i}{c_{pj}} T^{\infty} \quad (6.1)$$

From last two equations we have directly

$$p_n^{\infty} \operatorname{ctg} \varphi_0 + \gamma_j V_0^2 \beta_n^{\infty} = (1 - \gamma_j) \frac{c_i}{c_{pj}} p^{\infty}$$

Taking into account the second equation of system

(6.1) we receive

$$p_n^{\infty} = -\frac{\gamma_j - 1}{2 \operatorname{ctg} \varphi_0} \frac{c_i}{c_{pj}} p^{\infty}$$

which, after integration, gives

$$p^{\infty}(\eta) = p^{\infty}(0) e^{-k\eta}, \quad k = \frac{c_i(\gamma_j - 1)}{2c_{pj} \operatorname{ctg} \varphi_0}$$

After that we immediately obtain

$$\begin{aligned} T^{\infty}(\eta) &= T^{\infty}(0) e^{-k\eta}, & \beta^{\infty}(\eta) &= \beta^{\infty}(0) e^{-k\eta} \\ V^{\infty}(\eta) &= V^{\infty}(0) e^{-k\eta}, & \alpha_j^{\infty}(\eta) &= \alpha_j^{\infty}(0) e^{-k\eta} \end{aligned}$$

Now it is easy to integrate the fifth equation of

(6.1):

$$\varphi^{\infty}(\eta) = \frac{\beta^{\infty}(0) + \alpha_j^{\infty}(0)}{k\eta} (1 - e^{-k\eta})$$

Then,

$$\begin{aligned} p_{\varphi}(\varphi_0, r) &= \left( \frac{\partial p}{\partial \varphi} \right)_{\varphi=\varphi_0} = \frac{p^{\infty}(\eta)}{\varphi^{\infty}(\eta)} = \\ &= \frac{k p^{\infty}(0)}{\beta^{\infty}(0) + \alpha_j^{\infty}(0)} \frac{\eta e^{-k\eta}}{1 - e^{-k\eta}} \end{aligned}$$

i.e.,

$$p_{\varphi}(\varphi_0, r) = \frac{k p_{\varphi}(\varphi_0, 0)}{\beta_{\varphi}(\varphi_0, 0) + \alpha_{j\varphi}(\varphi_0, 0)} \frac{r e^{-kr}}{1 - e^{-kr}}$$

Thus, pressure gradient on line  $\varphi = \varphi_0$  diminishes with increase of distance from vertex of angle.

Analogous result is easy to obtain also for gradients of other quantities.

7. Results of calculations. Conditions of (2.5), (2.6) and equations of (3.2) constitute system of boundary conditions starting from which it is possible by method of characteristics, to find distribution of parameters of flow in region  $\varphi^* \leq \varphi \leq \varphi_0, r > 0$ .

Calculations were made for  $\gamma = 5/3$  which corresponds to simultaneous relaxation of rotational stages of three-dimensional rotator. (Equilibrium value  $\gamma_e$  is equal here to  $4/3$ ). Accuracy of calculations was controlled by comparison of derivatives received by method of characteristics and calculated by the formulas of Section 5. Mass flow rates through arcs  $\varphi^* \leq \varphi \leq \varphi_0$  of circle  $r = \text{const}$  limited by half-lines of  $\varphi = \varphi_0$  and  $\varphi = \varphi^*$ , with great degree of accuracy were equal to flow rates through radii  $r = \varphi_0$  of these circles.

Certain results of calculations are shown in Figs. 1 - 5. Here, everywhere  $V_0 = 2, \varphi^* = -20^\circ$ . In Fig. 1 are given temperature distributions  $T^x$  depending upon  $\varphi$  for various  $r^x$  at  $\Lambda = 1$ . In Fig. 2 - distributions  $T^x$  depending upon  $\varphi$  at  $\Lambda = 0.1, 1.0$  and  $10$  for  $r^x = 1$ . In both figures upper curve corresponds to equilibrium. In Figs. 3 - 5 are given pressure distributions  $p^x$ , temperature  $T^x$ , internal temperature  $\theta^x$  and entropy  $S^x$  along right side of angle  $\varphi = \varphi^*$  for various  $\Lambda$ . It is clear that influence of processes of relaxation during flow around an obtuse angle is considerable. Effects of relaxation strongly depend on length of time of relaxation.

The authors thank B. A. Ipatov for his help.

Submitted  
17 January 1963

#### Literature

1. J. F. Clarke. The linearized flow of a dissociating gas, J. Fluid Mech. 1960, vol. 7, No 4, 577 - 595.
2. V. P. Stulov. Flow around a convex angle of ideal dissociating gas taking nonequilibrium into account, News of Academy of Sciences of USSR, OTN, Mechanics and machine building, 1962, No 3, page 4 - 10.
3. W. W. Wood and F. R. Parker. Structure of a Centered Rarefaction Wave in a Relaxing Gas, Phys. Fluids, 1958, No. 3, 230 - 241.
4. F. R. Parker. Rotational and vibrational relaxation in diatomic gases,

ble

Phys. Fluids, 1959, vol. 2, No 4, 449 - 462, Russian trans: Parker, Rotational and oscillatory relaxation in diatomic gases, Coll. Gas dynamics and heat exchange in the presence of chemical reactions, IL, 1962, page 369-397.

axa-

5. L. Talbot. Survey of the Shock Structure Problem. ARS - Journal, 1962, vol. 32, No 7, 1009-1016.

of

as

ed

re

ling

?

ure

p\*

i  
1963

pch.,

ave

es,

## THEORY OF DIFFERENTIAL EJECTOR

B. A. Uryukov

(Moscow)

In single-stage gas ejector with cylindrical mixing chamber and supersonic speed of ejected gas, achievement of maximum total pressure of mixture at given ejection coefficient and given total pressure drop of miscible gases is limited by critical conditions at which ejected gas accelerates to speed of sound inside mixing chamber.

Multistage ejector (system of series connected ejectors) allows to obtain total pressure of mixture greater than in single-stage. This is caused by the fact that losses of total pressure during mixing of flows in ejector sharply decrease with decrease of ratio of total pressures of ejecting and ejected gases and also by the fact that in multistage ejector limitations, associated with critical conditions are weakened to a significant degree.

Calculations for multistage ejectors were made by Yu. N. Vasil'yev.

It is interesting to consider an extreme case - "differential" ejector - with continuous distribution of flow rate of ejecting gas on length of mixing chamber. Investigation of differential ejector allows to clarify main characteristics of ejector with large number of stages.

Equations of differential ejector were obtained by S. A. Khristianovich.

1. Differential ejector can consist of an infinite number of ejector "elementary". Diagram of differential ejector and separate elementary stage is given in Fig. 1.

During investigation the following assumption are made:

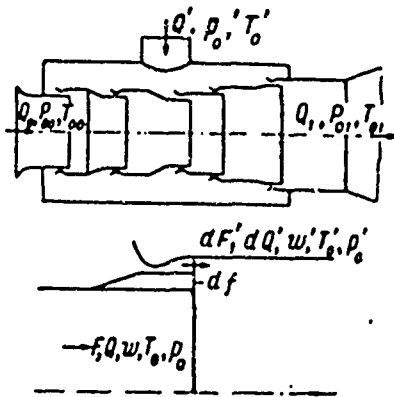
- 1) friction and heat transfer on walls of ejector are negligible;

- 2) miscible gases are ideal with identical chemical composition;  
 3) velocity, temperature, and pressure in initial section of every elementary ejector are evenly distributed.

We will introduce designations:  $F, Q, w, T_0, p_0$  — area, flow rate velocity, deceleration temperature and total pressure in given section of ejector respectively:  $dF', dQ', w', T_0', p_0'$  — the same parameters ejecting gas at nozzle section of elementary ejector;  $df$  — change of area of cross section of elementary ejector (Fig. 1).

Equations of inseparability and momentum for elementary ejector have form

$$dQ = dQ', d(T_0 Q) = T_0' dQ', d(Qw) - w' dQ' = p' dF' - d(pF) + p df \quad (1.1)$$



Change of area of mixing chamber

$$dF = dF' + df = F_0 (d\alpha + d\chi) \quad (1.2)$$

Dimensionless quantities (by index

0 are designated parameters ejecting gas at input to ejector) are

Fig. 1

$$\lambda = \frac{w}{a_0}; \quad n = \frac{Q'}{Q_0}, \quad \tau = \frac{T_0'}{T_{00}}, \quad \sigma = \frac{p_0'}{p_{00}}, \quad \varepsilon = \frac{p_0}{p_{00}}, \quad \varphi = \frac{F}{F_0}$$

$$\left( a_0 = \sqrt{\frac{2\kappa}{\kappa+1} RT_0}, \quad \kappa = \frac{c_p}{c_v} \right) \quad (1.3)$$

— reduced speed, coefficient of injection, temperature drop of deceleration, fall of total pressures, compression ratio, and relative area of mixing chamber respectively;  $a_0$  — critical speed of sound,  $c_p$  and  $c_v$  — ratio of heat capacities, and  $R$  — gas constant.

We will designate

$$z(\lambda) = \lambda + \frac{1}{\lambda}, \quad T(\lambda) = 1 - \frac{\kappa-1}{\kappa+1} \lambda^2, \quad \rho(\lambda) = T(\lambda)^{\frac{1}{\kappa-1}}$$

$$p(\lambda) = T(\lambda)^{\frac{\kappa}{\kappa-1}}, \quad q(\lambda) = \left( \frac{\kappa+1}{2} \right)^{\frac{1}{\kappa-1}} \lambda \rho(\lambda) \quad (1.4)$$

We will consider that  $P_0'$  and  $T_0'$  are constant along ejector, for consideration of a more general case does not introduce principal difficulties.

Ejection equations lead to form

$$\frac{dz}{dn} = \frac{\sqrt{\tau} q(\lambda_0)}{\sigma q(\lambda')}$$

$$\sqrt{\tau} z(\lambda') + \sqrt{(1+n)(1+n\tau)} \frac{T(\lambda)}{\lambda} \frac{1}{\varphi} \frac{d\chi}{dn} = \frac{d}{dn} [\sqrt{(1+n)(1+n\tau)} z(\lambda)]$$

$$\varepsilon = \frac{\sqrt{(1+n)(1+n\tau)} q(\lambda_0)}{\varphi q(\lambda)}, \quad \frac{a_{\infty}^2}{a_{\infty 0}^2} = \frac{1+n\tau}{1+n}, \quad \varphi = 1 + \alpha + \chi \quad (1.5)$$

Evidently length does not enter into ejection equations. As quantity replacing length along mixing chamber it is possible to take injection coefficient  $n$ .

Usually mixing chamber of ejector is terminated by diffuser. If in end of mixing chamber  $\lambda < 1$ , losses in diffuser are small. If however,  $\lambda > 1$ , then in diffuser various conditions can take place; losses in this case depend very strongly on design of diffuser can be very great at large values of  $\lambda$ .

In connection with this, we pose the problem of finding the optimum ejector in the following manner: at given total coefficient of injection  $n_1$  (value of  $n$  at end of ejector) at given  $\tau$  and  $\sigma$ , and also at given value of  $\lambda_1$  at end of ejector, to find distribution of velocities along ejector  $\lambda = \lambda(n)$  and  $\lambda' = \lambda'(n)$ , with which  $\varepsilon_1$  at end of ejector attains maximum value. Optimum value of  $\lambda_1$  can then be determined from joint consideration of work of ejector and diffuser.

Equations of (1.5) can be reduced to one equation by excluding geometric parameters  $\alpha$ ,  $\chi$  and  $\varphi$

$$dz = A dn, \quad A = \frac{\sqrt{\tau}}{\omega} \varepsilon \left\{ \frac{\lambda}{T(\lambda)} \left[ z(\lambda') - \frac{2\kappa}{\kappa+1} \lambda \frac{\omega'}{\sqrt{\tau}} \right] - \frac{\varepsilon q(\lambda)}{\sigma q(\lambda')} \right\} \quad (1.6)$$

$$\omega = \sqrt{(1+n)(1+n\tau)}, \quad \omega' = \frac{d\omega}{dn} = \frac{1/2(1+\tau) + n\tau}{\sqrt{(1+n)(1+n\tau)}} \quad (1.7)$$

It is important to note that in (1.6) there are no differentials  $d\lambda$  and  $d\lambda'$ . This is explained by the fact that in elementary ejector, change of total pressure

of mixture can depend only on increase of flow rate of ejecting gas.

From equation (1.6) it follows that for obtaining maximum value of  $\epsilon_1$  at end of ejector it is necessary that quantity  $A$  be at maximum for each elementary ejector. We have

$$\begin{aligned} \frac{\partial A}{\partial \lambda} &= e \frac{V\bar{\tau}}{\omega} \frac{T(\lambda')}{\lambda' T^2(\lambda)} \left\{ \frac{\lambda'}{T(\lambda')} \left[ z(\lambda') t(\lambda) - \frac{4x}{x+1} \frac{\omega'}{V\bar{\tau}} \right] + (\lambda^2 - 1) \frac{ep(\lambda)}{\sigma p(\lambda')} \right\} \\ \frac{\partial A}{\partial \lambda'} &= e \frac{V\bar{\tau}}{\omega} \frac{V\bar{\tau}}{\omega} \left( 1 - \frac{1}{\lambda'^2} \right) \frac{\lambda}{T(\lambda)} \left[ 1 - \frac{ep(\lambda)}{\sigma p(\lambda')} \right] \quad \left( t(\lambda) = 1 + \frac{x-1}{x+1} \lambda^2 \right) \end{aligned} \quad (1.8)$$

Assuming  $\partial A / \partial \lambda' = 0$ , find

$$\epsilon p(\lambda) = \sigma p(\lambda') \quad (1.9)$$

This equation has simple physical meaning: in each section of ejector static pressure of ejecting gas at nozzle section should be equal to static pressure of mixture.

Assuming  $\partial A / \partial \lambda = 0$  and using (1.9), we receive

$$\left[ \lambda' - \lambda \sqrt{\frac{1+n\tau}{\tau(1+n)}} \right] \left[ \lambda' - \lambda \sqrt{\frac{\tau(1+n)}{1+n\tau}} \right] = 0 \quad (1.10)$$

Since  $\epsilon < \sigma$ , from (1.9) it follows that always  $\lambda < \lambda'$ , so that equations (1.9) and (1.10) at any values of  $\tau$  allow only one solution  $\lambda = \lambda_*$ ,  $\lambda' = \lambda_*'$  having physical meaning. At the same time, so that ejector will operate, real velocity of gas at nozzle section should be larger or equal to velocity of mixture ( $u' \geq u$ ).

This condition has form

$$\lambda' - \lambda \sqrt{\frac{1+n\tau}{\tau(1+n)}} > 0 \quad (1.11)$$

It is obvious that (1.11) is always executed at  $\tau > 1$ , therefore  $\lambda_*$  and  $\lambda_*'$  at  $\tau > 1$  are found from (1.9) and

$$\lambda' - \lambda \sqrt{\frac{\tau(1+n)}{1+n\tau}} = 0 \quad (1.12)$$

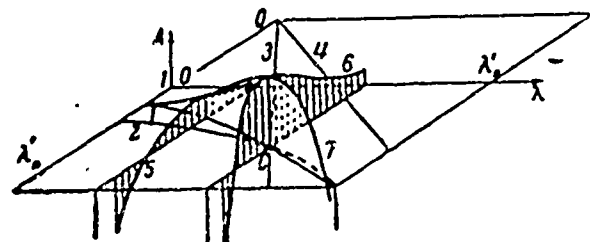


Fig. 2.

Equality (1.12) can also be presented in following form.

$$\rho' w' \left( \frac{\epsilon}{\sigma} \right)^{\frac{n-1}{n}} = \rho w \quad (\rho \text{ -- Density}) \quad (1.13)$$

At  $\tau < 1$  maximum value of A lies at limit of possible solutions determined by condition (1.11). Let us note that

$$\lambda_* = \lambda_*' = \sqrt{\frac{n+1}{n-1}} \quad \text{at} \quad \tau = 1$$

Structure of surface  $A = A(\lambda, \lambda')$  is shown in Fig. 2 in which 1 - line of equal pressures (equation (1.9)); 2 - line  $\partial A / \partial \lambda = 0$ , equation (1.8); 3 and 4 - solutions of (1.10); 5 - section A plane  $\lambda = \text{const}$ ; 6 - section A plane  $\lambda = \lambda_* = \text{const}$ ; 7 - section A on line of equal pressures; C - point  $(\lambda = \lambda_*, \lambda' = \lambda_*')$ .

It is possible to show that  $\lambda_*$  grows during increase of n. Therefore if  $\lambda_1 \leq \lambda_{*0}$  ( $\lambda_{*0}$  in beginning of ejector), the greatest value of A at any  $\epsilon$  is reached when  $\lambda = \lambda_1$  and at values of  $\lambda'$ , determined by equation (1.9). It follows from this that in this case optimum ejector corresponds to constant  $\lambda = \lambda_1$  along entire ejector. If  $\lambda_{*0} < \lambda_1$ , then in this case optimum ejector corresponds to  $\lambda = \lambda_{*0}$  at  $\lambda_* \leq \lambda_1$ , and then  $\lambda = \lambda_1$  to end of ejector.

2. Let us consider case  $\lambda = \lambda_*$  and  $\lambda' = \lambda_*'$  along entire ejector. Excluding  $\epsilon$  and  $\lambda$  from (1.6) with the help of (1.9) and (1.10), we receive

$$d\lambda_*' / dn = 0 \quad (2.1)$$

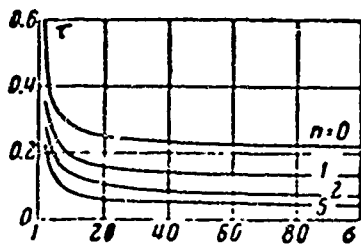


Fig. 3.

Thus,  $\lambda_*' = \text{const}$  along ejector.

In initial section of ejector we have from (1.9) and (1.10)

$$p(\lambda_{*0}) = \sigma p(\lambda_*') \quad (2.2)$$

$$\lambda_{*0} = \lambda_*' \sqrt{\tau} \quad (\tau < 1)$$

$$\lambda_{*0} = \frac{\lambda_*'}{\sqrt{\tau}} \quad (\tau < 1) \quad (2.3)$$

Hence are determined values of  $\lambda_*'$  and  $\lambda_{*0}$ . Excluding from (1.6)  $\epsilon$  and  $\lambda'$  with the help of (1.9) and (1.10) and integrating, we find distribution of  $\lambda_*$  along ejector. Then using equation (1.5), we find

$$\chi = 0, \quad \varphi = 1 + \alpha \quad (2.4)$$

$$\begin{aligned} \lambda_{*0}^2 &= \frac{\kappa+1}{\kappa-1} \frac{m-1}{(m/\tau)-1}, & \lambda_* &= \lambda_{*0} \sqrt{\frac{1+n}{1+n\tau}} & (\tau < 1) \\ \lambda_{*0}^2 &= \frac{\kappa+1}{\kappa-1} \frac{m-1}{m\tau-1}, & \lambda_* &= \lambda_{*0} \sqrt{\frac{1+n\tau}{1+n}} & (\tau > 1) \\ \varepsilon &= \left( \frac{1+n\tau}{1+n\tau/m} \right)^{\frac{\kappa}{\kappa-1}}, & \alpha &= \frac{n\tau}{m} & (\tau < 1) \\ \varepsilon &= \left( \frac{1+n}{1+n/m} \right)^{\frac{\kappa}{\kappa-1}}, & \alpha &= \frac{n}{m} & (\tau > 1) \left( m = \sigma^{\frac{\kappa-1}{\kappa}} \right) \end{aligned} \quad (2.5)$$

From (2.4) and (2.1) it follows that in interval  $\lambda_* < \lambda_1$  optimum will be single-stage ejector with cylindrical mixing chamber. In Fig. 3 are shown limits of regions  $\lambda_* < \lambda_1$  at  $\lambda_1 = 1$  and  $\tau < 1$ . Corresponding limit for  $\tau > 1$  at  $n = 0$  is obtain by replacement of  $\tau$  by  $\tau^{-1}$ . It is possible to see that at  $\lambda_1 = 1$  optimum ejector in which  $\lambda = \lambda_*$  and  $\lambda' = \lambda_*$  along entire ejector, practically, takes place only at very small or very large values of  $\tau$ .

It is interesting to note relationship between velocities of miscible gases in optimum ejector at  $\lambda_* < \lambda_1$ . If in case  $\tau > 1$   $w'/w = T_0'/T_0$ , i.e., difference between velocities is great and there is intense mixing, then at  $\tau < 1$  velocities are equal to  $w = w'$  and equalizing of flows occurs much less intensely.

3. Let us consider, practically, the most interesting case  $\lambda_1 < \lambda_{*0}$ . In optimum ejector we have  $\lambda = \lambda_1 = \lambda_*$ . Equation (1.6), taking into consideration (1.9), will be converted to form

$$\frac{\lambda'}{T(\lambda')} \frac{d\lambda'}{dn} - \frac{\sqrt{\tau}}{\omega} \frac{\lambda}{T(\lambda)} \left( \lambda \frac{\omega'}{\sqrt{\tau}} - \lambda' \right) = 0 \quad (3.1)$$

Initial value of  $\lambda_*$  is determined from equation (1.9)

$$p(\lambda) = \sigma p(\lambda_*) \quad (3.2)$$

Geometric characteristics and compression ratio of ejector are determined from equations

$$\begin{aligned} \frac{d\chi}{dn} &= \frac{1}{\sigma} \frac{p(\lambda)}{p(\lambda')} \frac{\lambda}{T(\lambda)} [z(\lambda) \omega' - \sqrt{\tau} z(\lambda')] \\ \varphi &= \frac{\omega}{\sigma} \frac{p(\lambda)}{p(\lambda')}, \quad \alpha = \varphi - 1 - \chi, \quad \varepsilon = \sigma \frac{p(\lambda)}{p(\lambda')} \end{aligned} \quad (3.3)$$

In case  $\tau = 1$  equation (3.1) is integrated

$$1 + n = \frac{\lambda_0' - \lambda}{\lambda' - \lambda} \sqrt{\frac{T(\lambda')}{T(\lambda_0')}} \left( \frac{1 - h\lambda_0' + h\lambda_0'}{1 + h\lambda' - h\lambda_0'} \right)^{\frac{1}{2k}} \quad (h = \sqrt{\frac{k-1}{k+1}}) \quad (3.4)$$

In Fig. 4 is shown change of area of mixing chamber as function of  $n$  at  $\lambda = 1$  and  $\tau = 1$  for several values of  $\sigma$ . It is clear that at sufficiently large  $\sigma$  mixing chamber at first contracts, and then expands. Position of minimum section is determined from relationship

$$\lambda_m' = \frac{\omega'}{\sqrt{\tau}} \frac{k+1}{2k} z(\lambda) \quad (3.5)$$

At  $\lambda_0' < \lambda_m'$  mixing chamber will be continuously expanded. At  $\lambda = 1$   $\tau = 1$ ,  $k = 1.4$ ,  $\lambda_m' = 1.714$ , which corresponds to value  $\sigma_m = 5.6$ . Let us note that  $d\lambda/dn < 0$  at  $\lambda = 1$ , i.e., mixing chamber of each elementary ejector in this case contracts.

Since compression ratio of ejector rises with increase of  $\lambda_1$ , and loss factor in diffuser even in simplest case of supersonic diffuser with normal shock, is small at values of  $\lambda_1$ , insignificantly exceeding unity one, application of ejector with low supersonic speed can be profitable.

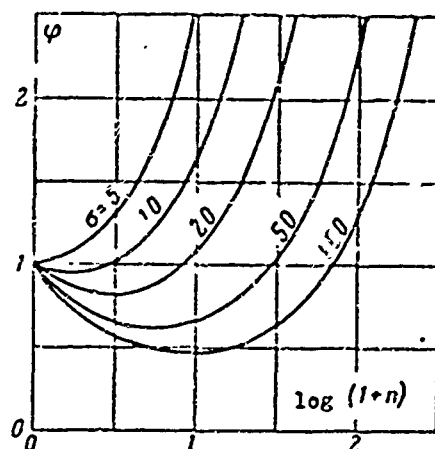


Fig. 4.

4. Let us consider the particular case of a differential ejector when  $\tau = 1$ , in which area of mixing chamber in each elementary stage does not change ( $\chi = 0$ ) and  $\lambda' = \text{const}$ . Equations of such ejector coincide with equations of single-stage ejector

$$\alpha_1 = \frac{n_1 q(\lambda_0)}{\sigma q(\lambda')}, \quad \epsilon_1 = \frac{1 + n_1 q(\lambda_0)}{1 + \alpha_1 q(\lambda_1)}$$

$$(1 + n_1) z(\lambda_1) = n_1 z(\lambda') + z(\lambda_0) \quad (4.1)$$

We will determine maximum compression ratio of such an ejector when velocity of mixture does not exceed speed of sound. For independent variables we take  $\lambda_0$  and  $\lambda_1$ . Derivatives  $\partial \epsilon_1 / \partial \lambda_0$  and  $\partial \epsilon_1 / \partial \lambda_1$  can turn into zero at four points of plane  $(\lambda_0, \lambda_1)$

- (1)  $(p(\lambda_0) = \sigma p(\lambda'), \lambda_1 = 1),$       (2)  $(p(\lambda_0) = \sigma p(\lambda'), \sigma p(\lambda') = \epsilon_1 p(\lambda_1)),$   
 (3)  $(\lambda_0 = 1, \lambda_1 = 1),$                       (4)  $(\lambda_0 = 1, \sigma p(\lambda') = \epsilon_1 p(\lambda_1))$

Analysis shows that points (1) - (3) do not correspond to maximum  $\epsilon_1$ .

Points (1) and (2) correspond to case  $\lambda_0 = \lambda_1 = \lambda' = 1$  and  $\sigma = 1$ . Investigation of second derivative at point (3) shows that it is a "saddle" point. Maximum  $\epsilon_1$  is at point (4). In all sections of ejector responding to point (4) except output, inequality occurs

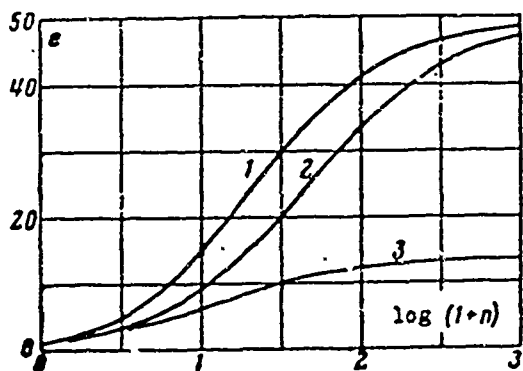


Fig. 5.

$$\sigma p(\lambda') > \epsilon p(\lambda) \quad (4.4)$$

In spite of coincidence of equations describing process of ejection under single-stage and differential ejector conditions corresponding to point (4), this cannot be realized in single-stage ejector, since here at values of  $\lambda < 1$  critical regime sets in. In differential ejector critical regime does not have place, since influence of infinitesimal ejecting stream on flow of mixture in each section of ejector is extremely slight.

During replacement of differential ejector by multistage, critical conditions will appear in each stage, but with increase of number of stops critical value of  $\lambda$  will continuously increase approaching  $\lambda = 1$ . This allows to receive,

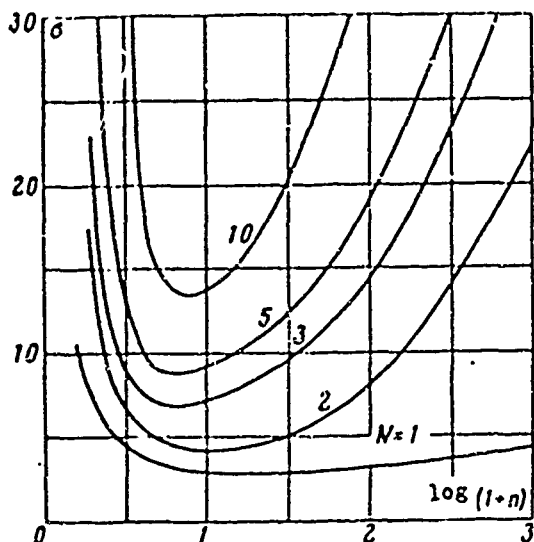


Fig. 6.

Comparison of these curves shows that multistage ejector can give very large increase of compression ratio. Narrowing of mixing chambers of elementary stages also gives essential increase of compression ratio.

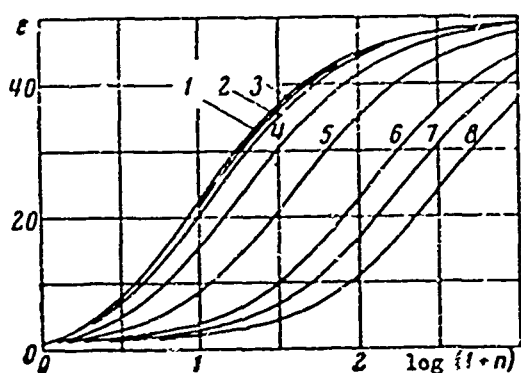


Fig. 7.

10. Compression ratios of multistage ejectors were calculated by Yu. N. Vasil'yev. Limits of fields correspond to difference of 10% of compression ratio of  $N$ -stage ejector from compression ratio of optimum differential ejector at  $\lambda_1 = 1$ . It is interesting to note that at small values of  $n$  and, practically, at any values of  $\sigma$ . and also at small values of  $\sigma$  (to  $\sigma = 2.5 - 3$ ), and any values of  $n$ , application of multistage ejectors is inexpedient. One may see also that field of application of ejector with given number of stages is expanded with increase of  $n$ , which is explained by decrease of losses in ejector with increase of flow rate of ejecting gas.

in multistage ejector, larger compression ratio than in single-stage.

In Fig. 5. for  $\sigma = 50$  at  $\tau = 1$  as function of  $n$  are given compression ratio curves: 1 - for optimum differential ejector at  $\lambda_1 = 1$ ; 2 - for differential ejector  $\chi=0$  and 3 - for optimum single-stage ejector under critical conditions.

Results obtained in work for optimum ejectors allow to indicate limits of application of multistage ejectors with determined number of stages. In Fig. 6 in coordinates of  $n, \sigma$  at  $\tau = 1$  are shown fields of use of  $N$ -stage ejectors for  $N = 1, 2, 3, 5,$

5. Equations for optimum ejector at  $\lambda_1 > \lambda_*$  allow to estimate simply influence of difference of temperatures of miscible gases on compression ratio of ejector. From (2.5) it is clear that heating of ejecting gas ( $\tau > 1$ ) does not affect compression ratio. Consequently, in this case weak change of compression ratio in multistage ejector can be expected depending on increase of temperature of ejecting gas. Conversely, at  $\tau < 1$  influence of temperature heated ejecting gas should be significant, since in optimum ejector at  $\tau < 1$  role of  $n$  is played by  $n\tau$ . This is seen in Fig. 7. where compression ratio curves of optimum ejectors are given at  $\lambda_1 = 1$  for  $\sigma = 50$  and various values of  $\tau$ :

- 1 -  $\tau = 30$ , 2 -  $\tau = 10$ ,  
 3 -  $\tau = 3.333$ , 4 -  $\tau = 1$ ,  
 5 -  $\tau = 0.3$ , 6 -  $\tau = 0.1$ ,  
 7 -  $\tau = 0.060$ , 8 -  $\tau = 0.0333$

#### 6. Efficiency of ejector

$$v^* = e/e_* \quad (6.1)$$

is determined as relation of compression ratio of ejector  $e$  to  $e_*$  — compression ratio obtained during isentropic process of mixing

$$e_* = \left( \frac{1 + n\tau}{1 + n} \right)^{\frac{n}{k-1}} \left( \sigma / \tau^{k-1} \right)^{\frac{n}{1+n}} \quad (6.2)$$

In Fig. 8 for  $\sigma = 50$  are given values of  $v^*$  as functions of  $n$  at various  $\tau$  for optimum differential ejector when  $\lambda_1 > \lambda_*$ :

- 1 -  $\tau = 30$ , 2 -  $\tau = 16.67$ , 3 -  $\tau = 10$ , 4 -  $\tau = 1$   
 5 -  $\tau = 0.3$ , 6 -  $\tau = 0.1$ , 7 -  $\tau = 0.06$ , 8 -  $\tau = 0.03$

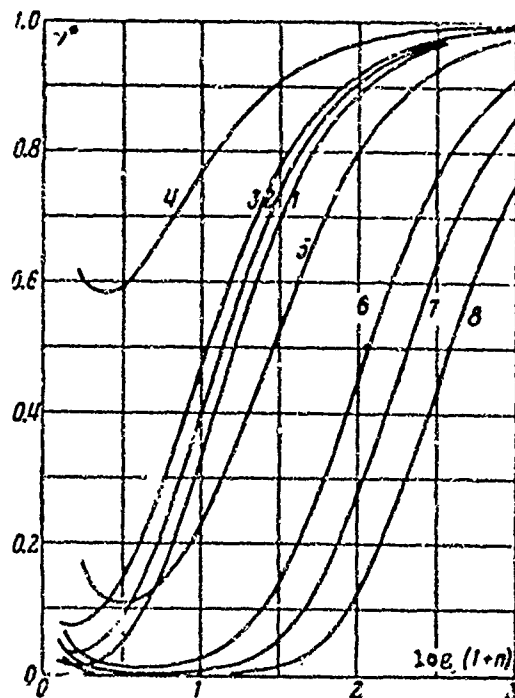


Fig. 8.

It is clear that efficiency of optimum ejector is very low at small values of  $n$  and is near to unit one at large  $n$ . Efficiency curves of optimum ejector at  $\lambda_1 = 1$ , have analogous form, since compression ratio of such ejector in entire range of  $n$  and  $\sigma$  differs insignificantly from compression ratio of optimum ejector  $\lambda_1 > \lambda_*$ .

Author thanks S. A. Khristianovich for formulation of problem and help in process of its solution.

ON CALCULATION OF THERMAL DIFFUSION IN LAMINAR FLOW OF VISCOUS  
LIQUID AT MODERATE VALUES OF THERMAL AND  
DIFFUSION PRANDTL NUMBERS

A. M. Suponitskiy

(Moscow)

If a stream of viscous incompressible liquid containing certain substance flows around a body, temperature of which is different than temperature of flow, then under action of temperature gradient transfer of components of solution occurs. Calculation of occurring thermal-diffusion separation is interesting for a series of problems of chemical technology. In previous article the author [1], was considered process of separation in case of large thermal and diffusion Prandtl numbers. In a liquid, the Prandtl diffusion number  $P$  is rather large ( $10^3$  and more). Meanwhile, thermal Prandtl number  $P_1$  for liquids changes in rather wide range (at  $20^\circ$  for water  $\sim 7$ , for lubricating oils  $\sim 10^3$ ), therefore, assumption made in [1],  $P_1 \gg 1$ , limits field of application of conducted calculations. Below is considered problem of calculation of thermal-diffusion separation at moderate values of thermal and diffusion Prandtl numbers ( $P \geq 1$ ,  $P_1 \geq 1$ ), and also elementary theory of thermal-diffusion separation in forced flow of viscous liquid is given.

1. Let us consider problem of thermal-diffusion separation in two-dimensional laminar boundary layer formed during flow around a wedge. We will assume that presence in stream of alien substance does not have influence on hydrodynamics of flow. This assumption is fully natural if substance is dissolved in comparatively small quantities or differs little by specific gravity, from substance of stream. We will draw for the body an orthogonal system of coordinates  $x, y$ , in such a manner that line  $y = 0$  coincides with contour of surface of wedge. Velocity distribution in hydrodynamic boundary layer of uniform

liquid is given by expressions of [2]

$$\begin{aligned} u &= Uf'(\eta), & v &= -\left(\frac{m+1}{2} \nu u_1 x^{m-1}\right)^{1/2} \left[f(\eta) + \frac{m-1}{m+1} \eta f'(\eta)\right] \\ \eta &= \left(\frac{m+1}{2} \frac{u_1}{\nu}\right)^{1/2} x^{\frac{m-1}{2}} y & (U &= u_1 x^m, \quad m = \frac{\beta}{2-\beta} = \text{const}) \end{aligned} \quad (1.1)$$

Here  $U$  - velocity distribution in external potential of flow;  $\pi\beta$  - aperture angle of wedge;  $\nu$  - coefficient of kinematic viscosity; function  $f(\eta)$  satisfies the Fokner-Skan equation.

Transfer of substance in considered problem is caused by joint action of convection and molecular devices. Flow of substance in liquid transferred, through surface by molecular device during calculation of thermal diffusion is given by expression [3]

$$J = -\rho D \left[ \frac{\partial c}{\partial y} + \sigma c(1-c) \frac{\partial T}{\partial y} \right] \quad (1.2)$$

where  $c(x, y)$  - concentration of substances;  $T(x, y)$  - temperature of liquid;  $\rho$  - density of liquid;  $D$  - diffusion factor;  $\sigma$  - Soret factor;  $y$  - normal to a surface.

Equations for determination of concentration of substance and temperature in diffusion and thermal boundary layers have form

$$u \frac{\partial c}{\partial x} + v \frac{\partial c}{\partial y} = \frac{\partial}{\partial y} \left\{ D \left[ \frac{\partial c}{\partial y} + \sigma c(1-c) \frac{\partial T}{\partial y} \right] \right\}, \quad u \frac{\partial T}{\partial x} + v \frac{\partial T}{\partial y} = \frac{\partial}{\partial y} \left( \chi \frac{\partial T}{\partial y} \right) \quad (1.3)$$

where  $\chi$  - thermal conductivity factor.

We assume that body is impervious to substance, and that concentration of substance  $c_0$  and temperature away from body  $T_0$ , just as surface temperature  $T_1$ , are constant; then boundary conditions have form

$$\begin{aligned} \left[ \frac{\partial c(x, y)}{\partial y} + \sigma c(x, y) (1-c(x, y)) \frac{\partial T}{\partial y} \right]_{y=0} &= 0 \\ T(x, 0) = T_1, & \quad c(x, \infty) = c_0, & \quad T(x, \infty) = T_0 \\ T(0, y) = T_0, & \quad c(0, y) = c_0 \end{aligned} \quad (1.4)$$

We assume that solution has constant physical characteristics. If we seek

solution in the form

$$T = T(\eta), \quad c = c(\eta) \quad \left( \eta = \left[ \frac{m+1}{2} \frac{u_1}{v} \right]^{1/2} x \frac{m-1}{2} y \right) \quad (1.5)$$

then, putting (1.5) in (1.3), and (1.4) and considering (1.1), we receive

$$\begin{aligned} -P f(\eta) c_n' &= c_n'' + \sigma [c(1-c) T_n']_n', & -P_1 f(\eta) T_n' &= T_n'' \\ c(\infty) &= c_0, \quad T(\infty) = T_0, & [c_n'(\eta) + \sigma c(1-c) T_n']_{\eta=0} &= 0, \quad T(0) = T_1 \end{aligned} \quad (1.6)$$

Here,  $P = v/D$ ,  $P_1 = v/\chi$  — diffusion and thermal Prandtl numbers. Heat transfer equation, second equation of system (1.6), has solution, expressed by quadrature

$$\begin{aligned} T(\eta) &= \alpha(P_1) (T_0 - T_1) \int_0^\eta \exp\left(-P_1 \int_0^\xi f(h) dh\right) d\xi + T_1 \\ \alpha(P_1) &= \left[ \int_0^\infty \exp\left(-P_1 \int_0^\xi f(h) dh\right) d\xi \right]^{-1} \end{aligned} \quad (1.7)$$

Values of function  $\alpha(P_1)$  for series of values  $P_1$  at various  $m$  were calculated by Evans [4]. Putting (1.7) in equation, and the boundary conditions of diffusion part of problem (1.6), we receive

$$\begin{aligned} -P f(\eta) c_n' &= c_n'' + \varepsilon \alpha(P_1) \left[ c(1-c) \exp\left(-P_1 \int_0^\eta f(h) dh\right) \right]' \\ [c_n' + \varepsilon \alpha(P_1) c(1-c)]_{\eta=0} &= 0, \quad c(\infty) = c_0, \quad \varepsilon = c(T_0 - T_1) \end{aligned} \quad (1.8)$$

From (1.8) it follows that quantity of separation  $\Delta = [c(0) - c_0] / c_0$  for wedge of given solution depends only on  $P$ ,  $P_1$  and  $\varepsilon$ .

2. Experimental investigations show that Soret factor  $\sigma$  has value of order  $10^{-2} - 10^{-3}$  1/deg, therefore, even significant temperature drops  $T_0 - T_1$  quantity  $\varepsilon = \sigma (T_0 - T_1)$  can be considered small.

We will seek solution of system (1.8) in the form of series on small parameter  $\varepsilon$

$$c(\eta) = c_0(\eta) + \varepsilon c_1(\eta) + \dots \quad (2.1)$$

Calculations give, for first two members of series (2.1) at  $\gamma = P_1 / P = D/\chi \neq 1$ , following expression

$$c = c_0 + \sigma (T_0 - T_1) \left\{ - \frac{c_0 (1 - c_0) \alpha (P_1)}{1 - \gamma} \left[ \int_0^{\xi} \exp \left( - P \int_0^{\xi} f(h) dh \right) d\xi - \right. \right. \\ \left. \left. - \gamma \int_0^{\xi} \exp \left( - P_1 \int_0^{\xi} f(h) dh \right) d\xi \right] + \frac{c_0 (1 - c_0) \left[ \frac{\alpha (P_1)}{\alpha (P)} - \gamma \right] \right\} + \dots \quad (2.2)$$

Concentration of substance on surface of wedge will be determined from (2.2):

$$c(0) = c_0 + \frac{\sigma (T_0 - T_1) c_0 (1 - c_0) \left[ \frac{\alpha (P_1)}{\alpha (P)} - \gamma \right]}{1 - \gamma} \quad (2.3)$$

In case of large values of quantity  $P_1$  during calculation of integral, determining  $\alpha (P_1)$ , for function  $f(\eta)$  we can assume its value close to  $\eta = 0$ . Considering  $f(\eta) = E\eta^2$ ,  $E = \text{const}$ , we receive

$$\alpha (P_1) = \frac{P_1^{3/2} E^{1/2}}{3^{3/2} \Gamma(3/2)} \quad (2.4)$$

Thus, at large values of thermal and diffusion Prandtl numbers, expression (2.3), taking into account (2.4), crosses to formula (3.3), [1]

$$c(0) = c_0 + \sigma (T_0 - T_1) c_0 (1 - c_0) \gamma^{1/2} (1 - \gamma^{1/2}) (1 - \gamma)^{-1} \quad (2.5)$$

In solutions of weak concentration, assuming  $c_0 (1 - c_0) \approx c_0$ , from (2.5) we receive

$$\Delta = \frac{c(0) - c_0}{c_0} = \frac{\sigma (T_0 - T_1) (\gamma^{1/2} + \gamma^{3/2})}{1 + \gamma^{1/2} + \gamma^{3/2}} \quad (2.6)$$

Function  $S(\gamma) = (\gamma^{1/2} + \gamma^{3/2}) (1 + \gamma^{1/2} + \gamma^{3/2})^{-1}$  in interval (0,1) will be continuously increasing. Let us remember that quantity  $\gamma = D/\chi$  for a liquid is less than one. From (2.6) it follows that during increase of  $\gamma$  separation  $\Delta$  increases. Physical interpretation of this fact is given in Section 5. Let us note that extrapolation of results by interval (1,  $\infty$ ) is groundless, which follows from method of obtaining of equation (1.8).

For aqueous solutions ( $\gamma \ll 1$ ) formula (2.3) takes form

$$c(0) = c_0 + \frac{\sigma (T_0 - T_1) c_0 (1 - c_0) \alpha (P_1)}{\alpha (P)} \quad (2.7)$$

Number  $P$ , for aqueous solutions is great; calculating  $\alpha(P)$  by formula (2.4), we receive

$$c = c_0 + \sigma (T_0 - T_1) c_0 (1 - c_0) 3'' \Gamma (4/3) \alpha (P_1) E^{-1} P^{-1/3} \quad (2.8)$$

If  $\gamma = 1$ , then first two members of series (2.1) have form

$$\begin{aligned} c = c_0 + \sigma (T_0 - T_1) c_0 (1 - c_0) & \left\{ -\alpha (P) \int_0^{\xi} \exp \left( -P \int_0^{\xi} f (h) dh \right) d\xi + \right. \\ & + \alpha (P) P \int_0^{\xi} \left[ \exp \left( -P \int_0^{\xi} f (h) dh \right) \right] \left( \int_0^{\xi} f (h) dh \right) d\xi + \left[ 1 - \frac{\alpha (P) P}{3 (P)} \right] \} + \dots \\ \beta (P) = & \left\{ \int_0^{\infty} \left[ \exp \left( -P \int_0^{\xi} f (h) dh \right) \right] \left( \int_0^{\xi} f (h) dh \right) d\xi \right\}^{-1} \end{aligned} \quad (2.9)$$

Concentration of substance on surface of wedge is given by expression

$$c(0) = c_0 + \sigma (T_0 - T_1) c_0 (1 - c_0) \left[ 1 - \frac{\alpha (P) P}{\beta (P)} \right] \quad (2.10)$$

At large values of  $P$ , formula (2.10) crosses to (2.6), in which is assumed  $\gamma = 1$ .

3. During solution of problem in preceding section small parameter method was used. We give approximate solution of problem in closed form, introducing certain changes of initial equations (1.3), owing to partial simplification of member expressing influence of thermal diffusion. Let us assume that thermal boundary layer is significantly thicker than that of diffusion. We expand, in Maclaurin series, expression for temperature distribution in flow (1.7) and limit ourselves to first two members

$$T(\eta) = T_1 + \alpha (P_1) (T_0 - T_1) \eta \quad (3.1)$$

Put (3.1) in equation and the boundary conditions of diffusion part of problem (1.6). In case of solution of weak concentration we receive ordinary second order differential equation with separable variables. Integration

gives

$$c(\eta) = - \frac{c_0 \alpha (P_1)}{1 - \alpha (P_1) J} \int_0^\eta \exp \left[ - P \int_0^\xi f(h) dh - \alpha (P_1) \xi \right] d\xi + \frac{c_0}{1 - \alpha (P_1) J} \left( J = \int_0^\infty \exp \left[ - P \int_0^\xi f(h) dh - \alpha (P_1) \xi \right] d\xi \right) \quad (3.2)$$

Concentration of substance on surface of wedge will be determined from (3.2):

$$c(0) = c_0 [1 - \alpha (P_1) J]^{-1} \quad (3.3)$$

At small values of parameter  $\alpha$  formula (3.3) transfers to (2.7), in which, considering weak concentration of solution, it is necessary to put  $c_0(1 - c_0) \approx c_0$ .

4. Let us consider class of laminar flows of viscous incompressible liquid, in which normal to surface of component of speed  $v_y$  depends only on distance on normal to surface  $y$ . To this class of flows, in particular, belong: flow, caused by rotation of a disk in liquid, flowing around forward stagnation point of body. Survey of problems of heat- and mass transfer for this class of flows can be found in [5].

We will study problem of thermal-diffusion separation for these flows under the assumption  $P \geq 1$  and  $P_1 \geq 1$ . It is not difficult to establish that equations of thermal and diffusion parts of problem of thermal-diffusion separation allow solutions, depending only from normal to surface of coordinate  $y$ . Taking into account this consideration, equations and boundary conditions take form

$$\begin{aligned} -Mf(y/N)c_v' &= D[c_v' + \alpha c(1-c)T_v']_{y'}, & -Mf(y/N)T_v' &= \chi T_v'' \\ c_v' + \alpha c(1-c)T_v' &= 0, & T &= T_1 \text{ when } y=0; & c=c_0, & T=T_0 \text{ when } y=\infty \end{aligned} \quad (4.1)$$

Here  $M$  and  $N$  constants. For case of rotation of disk with constant angular velocity  $\omega$  in liquids (Karman's problem)

$$M = (\omega v)''', \quad N = (v / \omega)''$$

normal to surface of disk of velocity component

$$v_y = -Mf(\omega''y / v'')$$

Function  $f(y/N)$  was determined by a number of authors from numerical solution of system ordinary differential equations [2]. For other flows of this class,

values of constants M, N can be found in [5].

We will introduce the following designations:

$$\eta = \frac{y}{N}, \quad P = \frac{MN}{D}, \quad P_1 = \frac{MN}{\lambda}, \quad c^*(\eta) = c(y), \quad T^*(\eta) = T(y) \quad (4.2)$$

If in system (4.1) we transfer to new variable  $\eta$  and introduce designations of (4.2) we will receive system (1.6). Thus, all results, received for problem of thermal diffusion separation on wedge, apply for considered class of flows.

5. We will list certain elementary considerations about the thermal-diffusion effect during forced convection, which are based on certain hypotheses about structure of thermal diffusion boundary layer, and similar considerations. These considerations represent interpretation of results obtained above.

Let liquid with initial concentration  $c_0$ , be located between two horizontal walls, upper of which has temperature  $T_0$ , and lower  $T_1$ . Let us assume that in layer no convection current is present (including free convection). Under action of temperature gradient transfer of substance appears with the help of a molecular device. After a certain time, process of transfer will be completed and stationary distribution of concentration will be established. From condition of equality of flow of substance  $j$  at zero, and from initial condition, we receive, for solution of weak concentration, following conditions:

$$j = D \left( \frac{\partial c}{\partial y} + \sigma c \frac{\partial T}{\partial y} \right) = 0, \quad \int_0^l c(y) dy = c_0 l \quad (5.1)$$

Here  $l$  - distance between plates;  $y$  - distance on normal to surface of plates. Considering that quantity  $\epsilon = \sigma (T_2 - T_1)$  is small, it is easy to receive from (5.1) quantity of separation

$$\Delta = \frac{c_1 - c_2}{c_0} = \sigma (T_0 - T_1) \quad (5.2)$$

where  $c_1, c_2$  - concentration of substance on lower and upper plates respectively.

In case of thermal diffusion in forced flow we will consider that thermal-diffusion layer can be smashed into two layers: thermal boundary layer and

within it the diffusion boundary layer. We assume that thermal boundary layer during forced flow gives the same separation, as in above considered case of motionless layer (this assumption is inherent to the so-called film theories). Further, let us assume that it "works", i.e., evokes separation of only part of thermal boundary layer, corresponding to diffusion boundary layer. We designate respectively  $\delta_{(1)}, \delta_{(2)}$ ,  $\delta$  — thicknesses of diffusion of thermal and hydrodynamic boundary layers. Amount of separation  $\Delta$  then is given by expression

$$\Delta = \sigma (T_0 - T_1) \delta_{(1)} \delta_{(2)}^{-1} \quad (5.3)$$

At large values of  $P$  and  $P_1$

$$\delta_{(1)} = \frac{\delta}{P^{1/2}} = \frac{\delta D^{1/2}}{v^{1/2}}, \quad \delta_{(2)} = \frac{\delta}{P_1} = \frac{\delta \gamma^{1/2}}{v^{1/2}} \quad (5.4)$$

Putting (5.4) in (5.3), we receive

$$\Delta = \sigma (T_0 - T_1) \gamma^{1/2} \quad (5.5)$$

Formula (5.5) coincides with (2.6) in case of small values of quantity  $\gamma^{1/2}$ .

During increase of  $\gamma$ , according to above-stated considerations, effective part of thermal boundary layer is increased, and amount of separation should increase, which also follows from (2.6).

In case  $P > 1$  and  $P_1 > 1$  we determine thicknesses of thermal and diffusion layers for wedge by expressions

$$\begin{aligned} \delta_{(2)} &= \frac{k(T_0 - T_1)}{j_1} = \frac{k(T_0 - T_1)}{k(T_0 - T_1) \alpha(P_1) \eta_{v'}|_{v=0}} = \frac{1}{\alpha(P_1) \eta_{v'}|_{v=0}} \\ \delta_{(1)} &= \frac{D(c_0 - c_*)}{j} = \frac{D(c_0 - c_*)}{D(c_0 - c_*) \alpha(P) \eta_{v'}|_{v=0}} = \frac{1}{\alpha(P) \eta_{v'}|_{v=0}} \end{aligned} \quad (5.6)$$

where  $j_1$  and  $j$  — respectively are flows of heat and substance on surface of wedge;  $c_*$  — concentration of substance of surface of wedge. Putting values for  $\delta_{(2)}$  and  $\delta_{(1)}$  in (5.3) we receive formula (2.7) for strongly diluted solutions.

6. Flow of substance through surface in gas mixtures under nonisothermal conditions, is given by expression of [3]

$$j = -\rho \left[ D \operatorname{grad} c + \frac{D_T^2 c (1-c) \operatorname{grad} T}{T} \right] \quad (6.1)$$

where  $D_T$  - thermaldiffusion factor.

A number of researchers use expression of (6.1) during description of thermal diffusion in liquids. During assignment of flow of substance in the form of (6.1), self-similarity of thermaldiffusion problem during forced convection, obviously, is not disturbed. Assuming further smallness of quantities

$$\sigma_1 \doteq D_T / D, \tau_1 = (T_0 - T_1) / T_1$$

it is easy to show justice of following situation: for calculation of thermal-diffusion separation during forced convection in case of assignment of molecular transfer of substance by expression (6.1) it is sufficient in solution, received during assignment of molecular transfer by expression (1.2), to exchange  $\sigma (T_0 - T_1)$  for  $D_T(T_0 - T_1) / DT_1$ .

Author thanks G. I. Barenblatt for attention and advice.

Submitted  
13 June 1963

#### Literature

1. A. M. Suponitskiy. On calculation of thermal diffusion in laminar flow of liquid of incompressible viscosity at large Prandtl numbers, PMTF, 1962, No 2.
2. G. Shlikhting. Theory of boundary layer, IL, 1956.
3. K. E. Grew and T. L. Ibbs. Thermal diffusion in gases, Gostekhizdat, 1956.
4. H. L. Evans. Mass transfer through laminar boundary layers, 3a Similar solutions of the b-equation, when  $B = 0$  and  $\sigma \geq 0.5$ , Internat. J. Heat and Mass Transfer, 1961, vol. 3, No 1.
5. A. M. Suponitskiy. Self-similar problems of convection diffusion in the presence of heterogeneous chemical reactions with mixed kinetics, PMTF, 1963, No. 2.

## ON FLOWS OF LIQUID WITH FORMATION OF CLOSED CAVITATION CAVITIES

A. Ye. Khoperskov

(Novosibirsk)

Considered is cavitation flowing around bodies on circuit, offered by M. A. Lavrent'yev [1] behind body will be formed closed region, in which liquid circulates; inside this region is included a cavitation recess with constant velocity: at its outer edge; flow is irrotational and velocity everywhere is final (Fig. 1). The problem: to create flow according to given diagram, i.e., to find complex potential  $w(z)$  of flow, if external boundary of flow and number of cavitations are given. Internal boundary (boundary of cavity) is not known beforehand, but two conditions on it are given - it is flow line and velocity on it is constant.

Below is considered a particular case of this problem - flow in infinite region with curvilinear boundary. Presented method will apply also for solution of analogous problem of flow in curvilinear channel.

Let doubly connected region of flow  $D$  be depicted in circular ring  $R < |\zeta| < 1$  boundary of cavity over to internal (Fig. 2) circumference  $C_R$ . For definiteness we will consider that point  $z = \infty$  corresponds to point  $\zeta = 1$ .

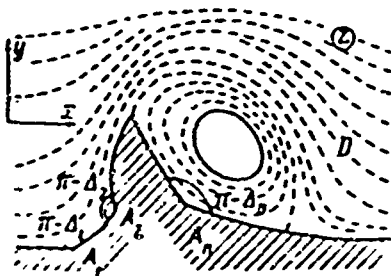


Fig. 1.

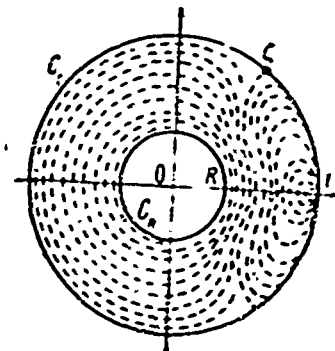


Fig. 2.

We will find complex potential  $w(\zeta)$  of flow in ring, considering that at point  $\zeta=1$  a doublet is located, and circumference  $C_R$  and  $C_1$  will be flow lines

$$w(\zeta) = Qi \left[ \frac{1}{\zeta-1} + \frac{1}{2} - \sum_{n=1}^{\infty} \frac{R^{2n}}{1-R^{2n}} (\zeta^n - \zeta^{-n}) + \frac{\Gamma}{2\pi} \ln \zeta \right] \quad (1)$$

Here  $Q$  - scale factor;  $Q\Gamma$  - circulation of velocity on boundary of cavity;  
 $Q \left[ \frac{1}{2} - (\Gamma / 2\pi) \ln R \right]$  - flow rate on circuit, connecting  $C_1$  with  $C_R$ .

In the future will be demanded derivative

$$\frac{dw}{d\zeta} = \frac{Qi}{\zeta} \left[ -\frac{\zeta}{(\zeta-1)^2} - \sum_{n=1}^{\infty} \frac{nR^{2n}}{1-R^{2n}} (\zeta^n + \zeta^{-n}) + \frac{\Gamma}{2\pi} \right] \quad (2)$$

Let us turn to variable  $u = - (iK / \pi) \ln \zeta$ , where  $K$  is found from relationship

$$R = \exp\left(-\frac{\pi K'}{K}\right) \quad (K'(k) = K(\sqrt{1-k^2}))$$

Here  $K$  and  $K'$  - full elliptic first integrals. Then series in expression (2) it is possible to sum

$$\begin{aligned} \frac{dw}{d\zeta} &= \frac{Qi}{\zeta} \left[ \frac{1}{4} \operatorname{csc}^2 \frac{\pi u}{2K} - 2 \sum_{n=1}^{\infty} \frac{nR^{2n}}{1-R^{2n}} \cos \frac{n\pi u}{K} + \frac{\Gamma}{2\pi} \right] = \\ &= \frac{Qi}{\zeta} \left[ \frac{K^2}{\pi^2} \frac{1}{\operatorname{sn}^2 u} - \frac{K(K-E)}{\pi^2} + \frac{\Gamma}{2\pi} \right] = \frac{Qi}{\zeta} \frac{K^2}{\pi^2} \left[ \frac{1}{\operatorname{sn}^2 u} - \frac{1}{\operatorname{sn}^2 u_0} \right] \end{aligned} \quad (3)$$

Here  $E = E(k)$  - full elliptic second integral,  $\operatorname{sn} u = \operatorname{sn}(u, k)$  - Jacobi's elliptic sine, and  $u_0$  - auxiliary parameter, associated with  $\Gamma$  relationship

$$\frac{1}{\operatorname{sn}^2 u_0} = 1 - \frac{E}{K} - \frac{\pi\Gamma}{2K^2} \quad (4)$$

Parameter  $u_0$  determines position of critical points of flow (points, where  $dw/d\zeta = 0$ ); depending upon quantity  $\Gamma$ , flow can have either two critical points on  $C_1$ , or two critical points on  $C_R$ , or one critical point inside flow.

If boundary has angular point in which angle, turned to flow is larger than  $\pi$ , then, during usual non-cavitational flowing around in this point, velocity turns to infinity. In order to avoid this, according to received diagram, we consider such points branching points of flow (critical points) and to analyze flow with critical points on external boundary of flow.

Based on found function  $w(\zeta)$ , we construct function  $z = f(\zeta)$ , depicting ring  $R \leq |\zeta| \leq 1$  on physical region of flow D. For solution of problem it is sufficient to determine complex velocity of flow

$$\frac{dw}{dz} = \frac{dw}{d\zeta} \frac{d\zeta}{dz}$$

Let us consider function  $\chi(\zeta) = U(r, t) + iV(r, t)$  such, that

$$\frac{dz}{d\zeta} = \frac{e^{i\chi(\zeta)}}{(\zeta-1)^2} \quad (\zeta = re^{it}) \quad (5)$$

Then from (5) we receive

$$U(r, t) = \ln \left| \frac{dz}{d\zeta} \right| + \ln(1 - 2r \cos t + r^2)$$

$$V(r, t) = \arg dz - \arg d\zeta + 2 \arctan \frac{r \sin t}{\cos t - 1}$$

We have

$$|dz/d\zeta| = |dz/dw| \cdot |dw/d\zeta|$$

But on surface of cavity  $|dw/dz| = v_0$ , and, consequently,

$$U(R, t) = \ln |dw/dz|_{r=R} - \ln v_0 + \ln(1 - 2R \cos t + R^2) \quad (6)$$

will be known function of  $t$ .

On circuit  $C_1$  we have  $\arg dz = \theta$  — angle tangential to circuit with axis  $x$ , and  $\arg d\zeta = t + 1/2 \pi$ , consequently,

$$V(1, t) = \theta - 1/2 \pi \quad (7)$$

Angle  $\theta$  as function of  $t$  is not known. If one were to temporarily assume that function  $V(1, t)$ , (7) has been found expression for function  $\chi(\zeta)$ , can be obtained. This allows solution of problem by integral equation.

Regular, in ring  $R < |\zeta| < 1$  single-valued function  $\chi(\zeta)$ , if its real part  $U(R, t)$  on circumference  $C_R$  and imaginary part  $V(1, t)$  on  $C_1$ , is given by following expression;

$$\chi(\zeta) = \frac{1}{2\pi} \int_0^{2\pi} U(R, t) dt + \frac{i}{\pi} \int_0^{2\pi} U(R, t) \sum_{n=1}^{\infty} \frac{R^n}{\zeta^n} [\cos nt (\zeta^n + \zeta^{-n}) - \sin nt (\zeta^n - \zeta^{-n})] dt + \frac{i}{2\pi} \int_0^{2\pi} V(1, t) dt +$$

$$\begin{aligned}
& + \frac{i}{\pi} \int_0^{2\pi} V(1, t) \sum_{n=1}^{\infty} \frac{R^n}{1+R^{2n}} \left[ \cos nt \left( \left( \frac{\zeta}{R} \right)^n + \left( \frac{\zeta}{R} \right)^{-n} \right) - \right. \\
& \quad \left. - t \sin nt \left( \left( \frac{\zeta}{R} \right)^n - \left( \frac{\zeta}{R} \right)^{-n} \right) \right] dt
\end{aligned} \tag{8}$$

If we introduce variable  $u = -t(K/\pi) \ln \zeta$ , then

$$\zeta^n + \zeta^{-n} = 2 \operatorname{ccs} \frac{n\pi u}{K}, \quad \zeta^n - \zeta^{-n} = 2 \sin \frac{n\pi u}{K}$$

Since  $\ln R = -\pi K'/K$ , then

$$\begin{aligned}
\left( \frac{\zeta}{R} \right)^n + \left( \frac{\zeta}{R} \right)^{-n} &= 2 \cos \frac{n\pi}{K} (u - tK') \\
\left( \frac{\zeta}{R} \right)^n - \left( \frac{\zeta}{R} \right)^{-n} &= 2t \sin \frac{n\pi}{K} (u - tK')
\end{aligned}$$

Putting these expressions in formula for  $\chi(\zeta)$ , we receive

$$\begin{aligned}
\chi(\zeta) &= \frac{1}{2\pi} \int_0^{2\pi} U(R, t) dt + \frac{1}{\pi} \int_0^{2\pi} U(R, t) \sum_{n=1}^{\infty} \frac{2R^n}{1+R^{2n}} \cos n \left( t - \frac{\pi u}{K} \right) dt + \\
& + \frac{i}{2\pi} \int_0^{2\pi} V(1, t) dt + \frac{i}{2\pi} \int_0^{2\pi} V(1, t) \sum_{n=1}^{\infty} \frac{2R^n}{1+R^{2n}} \cos n \left( t - \frac{\pi}{K} (u - tK') \right) dt
\end{aligned}$$

But

$$2 \sum_{n=1}^{\infty} \frac{R^n}{1+R^{2n}} \cos nr = \frac{K}{\pi} \operatorname{dn} \frac{Kx}{\pi} - \frac{1}{2}$$

Therefore

$$\chi(\zeta) = \frac{1}{\pi} \int_0^{2\pi} U(R, t) \operatorname{dn} \left( \frac{Kt}{\pi} - u \right) \frac{K}{\pi} dt + \frac{i}{\pi} \int_0^{2\pi} V(1, t) \operatorname{dn} \left( \frac{Kt}{\pi} - u + tK' \right) \frac{K}{\pi} dt \tag{9}$$

Here  $\operatorname{dn} u = \operatorname{dn}(u, k)$  - delta of amplitude, Jacobi's elliptic function. At  $K < |\zeta| < 1$  integrals in formula (9) do not have peculiarities, but at  $|\zeta| = R$  the first of them, and at  $|\zeta| = 1$  second is singular, and in these cases their principal values are put in formula (9).

Now we return to detecting of function  $V(1, t)$ , (7). Considering angle  $\theta$  as function of length of arc  $s$  of circuit, we receive

$$\frac{dV(1, t)}{dt} = \frac{d\theta}{ds} \frac{ds}{dt} \quad \left( \frac{ds}{dt} = \left| \frac{dx}{d\zeta} \right| \cdot \left| \frac{d\zeta}{dt} \right| = \frac{\exp U(1, t)}{2(1 - \cos t)} \text{ at } r=1 \right)$$

Considering curvature of boundary  $d\theta/ds = \kappa(s)$  given, we receive

$$\frac{dV(l, t)}{dt} = p[l, U(l, t)] e^{u(l, t)} \quad (10)$$

where  $p[l, U(l, t)]$  - operator of function  $U(l, t)$

$$p[l, U(l, t)] = \frac{x[s(t)]}{2(1-\cos t)} = \frac{1}{2(1-\cos t)} \times \left[ s(t_0) + \int_{t_0}^t \frac{\exp U(l, t) dt}{2(1-\cos t)} \right]$$

From formula (9) we find  $U(l, t)$

$$U(l, t) = -\frac{1}{\pi} \int_0^{2\pi} \frac{dV(l, \tau)}{d\tau} \ln \left| \frac{1 - \operatorname{dn}[(\tau-t)K/\pi]}{\operatorname{sn}[(\tau-t)K/\pi]} \right| d\tau + \\ + \frac{1}{\pi} \int_0^{2\pi} U(R, \tau) \operatorname{dn} \frac{K}{\pi} (\tau-t) \frac{K}{\pi} d\tau$$

Putting  $dV(l, t) / dt$  from (10) we receive nonlinear integral equation for determination of  $U(l, t)$

$$U(l, t) = \frac{1}{\pi} \int_0^{2\pi} p[\tau, U(l, \tau)] \ln \left| \frac{\operatorname{sn}[(\tau-t)K/\pi]}{1 - \operatorname{dn}[(\tau-t)K/\pi]} \right| e^{U(l, \tau)} d\tau + \\ + \frac{1}{\pi} \int_0^{2\pi} U(R, \tau) \frac{K}{\pi} \operatorname{dn} \frac{K}{\pi} (\tau-t) d\tau \quad (11)$$

Having determined  $U(l, t)$ , place it in (10) and integrated, we receive unknown function  $V(l, t)$ .

Let us consider function

$$y(t) = U(l, t) - g(t) \quad \left( g(t) = \frac{1}{\pi} \int_0^{2\pi} U(R, \tau) \frac{K}{\pi} \operatorname{dn} \frac{K}{\pi} (\tau-t) d\tau \right)$$

Here  $g(t)$  - known function, and crossing to dimensionless quantities, we receive for  $y(t)$  the following equation:

$$y(t) = \lambda \int_0^{2\pi} K(\tau, t, y(\tau)) e^{y(\tau)} d\tau \quad \left( \lambda = \frac{1}{\pi} \frac{Q}{lv_0} \right) \quad (12)$$

Here dimensionless quantities

$$K(\tau, t, y(\tau)) = p_1[\tau, g(\tau) + y(\tau)] \ln \left| \frac{\operatorname{sn}[(\tau-t)K/\pi]}{1 - \operatorname{dn}[(\tau-t)K/\pi]} \right| e^{y(\tau)} \\ p_1[l, u(t)] = \frac{1}{2(1-\cos t)} \times \left[ s(t_0) + \int_{t_0}^t \frac{\exp u(t) dt}{2(1-\cos t)} \right] \\ g_1(t) = g(t) + \ln v_0 - \ln Q$$

do not depend on parameters of  $v_0$  (velocity on surface of cavity),  $Q$  (flow rate) and  $l$  (characteristic dimension of streamlined body);  $\lambda$  — dimensionless parameter (unknown quantity, since flow rate  $Q$  is not previously known).

Besides  $\lambda$ , quantity  $\Gamma$  in formula (1) is also unknown. For their determination we use condition of uniqueness of function  $z = f(\zeta)$ ; for this it is necessary and sufficient that on any closed circuit  $L$  lying in ring  $R \leq |\zeta| \leq 1$

$$\oint \frac{dz}{d\zeta} d\zeta = 0 \quad (13)$$

for circuit  $L$  we take  $C_R$ , using (4), and receive

$$\left. \frac{dz}{d\zeta} \right|_{r=R} = \left. \frac{dz}{d\zeta} \right|_{r=R} \exp \left[ iV(R, t) + 2i \operatorname{arctg} \frac{R \sin t}{1 - R \cos t} \right]$$

and from (8)

$$V(R, t) = \frac{1}{\pi} \int_0^{2\pi} V(1, \tau) d\tau \frac{K}{\pi} (\tau - t) \frac{K}{\pi} d\tau - \\ - \frac{1}{\pi} \int_0^{2\pi} [U(R, \tau) - U(R, t)] \frac{\operatorname{cn}[(\tau - t)K/\pi]}{\operatorname{sn}[(\tau - t)K/\pi]} \frac{K}{\pi} d\tau$$

Here second integral exists, since  $U(R, t)$  satisfies Gelder condition.

Thus, condition (13) gives two equations, which, together with (12), is sufficient for finding solution of  $U(1, t)$  and of parameters  $\lambda$  and  $\Gamma$ . Besides  $Q/v_0 l$ , in problem there is still dimensionless parameter

$$\frac{v_0}{v_\infty} = \sqrt{1 - \sigma} \quad \left( \sigma = \frac{P_\infty - P_0}{\frac{1}{2} \rho v_\infty^2} - \text{number of cavitations} \right)$$

where  $v_\infty$  — velocity of flow at infinity. Parameter  $R$  depends on this relation, where  $R$  — is large at small  $v_0/v_\infty$ , and vice versa. Since to express  $R$  through  $v_0/v_\infty$  and other parameters is very difficult, we will consider flow at various  $R$  and determine  $v_0/v_\infty$  which are obtain here. It is easy to receive

$$v_\infty = e^{-U(1,0)} \lim_{\zeta \rightarrow 1} (\zeta - 1)^2 \left| \frac{dz}{d\zeta} \right| = Q e^{-U(1,0)}$$

It is interesting to consider case when boundary of flow has angular points. Let them correspond to  $\zeta_k = \exp(it_k)$ , and region of flow  $D$  will form,

in these points, angles  $\pi - \Delta_k$  ( $k = 1, \dots, n$ ) (Fig. 1).

We will express, through delta-function, the curvature of circuit

$$x[s(t)] = x^*[s(t)] + \sum_{k=1}^n \Delta_k \delta[s(t) - s(t_k)]$$

where  $x^*[s(t)]$  - piecewise continuous function. For

$$y^*(t) = U(t, t) - g(t) - \frac{1}{\pi} \sum_{k=1}^n \Delta_k \ln \left| \frac{\operatorname{sn}[(t_k - t)K/\pi]}{1 - \operatorname{dn}[(t_k - t)K/\pi]} \right| = U(t, t) - g^*(t)$$

we receive integral equation analogous to (12)

$$y^*(t) = \lambda \int_0^{2\pi} K^*(\tau, t, y^*(\tau)) e^{y^*(\tau)} d\tau \quad (14)$$

where

$$K^*(\tau, t, y^*(\tau)) = p_1^*[\tau, g^*(\tau) + y^*(\tau)] \ln \left| \frac{\operatorname{sn}[(\tau - t)K/\pi]}{1 - \operatorname{dn}[(\tau - t)K/\pi]} \right| e^{y^*(\tau)} \times \\ \times \prod_{k=1}^n \left| \frac{\operatorname{sn}[(t_k - \tau)K/\pi]}{1 - \operatorname{dn}[(t_k - \tau)K/\pi]} \right|^{\frac{\Delta_k}{\pi}} \\ p_1^*[t, u(t)] = \frac{1}{2(1 - \cos t)} x^* \left[ s(t_0) + \int_{t_0}^t \frac{\exp u(t) dt}{2(1 - \cos t)} \right]$$

remaining designations coincide with designations of formula (12).

Question of existence of solution of problem is complicated by the fact that equation (14) must be solved jointly with conditions of (13). If one were to put aside, for the moment, conditions (13), considering knowns  $\lambda$  and  $\Gamma$ , certain conclusions on solvability of fundamental equation (14) can be made.

Function  $K^*(\tau, t, y^*(\tau))$  weakly depends on  $y^*(\tau)$ , since

$$\frac{\min x^*}{2(1 - \cos t)} \leq p_1^*[t, U(t, t)] \leq \frac{\max x^*}{2(1 - \cos t)}$$

and has integrated particulars of type  $\ln|x|$  and  $|x|^{-\Delta_k/\pi}$  at  $x \rightarrow 0$ , since  $\Delta_k < \pi$  (for that, let us agree not to consider flow with region D forming zero angle).

Therefore, not knowing solution, it is possible to estimate integral

$$\int_0^{2\pi} K^*(\tau, t, y^*(\tau)) d\tau = M(t)$$

We assume, for simplicity, that curvilinear part of boundary is located in limited region. Then  $\max M(t)$  on  $0 \leq t \leq 2\pi$  will be finite quantity. Solution of equation (14) can be received by method of successive approximations if

$$\lambda \max M(t) < e^{-1} \quad \text{on } 0 \leq t \leq 2\pi$$

This inequality occurs at  $x^*(s) < 0$ , i.e., if all curvilinear sections are turned, by convexity, in the direction of flow, and also at sufficiently small

$$q = \int_{-\infty}^{+\infty} |x^*(s)| ds$$

i.e., at sufficiently small contribution introduced by curvilinear sections to change of angle of circuit along axis  $x$ .

Let us consider the most simple case - absence in circuit of curvilinear sections. Since  $x^*(s) \equiv 0$ , then  $y^*(t) \equiv 0$ , and we are relieved of necessity to solve integral equation (14). In this case  $V(1, t)$  - step function, determined with accuracy up to unknown parameters of  $t_k$  which determine position of angular points.

In this case, second integral in formula (9) takes form

$$\frac{i}{\pi} \int_0^{2\pi} V(1, t) dn \left( \frac{Kt}{\pi} - u + iK' \right) \frac{K}{\pi} dt = - \frac{i}{\pi} \sum_{k=1}^n \Delta_k \operatorname{am} \left( \frac{Kt_k}{\pi} - u + iK' \right) \quad (15)$$

where  $\operatorname{am} u = \operatorname{am}(u, k)$  - Jacobi amplitude.

It is easy to see that first integral in formula (9) gives solution of problem of flowing around a bubble above an even bottom (Fig. 3). Its solution can be found in appendix to work of Cox and Clayden [2]. Below it is given in designations made earlier.

If one were to make cut CD in region of flow shown in Fig. 3 (z) then region of variation of function

$$\chi = \ln \left( \frac{1}{v_0} \frac{dw}{dz} \right)$$

will have form shown on Fig. 3 (x). Depicting this region in parametric rectangle (Fig. 3 (u))

$$u = - \frac{iK}{\pi} \ln \zeta$$

$$\left( R < |\zeta| < 1, -\pi < \arg \zeta < \pi, R = \exp \left( - \frac{\pi K'}{K} \right) \right)$$

we receive

$$\frac{dw}{dz} = v_0 k^2 \frac{\operatorname{sn}^2 u_0 - \operatorname{sn}^2 u}{(\operatorname{dn} u_0 + \operatorname{dn} u)^2}$$

Using expression (3) for  $dw/d\zeta$ , we find

$$\frac{dz}{d\zeta} = \frac{dw}{d\zeta} \frac{d\zeta}{dw} = i \frac{QK^2}{\pi^2 v_0 k^2} \frac{1}{\zeta} \left( \frac{dn u_0 + dn u}{sn u_0 sn u} \right)^2$$

This formula gives solution of problem of bubble above even bottom, and simultaneously allows to calculate first integral in formula (9)

$$\frac{1}{\pi} \int_0^{2\pi} U(R, t) \sin \left( \frac{Kt}{\pi} - u \right) \frac{K}{\pi} dt = \ln \left[ i \frac{QK^2}{\pi^2 v_0 k^2} \frac{(\zeta - t)^2}{\zeta} \left( \frac{dn u_0 + dn u}{sn u_0 sn u} \right)^2 \right] \quad (16)$$

and, during absence of curvilinear sections, we receive from formulas (15), (16), and (5)

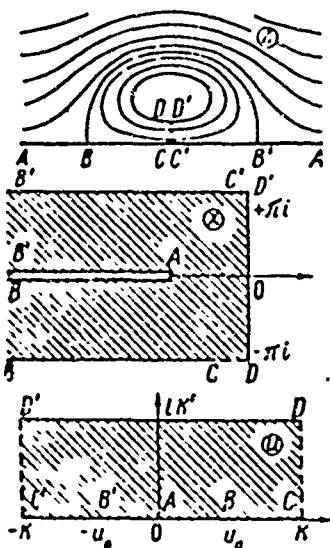


Fig. 3.

$$\frac{dz}{d\zeta} = \frac{iQK^2}{\pi^2 v_0 k^2} \frac{1}{\zeta} \left( \frac{dn u_0 + dn u}{sn u_0 sn u} \right)^2 \prod_{j=1}^n \left[ \operatorname{cn} \left( \frac{Kt_j}{\pi} - u + iK' \right) + i \operatorname{sn} \left( \frac{Kt_j}{\pi} - u + iK' \right) \right]^{-\Delta_j / \pi} \quad (17)$$

In solution of (17) enters  $n$  unknown parameters of  $t_j$  and unknown scale factor  $Q$ . Parameter  $u_0$  (through it is determined  $\Gamma$ , with the help of relationship (4)) is equal to  $Kt_0 / \pi$ , where  $t_0$  coincides with that from  $t_j$  for which  $\Delta_j < 0$  — this angular point should be branching point of flow. For the time being we consider that such an angular point is singular.

If obstacle is given, then lengths of  $(n - 1)$  - th section  $l_{j, j+1}$ , between angular points  $A_j$  and  $A_{j+1}$ ; are known; for determination of parameters of  $t_j$  and  $Q$  we obtain  $n - 1$  transcendent equation

$$l_{j, j+1} = \int_{t_j}^{t_{j+1}} \left| \frac{dz}{d\zeta} \right|_{r=1} dt = \frac{Q}{v_0} \frac{K^2}{k^2 \pi^2} \int_{t_j}^{t_{j+1}} \left( \frac{dn u_0 + dn(Kt/\pi)}{sn u_0 sn(Kt/\pi)} \right)^2 \times \prod_{i=1}^n \left| \frac{t - dn[(t_i - t)K/\pi]}{sn[(t_i - t)K/\pi]} \right|^{-\Delta_i / \pi} dt \quad (j = 1, \dots, n-1) \quad (18)$$

Joining two equations to them, ensuing from condition (13) of single-value of function  $z(\zeta)$

$$\int_0^{2\pi} \left( dn^2 u_0 \operatorname{sn}^2 \frac{Kt}{\pi} + \operatorname{cn}^2 \frac{Kt}{\pi} \right) \cos \gamma(t) dt = 0 \quad (19)$$

$$\int_0^{2\pi} \left( dn^2 u_0 \operatorname{sn}^2 \frac{Kt}{\pi} + cn^2 \frac{Kt}{\pi} \right) \sin \gamma(t) dt = 0$$

$$\left( \gamma(t) = -2 \operatorname{arc} \tan \frac{cn(Kt/\pi)}{dn u_0 \operatorname{sn}(Kt/\pi)} - \sum_{j=1}^n \frac{\Delta_j}{\pi} \operatorname{am} \frac{K}{\pi} (t_j - t) \right) \quad (20)$$

We arrive at a system of  $(n + 1)$  - th equations for determination of  $(n + 1)$  - th unknown:  $t_1, \dots, t_n$  and  $Q$ .

If however there are several points  $A_k$  for which  $\Delta_k < 0$ , generally, it would be necessary to consider triply, and more, connected region of flow  $D$ . During existence of two such points  $A^*$  and  $A^{**}$  region of flow will be doubly connected and fits our consideration if  $t^*$  and  $t^{**}$  corresponding to them are coupled by relationship  $t^{**} = -t^*$ ; this relationship can be satisfied if one were to decrease, per unit, the number of equations (18), (19), and (20). This can be done in two cases: if obstacle is taken as symmetric, equation (20) is transformed to identity  $\gamma(t)$  in this case is odd function of  $t$  and if we consider the previously unknown length of one of sections  $l_{j,j-1}$ .

Thus, the proposed problem has been reduced to solution of an integral equation, the solvability of which is clear for convex and for slightly bent obstacles. For circuits in the form of broken line, solution is written in closed form, but for determination of parameters it is necessary to solve system of transcendent equations.

Submitted  
13 March 1963

#### Literature

1. M. A. Lavrent'yev. Variational method in boundary value problems for systems of equations of elliptic type. Pub. House of Academy of Sciences of the USSR, 1962.
2. R. N. Cox and W. A. Clayden. Air entrainment at the Rear of a Steady Cavity. In coll. Cavitation in Hydrodynamics, London, 1956.

ON CRACKS SPREADING BETWEEN FLAT PLATES ON RECTILINEAR  
BOUNDARY OF GLUING

R. V. Gol'dstein and R. L. Salganik

(Moscow)

Propagation of cracks at place of gluing between two elastic materials differs by a number of peculiarities from well-studied (see survey [1]) propagation of cracks in uniform materials.

During quasi-static advance of end of crack in uniform material, local symmetry has a place, i.e., near this end only normal stresses act, symmetrically distributed relative to direction of propagation. Furthermore, form of crack and distribution of cohesive forces in terminal region of quasi-statically advancing end do not depend on applied loads (hypothesis of autonomy of terminal region).

Crack spreading on boundary of gluing between two elastic materials only in exceptional cases possesses these properties. In general, its behavior is different. In terminal region of such a crack, because of bulging of sides due to inequality of properties of glued bodies, overlap of one side on other occurs. In places of overlap appear forces of reaction influencing advance of ends of crack. Local symmetry in general, is also absent. On continuation of crack, near its end appear both sheering and normal stresses.

Nevertheless, if points of overlap of opposite sides are concentrated only near ends of crack, the hypothesis of autonomy can be generalized [2]. Generalized hypothesis of autonomy turns out to be equivalent to assumption about constancy of work, which reciprocal forces of opposed sides of crack distributed in the small terminal region produce, during formation of unit of length of crack.

For experimental check of permissibility of such assumption, it is necessary to obtain from it a number of results. In connection with this, in offered work are considered two problems of propagation of cracks along rectilinear boundary of gluing: the first problem about

a tension crack, caused by given normal stresses; the second - about wedging along boundary by a strictly smooth, semi-infinite wedge of constant thickness.

1. Rectilinear crack stretched by normal stresses under the conditions of flat deformation. Let us consider typical problem of theory of cracks. In infinite body, along axis  $x$  from  $x = 0$  to  $x = l$  is located a crack. At infinity to body are applied compressing stresses  $\sigma_y = -p$  ( $p > 0$ ). Crack is stretched in the middle by concentrated forces equal by absolute magnitude  $P$  and directed on perpendicular to crack. As always, it is necessary at first, to solve problem, assuming that crack and loads applied to its surface are absent. Then it is necessary to solve problem of a crack loaded on surface by forces and stresses applied to it equal to and opposite those which were obtained in first problem at place of discovery of crack. Here it is considered that other loads are absent. Sum of solutions of both problems, on account of linearity, will be solution of initial problem.

Materials on both sides of axis  $x$  are identical, solution of first problem in stresses will be

$$\sigma_y = -p, \quad \sigma_x = 0, \quad \tau_{xy} = 0 \quad (1.1)$$

If, however, these materials are not identical, then, assuming that gluing is not disturbed and that deformations of a thin layer of glue can be disregarded, we receive another solution. This solution, obviously, does not depend on  $x$  and in stresses has form

$$\begin{aligned} \sigma_y = -p, \quad \sigma_x = -\frac{\nu_1}{1-\nu_1} p, \quad \tau_{xy} = 0, \quad y > 0 \\ \sigma_y = -p, \quad \sigma_x = -\frac{\nu_2}{1-\nu_2} p, \quad \tau_{xy} = 0, \quad y < 0 \end{aligned} \quad (1.2)$$

where  $\nu$  - Poisson's ratio. Here, and in the future, by indices 1 and 2 will be marked quantities relating respectively to upper and lower half-spaces. From (1.2) ensures that presence of compressing stresses perpendicular to boundary leads to appearance of longitudinal compression where corresponding compressing stresses in both glued parts are different.

In contrast to preceding case, stress state described by formulas (1.2) is nonuniform. This is connected with the fact that formulas of (1.2) represent solution of problem of a strip glued along axis  $x$  from two different strips and compressed evenly by stresses distributed on its edges. Solution of (1.2) does not depend on stripwidth and therefore width of strip is considered infinite.

Turning to solution of second problem of a crack loaded on surface we will use, at  $y > 0$ , formulas of N. I. Muskhelishvili [3]

$$\begin{aligned} \sigma_x + \sigma_y &= 4 \operatorname{Re} \Phi(z), & \sigma_y - i\tau_{xy} &= \Phi(z) + \Omega(\bar{z}) + (z - \bar{z}) \overline{\Phi'(z)} \\ 2\mu_1 \left( \frac{\partial u}{\partial x} + i \frac{\partial v}{\partial x} \right) &= \kappa_1 \Phi(z) - \Omega(\bar{z}) - (z - \bar{z}) \overline{\Phi'(z)} \end{aligned} \quad (1.3)$$

where  $\mu$  - shear modulus;  $\kappa = 3 - 4\nu$ ,  $z = x + iy$ . In considered case, functions  $\Phi$  and  $\Omega$  in these formulas have form [4]

$$\begin{aligned} \Phi(z) &= \frac{1}{m} \Omega(z) = \frac{1}{2\pi i Z(z)} \int_0^l \frac{\varphi(t) Z(t+i0)}{t-z} dt \\ Z(z) &= z^{\beta} (z-l)^{\beta} (z+l)^{\beta}, & \beta &= \frac{1}{2\pi} \ln m, & m &= \frac{\mu_1 + \mu_2 \kappa_1}{\mu_2 + \mu_1 \kappa_2} \end{aligned} \quad (1.4)$$

Here

$$(\sigma_y - i\tau_{xy})_{z=x-i0} = (\sigma_y - i\tau_{xy})_{z=x+i0} = \varphi(x), \quad \lim_{z \rightarrow \infty} (Z(z)/z) = 1$$

Quantity  $\beta$  will be considered nonnegative. This can always be done, numbering glued bodies in the appropriate way.

Surface of crack is loaded by normal stresses of concentrated forces and by stresses of action of elastic field (1.2). This gives

$$\varphi(x) = p - P_0 (x - l/2) \quad (0 < x < l) \quad (1.5)$$

Due to symmetry of problem concerning line of action of concentrated forces, ends of crack are always disposed at identical distances from this line. Therefore, about propagation of crack, it is possible to judge, for example, by behavior of left end  $x = 0$  and to consider value  $x < (l/2)$ . Behavior of left end of crack is wholly determined by elastic field in its small environment.

From given solution, we find that on continuation of crack in this environment  
 $(z = x = -s, \quad s \rightarrow +0)$

$$\sigma_y - i\tau_{xy} = -\frac{1}{\sqrt{s}} \left\{ \left( \frac{s}{l+s} \right)^{1/2} (A_0 + iB_0) + c(1) \right\} \quad (1.6)$$

Opening of crack  $[u + iv]$ , equal to difference of displacements of its upper and lower sides at corresponding points, with accuracy within small [values] of a higher order, is determined when  $x \rightarrow +0$  by expression

$$[u + iv] = M \sqrt{x} \left( \frac{x}{l-x} \right)^{1/2} ((B_0 - 2\beta A_0) - i(A_0 + 2\beta B_0)) \quad (1.7)$$

Here  $M$  — certain positive quantity depending on elastic constants. Quantities  $A_0$  and  $B_0$  are expressed through applied loads in following manner

$$A_0 = -\frac{1}{2\pi} \frac{1+m}{\sqrt{l}} \frac{1+m}{\sqrt{m}} P + \frac{\sqrt{l}P}{2}, \quad B_0 = \beta P \sqrt{l} \quad (1.8)$$

From (1.7) it seems that during approach toward the end of crack, upper side would infinitely frequently intersect with the lower located beneath it. Actually this does not occur. Opposite sides of crack overlap one on the other. In places of overlap reaction forces appear, which it is necessary to add to already considered forces acting on surface of crack. To these forces it is necessary to add also cohesive forces of opposite sides of the crack which act near ends of crack. As a result, in formulas (1.6) and (1.7) instead of  $A_0, B_0$  it is necessary to place  $A_0 + A'$  and  $B_0 + B'$ , where quantities  $A', B'$  account for action of reactive forces and cohesive forces.

If given end of crack is in equilibrium, there should be

$$A_0 + A' = 0, \quad B_0 + B' = 0 \quad (1.9)$$

Here, in end of crack, sides are smoothly closed and stress in continuation of crack become terminal. Condition of (1.9) known for cracks in uniform materials as hypothesis of S. A. Khristianovich [5], was later proven with the help of variational principles [6, 7]. By the same method, it can be proven

also for cracks spreading on boundary of gluing [2].

Size of region of action of reactive forces can be various, depending upon relationship between loads  $p$  and  $p_*$ . If tensile force  $P$  is sufficiently great, points of overlap will appear only in the small terminal region. Actually, oscillatory character of dependence (1.7) disappears when  $x > x_*$ , where

$$x_* = l e^{-\pi/2\beta} (1 + e^{-\pi/2\beta})^{-1} \quad (1.10)$$

It is easy to show that  $\beta < (\ln x_*)/2\pi$ . Since Poisson's ratio  $\nu$  is always nonnegative, then, for all materials,  $x_* < 10^{-4}l$ . Derivative  $x$  on quantity [1], calculated without account of reactive forces and cohesive forces, at point  $x = x_*$  is equal  $-M(A_0 + 2\beta B_0)$ . If this derivative is positive, then the more to the right  $x = x_*$  upper side is located above the lower. From character of distribution of applied loads, it is clear that from this place and further, up to middle of crack, upper side will remain above lower. Condition of positiveness of derivative, taking into account expressions of (1.8) for  $A_0$ ,  $B_0$ , is reduced to inequality

$$P > P_*(l) \equiv \frac{pR \sqrt{ml}}{1+m} (1 + 4\beta^2) \quad (1.11)$$

Thus, during fulfillment of inequality (1.11), reactive forces and cohesive forces clearly act in small end region. This region remains small also, when  $P_*(l)$  somewhat exceeds  $P$ . When  $P_*(l)$  greatly exceeds  $P$ , size of region of action of reactive forces ceases to be small compared with length of crack.

A necessary condition of application of generalized hypothesis of autonomy is smallness of end region. Let us assume that this condition is satisfied. As was already noted, generalized hypothesis of autonomy is reduced to requirement of constancy of work of  $T$ , produced by forces of interaction of opposite sides of crack, during formation of unit of length of crack during quasi-static advance of its end. Quantity  $T$  is expressed through  $A'$ ,  $B'$  by the formula of [2]

$$T = \frac{\pi}{2} \frac{(\mu_1 + \mu_2 x_1)(\mu_2 + \mu_1 x_2)}{\mu_1 \mu_2 [\mu_2 (x_1 + 1) + \mu_1 (x_2 + 1)]} (A'^2 + B'^2) \quad (1.12)$$

Hence, from conditions of equilibrium (1.9) and formulas of (1.8) we obtain following expression for length  $\underline{l}$  of mobile-equilibrium crack

$$l = \frac{1+m}{\pi \sqrt{m(1+4\beta^2)}} \left\{ \frac{P}{p} + \frac{4T}{np^2} \pm 2 \sqrt{\frac{4T^2}{n^2 p^4} + \frac{2PT}{np^2} - \beta^2 \frac{P^2}{p^2}} \right\}$$

$$(n = \sqrt{(\mu_1 + \mu_2 x_1)(\mu_2 + \mu_1 x_2) / \mu_1 \mu_2})$$

In Fig. 1 is given graph of dependence of length  $\underline{l}$  of mobile-equilibrium

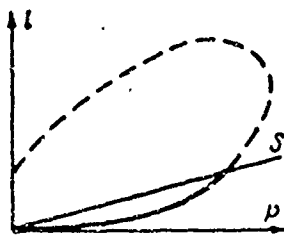


Fig. 1.

crack on quantity of concentrated force  $P$ , stretching

crack. This graph is a loop located in the

first quarter of plane  $P\underline{l}$ . In Fig. 1 is also

depicted straightline  $S (P = P_*(l))$ . Under

this straightline, and near it (above it) lie

points to which small end region corresponds,

and for which, consequently, application of generalized hypothesis of autonomy is permissible.

According to this hypothesis, during increase of load  $P$ , length of crack  $\underline{l}$  remains unchanged so long as quantity  $P$  does not attain value corresponding to given length  $\underline{l}$  on curve  $l(P)$ . If length  $\underline{l}$  is sufficiently small, after load  $P$  attains indicated value, quasi-static increase of length of crack begins on curve  $l(P)$ . Within limits of generalized hypothesis of autonomy, after this increase, it is possible to trace only up to values of  $\underline{l}$  which exceed somewhat length  $\underline{l}_1$ . This corresponds to point of intersection of straightline  $S$  with curve  $l(P)$ . It is easy to show that in region of such values of  $\underline{l}$ , dependence  $l(P)$  is single-valued.

For the largest values of  $\underline{l}$ , use of generalized hypothesis of autonomy is not possible, because terminal region of crack ceases to be small compared with length of crack. However, one can assume that for sufficiently large values

of length of initial crack quasi-static development, during increase of  $P$ , cannot continue indefinitely. Such an assumption is derived in the following manner.

During decrease of tensile force  $P$ , the crack is closed. In uniform material this would not lead to advance of its ends, in the interior of body. If however, materials, among which crack is located, are different, then, near ends of crack, small areas of contact will alternate with places where crack is open. As a result, on extent of crack concentration of stresses will appear. Due to this, ends will advance into interior of body. Increase of length of crack, during compression, is a characteristic peculiarity of brittle fracture of glued bodies. If we now start to increase tensile force  $P$ , this will lead to lowering of concentration of stresses, and ends of crack will stop. They, apparently, will remain motionless as long as the main part of crack is not freed from sites of contact and these sites are not concentrated near ends (full disappearance of sites of contact, as was already shown is generally impossible). In Fig. 1 to such a process corresponds transference of point depicted on horizontal above straightline  $S$  up to this straightline. During further increase of load  $P$ , body should be fractured, since by assumption, initial length of crack significantly exceeds quantity  $l_1$ , and from generalized hypothesis of autonomy in this case it ensures that equilibrium crack does not exist.

During infinite increase of compressing load  $p$ , characteristic length  $l_1$  aspires to zero. Together with it, minimum length of equilibrium crack decreases. This phenomenon is analogous to that, which takes place for crack in uniform material, stretched to infinity by stresses normal to the crack. Maximal equilibrium length of such a crack aspires to zero during infinite increase of tensile load (see, for example, [1]). However, an above mentioned interesting peculiarity of the considered case is the fact that this phenomenon sets in during compression, but not during tension.

If compressive stresses  $p$  decrease, then region under straightline S is increased, and within limit  $p \rightarrow 0$  occupies entire first quarter. Intersection point of curve  $l(P)$  with straightline S here departs to infinity. Thus, when only tensile loads act on crack, end region is always small, which is a necessary condition of application of generalized hypothesis of autonomy. Applying this hypothesis, we receive, for case  $p = 0$  a result, not qualitatively different from corresponding result for crack in uniform body.

We note also that if distinction in properties of glued bodies disappears, loop in Fig. 1 is turned into open curve departing to infinity, and straightline S occupies a certain limited position. Above this straightline, as before, lie points corresponding to case of mutual overlap of opposite sides of crack. But now stresses on extent of cracks are final, and a crack remains motionless during any changes of  $P$  in interval  $0 < P < P_*(l)$ . At  $P > P_*(l)$  spread of crack occurs, as was already described for small length  $l$  of, when glued materials are dissimilar. The only distinction is that now a part of the mobile-equilibrium development is not limited. At very large values of compressing stress  $p$ , influence of specific surface energy  $T$  becomes insignificant, and within limit, curve  $l(P)$  becomes straightline  $P = P_*(l)$ . Thus, in the same manner, without regard for cohesive forces, the problems of cracks in uniform rocks (see survey [1]), where large compressing stresses are caused by pressure of the overlying rock strata, are considered.

If a crack spreads in a non-uniform layer, and on the boundary between two uniform layers with various elastic properties, then at large values of compressing stresses, calculation of specific surface energy becomes immaterial in a certain intermediate interval of quasi-static development of the crack. This intermediate interval is wider, the less the distinction between properties of layers, and within limit when distinction disappears it becomes unlimited from above.

In problem analyzed in this paragraph, terminal region was small only during definite relationship between loads. Another case, when terminal region is always small, is represented by problem of wedging.

2. Wedging along glued boundary by wedge of constant thickness. Let us assume that along boundary of gluing (axis  $x$ ) is inserted a rigid, smooth, semi-infinite wedge of constant thickness  $2h$ , so that end formed before it a free crack of length  $l$  at origin of coordinates. Wedge itself is located in interval  $l < x < \infty$ . We assume also that to the wedge — body system no external forces are applied. Thickness of wedge  $2h$  will be considered small comparatively with length of free crack. The problem can be solved in linear placement analogous to that for problem of a uniform body [8]. Here boundary conditions fall on axis  $x$ . Assumption about smoothness of wedge means that friction is absent, on its sides, i.e., shear stresses are equal to zero. Since thickness of wedge is constant, along it transverse displacement  $v$  remains constant. Surface of crack is considered not loaded. Thus, we have

$$\begin{aligned} \tau_{xy} = 0, \quad \sigma_y = 0 & \quad (0 < x < l, \quad y = \pm 0) \\ (\partial v / \partial x) = 0, \quad \tau_{xy} = 0 & \quad (l < x < \infty, \quad y = \pm 0) \end{aligned}$$

Solution of problem of wedging at  $y > 0$  is given by formulas Muskhelishvili (1.2). On basis of results of work [4], it can be shown that

$$\Omega = m\Phi \tag{2.1}$$

where  $\Phi$  — function analytic in entire plane of complex variable  $z = x + iy$ , except perhaps, semiaxis  $x > 0$ . This function at  $z \rightarrow \infty$  becomes zero, and on semiaxes  $x > 0$  satisfies following boundary conditions:

$$\begin{aligned} \Phi(x + i0) + m\Phi(x - i0) = 0, \quad \text{Im } \Phi(x \pm i0) = 0 \\ (0 < x < l) \qquad \qquad \qquad (l < x < \infty) \end{aligned} \tag{2.2}$$

Introducing function  $\bar{\Phi}(z) \equiv \overline{\Phi(\bar{z})}$ , prob'em (2.2) can be reduced to conjugate problem for system of two functions [9]. In given case, problem for the system,

with the help of simple conversions, reduces to Riemann problem for one function [9, 11]. In result of solution of this problem is obtained,

$$\Phi = \frac{C}{\sqrt{z(z-l)}} \exp \left\{ i\beta \ln \frac{\sqrt{z-l} - i\sqrt{l}}{\sqrt{z-l} + i\sqrt{l}} \right\} \quad (2.3)$$

Here, at  $z = x < 0$

$$\sqrt{z-l} = i\sqrt{l-x}, \quad \sqrt{z(z-l)} = i\sqrt{x(x-l)} \quad (2.4)$$

and imaginary part of logarithm is equal to zero.

Constant C, in expression (2.3), is determined from condition, that opening of crack  $[v]$  during change of  $x$  from 0 to  $\underline{l}$ , changed from zero to  $2h$ . This constant is equal to

$$C = -\frac{4h}{\pi\beta} \operatorname{ch} \pi\beta \quad (2.5)$$

Investigating, as and in preceding paragraph, elastic field near end of crack, it is possible to show that size of region of action of reactive forces is always small as compared with length of crack  $\underline{l}$ . Application of generalized hypothesis of autonomy leads to following expression for length  $\underline{l}$  of a mobile-equilibrium crack

$$l = \frac{8h^2 \mu_1 \mu_2 c t^2 \pi \beta}{\pi T [\mu_2 (\kappa_1 + 1) + \mu_1 (\kappa_2 + 1)]} \quad (2.6)$$

where T specific surface energy.

Thus, as in analogous problem of wedging of uniform material, length of free crack  $\underline{l}$  is proportional to square of thickness of wedge  $2h$ . If elastic properties of glued bodies were identical, then in each of these bodies wedge would deepen by quantity  $h$ . In general, quantities of deepenings,  $h_1$  and  $h_2$ , first and second media, accordingly, are equal to

$$h_1 = 2h \left( 1 + \frac{\kappa_1 + 1}{\kappa_1 + 1} \frac{\mu_1}{\mu_2} \right)^{-1}, \quad h_2 = 2h \left( 1 + \frac{\kappa_2 + 1}{\kappa_2 + 1} \frac{\mu_2}{\mu_1} \right)^{-1} \quad (2.7)$$

Received qualitative and quantitative results it can be checked by experiment. In particular, using these results, one can find experimentally specific

surface energy  $T$ , and verify if it remains constant during change of external parameters.

Authors thank G. I. Barenblatt for suggestion to study questions analyzed here, and for constant attention to the work. Authors thank S. S. Grigoryan for discussion of results of work.

Institute of Mechanics  
Moscow State University

Submitted  
11 June 1967

#### Literature

1. G. I. Barenblatt. Mathematical theory of equilibrium cracks formed during brittle fracture. PMTF 1961, No 4.
2. R. L. Salganik. On brittle fracture of glued bodies. PMM, 1963, vol. XXVII, issue 5.
3. N. I. Muskhelishvili. Certain basic problems of mathematical theory of elasticity. Pub. House of Acad. of Sci. of USSR, 1954.
4. G. P. Cherepanov. On stressed state in nonuniform plate with notches. Pub. House of Academy of Sciences of USSR, OTN, Mechanics and machine building, 1962, No 1.
5. Yu. P. Zheltov and S. A. Khristianovich. On mechanism of hydraulic rupture of oil-bearing layer. Pub. House of Acad. of Sci. of USSR, OTN, 1955, No 5.
6. G. I. Barenblatt. On conditions of finiteness in mechanics of solid media, Static problems of theory of elasticity, PMM, 1960, vol. XXIV, issue 2.
7. G. I. Barenblatt and G. P. Cherepanov. On finiteness of stresses on edge of arbitrary crack, PMM, 1961, vol. XXV, issue 4.
8. G. I. Barenblatt. On certain problems of theory of elasticity, appearing during investigation of mechanism of hydraulic rupture of oil-bearing layer. PMM, 1956, vol. XX, issue 4.
9. N. I. Muskhelishvili. Singular integral equations. Fizmatgiz, 1962.
10. F. D. Gakhov. Boundary value problems. Fizmatgiz, 1963.
11. M. A. Lavrent'yev and B. V. Shabat. Methods of theory of functions of the complex variable, Fizmatgiz, 1958.

## EQUILIBRIUM CRACKS IN STRIP OF FINITE WIDTH

I. A. Markuzon

(Moscow)

Considered is problem of determination of length of equilibrium crack formed in strip of finite width under the conditions brittle fracture. With this aim, initially, is solved problem of distribution of stresses near slit of certain given length, and then results of work [1] are used, allowing to determine size of equilibrium crack depending upon applied loads. In connection with this, consideration is initially conducted without regard for cohesive forces acting near tip of crack.

Simultaneously considered is analogous problem of crack having form of round disk in plate of finite thickness.

1. Formulation of problem. Let us consider a strip of width  $2h$ , axis of symmetry of which we will take for axis of abscissas. Axis of ordinates  $y$  we direct upwards. Let on boundary of strip, i.e., at  $y = \pm h$ , distributed breaking load act of intensity  $p(x)$  symmetric with respect to axis ordinates and abscissas. We will create, in proximity of origin of coordinates along axis of abscissas, a crack (cut). Then under action of applied system of loads a crack will occur (Fig. 1), in general, of certain equilibrium length  $2a$ . Removing stresses on boundary of strip and considering, in view of symmetry, a halfstrip, we obtain following boundary conditions:

at  $y=0$

$$\tau_{xy} = 0 \quad (|x| < \infty) \quad (1.1)$$

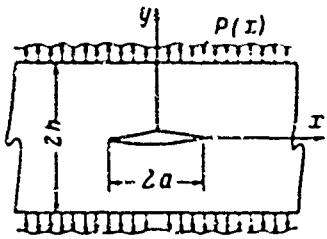


Fig. 1.

$$\begin{aligned} \sigma_y &= -g(x) & (|x| < a) \\ v &= 0 & (|x| \geq a) \end{aligned} \quad (1.2)$$

at  $y = h$

$$\tau_{xy} = 0, \quad \sigma_y = 0 \quad (|x| < \infty) \quad (1.3)$$

Here  $g(x)$  — stress appearing in solid strip on axis  $x$  from application of loads taking stresses on boundary.

2. Obtaining of integral equations. Following the method presented in Sneddon's book [2], and considering symmetry, we take following expressions for components stress tensor and displacement:

$$\sigma_y = -\frac{2}{\pi} \int_0^{\infty} \xi^2 G(y, \xi) \cos \xi x d\xi, \quad \tau_{xy} = \frac{2}{\pi} \int_0^{\infty} \xi \frac{dG}{dy} \sin \xi x d\xi \quad (2.1)$$

$$v = \frac{2(1+\nu)}{\pi E} \int_0^{\infty} \left[ (1-\nu) \frac{d^2 G}{dy^2} - (2-\nu) \xi^2 \frac{dG}{dy} \right] \cos \xi x \frac{d\xi}{\xi^2} \quad (2.2)$$

where

$$G(\xi, y) = (A + B\xi y) \operatorname{ch} \xi y + (C + D\xi y) \operatorname{sh} \xi y$$

Functions  $A(\xi), B(\xi), C(\xi), D(\xi)$  are determined from boundary conditions of problem.

Shown system of stresses and displacements satisfies equations of equilibrium and compatibility (components  $\sigma_x$  and  $u$  here are not written out). Using boundary conditions (1.1) and (1.3), we obtain system of three equations for  $A, B, C, D$ , whence, in particular, it follows

$$A(\xi) = \frac{\operatorname{sh}^2 \xi h - \xi^2 h^2}{\xi h + \operatorname{sh} \xi h \operatorname{ch} \xi h} B(\xi) \equiv H(\xi h) B(\xi)$$

We now demand fulfillment of boundary conditions (1.2). As a result, considering  $x = ax_1, \lambda = a\xi, h = a\delta$ , we obtain following system of dual integral equations:

$$\begin{aligned} \int_0^{\infty} \lambda H(\delta \lambda) B_1(\lambda) \cos \lambda x_1 d\lambda &= g_1(x_1), & \int_0^{\infty} B_1(\lambda) \cos \lambda x_1 d\lambda &= 0 \\ & (0 < x_1 < 1) & & (x_1 > 1) \\ \left( g_1(x_1) = \frac{\pi}{2} a^2 g(ax_1) \right) & & \left( B_1(\lambda) = \frac{\lambda}{a} B\left(\frac{\lambda}{a}\right) \right) & \end{aligned} \quad (2.3)$$

Let us note that displacement  $v = v^0$  and stress  $\sigma_v = \sigma_v^0$  at points of axis of abscissas are determined by formulas

$$v^0 = \frac{4(1-\nu^2)}{\pi k a^3} \int_0^{\infty} B_1(\lambda) \cos \lambda x_1 d\lambda, \quad \sigma_v^0 = -\frac{2}{\pi a^2} \int_0^{\infty} \lambda H(\delta\lambda) B_1(\lambda) \cos \lambda x_1 d\lambda \quad (2.4)$$

3. Reduction of system of dual integral equations to one Fredholm equation of second kind. Integrating the first of equations (2.3) from 0 to  $x$ , we obtain system

$$\int_0^{\infty} B(\lambda) H(\delta\lambda) \sin \lambda x d\lambda = G(x) \quad (0 < x < l) \quad \left( G(x) = \int_0^x g_1(\xi) d\xi \right) \quad (3.1)$$

$$\int_0^{\infty} B(\lambda) \cos \lambda x d\lambda = 0 \quad (x > l) \quad (3.2)$$

(index for  $B_1$  and  $x_1$  is omitted).

We will introduce new function  $\varphi(\lambda)$  is following form

$$B(\lambda) = \int_0^l \varphi'(t) J_0(\lambda t) dt \quad (3.3)$$

( $J_0$  - Bessel function of zero order).

On basis of formula

$$\int_0^{\infty} J_0(\lambda t) \cos \lambda x d\lambda = \begin{cases} (l^2 - x^2)^{-1/2} & (x < l) \\ 0 & (x > l) \end{cases}$$

equation (3.2) satisfies identity with the help of (3.3). We present equation (3.1) in following form:

$$\int_0^{\infty} B(\lambda) \sin \lambda x d\lambda + \int_0^{\infty} H_1(\delta\lambda) B(\lambda) \sin \lambda x d\lambda = G(x) \quad (0 < x < l) \\ (H_1(\delta\lambda) = H(\delta\lambda) - 1) \quad (3.4)$$

First component in (3.4), with the help of relationship (3.3) and formula

$$\int_0^{\infty} J_0(\lambda t) \sin \lambda x d\lambda = \begin{cases} 0 & (x < t) \\ (x^2 - t^2)^{-1/2} & (x > t) \end{cases}$$

will convert in following manner:

$$\int_0^{\infty} B(\lambda) \sin \lambda x d\lambda = \int_0^l \varphi'(t) dt \int_0^{\infty} \sin \lambda x J_0(\lambda t) d\lambda = \int_0^l \frac{\varphi'(t) dt}{\sqrt{x^2 - t^2}} \quad (3.5)$$

Integrating by parts (3.3), we obtain

$$B(\lambda) = \varphi(1) J_0(\lambda) + \lambda \int_0^1 \varphi(t) J_1(\lambda t) dt \quad (\varphi(0) = 0) \quad (3.6)$$

If we now place (3.6) in second component of left part of equation (3.4) and consider (3.5), then equation (3.4) can be written

$$\int_0^x \frac{\varphi'(t) dt}{\sqrt{x^2 - t^2}} + \varphi(1) A_1(x; \delta) + \int_0^1 A_2(x, t; \delta) \varphi(t) dt = G(x) \quad (0 < x < 1) \quad (3.7)$$

where

$$A_1(x; \delta) = \int_0^\infty H_1(\delta \lambda) J_0(\lambda) \sin \lambda x d\lambda$$

$$A_2(x, t; \delta) = \int_0^\infty \lambda H_1(\delta \lambda) J_1(\lambda t) \sin \lambda x d\lambda$$

We will introduce function  $f(x)$  by following relationship

$$f(x) = \int_0^x \frac{\varphi'(t) dt}{\sqrt{x^2 - t^2}} \quad \text{or} \quad \varphi(t) = \frac{2}{\pi} \int_0^t \frac{r f(r) dr}{\sqrt{t^2 - r^2}} \quad (3.8)$$

Using (3.8) and changing order of integration in iterated integral, we obtain from (3.7) the Fredholm integral equation with Kernel having a removable discontinuity

$$f(x) + \frac{2}{\pi} \int_0^1 [L(x, v; \delta) + K(x, v; \delta)] f(v) dv = G(x) \quad (0 < x < 1) \quad (3.9)$$

where

$$L(x, v; \delta) = \frac{v A_1(x; \delta)}{\sqrt{1 - v^2}}, \quad K(x, v; \delta) = v \int_0^1 \frac{A_2(x, t; \delta) dt}{\sqrt{t^2 - v^2}} \quad (3.10)$$

The same equation can be written in somewhat different form, more convenient for its solution

$$f(x) + \frac{2}{\pi} \int_0^1 K(x, v; \delta) f(v) dv = G_1(x) \quad (0 < x < 1) \quad (3.11)$$

Here

$$G_1(x) = G(x) - \varphi(1) A_1(x; \delta)$$

If one were to temporarily consider constant  $\varphi(1)$  known, then right side of

equation (3.11) will be given function. Then, solution of equation (3.11) can take the form [3]

$$f(x) = G_1(x) - \frac{2}{\pi} \int_0^1 G_1(v) K(x, v; \delta) dv + \dots$$

Formula (3.8) allows to obtain relationship, necessary for finding constant  $\varphi(1)$ .

4. Case of constant load. If strip breaks due to load of constant intensity  $p_0$ , applied to its surfaces, then  $G(x) = 0.5 \pi p_0 a^2 x$ , and consequently,

$$f(x) = \frac{\pi}{2} p_0 a^2 x - \varphi(1) A_1(x; \delta) - p_0 a^2 \int_0^1 v K(x, v; \delta) dv + \dots + \frac{2}{\pi} \varphi(1) \int_0^1 A_1(v; \delta) K(x, v; \delta) dv + \dots \quad (4.1)$$

We convert expressions  $A_1(x; \delta)$  and  $K(x, v; \delta)$ , entering (4.1). Here we use integral representations of Bessel functions  $J_0$  and  $J_1$ .

Thus

$$A_1(x; \delta) = \frac{2}{\pi} \int_0^\infty H_1(\delta \lambda) \sin \lambda x d\lambda \int_0^1 \frac{\cos \lambda u du}{\sqrt{1-u^2}} = \frac{2}{\pi} \int_0^1 H_{10}(x, u; \delta) \frac{du}{\sqrt{1-u^2}}$$

Here

$$H_{10}(x, u; \delta) = \int_0^\infty H_1(\delta \lambda) \sin \lambda x \cos \lambda u d\lambda$$

Analogous to

$$K(x, v; \delta) = \frac{2}{\pi} v \int_0^1 \frac{dt}{t \sqrt{t^2 - v^2}} \int_0^t H_{20}(x, u; \delta) \sqrt{t^2 - u^2} du$$

where

$$H_{20}(x, u; \delta) = \int_0^\infty \lambda^2 H_1(\delta \lambda) \sin \lambda x \cos \lambda u d\lambda$$

Let us note that expression  $H_1(z)$  entering into these formulas under the sign of integral can be represented in following manner:

$$\begin{aligned} zH_1(z) &= \frac{z(e^{-2z} - 1 - 2z^2 - 2z)}{2(z + \operatorname{sh} z \operatorname{ch} z)} \approx \frac{1}{4} (e^{-p_1 z} - 6.2 z e^{-p_2 z} + 8 z e^{-p_3 z} - \\ &- e^{-p_4 z} + 4.2 z e^{-p_5 z} + 10.4 z^2 e^{-p_6 z} + 12.4 z^2 e^{-p_7 z} - 8 z e^{-p_8 z} - \\ &- 16 z^2 e^{-p_9 z} - 16 z^2 e^{-p_{10} z}) \\ &(p_1 = 4.8, p_2 = 4.0, p_3 = 2.8, p_4 = 2.0) \end{aligned} \quad (4.2)$$

Here is used [2] that

$$\frac{u}{u + \sin u} \approx \left(\frac{1}{2} - 1.55 u\right) e^{-1.4u} + 2ue^{-u}$$

Calculating integrals entering into solution of (4.1) and expanding integrands in series by degrees of  $\delta^{-1}$ , we obtain

$$\begin{aligned} f(x) = & 1/2 \pi p_0 a^2 x - \varphi(1) c_1 x \delta^{-2} + \varphi(1) c_2 (2x^2 + 3x) \delta^{-4} + \\ & + 1/2 \pi p_0 a^2 c_3 x \delta^{-6} + \dots \\ (c_1 = & -2.31, c_2 = -0.83, c_3 = -0.63) \end{aligned} \quad (4.3)$$

Having found  $\varphi(t)$  by formula (3.8), we determine value of constant  $\varphi(1)$ , entering into (4.3). After that we immediately find that

$$\begin{aligned} \varphi'(t) = & 1/2 \pi p_0 a^2 t (1 + a_1 \delta^{-2} - (a_2 + a_2 t^2) \delta^{-4} + (a_3 + a_3 t^2 + a_3 t^4) \delta^{-6} + \dots) \\ (a_1 = & 1.15, a_2 = -0.71, a_3 = 1.25, a_4 = -0.38, a_5 = 0.00, a_6 = 0.77) \end{aligned} \quad (4.4)$$

Expression (4.4) allows, by formula (3.3), to find  $B(\lambda)$  and thereby, on basis of formulas of section 2, to obtain solution of problem of stress state in strip with crack. In particular, displacement of points of surface of crack ( $x \leq 1$ ) is expressed as

$$v^0 = \frac{4(1-\nu^2)}{\pi E a} \int_x^1 \frac{\varphi'(t) dt}{\sqrt{t^2 - x^2}} = \frac{2(1-\nu^2)}{E} p_0 a \sqrt{1-x^2} \Delta(x; \delta) \quad (4.5)$$

where

$$\begin{aligned} \Delta(x; \delta) = & 1 + a_1 \delta^{-2} - \left[ a_2 + \left( \frac{1}{3} + \frac{2}{3} x^2 \right) a_2 \right] \delta^{-4} + \left[ a_3 + \left( \frac{1}{3} + \frac{2}{3} x^2 \right) a_3 + \right. \\ & \left. + \left( \frac{1}{5} + \frac{4}{15} x^2 + \frac{8}{15} x^4 \right) a_3 \right] \delta^{-6} - \dots \end{aligned} \quad (4.6)$$

However, length of equilibrium crack has still not been determined, since, as was said, solution of problem was conducted neglecting cohesive forces. For finding of length  $2a$  of equilibrium crack, we demand smoothness of closing of its opposite surfaces near tip. This length can be determined from relationship written in dimensionless form

$$\lim_{x \rightarrow 1} \left( \frac{dv^0}{dx} \sqrt{1-x} \right) = \frac{2K(1-\nu^2) \sqrt{a}}{\pi E} \quad (4.7)$$

Hence

$$\frac{p_0 \sqrt{a}}{\sqrt{2}} \Delta(1; \delta) = \frac{K}{\pi}$$

$$\left( \Delta(1; \delta) = 1 + 1.15 \delta^{-2} - 0.55 \delta^{-4} + \right.$$

$$\left. + 0.49 \delta^{-6} + \dots = \frac{\Phi'(1)}{1/2\pi p_0 a^2} \right) \quad (4.8)$$

When  $\delta \rightarrow \infty$  ( $\Delta(1; \delta) = 1$ ), condition (4.8) takes form, coinciding with known solution for strip of infinite width.

Relationship (4.8) can be written in the form

$$\frac{\Delta(1; \delta)}{\sqrt{\delta}} = \frac{K \sqrt{2}}{\pi p_0 \sqrt{h}} = x_1 \quad (h = q\delta) \quad (4.9)$$

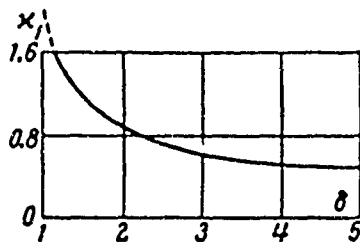


Fig. 2.

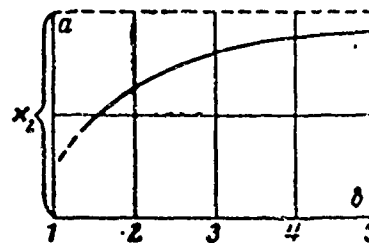


Fig. 3.

As can be seen from graph (Fig. 2), constructed formula (4.9) at given strip width, with increase of load  $p_0$ , size of equilibrium crack decreases. As expected equilibrium of cracks in considered case of load of constant intensity is unstable. From graph, furthermore, it is clear that instability of development of crack with decrease of parameter  $\delta = h/a$  assumes a sharper character. This may be seen also from Fig. 3, in which is given dependence of size  $a$  of equilibrium crack, at given load, on parameter  $\delta$ . Thus, for example, if  $h = 1.5a$ , then critical size of crack decreases approximately twice in comparison with that in infinite body. At  $h \geq 5a$  critical size of equilibrium crack in strip, practically, coincides with critical size

$$a = 2K^2 \pi^2 p_0^2 = x_2$$

of crack in infinite body.

5. Case of axial symmetry. Let us consider thick infinite plate with a round crack in the middle plane; selecting beginning of coordinates in center of crack, we direct axis  $z$  perpendicularly to middle plane of plate. Let, under

action of given symmetric, with respect to axis  $z$ , breaking load, crack open up. Removing stress at boundary, as was done in section 1, we obtain following boundary conditions:

when  $z = 0$

$$\tau_{rz} = 0 \quad (0 \leq r < \infty) \quad (5.1)$$

$$\sigma_z = -g(r) \quad (0 \leq r \leq a) \quad w = 0 \quad (r \geq a) \quad (5.2)$$

when  $z = h$

$$\tau_{rz} = 0, \quad \sigma_z = 0 \quad (0 \leq r < \infty) \quad (5.3)$$

Here  $g(r)$  — cracking stress at points of surface of crack (in converted stress state [1]),  $2h$  — thickness of plate,  $a$  — radius of equilibrium crack,  $r$  — radial coordinate.

Biharmonic function [4],

$$\begin{aligned} \vartheta(\rho, \zeta) = a^3 \int_0^{\infty} \lambda^{-3} \left\{ \left[ 2\nu + \frac{\lambda \zeta \operatorname{sh}^2 \lambda \delta}{\lambda \delta + \operatorname{sh} \lambda \delta \operatorname{ch} \lambda \delta} \right] \operatorname{ch} \lambda \zeta - \right. \\ \left. - \left[ \lambda \zeta - \frac{\lambda^2 \delta^2 - 2\nu \operatorname{sh}^2 \lambda \delta}{\lambda \delta + \operatorname{sh} \lambda \delta \operatorname{ch} \lambda \delta} \right] \operatorname{sh} \lambda \zeta \right\} \chi(\lambda) J_0(\lambda \rho) d\lambda \\ (\rho = r/a, \delta = h/a, \zeta = z/a) \end{aligned}$$

through which are expressed components of displacement and stress, allows to satisfy boundary conditions of (5.1) and (5.3), equations of equilibrium and compatibility. Here, on basis of boundary conditions (5.2), function  $\chi(\lambda)$  should appear by solution of following system of dual integral equations:

$$\begin{aligned} \int_0^{\infty} \lambda H(\lambda \delta) \chi(\lambda) J_0(\lambda \rho) d\lambda = \frac{\pi}{2} a^2 g(\rho) \quad (0 \leq \rho < 1) \\ \int_0^{\infty} \chi(\lambda) J_0(\lambda \rho) d\lambda = 0 \quad (\rho > 1), \quad \left( H(\lambda \delta) = \frac{\operatorname{sh}^2 \lambda \delta - \lambda^2 \delta^2}{\lambda \delta + \operatorname{sh} \lambda \delta \operatorname{ch} \lambda \delta} \equiv 1 + H_1(\lambda \delta) \right) \quad (5.4) \end{aligned}$$

It is interesting to note that, as and in problem of a stamp, plane and axisymmetric cases are described by equations, analogous in form, to replacement only of Bessel function (for case of axial symmetry) by cosine.

We will introduce new function [4, 5]

$$\chi(\lambda) = \int_0^1 \Phi(t) \sin \lambda t dt \quad (5.5)$$

Then, the second of equations (5.4) will be satisfied identically, and the first of equations (5.4), taking into account formulas of type (3.8), after corresponding conversions [4] takes form

$$f(\rho) + \frac{2}{\pi} \int_0^1 f(r) K(v, \rho; \delta) dv = \frac{\pi}{2} g(\rho) a^2 \quad (\rho \leq 1) \quad (5.6)$$

Here

$$f(\rho) = \int_0^{\rho} \frac{\Phi(t) dt}{V \rho^2 - t^2}, \quad K(v, \rho; \delta) = \frac{2}{\pi} v \int_0^1 \frac{dt}{V t^2 - r^2} \int_0^{\rho} N(u, t; \delta) \frac{du}{V \rho^2 - u^2}$$

where

$$N(u, t; \delta) = \int_0^{\infty} \lambda H_1(\delta \lambda) \sin \lambda t \cos \lambda u d\lambda$$

Solution of equation (5.6) can be taken in the form

$$f(\rho) = \frac{\pi}{2} a^2 \left\{ g(\rho) - \frac{2}{\pi} \int_0^1 K(v; \rho; \delta) g(v) dv + \left( \frac{2}{\pi} \right)^2 \int_0^1 K(z; \rho; \delta) dz \int_0^1 K(v; z; \delta) g(v) dv + \dots \right\} \quad (5.7)$$

Let us consider a particular case when plate is ruptured by constant load of intensity  $p_0$  applied on its edge. Using relationship (4.2) and expanding in (5.7) integrands by degrees of  $\delta^{-1}$ , after rather clumsy computations, we obtain

$$\Phi(t) = a^2 p_0 \left\{ t - \frac{2}{\pi} \sum_{m=1,3,5}^{\infty} (-1)^{1/2(m+3)} \frac{1}{\delta^{m+2}} a_{m+1} \sum_{k=0}^{1/2(m-1)} C_m^{2k} \frac{t^{2k+1}}{(2k+1)(m-2k+2)} + \dots \right\} \quad (5.8)$$

Here

$$\begin{aligned} a_1 &= -4.21, & a_2 &= -4.84, & a_3 &= -3.24, & a_4 &= -1.68 \\ a_5 &= -0.75, & a_6 &= -0.31, & a_7 &= -0.12, & a_8 &= -0.04 \end{aligned}$$

At sufficiently large  $m$

$$a_{1/2(m+1)} = 2^{-(m+2)} (m+3)^2 (m+2)$$

Now, by formula (5.5) can be found function  $\chi(\lambda)$ . However, for finding of displacements and stresses in points of middle surface of plate there is no necessity to find  $\chi(\lambda)$ . Indeed, stress  $\sigma_z^0$  outside crack ( $z=0, \rho > 1$ ) is determined by formula

$$\sigma_z^0 = \frac{2}{\pi a^2} \left\{ -\frac{\Phi(t)}{V \rho^2 - t^2} + \int_0^1 \frac{\Phi(t) dt}{V \rho^2 - t^2} + \int_0^1 \Phi(t) dt \int_0^{\infty} \lambda H_1(\lambda \delta) \sin \lambda t J_0(\lambda \rho) d\lambda \right\} \quad (5.9)$$

Displacement of points of surface of crack ( $\rho < 1$ ) is given by following expression;

$$w^0 = \frac{4(1-\nu^2)}{\pi E a} \int_0^1 \frac{\Phi(t) dt}{\sqrt{t^2 - \rho^2}} \quad (5.10)$$

Function  $\Phi(t)$  into both these formulas enters. We will show that for deter-

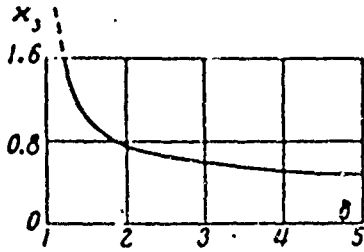


Fig. 4.

mination of previously known radius of equilibrium crack it is sufficient to know value  $\Delta(1; \delta) = \Phi(1) / a^2 p_0$ .

For finding of relationship, determining sought radius of equilibrium crack, we will demand, that stress  $\sigma_r^0$  when

$r \rightarrow a$  ( $\rho \rightarrow 1$ ) have order of magnitude  $K / \pi \sqrt{r-a}$ . As a result, we obtain

$$p_0 \sqrt{2a} \Delta(1; \delta) = K \quad (5.11)$$

The same condition can be obtained, using principle smooth closing of free surfaces of equilibrium crack (see (4.7)). From (5.10) we find that

$$\frac{dw^0}{d\rho} = \frac{4(1-\nu^2)}{\pi E a} \left\{ -\Phi(1) \frac{\rho}{\sqrt{1-\rho^2}} + \int_1^{\rho} \frac{\Phi'(pu) du}{u \sqrt{u^2-1}} - \frac{1}{\rho} \int_1^{\rho} \frac{\Phi(pu) du}{u^2 \sqrt{u^2-1}} \right\}$$

Hence, with the help of (4.7) we arrive anew at relationship (5.11).

When  $\delta \rightarrow \infty$ , from formula (5.8) we have  $\Phi(1) = a^2 p_0$ , therefore, relationship (5.11), when  $\delta \rightarrow \infty$  coincides completely with known result for space with crack.

Calculated with the help of formula (5.8), expression for  $\Delta(1; \delta)$  has form

$$\Delta(1; \delta) = 1 + (0.89 \delta^{-3} - 1.64 \delta^{-5} + 2.36 \delta^{-7} - 3.05 \delta^{-9} + 3.72 \delta^{-11} - \dots) + (0.80 \delta^{-6} - 2.57 \delta^{-8} + 5.46 \delta^{-10} - 9.69 \delta^{-12} + 14.4 \delta^{-14} - \dots) + \dots$$

In Fig. 4, with the help of relationship

$$\frac{\Delta(1; \delta)}{\sqrt{\delta}} = \frac{K}{p_0 \sqrt{2a}} = x_3 \quad (5.12)$$

obtained from formula (5.11), is built graph, allowing to find equilibrium radius of crack as a function of applied load. Comparison of graphs, built in

Figs. 2 and 4, shows that behavior of crack in axisymmetric case is analogous to behavior of straight crack in strip.

Submitted  
7 March 1963

Literature

1. G. I. Barenblatt. On equilibrium cracks formed during brittle fracture PMM, 1959, vol. XXIII, issues 3, 4, and 5.
2. I. Sneddon. Fourier transforms. II, 1955.
3. I. I. Privalov. Integral equations. ONTK, 1935.
4. M. Lowengrub. Stress in the vicinity of a crack in a thick elastic plate, Quart. Appl. Math., 1961, vol. XIX, No 2, 119 - 126.
5. N. N. Lebedev and Ya. S. Uflyand. Axisymmetric contact problem for elastic layer, PMM, 1958, vol. XXII, issue 3, 320 - 326.

## EQUILIBRIUM OF A TWIN FOR PLANE SURFACE OF ISOTROPIC MEDIUM

A. M. Kosevich and L. A. Pasmur

(Khar'kov)

Considered is dislocation model of quasi-static twinning on surface of crystal. General qualitative picture of hysteresis phenomena during such twinning is explained.

We will assume that twin is infinite in one direction parallel to surface of crystal, i.e., is formed by load created by infinitely long blade. Here, form of twin is completely characterized by its profile in plane perpendicular to indicated direction. In dislocation model such a twin is equivalent to totality of rectilinear dislocations, axes of which are located on its outline. Usually, thickness of twin is very small, therefore, it is natural to consider that all dislocations are located in one plane (plane of twinning), and besides, since number of them in macroscopic twin is sufficiently great, it is possible to introduce linear plane of dislocations which is continuous function of coordinate  $y$ , counted off along plane of twinning from surface to interior of crystal. These representations were assumed on the basis of works of authors [1 - 4]. In indicated works, for plane of dislocation  $\rho(y)$ , were formulated equations, which describe quasiequilibrium development of thin twin, and also their qualitative investigation is conducted.

In simplest case, when twin is formed purely by edge dislocations, and it is perpendicular to surface of isotropic body, indicated equation has form

$$\int_0^l K(y, \eta) \rho(\eta) d\eta = f(y) + S(y), \quad K(y, \eta) = \frac{1}{\eta - y} + \frac{y^2 + 4y\eta - \eta^2}{(y + \eta)^2} \quad (0.1)$$

where  $l$  - length of twin;  $f(y)$  - force, acting on dislocation from side of external load (we can always consider that  $f(y) > 0$ );  $S(y)$  - so-called force of nonelastic origin. Let us note that force of the same physical nature causes

presence "modulus of cohesion" in theories of fragile cracks, offered by G. I. Barenblatt [5].

If end of twin is free, i.e., there are no stoppers, preventing its growth into depth of crystal, then  $\rho_0$  is determined from following equation

$$\int_0^l \rho_0(\eta) \{f(\eta) + S(\eta)\} d\eta = 0 \quad (0.2)$$

where  $\rho_0(\eta)$  - solution of homogeneous equation, adjoint to (0.1).

In general, resisting force, acting on dislocation, depends on previous history of its given state.

Such dependence, as in [6], is cause of hysteresis during twinning under action of external load, infinitely slow, but non-monotonic varying with time (process of loading and subsequent unloading). It is interesting to note that for explanation of qualitative picture of hysteresis phenomena in dislocation model only certain things are essential, sufficiently general properties of function  $\rho_0(\eta)$ , entering into (0.2): fixed in interval  $(0, l)$  and definite asymptotics on ends of interval. To proof of these properties  $\rho_0(\eta)$  is devoted first part of present work. In second part is conducted qualitative analysis of hysteresis phenomena during twinning at surface of crystal, and also briefly considered is question of stability of twins.

1. As was already indicated,  $\rho_0(y)$  represents solution of uniform integral equation, adjoint to (0.1)

$$\int_0^l \left\{ \frac{1}{\eta - y} + \frac{y^2 - 4y\eta - \eta^2}{(y + \eta)^2} \right\} \rho_0(\eta) d\eta = 0 \quad (1.1)$$

By substitution  $\eta = lx, y = ly$ , equation (1.1) we come to form

$$\int_0^1 \left\{ \frac{1}{t - x} + \frac{x^2 - 4xt - t^2}{(x + t)^2} \right\} \varphi(t) dt = 0 \quad (\varphi(t) = \rho_0(lt)) \quad (1.2)$$

Nonuniform equation of such type was considered by Wigglesworth [7] in connection with problem of crack at surface of solid body, where solution was

obtained by method of Wiener - Hopf. We will solve equation (1.2), following essentially the method of work [7].

We will introduce functions

$$\varphi_-(x) = \begin{cases} \varphi(x) & (0 < x < 1), \\ 0 & (1 < x < \infty), \end{cases} \quad \varphi_+(x) = \begin{cases} 0 & (0 < x < 1) \\ \gamma_+(x) & (1 < x < \infty) \end{cases}$$

$$\gamma_+(x) = \int_0^1 K(t, x) \varphi_-(t) dt$$

With the help of these functions, and also taking into account homogeneity  $K(t, x)$ , we write (1.2) in the form

$$\int_0^{\infty} \varphi_-(x) k\left(\frac{y}{x}\right) \frac{dx}{x} = \varphi_+(y) \quad \left(k(x) = -\frac{1}{1-x} + \frac{1+4x-x^2}{(1+x)^2}\right) \quad (1.3)$$

By Mellin transform, considering that left part of (1.3) has the form Mellin convolution, we bring (1.3) to form

$$\Phi_-(s) = 2\pi \frac{\sin^2(1/2 \pi s) - s^2}{\sin \pi s} = \Phi_+(s) \quad (1.4)$$

Here  $\Phi_{\pm}(s)$  is Mellin transform of functions  $\varphi_{\pm}(x)$ , i.e.,

$$\Phi_+(s) = \int_0^{\infty} \varphi_+(x) x^{s-1} dx, \quad \Phi_-(s) = \int_0^1 \varphi_-(x) x^{s-1} dx$$

We will solve functional equation (1.4) by method of Wiener - Hopf (see, for example, [8]). Following main idea of this method, we will explain first of all, general strip of analyticity of both parts of equation. If we assume that  $\varphi_-(x)$ , when  $x \rightarrow 0$  conducts self, as  $x^{\alpha}$  ( $\alpha > -1$ ), then  $\Phi_-(s)$  will be analytic in half-plane  $\text{Re } s > -\alpha$ . Further, since

$$\varphi_+(x) = \int_0^1 \varphi_-(t) k\left(\frac{x}{t}\right) \frac{dt}{t} \sim \frac{A}{x^2} \text{ when } x \rightarrow \infty$$

$\Phi_+(s)$  is analytic in half-plane  $\text{Re } s < 2$ . Therefore, general strip of analyticity of equation (1.4) will be  $\beta < \text{Re } s < 1$ , where  $\beta = \max(-\alpha, 0)$ ; function is analytic in each of strips, shown in parentheses.

$$\kappa(s) = \frac{\sin^2(1/2 \pi s) - s^2}{\sin \pi s} \quad (2\pi < \text{Re } s < 2\pi + 1, \pi - 0, \pm 1, \dots)$$

Following stage of solution consists of factorization of  $\kappa(s)$ , i.e., in

its representation in the form  $x(s) = x_-(s) / x_+(s)$ , where  $x_{\pm}(s)$  - analytic, and functions not turning into zero, corresponding, in half-planes, to  $\text{Re } s > \beta$  and  $\text{Re } s > 1$ . This was performed in work [7]; here is given only expression for  $x_-(s)$ , which will be needed in the future

$$x_-(s) = \frac{h_-(s) \Gamma(1/2(s+1))}{\Gamma(1/2s)} \quad (1.5)$$

where  $\Gamma(s)$  - Euler gamma function, and

$$h_-(s) = (1+s) \prod_{n=1}^{\infty} \left(1 + \frac{s}{\mu_n}\right) \left(1 + \frac{s}{\mu_n^*}\right) \left(1 + \frac{s}{2n}\right)^{-1} \quad (1.6)$$

Here  $\mu_n$  - roots of equation  $\sin^2(1/2 \pi s) - s^2 = 0$ , lying in first quadrant, except for 0 and 1 ( $\text{Im } \mu_n > 0, \text{Re } \mu_n > 0$ ). and dash designates complex union. For  $h_-(s)$  can be obtained also integral representation, from which is established [7, 8], that  $\lim_{s \rightarrow \infty} h_-(s) = 1$  ( $\text{Re } s > \beta$ ).

Using factorization function  $x(s)$ , we represent (1.4) in the form

$$\Phi_-(s) x_-(s) = \Phi_+(s) x_+(s) \quad (1.7)$$

Hence, it follows that both parts of (1.7) are equal the same entire function  $P(s)$ , which, as usually, in Wiener - Hopf method, can always be selected polynomial. Thus

$$\Phi_{\pm}(s) = \frac{P(s)}{x_{\pm}(s)} \quad (1.8)$$

From (1.5) it follows that  $x_-(s) \sim \sqrt{s}$  when  $|s| \rightarrow \infty, \text{Re } s > \beta$ . Since  $\Phi_-(s)$  should disappear to infinity (this is necessary condition for application of Mellin transform [8]), then  $P(s)$  can be only a constant. Finally we obtain that  $\Phi_{\pm}(s) = C / x_{\pm}(s)$ , and means

$$\varphi_-(x) = \frac{1}{2\pi i} \int_L \frac{C}{x_-(s)} x^{-s} ds \quad (1.9)$$

where  $L$  - straightline  $\text{Re } s = \delta > 0$ . Since here  $0 < x < 1$ , it is possible to add contour  $L$  to semicircle of infinite radius, lying more to the left of  $L$ , and then  $\varphi_-(x)$  will be equal to sum of residues of  $\Phi_-(s)$  at poles, lying

more to the left of  $L$ , i.e.,

$$\varphi(x) = C_0 + \sum_{n=1}^{\infty} \operatorname{Re}(C_n x^{\mu_n}) \quad (1.10)$$

Here  $C_0$  and  $C_n$  - residues of  $\Phi_-(s)$  at points  $s=0$  and  $s=\mu_n$  respectively. From (1.10) one may see, that  $\varphi(0) = C_0$  (since  $\operatorname{Re} \mu_n > 0$ ).

For explanation of behavior of  $\varphi(x)$  when  $x \rightarrow 1$  we will use following affirmation [9]: if  $f(s)$  is "half-plane" of Mellin transform, functions of  $\psi(t)$ , then are

$$\lim_{t \rightarrow 1} \psi(t) = \lim_{s \rightarrow \infty} s f(s) \quad \left( f(s) = \int_0^1 \psi(t) t^{s-1} dt \right) \quad (1.11)$$

Here, from existence of limit in left part, follows existence of limit on the right. We assume now that

$$\varphi(x) \sim A(1-x)^\gamma \quad \text{when } x \rightarrow 1 \quad (A = \text{const}, \gamma > -1)$$

Then from (1.11), it follows, first of all, that  $\gamma < 0$ , since  $s\Phi_-(s)$ , when  $s \rightarrow \infty$ , also aspires to infinity ( $s\Phi_-(s) \sim \sqrt{s}$  when  $s \rightarrow \infty$ ). Further, applying (1.11) to  $\psi(t) = \varphi(t) - A(1-t)^\gamma$ , we conclude that necessarily

$$\lim_{s \rightarrow \infty} s \left\{ \Phi_-(s) - A \frac{\Gamma(1-\gamma)}{s^{1-\gamma}} \right\} = 0$$

and since at large  $s$

$$\Phi_-(s) = Cs^{-1/2} + O(s^{-3/2})$$

then obviously

$$\gamma = -\frac{1}{2}, \quad A = \frac{C}{\Gamma(1/2)}$$

Thus, finally

$$\varphi(x) \sim \frac{C}{\sqrt{\pi}} (1-x)^{-1/2} \quad \text{when } x \rightarrow 1$$

We will now prove nonnegative character of function  $\varphi(x)$ . This, its property, is result of one theorem of S. N. Bernstein [10], which, as applied to considered case, is formulated thus: so that function  $\varphi(x)$  is nonnegative, it is necessary and sufficient, that its "half-plane" Mellin transform

$$\Phi_-(s) = \int_0^1 \varphi(x) x^{s-1} dx$$

be an absolutely monotonic function, i.e.,

$$\Phi_-(s) \geq 0, \quad \Phi_-'(s) \leq 0, \quad \Phi_-'(s) \geq 0 \dots, \quad (0 < s < \infty) \quad (1.12)$$

Because of this theorem, it is necessary only to be convinced of the fact that  $\Phi_-(s)$  satisfies condition (1.12). For that we will use expression (1.8) for  $\Phi_-(s)$ , from which, taking into account form of  $\kappa_-(s)$ , given in (1.5), it is immediately clear that  $\Phi_-(s) > 0$  ( $0 < s < \infty$ ). Further, we examine

$$\Psi(s) \equiv \ln \Phi_-(s) = \left[ \frac{1}{s+3} - \frac{1}{s} + \sum_{n=1}^{\infty} \left( \frac{1}{s+2n+3} - \operatorname{Re} \frac{1}{s+\mu_n} \right) \right]$$

It can be shown that  $\operatorname{Re} \mu_n - (2n+3) < 0$  at any  $n$ , whence it follows that  $\Psi'(s) < 0$ ,  $\Psi''(s) > 0, \dots$ . Now applying method of mathematical induction, it is easy to prove that  $\Phi_-(s)$  satisfies (2.12), and means  $\varphi_-(s)$  is nonnegative.

2. Let us consider development of twin during infinitely slow, but non-monotonic change of load. For basis we will take equation (0.2), which gives connection of length of free twin with quantity and character of forces, acting on dislocation. We note, first of all, that force of resistance  $S(x)$  consists of two considerably different parts

$$S = s + S^\circ$$

where  $s(x)$  — braking force (Peierls force), and  $S^\circ(x)$  — force of surface tension.

Regarding  $s$ , we will assume that it is directed against possible motion of dislocations and in limit of infinitesimal speed is equal to constant:  $|s| = S_0 = \text{const}$ . During monotonic buildup of external load  $s = -S_0$ , and during its non-monotonic change, in general,  $-S_0 \leq s \leq S_0$ .

Force of surface tension  $S^\circ(x)$  is applied directly to "mouth" of twin and therefore, it can be considered non-zero only near end of twin, i.e.,  $S^\circ(x) = Q(l-x)$ , where  $Q(x) \neq 0$  only at  $0 \leq x \leq d$  and  $d$  is small.

External load  $f(x)$ , let us assume, is proportional to certain parameter  $A$  ( $f(x) = Ag(x)$ ), so that increase or decrease of load is caused by increase or decrease of  $A$ . Then, for case of load, equation (0.2) is written in the

form

$$F(l) = S_0 + J(l) \quad (2.1)$$

Here

$$F(l) = \frac{A}{B} \int_0^l g(x) \eta(x) dx, \quad J(l) = \frac{1}{B} \int_0^l S^0(x) \eta(x) dx$$

$$B = \int_0^1 \varphi(x) dx = \Phi_-(1), \quad \eta(x) = \frac{\varphi(x, l)}{l}$$

It is not difficult to show now, considering results of Section 1, that equation (2.1) has the same properties as corresponding equations in [5, 6]. Thus  $J(l)$  will be monotonely diminishing function  $l$ , of and its main member at  $l \gg d$  equals

$$J(l) \approx \frac{M}{\sqrt{l}}, \quad M = \frac{C}{B \sqrt{\pi}} \int_0^{\infty} \frac{Q(x) dx}{\sqrt{x}}$$

Further,  $F(l)$  also will be monotonically diminishing function of  $l$ , if  $f(x)$  monotonically diminishes. If however,  $f(x)$  non-monotonically depends on  $x$ , then  $F(l)$  can have several maxima and minimums (however, always  $F(\infty) = 0$ , only if  $f(x)$  is integrated in infinite interval). Marked coincidence of properties of equation (2.1) and corresponding equations of [5, 6] allows to affirm that all basic conclusions and results of these works will also be correct and in given case. In brief, we will formulate these results.

Loading. During increase of external force  $Ag(x)$  while parameter  $A$  less than certain  $A^*$ , twin does not appear. Quantity  $A^*$  is determined by the condition that external force at locus point of source is equaled by full resisting force at this point  $S(0)$ . When  $A = A^*$  twin appears, which is increased with further rise of  $A$ . Depending upon form of  $g(x)$ , length of twin, when  $A = A^*$ , can be either as small as desired (during monotonous and is sufficiently fast decrease of  $g(x)$ , when equation (3.1) has only one solution), or finite (during slow decrease or non-monotonous change of  $g(x)$ , when equation (2.1) has two or more roots). In latter case, twin of finite dimensions intermittently develops.

Unloading. During examination of unloading, a simplifying assumption is

made about form of  $g(x)$ , which is considered monotonely diminishing with rise of  $x$ . It turns out that a determining role is played here by relation  $S_0$  to  $S^\circ$ , depending upon size of which, two cases can be represented.

1. Surface tension is slight,  $S^\circ(0) < S_0$ . Then, if twin is formed by comparatively little force, such that always  $f(0) < 2S_0$ , then after removal of load, dimensions of twin remain unchanged. Otherwise, when external stress at point  $x = 0$  in end of load is larger than  $2S_0$ , during removal of load, a certain thinning of twin occurs in its mid part, without change of length.

2. Surface tension is great. In this case, twins of large dimensions, such that  $S_0\sqrt{l} > M$ , conduct themselves just as in case 1, i.e., only then without changing length. If length of twin is not very great, and reverse inequality  $S_0\sqrt{l} < M$  occurs, then, during removal of load, at first occurs decrease of thickness, at constant length, and then, at most extreme decrease of external force, length also starts to decrease, and finally twin completely disappears.

Apparently, case 2 corresponds to real twin layers, whereas case 1 is more probable for incomplete shifts.

In conclusion, we will list certain considerations about stability of twins at surface of crystal. Twin will be called stable, if its length increases with increase of load, i.e., if  $dl/dA > 0$ .

Considering equation (2.1) as implicit assignment of function  $l(A)$ , we will find that from condition  $dl/dA > 0$ , it follows that  $F'(l) < J'(l)$ .

During sufficiently large  $l$

$$F(l) \sim \frac{F_0}{l} \quad \left( F_0 \approx \frac{1}{B} \int_0^\infty f(x) dx \right), \quad J(l) \approx \frac{M}{\sqrt{l}}$$

and, consequently, condition stability is fulfilled. This means that long twins are always stable, where, under long, one should understand such twins, length of which is great as compared with dimensions of region of application of load to surface of crystal.

## Literature

1. A. M. Kosevich and L. A. Pastur. On dislocation model of twin, Phys. of solid body, 1961, vol. III.
2. A. M. Kosevich and L. A. Pastur. Form of thin twin, located at an angle to surface, Phys. of solid body, 1961, vol. III.
3. A. M. Kosevich and L. A. Pastur. Works of second conference of physics of alkali halide crystals. Riga, 1962.
4. A. M. Kosevich and L. A. Pastur. Thin twin at plane surface of anisotropic body. Phys. of solid body, 1962, vol. IV.
5. G. I. Barenblatt. Mathematical theory of equilibrium cracks formed during brittle fracture, PMTF, 1961, No 4.
6. A. M. Kosevich. Dislocation theory of hysteresis phenomena during twinning and generation of dislocations in unlimited medium. Phys. of solid body, 1961, vol. III.
7. L. A. Wigglesworth. Stress distribution in a notched plate. Mathematika, 1957, No 4, 76 - 96.
8. F. Morse and G. Fishbach. Methods of theoretical physics. II, vol. 1, 1958.
9. B. Vanderpol and H. Bremmer. Operational calculus on the basis of bilateral Laplace transform, II, 1952.
10. N. I. Akhiezer. Classical problem of moments, Fizmatgiz, 1961.

## ON STRAIN WAVES IN DURABLE ROCKS

Ye. I. Shemyakin

(Novosibirsk)

1°. During dynamic loadings of solid media by explosion or shock, strain waves appearing in these media have, as a rule, small spatial extent of region of loading. If the biggest dimension of this region,  $s_1$ , is significantly less than distance  $r_0$  from source (in center of charge or at point application of impact load), for example,  $s_1 \sim 0.1 r_0$ , or still less, then such a strain wave can be considered short [1, 2].

In significant range of distances from source, strain waves in solid media can be considered weak. This is due to fact that compressibility of solid bodies is small: bulk modulus of compression of majority of durable rocks has a magnitude of  $\sim 10^5$  kg/cm<sup>2</sup>, so that relation of amplitude of strain in wave to magnitude of this modulus is of small size of order 0.1 for waves with amplitude of  $10^5$  kg/cm<sup>2</sup>.

As an example, of short strain waves can serve waves on section of load in durable rocks, appearing during underground explosion of high explosive charge. Practically, in entire range distances, starting from 2-5 radii of charge and further, these strain waves are weak. These facts allow to apply to study of strain waves methods of theory of short waves [1, 2].

2°. On basis of given measurements of strains and particle velocities in durable rocks (diabase, limestone, granite, marble [3]) it is possible to note following peculiarities of strain waves, appearing during underground explosions:

1) in entire range of measurements, starting with 10-15  $R_*$  ( $R_*$  - radius of charge), on stress curves shock waves are not observed.

2) starting from distances 10-15  $R_*$  to 100, relation of length of section of stress build-up  $s_1$  to distance from point of explosion has magnitude of order of 0.1, and then approximately proportionally decreases with distance from point of explosion;

3) build-up of strain occurs sharply, and decay of strain has smooth character; ration of stress gradients in regions of loading and unloading can be estimated by ration of magnitudes  $s_1/s_2$ , where  $s_2$  - extent of zone of compression in region of unloading. This ratio in zone near charge has magnitude  $\sim 0.05-0.1$ , and at great distances, where stresses are

already small, equal 0.25-0.3;

4) length of zone of compression  $s_1 + s_2$  increases slightly with distance from point of explosion (with increase of distance from 30 to 150  $R_*$  magnitude of  $s_1 + s_2$  is increased approximately by 10-20%).

Region of stresses build-up  $s_1$ , approximately up to 100  $R_*$  grows significantly faster, than  $s_1 + s_2$ , so that position of peak on stress curve sharply shifts from beginning of curve to sides toward point of explosion-peak of stresses "will lag" behind entry of wave;

5) starting from distances of order 20-30  $R_*$ , entire stress curve, on the whole, travels approximately with speed of sound  $a_0$  and in stationary medium. Difference of prepropagation speed between peak of stresses and wave front is approximately equal to 5-10% at distances  $\sim 30 R_*$  and  $\sim 1-2\%$  at distances of 100  $R_*$ ; difference of these speeds decreases with distance from point of explosion;

6) peaks of stress and strain in section of stress build-up decrease with distance approximately proportionally with  $r^{-n}$ , where  $n = 1.6 - 1.8$ ;

7) at distances  $\sim 50 R_*$  ratio of maximum travelling speeds  $u$ , to speed of sound in stationary medium is  $u/a_0 \sim 10^{-4}$ : longitudinal deformation has the same order.

Peaks of stress  $\sigma_r$  at distances  $\sim 50 R_*$  have magnitude of order 100  $\text{kg/cm}^2$ ; for a given particle, these stresses increase for a time  $\sim 10^{-3}$  sec (for charge of TNT weighing 1 t).

3°. In article are considered short strain waves in medium, which, during rapid dynamic loadings, changes to maximum state in part of loading, it is assumed that in this state principal normal stress in wave are connected with certain condition of type of Coulomb-Mohr-Prandtl conditions. Dependence of hydrostatic pressure on volume strain is assumed weak-nonlinear.

Solution of problems for spherical and cylindrical symmetry, and also for plane wave is constructed by method of theory of short waves; all main results about loading waves coincide in accuracy with results of article [4]. New data relate to generalization of condition of limiting state in case of weak nonlinearity and to appraisal of influence of unloading law of attenuation of maximum amplitudes.

1.1. Let us consider one-dimensional problems of propagation of strain waves in continuous medium. We will select, as independent variables, the Lagrange variables:  $r_0$ -initial coordinate of particle,  $r$ -coordinate at moment of time  $t$ .

Equations of motion and inseparability in Lagrange variables have following form\*

$$\rho \frac{\partial u}{\partial t} + \frac{1}{\partial r / \partial r_0} \frac{\partial \sigma_r}{\partial r_0} + \frac{2(\sigma_r - \sigma_\theta) r_0}{r_0} \frac{r_0}{r} = 0, \quad \frac{\partial r}{\partial r_0} = \frac{\rho_0}{\rho} \left( \frac{r_0}{r} \right)^3 \quad (1.1)$$

Here  $\sigma_r, \sigma_\theta = \sigma_r$ -principal normals of stress;  $\rho$ -density,  $\rho_0$ -its initial value;  $u$  speed of travel in direction  $r$ .

\*In equation of motion, compressive stresses are considered positive quantities. Equations of (1.1) are written for case of spherical symmetry, but all subsequent calculations, with elementary changes, can be applied to cylindrical and plane cases.

If one were to introduce instead of  $\rho$  volume strain of particle  $\epsilon = \rho_0 / \rho - 1$  and to differentiate second equation of (1.1) by  $t$ , this equation of inseparability can be represented in the form

$$\frac{\partial u}{\partial r_0} = \left(\frac{r_0}{r}\right)^2 \frac{\partial \epsilon}{\partial t} - \frac{r_0}{r} \frac{\partial r}{\partial r_0} \frac{2u}{r_0} \quad \left(u = \frac{\partial r}{\partial t} = \frac{\partial}{\partial t}(r - r_0), \quad \epsilon = \frac{\rho_0}{\rho} - 1\right) \quad (1.2)$$

In equations of motion and inseparability we shall turn from stresses to deformations; let  $u(r_0, t)$  - velocity of a particle;  $\epsilon(r_0, t)$  - volume strain;  $r(r_0, t)$  - position of particle,  $w(t)$  - dislocation of particle; then

$$r(r_0, t) = \int_0^t u dt' + r_0 \quad \text{or} \quad w = \int_0^t u dt' \quad (1.3)$$

We introduce new independent variables  $\delta, \tau$ , and new unknown functions  $m$  and  $e$  with the help of relationships

$$r = a_0 t (1 + \Delta_0 \delta), \quad \tau = \ln t, \quad u = a_0 M_0 m(\delta, \tau), \quad \epsilon = \epsilon_0 e(\delta, \tau) \quad (1.4)$$

Here  $a_0$  - speed of sound in stationary medium;  $M_0$  and  $\epsilon_0$  - small quantities, having order of maximum Mach number and of maximum deformation. Assumption of smallness of  $M_0$  and  $\epsilon_0$  is assumption of weakness of amplitudes in wave. As was indicated above,  $M_0$  has order of magnitude  $10^{-3}$  to  $10^{-4}$ , quantity  $\epsilon_0$  also is small; as will be shown below (during derivation of equations of short waves),  $\epsilon_0 \approx M_0$ ; quantities  $\delta, \tau$  - are of order of one unit.

In (1.5) is considered that  $\Delta_0 \delta \ll 1$  due to smallness of  $\Delta_0$ .

Assumption on smallness of  $\Delta_0$  is assumption of shortness of wave. This signifies, as follows from (1.4) and from determination of  $s_1$  (see above), that length of region of stress build-up  $s_1 = a_0 t \delta \Delta_0$  is significantly less than distance, passed by wave from point of explosion  $r_0 \approx a_0 t$

$$s_1 \ll r_0 \quad (1.5)$$

In short ( $\Delta_0 \ll 1$ ) and weak ( $M_0 \ll 1; \epsilon_0 \ll 1$ ) waves, following appraisals of lateral and longitudinal deformations in spherical-symmetric wave are correct:

$$\epsilon_0 = \frac{w}{r_0} \sim \frac{a_0 M_0 m \Delta_0 t}{a_0 t (1 + \Delta_0 \delta)} \sim \Delta_0 M_0, \quad \epsilon_r = \frac{\partial u}{\partial r_0} \sim M_0 \quad (1.6)$$

From comparison of appraisals of (1.6), it follows that  $\epsilon_r$  is small quantity of order of  $M_0$ , and  $\epsilon_0$  - is small quantity of a higher order, since  $\epsilon_0 \sim \Delta_0 M_0$ .

1.2. We assume that during dynamic loading behavior of medium is described by the following two functions:

$$-\sigma = \Psi(\epsilon), \quad \sigma = 1/2(\sigma_r + 2\sigma_\epsilon), \quad \sigma_r - \sigma_\epsilon = f(\sigma) \quad (1.7)$$

Connection of average stress  $\sigma$  with volume strain will be obtained, further, in the form

$$-\sigma = K\epsilon(1 + l'\epsilon), \quad |l'\epsilon| \ll 1 \quad (K = \lambda + 2/3\mu, \quad l' = \text{const}) \quad (1.8)$$

Here  $K$  - bulk modulus,  $\lambda, \mu$  - Lamé constants.

In (1.7), function  $f(\sigma)$  describes limiting state of medium and connects first and second invariants of stress tensor; we obtain

$$f(\sigma) = 3m\sigma(1 - \chi'\sigma) \quad (\chi'\sigma \ll 1; \quad m, \chi' = \text{const} > 0)$$

This corresponds to decrease of shearing stress at site of slipping with increase of normal stress at this site (or with increase of average stress  $\sigma$ ). In this case, using smallness  $\chi'\sigma$ , we have

$$\sigma_\epsilon = \alpha\sigma_r(1 + \chi\sigma) \quad \left(\alpha = \frac{1-m}{1+2\nu}, \quad \chi = \frac{(1-\alpha)(1+2\nu)}{3\nu} \chi', \quad \chi\sigma \ll 1\right) \quad (1.9)$$

Unknown parameters  $\alpha, \chi$  will be considered constant in range of high speeds of loading, near shock loads. With the help of (1.8) and (1.9) we obtain

$$\begin{aligned} -\sigma_r &= \frac{3K\epsilon}{1+2\nu}(1 + l\epsilon) & l &= l' + \frac{2\nu}{1+2\nu} \chi K \\ \sigma_r - \sigma_\epsilon &= \frac{3K(1-\alpha)}{1+2\nu} \epsilon(1 + l'\epsilon), & l' &= l'' + \chi' K \end{aligned} \quad (1.10)$$

We put these expressions in equations of motion (1.1), replace in it,  $\rho, r, r_0$  by expressions through deformations

$$\frac{1}{(1+\epsilon_0)^2} \frac{\partial u}{\partial t} - a_{10}^2(1+2l\epsilon) \frac{\partial \epsilon}{\partial r_0} - \frac{2a_{10}^2(1-\alpha)\epsilon(1+l'\epsilon)}{r_0} \frac{1+\epsilon_r}{1+\epsilon_0} = 0 \quad (1.11)$$

Here  $a_{10}$  - local speed of sound in region of limiting state; it is determined by factor  $\partial e / \partial r_0$ ; we have

$$-\frac{1}{\rho_0} \frac{ds_r}{de} = a_1^2 = a_{10}^2 (1 + 2\epsilon), \quad a_{10}^2 = \frac{3K}{\rho_0(1+2\alpha)} \quad (1.12)$$

In elastic medium, instead of (1.10), we have Hooke law

$$-\sigma_r = (\lambda + 2\mu) \epsilon_0 - 4\mu\epsilon_0, \quad \sigma_r - \sigma_\theta = 2\mu (\epsilon - 3\epsilon_0) \quad (1.13)$$

Equations of motion of elastic medium have form

$$\frac{1}{(1+\epsilon_0)^2} \frac{\partial u}{\partial t} - a_0^2 \frac{\partial}{\partial r_0} + \left[ \frac{4\mu}{\rho_0 r_0} (\epsilon - 3\epsilon_0) \right] - \frac{4\mu}{\rho_0 r_0} (\epsilon - 3\epsilon_0) \frac{1+\epsilon_r}{1+\epsilon_0} = 0$$

$$\left( a_0 = \sqrt{\frac{\lambda + 2\mu}{\rho_0}} \right). \quad (1.14)$$

Here component in parentheses is obtained during differentiation of  $\epsilon_0$  with respect to  $r_0$ .

1.3. We will derive equation of short waves for medium in limiting state and for elastic medium. In equations (1.11) and (1.14) let us turn to variables of (1.4); here we will consider appraisal of (1.6) for  $\epsilon_0$  and  $\epsilon_r$  and use following transfer formulas

$$\frac{\partial u}{\partial r_0} = \frac{M_0}{i\Delta_0} \frac{\partial m}{\partial \delta}, \quad \frac{\partial u}{\partial t} = \frac{a_0 M_0}{t} \left( \frac{\partial m}{\partial \tau} - \frac{1 + \Delta_0 \delta}{\Delta_0} \frac{\partial m}{\partial \delta} \right)$$

$$\frac{\partial r}{\partial r_0} = \frac{r_0}{a_0 i \Delta_0} \frac{\partial \epsilon}{\partial \delta}, \quad \frac{\partial \epsilon}{\partial t} = \frac{\epsilon_0}{t} \left( \frac{\partial \epsilon}{\partial \tau} - \frac{1 + \Delta_0 \delta}{\Delta_0} \frac{\partial \epsilon}{\partial \delta} \right) \quad (1.15)$$

Transforming equation of inseparability of (1.2) we have

$$\frac{M_0}{i\Delta_0} \frac{\partial m}{\partial \delta} = \frac{1}{(1+\epsilon_0)^2} \frac{\epsilon_0}{t} \left[ \frac{\partial \epsilon}{\partial \tau} - \frac{1 + \Delta_0 \delta}{\Delta_0} \frac{\partial \epsilon}{\partial \delta} \right] - \frac{1 + \epsilon_r - 2\epsilon_0}{1 + \epsilon_0} \frac{2a_0 M_0 m}{a_0 t (1 + \Delta_0 \delta)}$$

Hence, with accuracy within small parts of a higher order, respectively  $M_0, \Delta_0$ .

$$\frac{\partial m}{\partial \delta} + \frac{\epsilon_0}{M_0} \frac{\partial \epsilon}{\partial \delta} = \Delta_0 \frac{\epsilon_0}{M_0} \left[ \frac{\partial \epsilon}{\partial \tau} - \delta \frac{\partial \epsilon}{\partial \delta} - 2 \frac{M_0}{\epsilon_0} m \right] \quad (1.16)$$

Transformation for equation of motion gives:

for limiting state of medium

$$\frac{\partial m}{\partial \delta} + N \frac{\epsilon_0}{M_0} \frac{\partial e}{\partial \delta} = \Delta_0 \left[ \frac{\partial m}{\partial \tau} - \delta \frac{\partial m}{\partial \delta} - 2hN \frac{\epsilon_0}{\Delta_0} \frac{\partial e}{\partial \delta} - 2N(1-\alpha)e \right] \left( N = \frac{a_{10}^2}{a_0^2} \right) \quad (1.17)$$

for elastic medium

$$\frac{\partial m}{\partial \delta} + \frac{\epsilon_0}{M_0} \frac{\partial e}{\partial \delta} = \Delta_0 \left[ \frac{\partial m}{\partial \tau} - \delta \frac{\partial m}{\partial \delta} \right] \quad (1.18)$$

From comparison of (1.16) and (1.17), and also (1.16) and (1.18), assuming that right sides of equations - small quantities, we find

$$\epsilon_0 = M_0, \quad N = 1 - 2h\Delta_0 \quad (h = \text{const} > 0, h \sim 1) \quad (1.19)$$

From (1.16), (1.18) and from (1.16), (1.17) of equation of short waves will obtain:

for elastic medium

$$\frac{\partial m}{\partial \delta} + \frac{\partial e}{\partial \delta} = 0, \quad \frac{\partial m}{\partial \tau} - \delta \frac{\partial m}{\partial \delta} + m = 0 \quad (1.20)$$

for medium in limiting state

$$\frac{\partial m}{\partial \delta} + \frac{\partial e}{\partial \delta} = 0, \quad \frac{\partial m}{\partial \tau} - (\delta + \kappa m + h) \frac{\partial m}{\partial \delta} + (2 - \alpha)m = 0 \quad \left( \kappa = l \frac{\epsilon_0}{\Delta_0} \sim 1 \right) \quad (1.21)$$

If  $\kappa \ll 1$ , it is possible to show that speed of propagation of deformations in regions of limiting state will be constant, and that quantity  $\kappa m$  in equation (1.21) should be disregarded.

From first equations of (1.20) and (1.21) it follows

$$m = -e \quad (1.22)$$

(arbitrary function of  $\tau$  is equal to zero due to continuity of  $m$  and  $e$  on boundary of elastic zone and state of rest on boundaries of zones of elastic and limiting states).

During derivation of equation of short waves with acceptable accuracy (to small parts of first order inclusively) into final equations did not enter quantity  $\epsilon_0$ , since it is small of order of  $\Delta_0 M_0$ . Since Lagrange coordinate  $r_0$  differs from  $r$  by  $\epsilon_0$ , then with acceptable accuracy  $r = r_0$ .

Therefore equations of short waves (1.20) and (1.21) have the same form in Lagrange and Euler coordinates.

If, in expression for  $N$  from (1.19), we replace  $a_{10}$ ,  $a_0$  by their expressions through Lamé parameters and quantity  $\alpha$  from conditions of limiting state, it is possible to establish following relation

$$\alpha = \frac{\lambda}{\lambda + 2\mu} - h\Delta_0 \left(1 + \frac{\lambda}{\lambda + 2\mu}\right), \text{ or } \alpha = \frac{\nu}{1-\nu} \left(1 - \frac{h\Delta_0}{\nu}\right) \quad (h\Delta_0 \ll 1) \quad (1.23)$$

Here  $\nu$  - Poisson's ratio. Quantity  $h\Delta_0$ , as follows from formula for  $N$ , determines jump of local speed of sound during transition from elastic region to region of limiting state

$$a_{10} = a_0 (1 - h\Delta_0) \quad (1.24)$$

i.e., in case of weak short wave  $(a_{10} - a_0) / a_0$  - small quantity of order of  $\Delta_0$ . From (1.23) it follows that for such wave  $\alpha = \nu / (1 - \nu)$  with accuracy within small part of order  $\Delta_0$ .

If speed of sound changes continuously, then  $h = 0$  and quantity  $\alpha$  in accuracy, is equal to  $\nu / (1 - \nu)$ , as was noted in [4].

We return to relationships of (1.10). Let us consider simplest case, considering  $\alpha = \nu / (1 - \nu)$  and disregarding nonlinearity  $\underline{1} = \underline{1}'' = 0$ ; we have

$$- \sigma_r = (\lambda + 2\mu) \varepsilon, \quad - \sigma_\theta = \lambda \varepsilon$$

We will compare these and elastic dependences

$$- \sigma_r = (\lambda + 2\mu) \varepsilon - 4\mu \varepsilon_\theta, \quad - \sigma_\theta = \lambda \varepsilon + 2\mu \varepsilon_\theta$$

One would think, that due to smallness of  $\varepsilon_\theta$  in comparison with  $\varepsilon_r$ , there should be no difference both in laws of propagation and wave attenuations in elastic and limiting zones. However, this is not so. Into equation of dynamics of elastic media (1.14) enters derivative  $\partial \varepsilon_\theta / \partial r_0$ , having the same order  $M_0$  as longitudinal deformation  $\varepsilon_r$  (see (1.6)), and size of this derivative can be disregarded no longer. This determines faster attenuation of stresses in region of limiting state as compared with attenuation of stresses in short

elastic wave (compare second equations in (1.20) and (1.21)). We will show, at last, that if into conditions of limiting state (1.7) or 1.19) we introduce constant component  $\beta$  (let us consider, for example, linear condition (1.9) and connection  $\alpha$  and  $\nu$  in the form (1.23))

$$\sigma_0 = \alpha \sigma_r - \beta, \quad \frac{\sigma_r}{\lambda + 2\mu} \sim \epsilon_0 \quad (1.25)$$

then, for short wave  $\beta / (\lambda + 2\mu)$  will be small of order  $\Delta_0 \epsilon_0$ , and quantity  $\beta$  in equation of motion should be disregarded.

We make following appraisal. From condition (1.25) we have

$$\dot{\sigma}_0 = \frac{\nu}{1-\nu} \dot{\sigma}_r - \beta - \frac{k \Delta_0}{1-\nu} \sigma_r$$

and from elastic connection

$$\sigma_0 = \frac{\nu}{1-\nu} \sigma_r - 3 \frac{1-2\nu}{1+\nu} (\lambda + 2\mu) \epsilon_0$$

Since, during transition from elastic region to region of limiting state, stresses are continuous, then

$$\frac{\beta}{\lambda + 2\mu} = \Delta_0 M_0 \left( 3 \frac{1-2\nu}{1+\nu} - \frac{k}{1-\nu} \right) \sim \Delta_0 M_0 \quad (1.26)$$

In this case, during derivation of equations of short waves (1.21) under condition of (1.25), into the right part of (1.17) would enter a quantity of order  $\Delta_0 M_0$ , which one should reject. Thus, during the study of continuous strain waves, one should use condition (1.9) and consider  $\alpha$  and  $\nu$  connected by relationship (1.23).

1.4. We will find common integrals of equations (1.20) and (1.24).

Integrating ordinary differential equations

$$\frac{d\tau}{\tau} = \frac{d\delta}{-(\delta + \alpha m + h)} = \frac{dm}{-(2-\alpha)m}$$

we determine

$$C_1 = m t^{2-\alpha}, \quad \delta = C_2 m^{\frac{1}{2-\alpha}} + \frac{\alpha m}{1-\alpha} - h$$

Hence, common integral

$$\delta = m^{\frac{1}{2-\alpha}} \Phi(m t^{2-\alpha}) + \frac{\alpha m}{1-\alpha} - h \quad (1.27)$$

where  $\Phi$  - arbitrary function.

Common integral can be rewritten in the form

$$m = T^{-(2-\alpha)} \Psi \left[ \left( \delta - \frac{\kappa m}{1-\alpha} + h \right) T \right], \quad T = \frac{t}{t_0} \quad (1.28)$$

where (by meaning of problem)  $\Psi$  - arbitrary positive, monotonically increasing function; entry with variable  $T$  was selected for convenience of determination of  $\Psi$  from initial data at  $t = t_0$ .

We will write (1.28) in variables  $(r, t)$

$$\frac{u}{a_0} = \frac{1}{r^{2-\alpha}} \Psi(\xi), \quad \xi = r \left( 1 - \frac{\kappa m \Delta_0}{1-\alpha} \right) - a_0^2 (1 - h \Delta_0) t \quad (1.29)$$

coinciding, at  $h = 0$ , with integral, shown in [4].

Common integral of equation of short elastic waves has form

$$m = \delta \Phi(\delta T), \quad \text{or} \quad m = \frac{\Phi_0(\delta T)}{T} \quad (1.30)$$

where  $\Phi_0$  - arbitrary function. Or

$$\frac{u}{a_0} = \frac{\Phi_1(r - a_0 t)}{r} \quad (1.31)$$

From comparison of (1.29) and (1.31), it follows that in region of limiting state, decrease of amplitudes with distance occurs reciprocally to  $r^{2-\alpha}$ , independently of quantity  $\kappa$ , which determines change of speed of sound as function of size of load. In elastic medium it is reciprocal to  $r$ .

Comparison of formulas (1.10) and (1.13) shows that at  $\alpha \doteq \nu / (1 - \nu)$  connection  $\sigma_r(\varepsilon)$ , in elastic and limiting states, hardly differ. This fact is well illustrated by experiments with fast loading, for example, Fig. 1 from [8] (with increase of velocity of loading, function  $\sigma_r(\varepsilon)$  changes from (5) to (1)). But, as follows from presented [example], law of attenuation of amplitudes does not determine this connection, but derivative of  $\sigma_r$  in respect to  $r$ , which is various for elastic and limiting states.

In concluding this section we will introduce integrals of equations for short waves in elastic medium and in medium of limiting state.

#### In cylindrical case

$$\frac{\partial m}{\partial \delta} + \frac{\partial \varepsilon}{\partial \delta} = 0, \quad \frac{\partial m}{\partial r} - (\delta + \kappa m) \frac{\partial m}{\partial \delta} + \frac{2-\alpha}{2} m = 0 \quad (1.32)$$

These equations allow common integral ( $h = 0, \psi(\tau) = 0, \text{ i.e., } m = -e$ )

$$\delta = m^{\frac{2}{2-\alpha}} \Phi\left(mt^{\frac{2-\alpha}{2}}\right) + \frac{\alpha}{2} \kappa m \quad \text{or} \quad m = T^{\frac{\alpha-2}{2}} \Phi_0\left[\left(\delta - \frac{\alpha}{2} \kappa m\right) T\right] \quad (1.33).$$

Here  $\Phi_0$  - arbitrary positive, monotonically increasing function. In cylindrical case, common integral of equation of short elastic waves has form

$$m = T^{-\nu} \Phi(\delta T)$$

which coincides with main member of asymptotic expansion of known solution for elastic waves.

In case of plane wave (or for wave in rod, included in rigid shell) connections of stresses and deformations in elastic and limiting states do not differ, since as before, from continuity of speeds, follows connection  $\alpha = \nu/(1-\nu)$ , and lateral deformations are absent.

Equations of short waves for medium in limiting state will differ from equations of short elastic waves only by component, allowing for nonlinearity of volume strain ( $\underline{l} \neq 0$ ), which influences only rebuilding of stress profile, and does not affect attenuation, if we disregard unloading

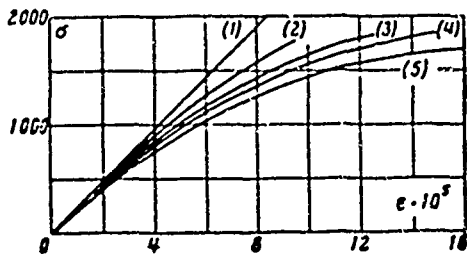


Fig. 1.

$$\begin{aligned} \frac{\partial m}{\partial \delta} + \frac{\partial e}{\partial \delta} &= 0 \\ \frac{\partial m}{\partial \tau} - (\delta + lm) \frac{\partial m}{\partial \delta} &= 0 \end{aligned}$$

Hence, it follows that

$$m = \Phi[(\delta + lm)t] \quad (1.34)$$

Here  $\Phi$  - arbitrary function. Case of

plane elastic wave follows from (1.34) at  $\underline{l} = 0$ .

As in elastic medium, so also in medium, located in limiting state (disregarding unloading), decrease of amplitudes of continuous plane wave of loading with distance does not occur. This agrees with known facts.

2.1. We will investigate influence of elastic unloading on attenuation of amplitudes in spherically-symmetrical strain wave, region of loading of which is described by solution of Section 1.

Influence of irreversible losses on lowering of peaks of stresses in spherical (and cylindrical) case can appear in two-fold manner:

1) in region of loading, velocity of propagation of perturbations (speed of sound)  $a_1$  is less than speed of sound  $a_0$  in stationary medium (or in zone of elastic unloading), because of this, wave of unloading continuously lowers peaks of stress in wave;

2) presence of irreversible losses during loading (limiting state of medium) leads to faster lowering of all stresses in zone of loading, as compared with case of elastic (reversible) deformations. As was shown above, in region of load faster lowering of amplitudes of all stresses occurs, as compared with lowering in elastic wave ( $r^{-(2-\alpha)}$ ,  $\alpha < 1$  instead of  $r^{-1}$ ).

Influence of unloading wave on decrease of peaks of stresses in strain wave is determined by conditions of reflection and refraction of waves at boundary of region of elastic unloading and region of loading. Influence of unloading depends on difference in velocities of propagation of perturbations and on relative magnitude of gradients of stress curve in regions of loading and unloading [5, 6].

Knowing solution of problem of wave propagation in region with limiting state, for determination of unloading wave it is necessary to solve boundary problem for equations of theory of elasticity (data on one of characteristics and data on unknown curve, near characteristic of second family), which can be done by numerical methods (for example, method of characteristics).

If, however, we consider only appraisal of influence of unloading on attenuation of maximum amplitudes, it is possible to use following method: to derive formula for initial velocity of unloading front (by analogy with derivation for plane elastic-plastic wave [5, 6]), and then by deviation of speed of unloading front from speed of sound to estimate contribution of unloading to decrease of amplitudes.

2.2. We will derive equation of elastic unloading. Equations of motion and inseparability of small elastic deformations have form

$$\rho_0 \frac{\partial u}{\partial t} + \frac{\partial \sigma_r}{\partial r} + 2 \frac{\sigma_r - \sigma_\theta}{r} = 0, \quad \frac{\partial u}{\partial t} + 2 \frac{u}{r} - \frac{\partial e}{\partial t} = 0 \quad (2.1)$$

During unloading, differences between stresses and deformations obey the Hooke law

$$\begin{aligned} -(\sigma_r - \sigma_{r-}) &= (\lambda + 2\mu) e - 4\mu e_0 - (\lambda + 2\mu) e_- + 4\mu e_{0-} \\ -(\sigma_\theta + \sigma_{\theta-}) &= \lambda e + 2\mu e_0 - \lambda e_- - 2\mu e_{0-} \end{aligned} \quad (2.2)$$

where quantities with minus index are calculated on front of unloading  $t = f(r)$  from side of region of loading ( $f(r)$  - unknown function).

Using connection of stresses and deformations in region of limiting state (not limiting generality of conclusion, we assume below  $h = 0$ , so that  $\alpha = \nu / (1 - \nu)$ )

$$-\sigma_{r-} = (\lambda + 2\mu) e_- (1 + \alpha e_-), \quad -\sigma_{\theta-} = \lambda e_- (1 + \alpha e_-) \quad (2.3)$$

From (2.2) we find

$$\begin{aligned} -\sigma_r &= (\lambda + 2\mu) e - 4\mu e_0 + (\lambda + 2\mu) \alpha e_-^2 + 4\mu e_{0-} \\ \sigma_r - \sigma_\theta &= -2\mu (e - 3e_0) - 2\mu \alpha e_-^2 - 6\mu e_{0-} \end{aligned} \quad (2.4)$$

Putting (2.4) in equation of motion (2.1), we find

$$\rho_0 \frac{\partial u}{\partial t} - (\lambda + 2\mu) \frac{\partial e}{\partial r} = \rho_0 \alpha e_-^2 G(r) \quad (2.5)$$

where

$$G(r) = \left( \frac{a_1^2}{a_0^2} - 1 \right) \left[ \frac{\partial e_-}{\partial r} + 2(1 - \alpha) \frac{e_-}{r} \right] + 2(1 - \alpha) \frac{e_-}{r} \quad (2.6)$$

If we introduce characteristic variables

$$\xi = r - a_0 t, \quad \eta = r + a_0 t \quad (2.7)$$

in region of elastic unloading, equations of (2.1) can be written in following form

$$\frac{\partial F_1}{\partial \eta} = -\frac{u}{r} + a_0 \frac{G(r)}{2}, \quad \frac{\partial F_2}{\partial \xi} = -\frac{u}{r} - a_0 \frac{G(r)}{2} \quad \begin{cases} F_1 = u - a_0 e \\ F_2 = u + a_0 e \end{cases} \quad (2.8)$$

Relationships of (2.8) will be represented in following form, convenient for further computations:

along characteristic  $\xi = \text{const}$

$$u = a_0 e - \int_{\xi_0}^{\xi} \left[ \frac{u}{r} - a_0 \frac{G(r)}{2} \right] d\eta + F(\xi) \quad \left( r = \frac{\xi + \eta}{2} \right) \quad (2.9)$$

along characteristic  $\eta = \text{const}$

$$u = -a_0 e - \int_{\xi_0}^{\xi} \left[ \frac{u}{r} + a_0 \frac{G(r)}{2} \right] d\xi + E(\eta) \quad (2.10)$$

2.3. We will derive formula for initial velocity of unloading  $c$ , following method, shown in [6], for plane of unloading wave.

Let, at  $r = r_0$  deformation curve be given  $\epsilon_0(t)$ , having corner at  $\epsilon_0 = \epsilon_{\text{max}}$ ,  $t = t_0$ . In vicinity of this point, it is possible, approximately, to describe curve by formulas (Fig. 2)

$$\begin{aligned} \epsilon_0 &= \epsilon_{\text{max}} - k_1(t - t_0) & (t < t_0) \\ \epsilon_0 &= \epsilon_{\text{max}} + k_2(t - t_0) & (t \geq t_0) \end{aligned} \quad (2.11)$$

Loading corresponds to  $t < t_0$ , unloading -  $t \geq t_0$ ,  $k_1, k_2$  - positive values of gradients of deformation.

Solution of problem of unloading is based on joint solution of equations of short waves for region of limiting state and equations (2.9), (2.10) for elastic unloading, taking into account boundary conditions of (2.11) at  $r = r_0$  and conditions of continuity of particle velocities and deformations on unloading front  $t = f(r)$ , position of which is not known.

Using approximations of (2.11), we will define values of deformations at points A, B, and C, on characteristics in region of loading and unloading respectively, considering quantities of velocities  $c$  and  $a_1$  constant in section  $(r_0, r_0 + dr^*)$ :

$$\begin{aligned} \epsilon_A &= \epsilon_{\text{max}} - k_1 \left( dt^* - \frac{dr^*}{a_1} \right) \\ \epsilon_B &= \epsilon_{\text{max}} + k_2 \left( dt^* - \frac{dr^*}{a_0} \right) \\ \epsilon_C &= \epsilon_{\text{max}} + k_2 \left( dt^* + \frac{dr^*}{a_0} \right) \end{aligned} \quad (2.12)$$

At point M  $(r_0 + dr^*, t_0 + dt^*)$  on front of unloading, we will calculate deformation and particle velocity by the formulas for region of limiting

state

$$\varepsilon = r^{-(2-\alpha)} \Psi [r - r_0 - a_1(t - t_0)], \quad u = -a_0 \varepsilon \quad (2.13)$$

Hence, with the help of (2.11), for section of load it follows

$$\varepsilon = \left(\frac{r_0}{r}\right)^{2-\alpha} \left\{ \varepsilon_{\max} - \frac{k_1}{a_1} [a_1(t - t_0) - (r - r_0)] \right\} \quad (2.14)$$

Thus, on front of unloading

$$r - r_0 = c(t - t_0) \quad \text{OR} \quad dr^* = c dt^* \quad (c = dr/dt = 1/f')$$

will be

$$\varepsilon_M \approx \varepsilon_{\max} - (2-\alpha) \varepsilon_{\max} dr^*/r_0 - k_1 dt^*(1 - c/a_1) \quad (2.15)$$

$$u_M \approx u_{\max} - (2-\alpha) u_{\max} dr^*/r_0 + a_0 k_1 dt^*(1 - c/a_1) \quad (2.16)$$

with accuracy within first degrees of  $dr^*$ ,  $dt^*$  inclusively.

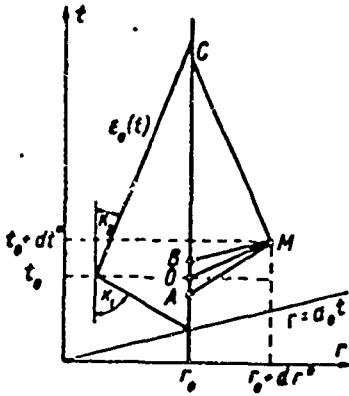


Fig. 2.

We will determine "reflectivity factor" of

waves in region of elastic unloading from front of unloading.

From proximity of points B and C to point O it follows

$$\begin{aligned} u_B - u_{\max} &= \frac{\partial u}{\partial t} \Big|_{t=t_0+0} (t_B - t_0) = I \left(1 - \frac{c}{a_0}\right) dt^* \\ u_C - u_{\max} &= \frac{\partial u}{\partial t} \Big|_{t=t_0+0} (t_C - t_0) = I \left(1 + \frac{c}{a_0}\right) dt^* \end{aligned} \quad (2.17)$$

where  $I$  - acceleration at origin of unloading.

Hence,

$$\frac{u_B - u_{\max}}{u_C - u_{\max}} = \frac{1 - c/a_0}{1 + c/a_0} \quad (2.18)$$

For calculation of  $u_B - u_{\max}$  and  $u_C - u_{\max}$  we will use relationships on characteristics in region of elastic unloading, will calculate  $u_B - u_M$  and  $u_C - u_M$  with the help of (2.9) and (2.10), and then, with the help of formula (2.16) for  $u_M$ , let us turn to required quantities. Inasmuch as relationship along characteristic (2.9) and (2.10) is applied in immediate vicinity of point  $(r_0, t_0)$ , integrals in (2.9) and (2.10) are calculated approximately; integrand is calculated at point M (or point O) and is multiplied by length of interval of integration

2dr\*.

Omitting intermediate calculations, we arrive at final expressions

$$u_B - u_{max} = a_0 k_2 (1 - c/a_0) dt^* + 2a_0 k_1 (1 - c/a_1) dt^* + G_1 a_0 k_1 dt^*$$

$$u_C - u_{max} = -a_0 k_2 (1 + c/a_0) dt^* - 2a_0 \epsilon_{max} dr^* / r_0 - G_1 a_0 k_1 dt^*$$

where

$$G_1 = \left( \frac{a_1^2}{a_0^2} - 1 \right) \left[ \frac{\epsilon_{max} c}{k_1 r_0} + \left( 1 - \frac{c}{a_1} \right) \right]$$

Putting these expressions in (2.18), we obtain equation for unknown quantity  $U$

$$\frac{1 - c/a_0}{1 + c/a_0} = \frac{(k_2/k_1)(1 + c/a_0) + 2(1 - c/a_1) + G_1}{-(k_2/k_1)(1 + c/a_0) + 2\pi U - G_1} \quad \left( U = -\frac{\epsilon_{max} c}{k_1 r_0} \right) \quad (2.19)$$

Quantity  $U$ , as easily shown, will be small, due to shortness of wave. Indeed, for curve with linear build-up of quantity of deformation  $U = s_1/r_0$ , so that  $U$  has order of smallness  $\Delta_0$ .

Using experimental data on proximity of quantity  $c$  and  $a_0$  ( $1 - c/a_0 = \omega_1, \omega_1 \ll 1$ ), and assuming that  $1 - a_1/a_0 = \omega_2, \omega_2 \ll 1$ , from (2.19), we obtain, with an accuracy to the small order of the products  $\omega_1, \omega_2, \Delta_0$ .

$$\frac{c}{a_1} = 1 + \frac{k_2}{k_1} \left( 1 - \frac{c}{a_0} \right) \quad (2.20)$$

i.e., velocity of front of unloading is nearer to velocity of propagation of

deformations in limiting region  $a_1$ , the less  $k_2/k_1$  - ratio of gradients in region of unloading and loading - and the less  $\omega_1$  - deviation of velocity of propagation of peak  $c$  from  $a_0$ .

Formula (2.20) coincides with analogous formula for plane wave of unloading [5, 6], if in the latter, are consider  $\omega_2 \ll 1$ . Coincidence of (2.20) with results for plane wave is result of shortness of loading wave.

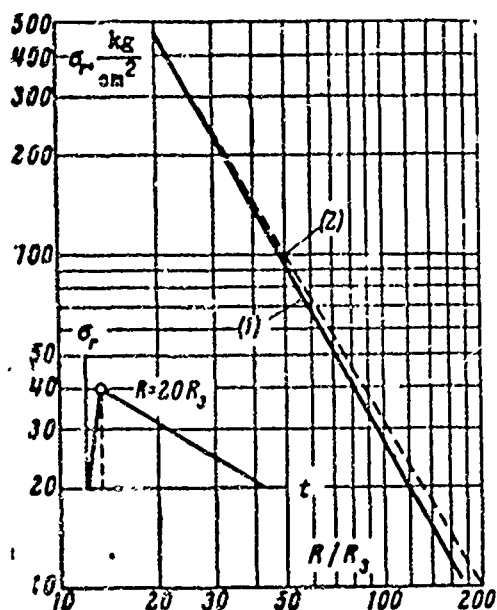


Fig. 3.

Application of (2.20) to appraisal of influence of unloading on attenuation of peak amplitudes of strain waves during explosions in durable rocks, shows that this influence is insignificant, since at short distances, where  $\omega_1 \sim 0.1$ , ratio  $k_2/k_1$  is small, and at great distances, where  $k_2/k_1 \sim 0.26 - 0.3$ , there is minute difference  $1 - c/a_0$ . For appraisal of influence of unloading, following calculation was performed, in which experimental strain curves were used [3]. Law of attenuation of maximum stresses, according to this data, is represented by dependence 1 (Fig. 3). As initial curve was taken stress curve at distance of  $20 R_*$ , shown in Fig. 3. Using experimental data on quantities  $k_2$  and  $k_1$ , and on speeds  $a_0$  and  $c$ , with the help of formula (2.20), was calculated decrease of maximum amplitude owing to unloading at all distances from point of explosion. For intermediate distances between empirical curves, interpolation was made. Thus, dependence 2 (Fig. 3) was determined, which corresponds to change of maximum stress, without influence of unloading.

At distance  $150 R_*$ , as seen from Fig. 3, amplitude of stresses, measured in experiment, is equal to  $13.8 \text{ kg/cm}^2$ , without regard for influence of unloading, amplitude  $\sigma_0 = 16 \text{ kg/cm}^2$ . If we calculate attenuation of amplitudes, without regard for transfer of rock in limiting state in regions of loading (i.e., for elastic medium), amplitude of stresses is equal to  $62 \text{ kg/cm}^2$ .

In [7], remarks concerning our article from N. S. Medvedeva [4] were expressed in which preliminary results of investigations of waves of loading in rocks were presented. These notes relate to connection between  $\alpha$  and  $\nu$  and to possible influence of unloading (which was not estimated in [4]). This criticism forced return to problem of strain waves and re-examination, once again, of basic conclusions of [4]. As reader may note, all basic assertions of [4] are true.

Author extends sincere gratitude to S. A. Khristianovich for valuable advice and instructions, given during execution of present work.

Submitted  
1 June 1963

## Literature

1. S. A. Khristianovich. Shock wave at great distances from point of explosion, PMM, 1956, No 6.
2. A. A. Grib, O. S. Ryzhov, and S. A. Khristianovich. Theory of short waves, PMTF, 1960, No 1.
3. A. N. Khanukayev, I. F. Vanyagin, V. M. Gogolev, and V. G. Markin. On propagation of strain waves during explosion in hard rocks. Records of Leningrad Mining Institute im. G. V. Plekhanov, 1961, Vol. XIV, No. 1.
4. N. S. Medvedeva and Ye. I. Shemyakin. Loading waves during underground explosion in rocks, PMTF, 1961, No 6.
5. Kh. A. Rakhmatullin, and Yu. A. Dem'yanov. Durability during intense short-term loadings. 1961.
6. V. L. Biderman. Calculations on impact load. Bases of contemporary methods of calculation on durability in machine building, Coll. under editorship of S. D. Ponomarev, Mashgiz, 1952.
7. S. S. Grigor'yan, A. A. Grib, N. V. Zvolinskiy, L. M. Kachanov, and G. I. Petrashen'. On works of Ye. I. Shemyakin "Expansion of gas cavity in incompressible elastic-plastic medium (to study of action of explosion on soil)," and N. S. Medvedeva, and Ye. I. Shemyakin "Waves of loading during underground explosion in rocks," News of Academy of Sciences USSR, series. Mechanics and machine building, 1962, No 5.
8. W. Glanvill. The creep or flow of reinforced concrete, London, 1930.

## APPROXIMATE EQUATION OF STATE OF SOLID BODIES

V. M. Gogolev, V. G. Myrkin, and  
G. I. Yablokov

(Leningrad)

In series of problems, coupled with study of strong shock waves in solid bodies, information is necessary about their thermodynamic properties during high loads. At present, for study of mentioned properties, so-called method of shock compression [1-10], is widely used. This method allows to obtain shock adiabat for investigated material. Using shock adiabat and theoretical model of solid body in Debye approximation or in more accurate approximation, equation of state and other thermodynamic relationships can be obtained.

Large variety of solid materials and insufficient knowledge their properties during shock compression pose question of consideration of possibility of generalization of experimental data and obtaining of unified relationships, describing thermodynamic properties of definite class of solid materials, which would allow to make extrapolation of these properties on other materials. Such generalization, in accurate meaning, is hardly possible. However, for problems of applied character, in many cases presence of approximate information is sufficient for this question.

Below are given results of generalization of experimental data of [1-10] concerning shock compression of metals, rocks, and several other solid materials. Offered is single shock adiabat for shown materials. On the basis of theoretical model of solid body in Debye approximation and shock adiabat, generalized equation of state expression for internal energy and several other thermodynamic relationships for solid bodies are given. These results have an approximate character.

1. Generalized shock adiabat. At present, in sufficient detail, shock compressibility of metals has been studied [1-5, 8-10]. Furthermore, in published literature there are experimental data on shock compression of series of rocks

[6, 11] and certain other solid materials [6, 7]. Let us consider possibility of their generalization and obtaining of single shock adiabat. For comparison of shown data, it is necessary to bring them to dimensionless form. As measured parameters, which would characterize form of hard material, it is rational to select speed of sound  $c_0$  in undisturbed medium and density  $\rho_0$ .

In Fig. 1 are given experimental points on shock compression of solid rocks and related materials in system of coordinates

$$\Delta P = \frac{p - p_0}{\rho_0 c_0^2}, \quad M = \frac{u}{c_0}$$

where  $p - p_0$  - pressure jump at front of shock wave, spreading in undisturbed medium,  $u$  - particle velocity at front of shock wave. From consideration of figure, it is clear that for various materials, experimental points are sufficiently well coordinated among themselves without any noticeable systematic deviation.

In Fig. 2, in that same system of coordinates are given experimental points for dimensionless pressures up to magnitudes  $\sim 35$ . Since, for large pressures, information about shock compressibility of solid rocks is absent, on figure are given points for metals; in given case, experimental points for various materials are well coordinated.

Below, on basis of given data, is made an attempt to obtain single shock adiabat for solid rocks, metals, and several other materials.

During approximation of experimental data on compressibility of liquids and solid bodies analytic function is frequently used, of form

$$\Delta P = \frac{p - p_0}{\rho_0 c_0^2} = \frac{1}{A} \left[ \left( \frac{p}{p_0} \right)^n - 1 \right] \quad (1.1)$$

where  $A$  and  $n$  - constants, determined by experimental data. Using conditions of dynamic compatibility, we proceed in (1.1) to variables  $\Delta P$ ,  $M$

$$M^2 = \Delta P \{1 - (A \Delta P + 1)^{-1/n}\} \quad (1.2)$$

As a result of approximation of data of Figs. 1 and 2, we obtain

$$A = 5.5, \quad n = 5 \quad \text{when} \quad 0.1 \leq \Delta P \leq 35 \quad (1.3)$$

$$A = 3, \quad n = 3 \quad \text{when} \quad 0 \leq \Delta P < 0.1 \quad (1.4)$$

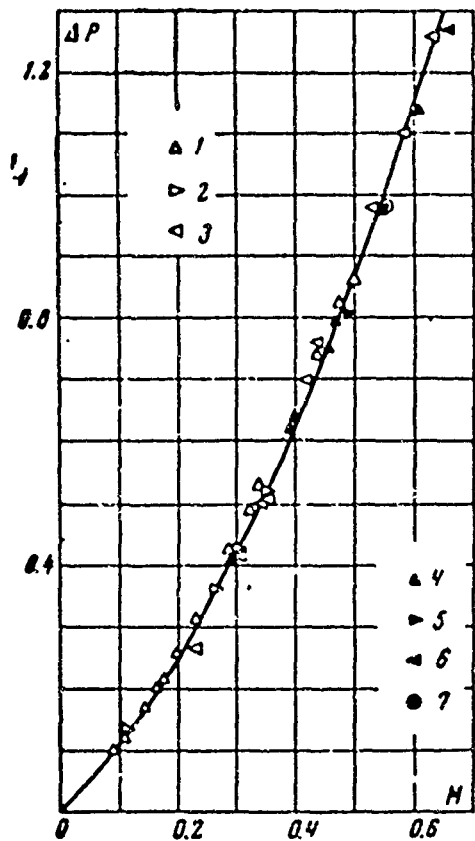


Fig. 1. Curve-calculation by formula (1.2); points:

- 1 - marble ( $\rho_s = 275$ ,  $c_s = 3610$ )
  - 2 - quartz ( $\rho_s = 270$ ,  $c_s = 3700$ )
  - 3 - paraffin ( $\rho_s = 92.8$ ,  $c_s = 3000$ )
  - 4 - NaCl, single crystal ( $\rho_s = 220$ ,  $c_s = 3318$ )
  - 5 - CO<sub>2</sub> solid ( $\rho_s = 157$ ,  $c_s = 2660$ )
  - 6 - tuff, rose ( $\rho_s = 194$ ,  $c_s = 1950$ )
  - 7 - tuff, white ( $\rho_s = 163$ ,  $c_s = 1300$ )
- $(\rho_s) = \text{sec}^2/\text{m}^4$      $(c_s) = \text{m}/\text{sec}$

In Figs. 1 and 2, graph of dependence of (1.2) with respect to (1.3) and (1.4) is shown by solid lines. This graph is sufficiently well coordinated with experimental points. Relative deviation of experimental points from curve lies within limits ten percent.

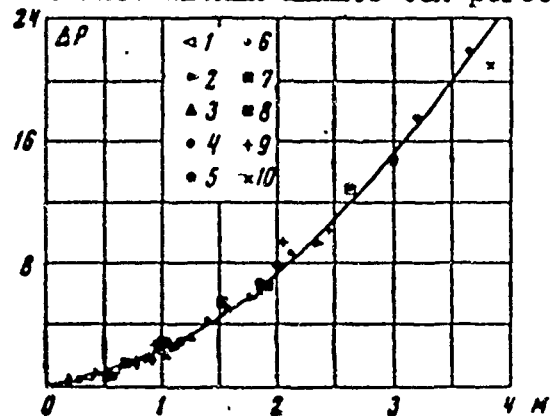


Fig. 2. Curve-calculation by formula (1.2); points:

- 1 - paraffin
- 2 - CO<sub>2</sub>, solid
- 3 - NaCl, single crystal
- 4 - Cd ( $\rho_s = 891$ ,  $c_s = 2110$ )
- 5 - Cu ( $\rho_s = 896$ ,  $c_s = 3200$ )
- 6 - Pb ( $\rho_s = 1154$ ,  $c_s = 2220$ )
- 7 - Sn ( $\rho_s = 743$ ,  $c_s = 2700$ )
- 8 - Zn ( $\rho_s = 728$ ,  $c_s = 3000$ )
- 9 - tuff, white
- 10 - tuff, rose

It is necessary to note that formula (1.2), under condition of (1.4), has interpolating character, since, in this range of pressures, experimental data are absent.

Detailed comparison of approximation (1.2), under conditions (1.3) and (1.4), with experimental data for various metals is given in Fig. 3. This comparison once again shows good coincidence of experimental data with approximation (1.2) - (1.4).

In plane of variables  $\Delta P$  and  $\rho/\rho_s$  there is rather large scattering of experimental points. In connection with this, deviation of experimental points

from curve (1.2) reaches 20%.

Thus, conducted comparison of experimental data for various solid rocks, metals, and several other materials shows that for approximate description of shock compressibility of these materials it is possible to use generalized shock adiabat (1.1).

2. Equation of state for solid bodies. Knowledge of shock adiabat of solid body allows to receive equation of state and other thermodynamic characteristics, if one were to use theoretical model of solid body Debye approximation. It is known [12], that in this approximation, internal energy and equation of state can be represented in the form

$$E = E_x(v) + E_m(v, T) \quad (2.1)$$

$$p = \frac{\partial E_x}{\partial v} + \gamma(v) \frac{E_m}{v} \quad (2.2)$$

Here,  $p$  - pressure;  $T$  - temperature;  $v$  - specific volume;  $E_x$  - energy of cold compression;  $E_m$  - energy, connected with thermal motions of particles;  $\gamma$  - Grüneisen coefficient. In these expressions  $E_m$ ,  $E_x$ , and  $\gamma$  are unknown functions. If they will be determined, then full thermodynamic description of solid body will be obtained. Let us consider their determination. Thermal energy, in this case, can be calculated in following manner [12]:

$$E_m = c_v T \quad (2.3)$$

If we assume that temperature of body, on the one hand, is noticeably above room temperature, and, on the other hand, does not exceed tens of thousands degrees, then, according to Dulong and Petit law [12], we have

$$c_v \approx c_p = \text{const} \quad (2.4)$$

i.e., heat capacities, during constant volume and pressure, are identical and constant. Thus, thermal energy is determined completely by (2.2) and (2.3), in the above mentioned interval of temperatures. For determination of energy of

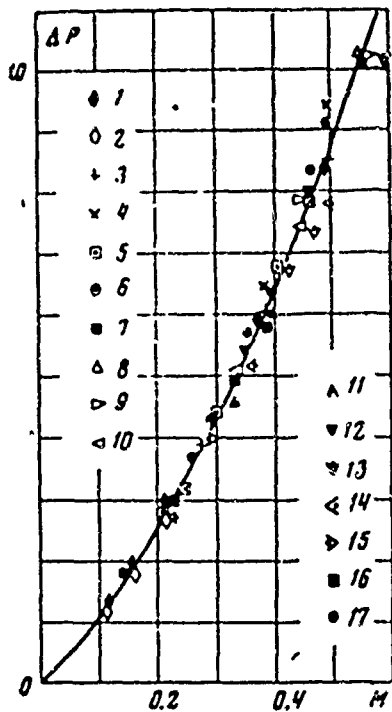


Fig. 3. Curve-calculation by formula (1.2); points:

- |  |
|--|
| 1 - Co ( $\rho_0 = 8800$ , $c_0 = 4630$ )  |
| 2 - Be ( $\rho_0 = 188$ , $c_0 = 7800$ )   |
| 3 - Th ( $\rho_0 = 11900$ , $c_0 = 2050$ ) |
| 4 - Tl ( $\rho_0 = 1210$ , $c_0 = 1830$ )  |
| 5 - Zn                                     |
| 6 - Cd                                     |
| 7 - Zr ( $\rho_0 = 662$ , $c_0 = 3330$ )   |
| 8 - Ag ( $\rho_0 = 1070$ , $c_0 = 3190$ )  |
| 9 - Au ( $\rho_0 = 1930$ , $c_0 = 3050$ )  |
| 10 - Cr ( $\rho_0 = 725$ , $c_0 = 5150$ )  |
| 11 - Mo ( $\rho_0 = 1040$ , $c_0 = 5190$ ) |
| 12 - Ni ( $\rho_0 = 905$ , $c_0 = 4630$ )  |
| 13 - Ti ( $\rho_0 = 450$ , $c_0 = 4310$ )  |
| 14 - V ( $\rho_0 = 622$ , $c_0 = 5160$ )   |
| 15 - W ( $\rho_0 = 1955$ , $c_0 = 4050$ )  |
| 16 - Sn ( $\rho_0 = 743$ , $c_0 = 2760$ )  |
| 17 - Cu ( $\rho_0 = 908$ , $c_0 = 3980$ )  |

immaterial additive constant.

For determination of Grüneisen coefficient by L. D. Landau and Slater [1-4], was offered dependence

$$\gamma = -\frac{2}{3} - \frac{v}{2} \frac{d^2 p_x / dv^2}{dp_x / dv} \quad \left( p_x = -\frac{\partial E_x}{\partial v} \right) \quad (2.6)$$

Here  $p_x(v)$  pressure of cold compression;  $E_x$  - energy of cold compression.

Some time later, MacDonald and Dugdale offered a more accurate, though bulkier,

cold compression, shock adiabat is used [1, 8]. For that, from condition of dynamic jointness

$$E - E_0 = \frac{1}{2}(p + p_0)(v - v_0)$$

where  $E_0$ ,  $p_0$ ,  $v_0$  - values of parameters before front of shock wave, thermal part of energy, is excluded with the help of (2.1) and (2.2). As a result, equation for determination of energy of cold compression is obtained by shock adiabat

$$\frac{d\Delta E_x}{dv} + \frac{\gamma}{v} \Delta E_x = -\frac{\gamma}{2} \left( \lambda - \frac{v_0}{v} \right) (p - p_0) + \gamma p_0 \left( \frac{v_0}{v} - 1 \right) - p_0 + \frac{\gamma}{v} E_{m_0} \quad (2.5)$$

Here index 0 designates quantity of parameters of medium in undisturbed state, value of pressures is taken on shock adiabat (1.1)

$$\Delta E_x = E_x - E_{m_0}, \quad \lambda = (2 + \gamma) / \gamma$$

This equation determines energy of cold compression with accuracy within

formula [1 - 4, 8]. For aims of present work, it was more convenient to use dependence (2.6). Totality relationships (2.5) and (2.6) gives differential equation for determination of energy of cold compression. However, accurate solution of this equation is possible only by numerical methods and entails great difficulties. Therefore, we will make approximate solution of shown equation. Calculations show that Gruneisen coefficient is a slowly variable function as compared with remaining variables in (2.5). In connection with this, we will integrate (2.5), considering that  $\gamma$  is constant. Then with the help of (2.6), we will determine dependence of  $\gamma$  on  $v$ . Before doing this, let us turn to dimensionless variables.

$$P = \frac{P}{\rho_0 c_0^2}, \quad V = \frac{v}{v_0}, \quad e_x = \frac{\Delta E_x}{c_0^2}, \quad e_m = \frac{c_v T}{c_0^2} \quad (2.7)$$

Making replacement in (2.5), according to (2.7), and executing integration, we receive

$$e_x = e_x^{(1)}(v) + \frac{P_0}{2} \left[ 1 - \frac{\gamma+2}{\gamma+1} V \right] + V^{-\gamma} \left[ \frac{P_0}{2(\gamma+1)} - e_{m0} \right] + e_{m0} \quad (2.8)$$

where

$$e_x^{(1)} = -\frac{\gamma}{2A} \left\{ \frac{1}{\gamma} \left[ 1 - \frac{(\gamma+2)}{(\gamma+1)} V \right] + \frac{1}{(n-\gamma)} \left[ 1 - \frac{(\gamma+2)(n-\gamma)}{\gamma(n-\gamma-1)} V \right] V^{-n} + \frac{n(n+1)}{\gamma(\gamma+1)(n-\gamma)(n-\gamma-1)} V^{-\gamma} \right\} \quad (2.9)$$

Quantities A and n are determined according to (1.3) - (1.4).

Thus, relationships (2.1), (2.3) and (2.8) allow to receive expression for internal energy. From (2.2), (2.7), and (2.3) we obtain equation of state

$$P = P_x(V) + \frac{\gamma}{V} e_m \quad (2.10)$$

where

$$P_x = P_x^{(1)}(V) + \frac{P_0}{2} \frac{\gamma+2}{\gamma+1} + \frac{\gamma}{V^{\gamma+1}} \left[ \frac{P_0}{2(\gamma+1)} - e_{m0} \right] \quad (2.11)$$

$$P_x^{(1)}(V) = \frac{\gamma}{2A} \left\{ \frac{n}{n-\gamma} \left[ \frac{(\gamma+2)(n-\gamma)(n-1)}{\gamma(n-\gamma-1)n} V^{-1} \right] V^{-(n+1)} - \frac{n(n+1)}{(\gamma+1)(n-\gamma)(n-\gamma-1)} V^{-(\gamma+1)} - \frac{1}{\gamma} \frac{(\gamma+2)}{(\gamma+1)} \right\} \quad (2.12)$$

Quantity  $\gamma$  is determined from (2.6) and (2.11). Disregarding initial values

of parameters in (2.11), we obtain

$$\gamma = -\frac{2}{3} + \frac{1}{2} \frac{B_1(n+1) - B_2(n+2)V^{-1} - B_3(\gamma+2)V^{n-\gamma-1}}{B_1 - B_2V^{-1} - B_3V^{n-\gamma-1}} \quad (2.13)$$

where

$$B_1 = \frac{(\gamma+2)(n-1)n}{n-\gamma-1}, \quad B_2 = \frac{n(n+1)}{n-\gamma}, \quad B_3 = \frac{\gamma n(n+1)}{(n-\gamma)(n-\gamma-1)}$$

Graph of function  $\gamma(V)$  is shown in Fig. 4. Analytic dependence

$$\gamma = 2.3V^{1.23} \quad (2.14)$$

gives sufficiently good approximation of graph of Fig. 4.

Thus, relationships (2.1), (2.3), (2.8), (2.10), and (2.14) give expression for internal energy and equation of state for metals, solid rocks, and several other materials.

In Fig. 5, are given curves for comparison shock adiabat and isotherm of cold compression (2.11) with regard to (2.14). At comparatively small pressures, these curves differ little one from another. Of interest is analytic appraisal of difference of these quantities. We will introduce, for this quantity

$$\delta = \frac{P - P_0}{P_0}$$

Considering it small, as compared with one, and expanding expressions (1.1) and (2.11) in a series along  $\delta$ , we obtain

$$\Delta P - P_x^{(1)} = \frac{1}{A} \left\{ \frac{n\gamma(n+1)[(n-1)(n-2\gamma) + \gamma(\gamma-1)]}{12(n-\gamma)(n-\gamma-1)} \delta^2 + \frac{\gamma n(n+1)[(n-1)(n-2)(2n-3\gamma) - \gamma(\gamma-1)(\gamma-2)]}{2 \cdot 4! (n-\gamma)(n-\gamma-1)} \delta^4 + \dots \right\} \quad (2.15)$$

Since  $V$  changes little here, we consider  $\gamma$  constant. From (2.15), it follows that difference between shock adiabat and isotherm of cold compression, at relatively low pressures, is proportional to  $\delta^2$ .

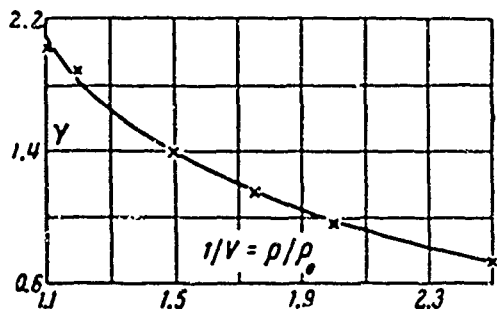


Fig. 4. Curve-calculation by formula (2.13); points - calculation by formula (2.14).

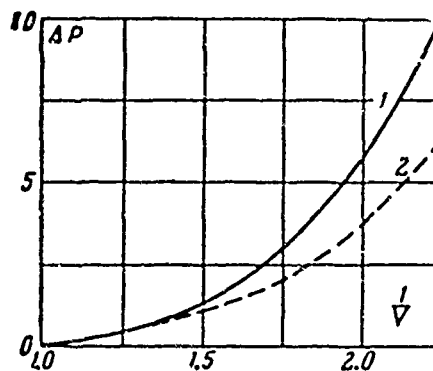


Fig. 5. Comparison of shock adiabat 1, with isotherm of cold compression 2.

3. Expression for entropy of solid body. According to definition, entropy differential has form

$$ds = \frac{dE}{T} + \frac{p dv}{T} \quad (3.1)$$

In accordance with assumptions made above, we have

$$dE = \frac{\partial E_x}{\partial v} dv + c_v dT \quad (3.2)$$

Placing (3.2) in (3.1), we obtain

$$ds = \frac{1}{T} \left[ \frac{dE_x}{dv} + p \right] dv + c_v \frac{dT}{T} \quad (3.3)$$

We proceed, in (3.3), to dimensionless quantities

$$S = \frac{s}{c_v}, \quad P = \frac{p}{\rho_0 c_0^2}, \quad V = \frac{v}{v_0}; \quad e_x = \frac{\Delta E_x}{c_v^2}, \quad e_m = \frac{c_v T}{c_0^2}$$

Using equation of state (2.10), we obtain

$$dS = \frac{1}{V} dV + \frac{de_m}{e_m} \quad (3.4)$$

Integrating this equality from point of initial state ( $S = S_0, V = 1, e_m = e_{m0}$ ) up to arbitrary state, we obtain

$$S - S_0 = \ln \frac{e_m V^{\gamma}}{e_{m0}} \quad (3.5)$$

This relationship represents generalized expression of entropy  $S$  of solid body, through parameters of its state. It is necessary to note external similarity of expression (3.5) to expression for entropy of ideal gas. In latter case, role

of Grüneisen coefficient is different

$$\left(\frac{c_p}{c_v} - 1\right)$$

If, in solid body, there is isoentropic process, then, from (3.5) and (2.10), we obtain following expression for Poisson's adiabat

$$V^{\gamma+1} [P - P_x(V)] = \text{const} \quad (3.6)$$

From (3.6), it follows that product of thermal pressure on specific volume in degrees  $(\gamma + 1)$  is constant quantity, i.e., in given case, there is also the above-noted analogy to ideal gas. This analogy is associated with assumption of (2.3).

In order to receive appraisal of jump of entropy on front of shock wave, depending upon its intensity, we exclude, from (3.5), thermal energy, with the help of equation of state (2.10)

$$S - S_0 = \ln \left\{ 1 + \frac{[P - P_x] V^{\gamma+1} - \gamma e_{m0}}{\gamma e_{m0}} \right\} \quad (3.7)$$

During comparatively slight intensity of shock wave, fraction in expression (3.7) is small. Therefore, we represent logarithm in the form of a series

$$S - S_0 = \frac{[P - P_x] V^{\gamma+1} - \gamma e_m}{\gamma e_{m0}} + \dots$$

Using (2.15) and expanding  $V^{\gamma+1}$  in series along  $\delta$ , we obtain

$$S - S_0 = \frac{1}{\gamma e_{m0}} \{A_1 \delta^2 + [A_2 - A_1(\gamma + 1)] \delta^3 + \dots\} \quad (3.8)$$

where  $A_1$  - coefficient from (2.15) at  $\delta^2$ ;  $A_2$  - coefficient from (2.15) at  $\delta^3$ .

From this expression, it follows that jump of entropy on front of shock wave is proportional to jump of density in degrees not lower than 3.

Thus, on basis of generalization of experimental data on shock compression of metals, solid rocks, and several other nonporous materials, we managed to obtain single, for these materials, shock adiabat. As a result of use of theoretical model of solid body and of single shock adiabat, generalized equation of

state, expression for internal energy and entropy are obtained, which can be used for approximate description of thermodynamic properties of metals, solid rocks, and several other hard nonporous materials.

Submitted  
25 February 1963

#### Literature

1. L. V. Al'tshuler, K. K. Krupnikov, and M. I. Brazhnik. Dynamic compressibility metals at pressures from four hundred thousand to four million atmospheres. Zhurn. eksperim. and teoret. fiz., 1958, Vol. 34, No 4.
2. L. V. Al'tshuler, K. K. Krupnikov, B. N. Lednev, V. I. Zhuchikhin, and M. I. Brazhnik. Dynamic compressibility and equation of state of iron at high pressures. Zhurn. eksperim. and teoret. fiz., 1958, Vol. 34, No 4.
3. L. V. Al'tshuler, L. V. Kuleshov, and M. N. Pavlovskiy. Dynamic compressibility, equation of state, and electrical conductivity of sodium chloride at high pressures. Zhurn. eksperim. and teoret. fiz., 1960, Vol. 39, No 1.
4. L. V. Al'tshuler, A. A. Babanov, and R. F. Trunin. Shock adiabats and zero isotherms of seven metals at high pressures. Zhurn. eksperim. and teoret. fiz., 1962, Vol. 42, No 1.
5. V. N. Zhapkov and V. A. Kalinin. Equation of state of iron up to pressures in several million atmospheres. Reports of Academy of Sciences of USSR, 1960, Vol. 135, No 4.
6. A. N. Dremin. Investigation of shock compression of marble and quartz. Scientist's council on national-economic use of explosion, Siberian Branch of Academy of Sciences of USSR, 1960, No 16.
7. V. N. Zubarev and G. S. Telegin. Shock compressibility of liquid nitrogen and solid carbon dioxide, Reports of Academy of Sciences of USSR, 1962, Vol. 142, No 2.
8. J. M. Walsh, M. H. Rice, and R. G. McQueen. Shock-Wave Compressions of Twenty-seven Metals, Equations of state of Metals, Phys. Rev., 1957, 108, 2.
9. D. Bancroft, E. Peterson, and S. Minshall. Polymorphism of Iron at High Pressure, J. Appl. Phys., 1956, Vol. 27, No 3.
10. R. G. McQueen and S. P. Marsh. Equation of state for Nineteen Metallic Elements from Shock-Wave Measurements to Two Megabars, J. Appl. Phys., 1960, 31, 7.
11. G. W. Johnson, G. H. Higgins, and C. E. Violet. Underground Nuclear Detonations, J. Geophys. Res., 1959, 64, 10.
12. L. Landau and Ye. Lifshits. Statistical physics, 1951., Moscow Leningrad.

EXPERIMENTAL INVESTIGATION OF DYNAMIC STRESSFIELD IN  
SOFT EARTH, DURING CONTACT EXPLOSION

V. D. Alekseyenko

(Moscow)

Contact explosion occurring at boundary of two strongly differing (by properties) media - air, and ground, creates, in latter, non-stationary axisymmetrical stress fields and speeds, and leads to motion of air. Theoretical solution of corresponding problem arising for equation of gas dynamics describing motion of air, and equations of mechanics of ground (eight of which are considered here), present great difficulties. Difficulties also appear during experimental study of this phenomenon.

Below are expounded certain results of experimental investigation of non-stationary stress field, created by contact explosion, in medium-granular sand of undisturbed structure with specific weight  $\gamma = 1.6 \text{ g/cm}^3$  and absolute humidity  $w = 7 - 10\%$ . The following scheme of measurements was used (Fig. 1). On spherical surfaces, far from center of explosion, to relative distances  $r$ , equal to 15, 20, 30, and 40 ( $r = R/r_0$ ,  $R$ —distance from center of explosion,  $r_0$  — radius of charge), at points 1 - 9, were established four-component tensometric data units. With the help of these, were measured normal stresses  $\sigma_1, \sigma_2, \sigma_3$ , acting in coordinate areas of cylindrical system of coordinates  $r, \theta$ , and normal stress  $\sigma_n$ , acting in meridian plane  $\theta$  on area, normal of which constituted, with axis  $\rho$ , fixed angle  $\alpha = \pi/4$ . Details, connected with necessity of such measurements, are contained in [1]. We will give only necessary formulas, allowing, by results of measurement of  $\sigma_1, \sigma_2, \sigma_3, \sigma_n$  to calculate main characteristics of stress field:  $\tau_{\rho z}$  - shear stress,  $\sigma_1, \sigma_2$  - main stresses in meridian plane,  $\varphi$  - angle between one of main directions and direction  $z$

$$\tau_{\rho z} = \frac{\sigma_n \cdot (\tau_\rho \cos^2 \alpha + \tau_z \sin^2 \alpha)}{\sin 2\alpha} \quad (1)$$

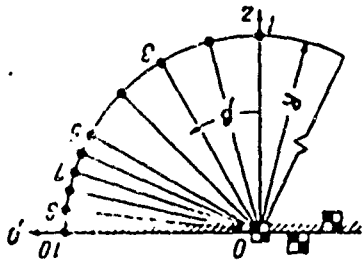


Fig. 1.

$$\sigma_1 = \sigma_x \cos^2 \varphi + \sigma_y \sin^2 \varphi + \tau_{xy} \sin 2\varphi \quad (2)$$

$$\sigma_2 = \sigma_x \sin^2 \varphi + \sigma_y \cos^2 \varphi - \tau_{xy} \sin 2\varphi \quad (3)$$

$$\varphi = 0.5 \arctan \left[ \frac{2\tau_{xy} - 2(\sigma_x \cos^2 \alpha + \sigma_y \sin^2 \alpha)}{(\sigma_x - \sigma_y) \sin 2\alpha} \right] \quad (4)$$

At point 10, capsule-microphones, were established fixing moment of arrival of front of air shock wave. Signals from strain gauges through amplifier UTS-12/35 were recorded by loop oscillographs MPO-2 or N-102, and from capsule-microphones directly by oscillographs. Angular distance between points of measurement 1 - 5 constituted  $15^\circ$ , and  $6^\circ$  between points 5 - 10. Trotyl charges of cubic form, by weight 1.6, 5.4, 12.8 kg, were disposed as shown in Fig. 1.

1. Kinematic characteristics of motion. Experimental investigation showed that in significant region of ground half-space, adjacent to axis of symmetry  $z$  ( $0^\circ \leq \beta \leq 60^\circ - 66^\circ$ ), blast wave has one stress peak, but near surface of ground ( $60^\circ - 66^\circ \leq \beta \leq 90^\circ$ ) - two peaks, corresponding to two longitudinal waves, generated by perturbation, proceeding through the ground from focus of explosion and by air shock wave, spreading on surface of ground [1, 2]. In Fig. 2 are depicted stress oscillograms at point 1, when  $r = 20, \beta = 0^\circ$  (oscillogram 48-1), and at point 7, when  $r = 20, \beta = 72^\circ$  (oscillogram 34-6). Lines downward correspond to  $\sigma_r, \sigma_z, \sigma_n, \sigma_\theta$ , time marking - sinusoid of 500 cps. Region, in which are observed waves with two peaks, we will call surface.

Experiments showed that at relative distances from center of explosion,  $r < 20$ , wave in the ground is characterized by discontinuity of stresses. Here the greatest of stresses at the front constitutes 4 - 5 kg/cm<sup>2</sup>. At distances

$r > 20$ , there are waves with smooth build-up of stresses to a maximum value. Above information relates to waves, having one peak. Waves having two peaks, at distances  $r \leq 20$  also have shock fronts at both maxima, and at  $r > 20$ , stress in second maximum grows for some time, but first maximum preserves intermittent character longer, the nearer point of observation is to surface of ground. Here, time increase of stress in first maximum decreases with approach to free surface, and at  $\beta = 90^\circ$ , obviously, equals zero. Time increase in second maximum, at fixed distance from center of explosion, does not depend on angle coordinate  $\beta$ . Time increase relative to second maximum, is determined as time between minimum and second maximum. In Fig. 3 are represented experimental function of time of build-up  $\tau_1^*$  on linear  $r$ , and angle  $\beta$  coordinates for wave having one maximum, and on first maximum for waves having two maxima\*. Curve 1 corresponds to value of angle  $\beta$  from 0 to  $66^\circ$ , curves 2, 3, 4 for  $\beta = 72^\circ, 78^\circ, 84^\circ$ . Let us note that difference from zero of time, corresponding to dotted line in Fig. 3., should be subtracted from true time of build-up, since it characterizes boundedness of resolving power of applied equipment. By given data of Fig. 3 is obtained formula for determination of time of build-up for waves shown

$$\tau_1 = (lR - d_1^3) \bar{C} \quad (1.1)$$

In all formulas (including (1.1)) are obtained following units of measurement:

msec for time, m for length, kg for weight of charge,  $\text{kg/cm}^2$  for stresses,  $\text{kg sec/cm}^2$  for specific impulses, and m/sec for velocity. Numerical (dimensional) coefficients  $l$  and  $d$  in formula (1.1) depend on angle coordinate  $\beta$ . In subsequent formulas, analogous coefficients will also be functions of  $\beta$ . On graphs,



Fig. 2

\*Here, and in the future, superscript \* means that given parameter is related to linear scale of charge  $\tau_1^* = \tau_1 \cdot \bar{C}$  [msec/kg<sup>1/3</sup>] (C-weight of charge in kg).

depicting this dependence on  $\beta$ . dotted parts are natural extrapolation. In Fig. 4 are shown functions of  $l$  and  $d$  on  $\beta$ . Data on time of stress build-up in second maximum is more conveniently given later.

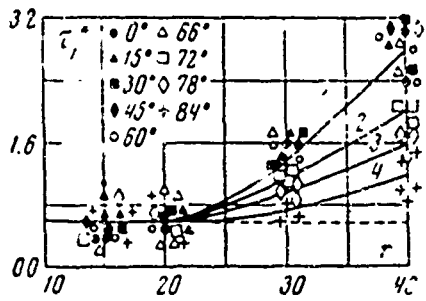


Fig. 3

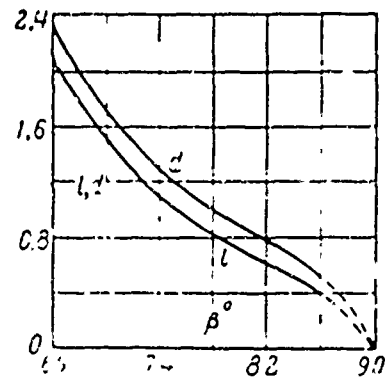


Fig. 4

For determination of velocity of propagation of blast wave in ground, by experimental data on time of its arrival at points of measurement, hodographs of fronts of shock waves or maximum stresses for unstressed waves were constructed. Hodographs of fronts of sound waves, arising at a definite stage before shocks were also constructed. By means of differentiation of these curves was determined velocity of propagation of maximum stresses at various points of ground half-space. In Fig. 5, in coordinates  $t_0^*$ ,  $r$ , are depicted hodographs of waves; by dash lines is depicted front of sound wave, solid lines - front of first maximum, and dash-dotted - second maximum of stresses. From Fig. 5 it is clear that at any fixed value of  $r$ , in certain region adjoining axis  $z$  and having angle dimension  $0 < \beta \leq \beta(r)$ . only one stress maximum is observed in wave, time of arrival of which, within limits given region, does not depend on  $\beta$ . Beyond limits of this region, i.e., at  $\beta > \beta(r)$ , wave has two maxima. Here, time of arrival of first stress maximum  $t_{01}^*$  decreases as compared with time of arrival of wave in region  $0^\circ < \beta < \beta(r)$ , and the more intense, the nearer to free surface is the considered point. It is obvious, that at  $\beta = 90^\circ$ ,  $t_{01}^*$  is equal to time of arrival, at given point, of front of air shock wave. Arrival

time of second stress maximum  $t_{02}^*$ , beyond limits of region  $0^\circ < \beta < \beta(r)$ , on the contrary, increases as compared with arrival time of wave within limits of this region. However, as seen from Fig. 5, this increase is insignificant.

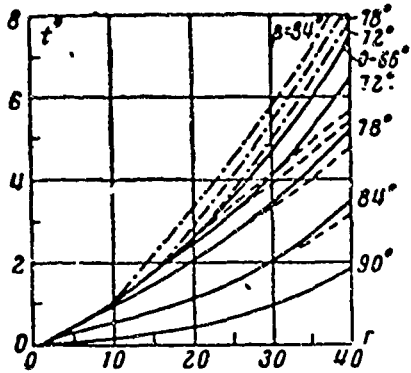


Fig. 5

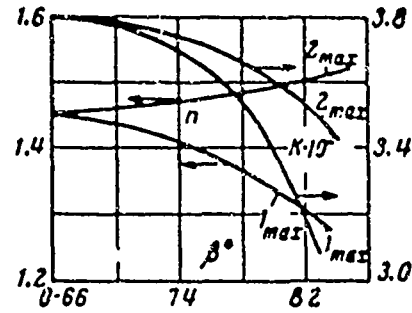


Fig. 6

Data of Fig. 5 are well described by formula

$$t_0^* = k(18.5R^* - 1)^n \quad (1.2)$$

Differentiating (1.2) in respect to  $t$ , we obtain formula for determination of propagation velocities of stress maximums

$$D = \frac{54}{kn(18.5R^* - 1)^{n-1}} \quad (1.3)$$

Graphic functions of coefficients  $k$  and  $n$  are represented in Fig. 6. By data of Fig. 5 is obtained formula for determination of time between arrivals of first and second maxima

$$\Delta t_{12} = (aR^* - b)^2 \sqrt{c} \quad (1.4)$$

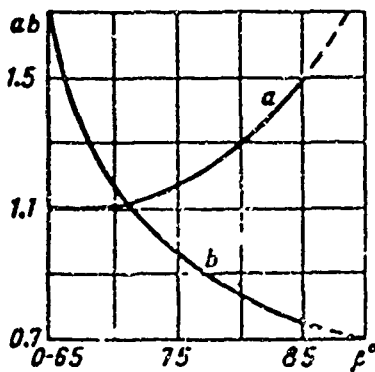


Fig. 7

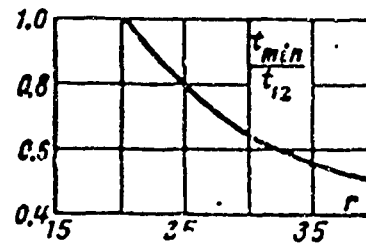


Fig. 8

Coefficients a and b are determined by graph in Fig. 7. Position of minimum of stresses, as experiments show, depends mainly on distance from center of explosion. If fronts of first and second maxima are shock, the minimum of stresses coincides in time, with second maximum, i.e., time between arrival of first maximum and minimum  $t_{\min} = t_{12}$ . When stresses in second maximum increase smoothly for some time, minimum of stresses is displaced in direction of first maximum. In Fig. 8 is depicted function of  $t_{\min}/t_{12}$  on r. Using for la (1.4) and data of graph of Fig. 8, one can determine rise time of stress in second maximum by the formula

$$t_2 = t_{12} - t_{\min} \quad (1.5)$$

Full time of action of blast wave, within limits region where wave has one maximum ( $0^\circ < \beta < 60^\circ - 66^\circ$ ), practically, does not depend on angle of  $\beta$  at fixed value of r. At  $\beta > 66^\circ$ , full time of action diminishes with increase of angle of  $\beta$ , in spite of the fact that in surface region there is a composition of two waves displaced in time. In this, apparently, is developed essential influence of rarefaction wave on stress field in surface region. Data of experiments are well described by formula

$$\theta = (\eta R^* + f) \sqrt{C} \quad (1.6)$$

Function of  $\eta$  and f on  $\beta$  are depicted in Fig. 9.

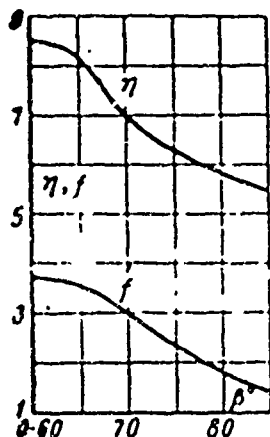


Fig. 9.

On basis of data of Fig. 5, it is possible to construct wave fronts in half-space at various moments of time and, thus, to trace transformation of wave front in process of propagation. During construction of wave front, for characteristic moments of time were taken arrival times of wave at points

of measurement on axis of symmetry ( $\beta = 0^\circ$ ), far from center of explosion at

$r = 15, 20, 30,$  and  $40$ . At distances of  $r > 20$ , during construction wave front, arrival time of sound front and arrival time of stress maximum were considered. In wave with two maxima, arrival times of beginning of wave of first and second maxima were considered. In Fig. 10 is depicted meridian section of wave front at various distances from center of explosion. Points of measurement were disposed on spherical planes with center coinciding with center of charge. Therefore, in regions where arrival time of wave does not depend on angle coordinate  $\beta$ , wave front has spherical form. In surface region, fronts of first and second stress maxima, due to dependence of their arrival times on angle of  $\beta$  are not spherical in form. Here, front of first stress maximum, as seen in Fig. 10, with approach to free surface, seems to "follow" front of air shock wave. Front of second stress maximum deviates slightly from spherical.

In Fig. 10, it is clear that magnitude of value  $\beta$ , separating surface region from remaining space, changes together with  $r$ . Increase of angular dimension of surface region occurs due to faster deceleration of propagation of spherical wave spreading through ground from center of explosion, as compared with wave generated by air shock wave. Slope of front of latter wave, due to decrease of ratio of velocity of air wave to velocity of ground wave  $D_f / D$ , is increased with departure from center of explosion. However, absolute values of angle of inclination  $\psi$  are small, and at distance  $r = 40$  constitutes approximately  $16^\circ$ .

Thus, wave front in meridian section represents semicircle with center coinciding with center of charge, and a certain slightly distorted line, convex in the direction of free surface, and inclined towards it under certain angle  $\psi$ , magnitude of which increases together with  $r$ . The above refers to fronts of maximum stresses. Regarding,

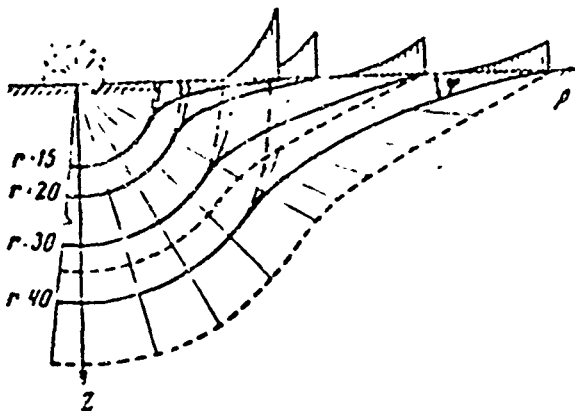


Fig. 10

sound wave, however, with removal from center of explosion, its outline, in half-space, approaches configuration of longitudinal waves, appearing in elastic isotropic half-space during action on its surface of a concentrated force and weak air wave.

2. Main characteristics of stress waves. During investigation of dynamic stress field, at every point of measurement, four normal stresses  $\sigma_x, \sigma_y, \sigma_z, \sigma_n$  were fixed in time. Measurements of shown stresses give full information about state of strain at point of ground half-space, which allows to produce manifold analysis of dynamic stress field. Furthermore, with the help of data on stressed state, it is possible to check derivations made from kinematic parameters.

In Fig. 11, by solid lines are represented experimental functions of maximum

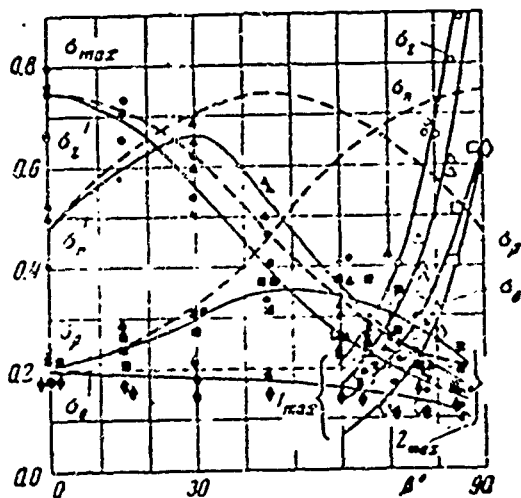


Fig. 11

values of components of stresses

$\sigma_x, \sigma_y, \sigma_z, \sigma_n$  of angle  $\beta$  at distance from center of explosion  $r = 40$ , when center of charge coincided with surface of ground. In this figure, by dotted lines are depicted curve changes of shown stresses in centrally symmetric field constructed from formulas

$$\sigma_x = \sigma_{x0} \cos^2 \beta + \sigma_{z0} \sin^2 \beta \quad (2.1)$$

$$\sigma_y = \sigma_{z0} \sin^2 \beta + \sigma_{x0} \cos^2 \beta \quad (2.2)$$

$$\sigma_n = 0.5 [(\sigma_{z0} + \sigma_{x0}) + (\sigma_{z0} - \sigma_{x0}) \sin 2\beta] \quad (2.3)$$

$$\sigma_z = \sigma_{z0} = \text{const} \quad (2.4)$$

where  $\sigma_{x0}, \sigma_{y0}, \sigma_{z0}$  - experimental values of stresses at  $\beta = 0^\circ$ . There are analogous data for other relative distances, however, they are not listed here due to lack of space. It is natural that each curve, relating to any component of

stress, starting from certain value of angle  $\beta$ . consists of two branches, expressing change of maximum stress in first and in second maxima. Relationship of maximum magnitudes of stresses in first and in second maxima depends on angle  $\beta$ . In beginning (on  $\beta$ ) surface region, stress has large magnitude in second maximum, but with approach to free surface - in the first. This is explained, by various laws, as wave attenuation, spreading from center of explosion, and wave generated by air shock wave. Stress in wave, propagated through the ground from center of explosion, decreases with approach to free surface, and increases in wave, generated by air shock wave and diffused from free surface. From Fig. 11, it is clear that unloading influence of free surface on wave, propagated through the ground from center of explosion, is so intense that, in spite of the fact that second maximum is result of imposition of this wave on wave, propagated from free surface, this maximum, during approach to free surface, becomes minute.

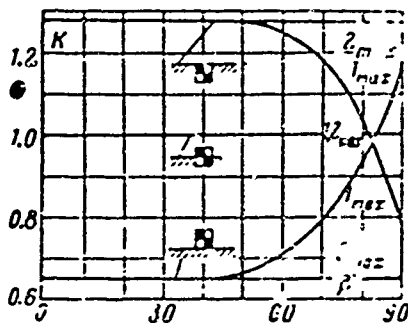


Fig. 12

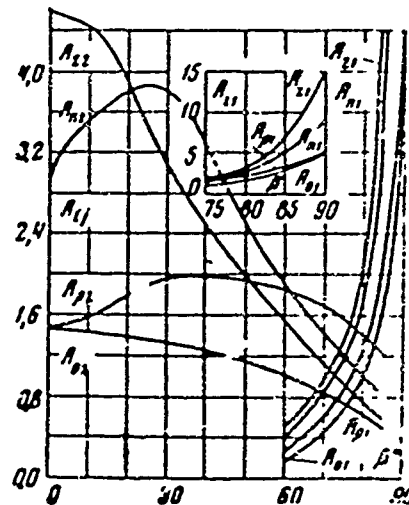


Fig. 13

During conduction of experiments position of center of charge changed relative to surface of ground. Results of measurements of stress field showed that maximum stress rather considerably depends on this factor. Thus, for example, when location of charge is directly on surface, maximum stress in region, where wave has one maximum, is twice as low as when charge is flush with free surface. Influence of position of charge on magnitudes stresses in first and in second

maxima spreading in surface region, is varied. Change of stress in second maximum is approximately the same as in regions with one maximum in wave. Change of stress in first maximum, depending upon position of charge, occurs in opposite manner. When charge is directly on surfaces of ground, stress in first maximum is larger than when charge is located flush with surface. All this is natural, and is connected with varied distribution of energy of explosion between movements of ground and air in initial moments of development of process at varied location of charge relative to surface of ground. In Fig. 12 are presented data on dependence on  $\beta$  of ratio  $K$  of maximum stresses at above mentioned two extreme locations of center of charge (in reference to free surface) to maximum stresses where center of charge is on surface of ground.

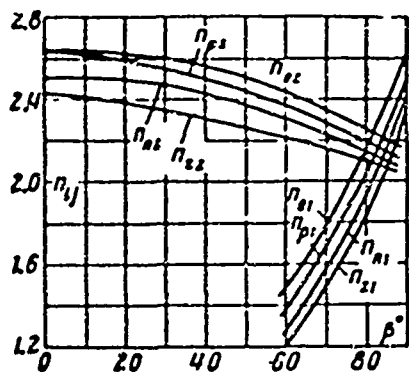


Fig. 14

Maximums of measured components of stresses can be described by formula

$$\sigma_{ij}^{\max} = K A_{ij} \left( \frac{1}{R^0} \right)^{n_{ij}} \quad (i = \theta, z, n, p; j = 1, 2) \quad (2.5)$$

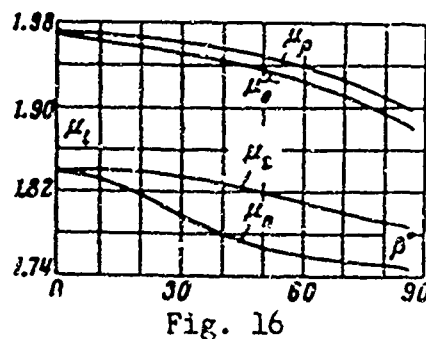
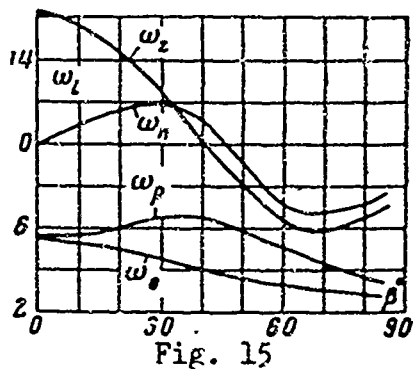
Coefficients  $K$ ,  $A_{ij}$ , and  $n_{ij}$  are determined by graphs in Figs. 12, 13, and 14. Here, value of index  $j = 1, 2$  indicates in which maximum  $\sigma_i^{\max}$  is

determined.

Analysis of experimental data showed that within limits of region with one maximum in wave, laws of change of specific impulses are similar to laws of change of corresponding components of stresses. This is explained by the fact that, as shown above, total time of action of wave in this region does not depend on angle  $\beta$ . In surface region, specific impulses for each component of stresses are total throughout entire wave with two maxima. Obviously, on free surface, specific impulse is equal to specific impulse of air shock wave. Experiments showed that position of charge of, in reference to free surface, noticeably influences the magnitude of specific impulse. We note, however, that influence

of this factor shows up, mainly, in regions where wave has one maximum. Since in this region, time of action does not depend on angle coordinate  $\beta$ , specific impulse changes here proportionally to coefficient  $K$ . In surface region, because position of charge, in reference to free surface, affects magnitude of stresses in first and in second maxima differently, magnitude of total (by wave) specific impulse, practically, does not depend on position of charge. By data of experiments, it is possible to construct following formula for determination of magnitude of specific impulse.

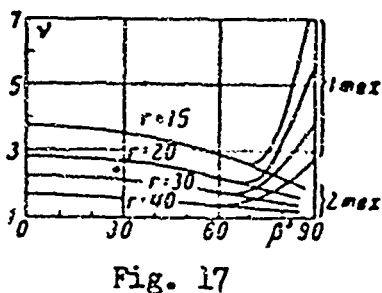
$$I_1 = K \omega^3 \sqrt{C} \left( \frac{1}{R^2} \right)^{1/2} \quad (2.6)$$



Coefficients  $\omega_i$  and  $\mu_i$  are determined by graphs in Figs. 15 and 16. On basis of data on stresses, time of action, and specific impulses, is obtained dependence, characterizing law of change of stress in wave in time. Here, it was assumed that blast wave, in time, is described by binomial law.

$$\sigma_{ij}(t) = \sigma_{ij}^{\max} \left( 1 - \frac{t}{\theta} \right)^v \quad (2.7)$$

In Fig. 17 is shown change of exponent  $v$  depending upon  $r$  and  $\beta$ .



Obtained experimental data allow to analyze in detail the qualitative and quantitative sides of dynamic stress field. By above mentioned data are calculated maximum magnitudes of principal normal stresses, and their orientation in meridional planes ( $\sigma_1^{\max}$ ,  $\sigma_2^{\max}$ ,  $\varphi$ ) is determined along with maximum

value of shear stress  $\tau_{\theta r}$ , effective in that same plane. In Figs. 18, 19, 20, and 21 respectively are presented results of calculations for  $\sigma_1^{\max}, \sigma_2^{\max}, \varphi, \tau_{\theta r}$ .

From Fig. 20, it is clear that angle  $\varphi$ , calculated by maximum values of stresses in wave with one maximum and by stresses in second maximum, in surface region, within limits all half-space, is very near in magnitude to angle  $\beta$ . Proximity of angles  $\varphi$  and  $\beta$  indicates that wave front, spreading from center of explosion, can be considered spherical. Angle  $\varphi$ , calculated by stresses in first maximum, in the beginning, in surface region, sharply diminishes, and then, practically, is equal to angle  $\psi$  of slope of wave front, spreading from free surface. Thus, outline of wave front is half-space, constructed from kinematic data, is confirmed by data of measurements of stresses.

Examination of Fig. 11 shows that experimental curves, within limits of region  $0^\circ \leq \beta \leq 30^\circ$ , is immaterially deviate from dotted curves expressing laws of change of corresponding components of stresses in centrally symmetric field. This fact, jointly with received data on sphericity of front, justifies conclusion that distribution of stresses in this region (we will call it axial) can be considered approximately the same, as in case of centrally symmetric field. Indeed, in Figs. 18, and 19, it is clear that principal normal stresses  $\sigma_1, \sigma_2, \sigma_{\theta}$  within limits of axial region, depend little on angle coordinate  $\beta$ , and that

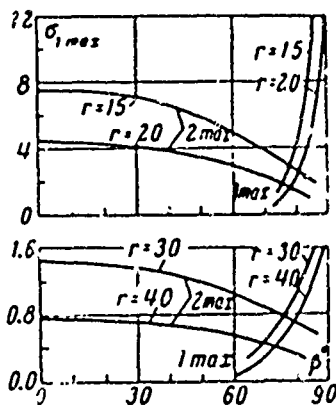


Fig. 18

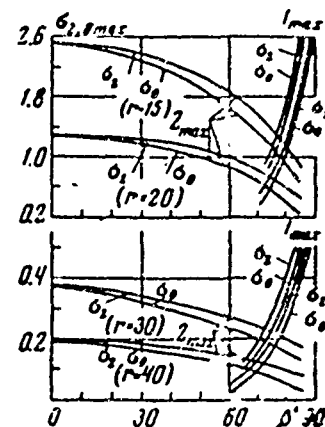


Fig. 19

smaller of them are close by absolute magnitude, i.e.,  $\sigma_1 \approx \sigma_{\theta}$ .

Data of

Fig. 21 also confirm expressed affirmation. Thus, in axial region, character of wave propagation, distribution of stresses, and consequently, the movement of ground are qualitatively similar to case of centrally symmetric field, created by canouflet explosion. This means that influence of free surface (from the viewpoint of distortion of stress state in axial region, by comparison with stress state on axis of symmetry  $z$ , where, as known, conditions of central symmetry are satisfied) is insignificant. Beyond the limits of axial region, as seen from Figs. 11 and 21, experimental and dotted curves strongly differ. Let us note that comparison of these curves has meaning only in region where wave has one maximum. It is characteristic that in region  $30^\circ \leq \beta < 60^\circ - 66^\circ$  (we will call it the mean region), in spite of sphericity of front, is observed essential deflection in distribution of stresses, as compared with centrally symmetric field (Figs. 18 and 19). In addition, we note that smaller main stresses are close in absolute magnitude at any fixed value of angle  $\beta$ . Consequently, it is possible to consider that, in mean region conditions of central symmetry are approximately satisfied, i.e.,  $\varphi \approx \beta$ ,  $\sigma_1 \approx \sigma_0$ , and main stresses depend on  $\beta$ , as on parameter.

The greatest influence free surface appears in surface region. This is confirmed by the very fact of existence of a wave with two maxima. Due to this, stress field in surface region is the most complicated. From Fig. 19 it is clear that front of wave of generated air shock wave, has small angle of inclination, in reference to free surface. This circumstance and the fact that smaller main stresses are approximately equal, gives possibility to assume that stress state created by this wave, insignificantly differs from stress field in plane wave. Analysis of differential equations describing movement of ground evoked by waves of similar kind, by method of estimations presented in [3], showed that movement of ground, due to smallness of angle  $\varphi$ , occurs practically vertically. Allowable error proportional to  $\sin^2 \varphi$ . However, because pressure on front of air shock wave is function of distance from center of explosion, movement of ground, in

various vertical sections of half-space, will be varied. Thus, the process of wave propagation, excited by air shock wave, is analogous to phenomenon of flow around thin, pointed bodies by stationary gas stream with very great supersonic speed. Distribution of stresses beyond second maximum, generated by wave, spreading from center of explosion, during its imposition on wave, generated by air shock wave, is very complicated. Principal normals of stress depend considerably on  $\beta$ , the smaller of them are not equal to one another which is especially noticeable

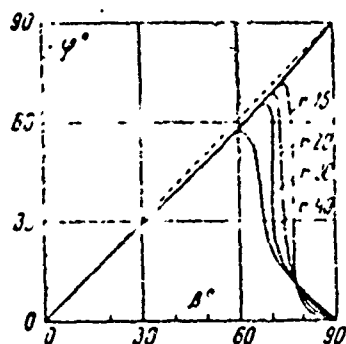


Fig. 20

in direct proximity to free surface.

Front of second maximum, as seen from Fig. 10, although insignificantly, differs from sphere. Thus, by experimental means, are revealed characteristic sides of the dynamic stress field in

soft ground during a contact explosion.

In conclusion, let us consider the very significant question of distribution of energy of a contact explosion in ground and in air. By experimental means, by method of intersection of front of air shock wave, spreading along free surface, were obtained dependences of time of arrival of wave front  $t^*$  on distance from

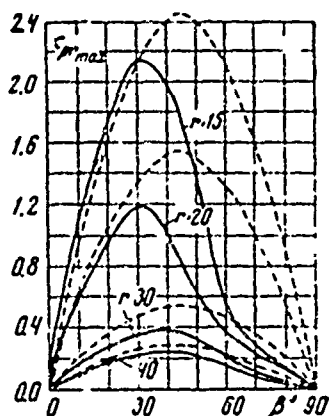


Fig. 21

center of explosion  $r$ , at varied position of center of charge, relative to free surface. By means of differentiation of these dependences and use of gas-dynamic relationships on front of shock wave, were constructed dependences of pressure on wave front  $\Delta P$ , as functions of  $r$ . By comparison of these dependences

with dependence  $\Delta P(r)$ , for case of explosion in incompressible half-space, established by M. A. Sadovskiy [4], was determined share of energy, radiated

in air and expended on excitation of air shock wave. Remaining energy, obviously, is transmitted to ground. In our experiments, it was found that during location of charge in such a way that its center coincided with surface of ground, in air and in ground is radiated, coorespondingly, 65 and 35% of the energy of the explosion. In cases, when upper or lower bounds of charge were disposed on surface of ground, in air and in ground are radiated 78 and 22, 53 and 47% of the energy of the explosion, respectively.

These data give possibility, in axial region, to use theoretical or experimental dependences, by which are determined parameters of waves in spherical stress field, and also more accurately to calculate parameters of air shock wave, as compared with case, assuming half-space to be incompressible.

The author thanks S. S. Grigoryan for direction and help during execution of given work, G. V. Rykov and A. F. Novgorodov for help in conduction of experiments.

Submitted  
28 May 1963

#### Literature

1. V. D. Alekseyenko, S. S. Grigoryan, A. F. Novgorodov, L. I. Koshelyev, and G. V. Rykov. Measurement of stress waves in soft soils, PMTF, 1953, No 2.
2. V. D. Alekseyenko. Waves in surface region of ground half-space during contact explosion PMTF, 1963, No 3.
3. S. S. Grigoryan. On approximate solution of certain problems of dynamics of soils, PMM, 1962, No 5.
4. M. A. Sadovskiy. Physics of explosion, No 1, Izd. AN SSSR, 1952.

FORMING OF SHOCK WAVE AND SCATTERING OF PRODUCTS  
OF EXPLOSION IN AIR

V. V. Adushkin

(Moscow)

With the help of piezo apparatus, high-speed photographing, and ionization probe were studied laws of movement of front of shock wave and products of explosion (PE), during explosion in air of spherical charges of certain types of explosives (HE). By speed of front, were constructed dependences of main parameters of front near charge to distances, at which formulas of M. A. Sadovskiy [1] are correct. In region of action of PE is constructed dependence of width of layer, compressed in wave of air between front and PE on distance.

By method, developed in [2] similar to method of film [3, 4], on basis of measurements of parameters of front of shock wave is obtained distribution of pressure and density in layer of air behind front to contact surface. Calculated pressure distribution in layer is augmented by diagrams of  $\Delta p = f(t)$ , obtained during measurement of parameters of shock waves in air near a charge of HE [5]. By distribution of pressure, density, and velocity of air in shock wave is calculated energy, which air acquires from expanded HE as result of its intense braking. Shown is at what stage and how energy of air is distributed behind front of shock wave. Comparison is conducted of certain obtained results with results of numerical calculation of shock wave from explosion of spherical charge of trotyl [6], strong point explosion [7], and point explosion with counterpressure [8].

1. Description of experiment. In experiment were measured arrival times  $t$  of wave front and PE at various distances  $r$  from center of charge in three series of experiments on charges of various types of HE of spherical form. Charges were triggered from center. In Table 1 are given data on charges of trotyl-hexogen 50/50 (TH) and PETN, used in experiment.

Table 1.

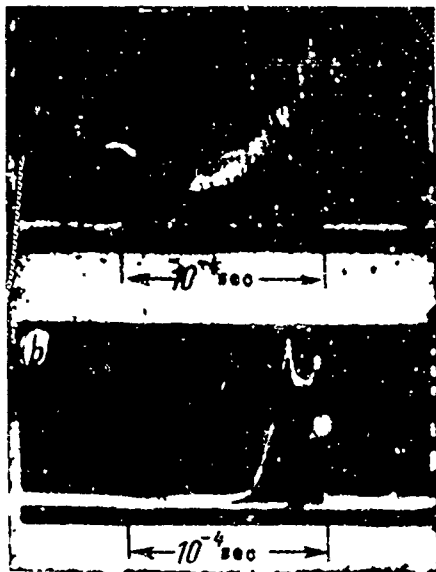
(a) Серия	(b) Тип заряда ВВ	(c) $\rho$ , г/см <sup>3</sup>	(d) C, кг	(e) $\epsilon$ , ккал/кг	$\delta$ , мм	$\beta$
(f) 1	ТГ литой	1.68	24·10 <sup>-3</sup> , 135·10 <sup>-3</sup>	1140	0	0.052
(g) 2	ТГ насыпной	0.9	36·10 <sup>-3</sup> , 150·10 <sup>-3</sup>	1030	2	0.064
(h) 3	ТГ прессованный	1.6	0.8·10 <sup>-3</sup> , 2.5·10 <sup>-3</sup>	1400	0.2	0.053

KEY: (a) Series; (b) Type of charge HE; (c)  $\rho$ , g/cm<sup>3</sup>;  
 (d) C, kg; (e)  $\epsilon$ , kcal/kg; (f) TH, cast; (g) TH granular;  
 (h) PETN, pressed.

Here  $\rho$ -density of charges, C-weight of charges,  $\epsilon$ -specific energy of explosion,  $\delta$ -thickness of scattered layer of HE,  $\beta = r_0/C^{1/3}$ , where  $r_0$ -radius of charge in meters after subtracting scattered layer.

In series of experiments 1 and 2 movement of wave front and PE in region from surface of charge to  $13 r_0$  was obtained by method of ionization probe, bared ends of which were connected by front of strong shock wave, where air was partially ionized. Recording was done on cathode-ray oscillographs OK-17 and OK-24. Furthermore, in realm of distances above  $4 r_0$ , arrival times of wave front were measured in records of  $\Delta p - f(t)$ , obtained with the aid of piezo-probes. Results of measurements of parameters of shock waves by piezo-probes, in near zone of explosion, and their organization are given in [5]. In Fig. 1 are shown samples of recordings obtained with the help of piezo-probe (a) and ionization probe (b) at a distance of  $11.1 r_0$ .

Movement of PE was photographed by instrument SFR-2M, which, besides continuous scan in time, allows to receive a series of frames with frequency of shots from 20 thousand to 2 million frames per second. Some frames of photographs of explosion from series 1 of charges weighing 135 g are presented in Fig. 2. Near frames is designated dimension of visible cloud from center of explosion in radii of charge  $r_0$ . Let us note that in direct proximity to charge, source of light is surface of front of shock wave formed by expanding PE. Then possibly, glow comes from deeper layers of turbulent air behind wave front. In region above  $3-4 r_0$ , which is especially well seen in photographs, obtained on SFR by method of stereo survey, surface

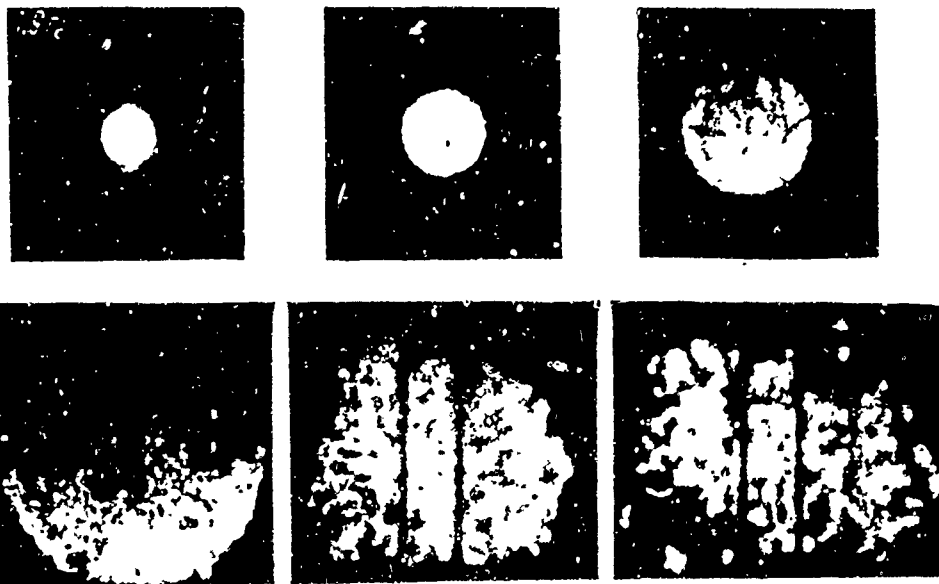


GRAPED NOT  
REPRODUCIBLE

Fig. 1

"is bared" of PE's themselves in the form of a rough cloud. However, it is possible that source of light, nevertheless, is a thin layer of air, adjoining the surface of PE, especially so since temperature of the air behind wave front increases (especially sharp near contact surface) while temperature of PE's themselves is significantly lower

than temperature of air behind wave front [9].



GRAPED NOT  
REPRODUCIBLE

Fig. 2

Results of measurements on movement of wave front (curve 1) and PE (curve 2), for explosions of series 1, are shown in Fig. 3 in the form of dependence of shown time,  $t^0 = t / C^{1/3}$  in  $\text{sec}/\text{kg}^{1/3}$ , on distance in radii of charge. Since temperature of PF's, during their expansion, is many times lower than temperature of the compressed air behind front of shock wave, it was expected that ionization probe would sense difference in electrical conductivities of air, compressed in wave, and PE. In Fig. 3, results of measurements by ionization probe, of arrival times of PE in region up to  $13 r_0$ , are designated by crosses. On recordings of

ionization probe (Fig. 1b), the arrival time of PE was taken as the moment of sharp drop after second peak of the recording. These measurements of arrival

times of PE coincided with optical observations. Thus, under the conditions experiment, during photographing of the intrinsic glow of process of explosion

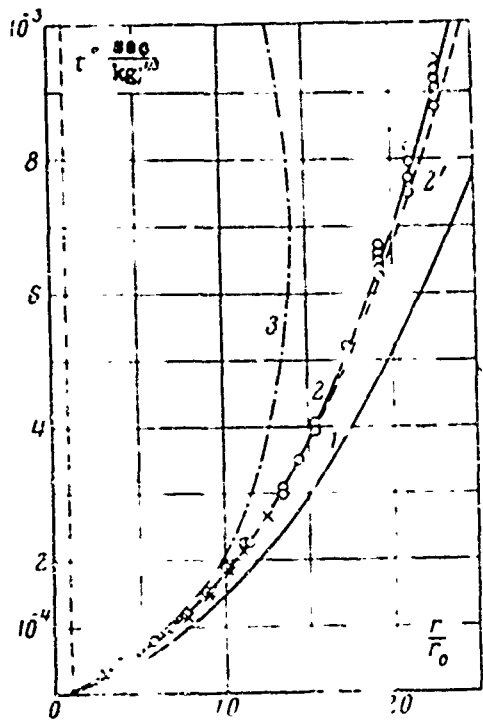


Fig. 3

**GRAPHIC NOT  
REPRODUCIBLE**

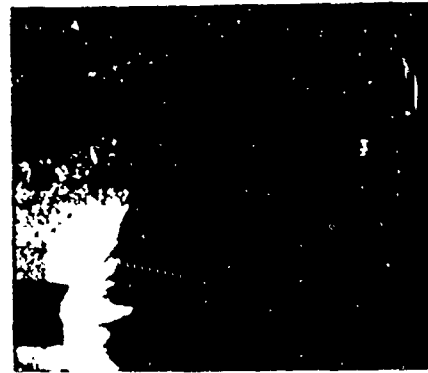


Fig. 4

of HE are recorded the hottest layers of air at the very contact surface, or external layers of PE.

In the case of explosion of charges of PETN, movement of front in region up to  $25 r_0$  was obtained during photographing of explosions in parallel bundle of light (schlieren method) slave photo recorder ZhFR. Photograph of unfolding of explosion of 2.5 g of PETN is shown in Fig. 4. Scattering PE was photographed by instrument SFR-2M. As a result, was obtained dependence  $r = r(t)$  for front and PE of charges of PETN.

In Fig. 3, by dash-dotted line 3 is presented movement of contact surface, obtained during calculation of trotyl explosion Brode [6]. It is clear that movement of contact surface, from center of explosion, in [6], ceases at distance 13 to 14  $r_0$ , in contrast to movement of PE observed in experiment, which starts approximately from 5 to 7  $r_0$ .

2. Width of layer of air between front and products of explosion. By law

of motion,  $r = r(t)$  of wave front and PE is built an empirical formula, presenting dependence of width of layer of air  $\Delta$  between PE and front from a distance to wave front  $r_0$

$$\frac{\Delta}{r_0} = 0.045 \left[ \left( \frac{r}{r_0} \right)^{1.4} - 1 \right], \quad 1 < \frac{r}{r_0} < 35 \quad (2.1)$$

Within limits experimental variance (near 10%), difference in width of layer,

depending upon form of HE was not observed.

### 3. Parameters of front near charge

of HE. By graphic differentiation of experimental dependences  $r = r(t)$ , for front and PE were determined velocities of their movement, as functions of distance. By speed of front, with the help of known tables of parameters of

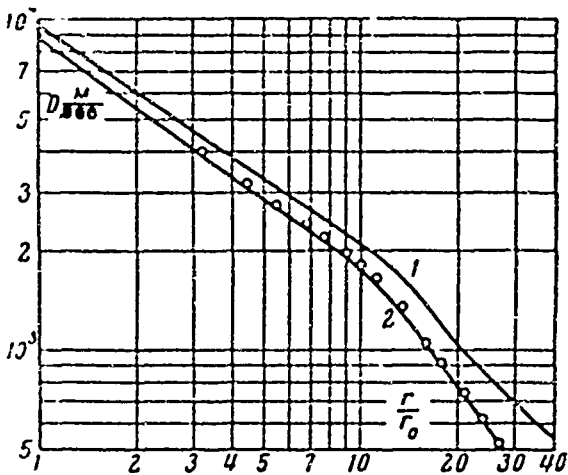


Fig. 5

front of a shock wave in air, composed by A. S. Kompaneyts and N. M. Kuznetsov, and also presented in [10, 11], functions were plotted of maximum pressure and mass velocity at wave front on distance. In Fig. 5, curve 1 represents dependence

of velocity of front on distance, in case of experiments of series 1; curve 2 - dependence of mass velocity of air at wave front. Circles represent experimental velocities of boundary of PE - air, at that same moment of time, at which velocity of front is measured.

Similar plotting was done for explosions of series 2 and 3. Location of experimental points, in reference to curve 2, indicates that measured velocities of

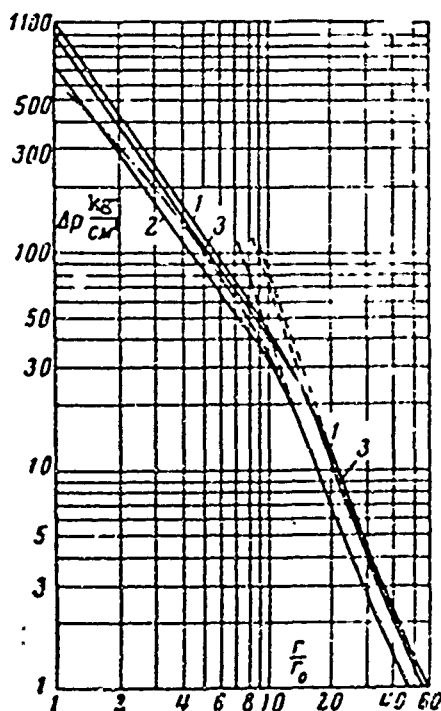


Fig. 6

boundary PE - air agree, with accuracy up to 10 to 15%, with magnitude of mass velocity of air at front. In connection with this, the layer of air between front and PE, within limits of indicated accuracy, consists of particles, which move with nearly identical velocity, varying only with time (or radius of front).

In Fig. 6 are presented dependences of maximum pressure on distance: figures on curves designate series of explosions, by dashed line are continued the dependences of pressure, corresponding to trinomial formula of M. A. Sadovskiy [1]. Dash-dotted line shows result of Brode calculation [6], under conditions, noted in [5].

In near zone of explosion, dependences of maximum pressure and velocity of front on radius of front, and also dependence of radius of front on given time  $t^0$ , obtained by integration of expression for velocity of front under the condition that  $t = t_d$  at  $r = r_0$ , where  $t_d$  - time of detonation of charge of HE, can be described by following empirical formulas corresponding to the three series of experiments:

at  $(1 \leq r/r_0 \leq 12)$

$$\Delta p = \frac{1100}{(r/r_0)^{1.4}}, \quad D = \frac{9500}{(r/r_0)^{0.66}}, \quad \frac{r}{r_0} = [3 \cdot 10^3 (t^0 - t_d^2) + 1]^{0.803} \quad (3.1)$$

at  $(1 \leq r/r_0 \leq 10)$

$$\Delta p = \frac{730}{(r/r_0)^{1.35}}, \quad D = \frac{8000}{(r/r_0)^{0.61}}, \quad \frac{r}{r_0} = [2 \cdot 10^3 (t^0 - t_d^2) + 1]^{0.61} \quad (3.2)$$

at  $(1 \leq r/r_0 \leq 12)$

$$\Delta p = \frac{1000}{(r/r_0)^{1.35}}, \quad D = \frac{9200}{(r/r_0)^{0.63}}, \quad \frac{r}{r_0} = [2.8 \cdot 10^3 (t^0 - t_d^2) + 1]^{0.606} \quad (3.3)$$

In the future, exponent, in law of attenuation of pressure with distance, starts to increase, attaining greatest magnitude 2.7 at pressure near  $20 \text{ kg/cm}^2$ , then, starting from distance 15 to 18  $r_0$ , dependence of maximum pressure corresponds formula of M. A. Sadovskiy, which occurs in realm of distances, where influence of PE is absent and pressure at wave front from charge of various type of HE is determined only by amount of energy of explosion.

4. Parameters of air behind front of shock wave. Obtained experimental results characterizing, basically, front of shock wave, with the help of method presented and well-grounded in [2], were used for calculation of parameters of air entrapped by shock wave, during explosion of charge of HE. This determination of parameters is made according to accurate values of derivatives of main gas-dynamic quantities at wave front in Lagrange (mass) coordinates. By experimental data for explosions of series 1, derivatives were calculated of pressure  $a$  and speed  $b$ , taking counterpressure into account, in the case of spherically-symmetric motion ( $\nu = 3$ )

$$\begin{aligned} a &= \frac{\partial p}{\partial m} \frac{M}{\rho_0}, & b &= \frac{\partial u}{\partial m} \frac{M}{u_0}, & U' &= \frac{d \ln u_0}{d \ln M} \\ u_0 &= \frac{2D}{k+1} \left(1 - \frac{c_0^2}{D^2}\right), & M &= \frac{4\pi}{3} \rho_0 (r_0^3 - r_0'^3) \end{aligned} \quad (4.1)$$

For undisturbed air  $k_0 = 1.4$ ,  $c_0 = 330$  m/sec,  $\rho_0 = 1.29 \times 10^{-3}$  g/cm<sup>3</sup>.

Results of calculation of  $a$ ,  $b$ ,  $U'$ , depending upon amount of pressure at front  $\Delta p$ , are given in graph of Fig. 7 and designated, respectively, 1, 2, and 3. For comparison, in the same graph, by dash-dotted lines 1', 2', and 3' are shown corresponding magnitudes of  $a$ ,  $b$ , and  $U'$  calculated by results of calculation of point explosion with counterpressure [8]. From graph of Fig. 7, one may see that magnitude of derivatives of  $a$ ,  $b$  and  $U'$ , in case of explosion of real charge of HE, considerably differ from case of point (without mass) explosion, in region of strong shock wave, there, where  $\Delta p_0 > 10 - 20$  kg/cm<sup>2</sup>. Thus, in case of explosion of charge of HE, derivative of pressure  $a$  is almost three times less than corresponding derivative of point explosion, and derivative of mass velocity  $b$  vanishes to zero.

Assuming profiles of pressure and velocity to be linear by mass of air compressed by wave [2], distribution of pressure, density and velocity in Lagrange coordinates, in that layer of air, can be written in the form

$$p_0 = 1 - \mu(1 - \mu), \quad \rho_0 = \rho / \rho_0, \quad \mu = r_0 / M \quad (4.2)$$

$$r_0 = \frac{\rho(m)}{\rho_s(M)} = \frac{\rho_s(m)}{\rho_s(M)} \left\{ [1 - a(1-\mu)] \frac{\rho_s(M)}{\rho_s(m)} \right\}^{-\frac{1}{k(m)}} \quad (4.3)$$

$$s_0 = 1 - b(1-\mu), \quad u_s = u/u_s \quad (4.4)$$

In expression (4.3), for air density it is assumed that process of expansion of compressed air, behind front of shock wave, is adiabatic with its own effective adiabatic exponent  $k(m)$ , at fixed  $m$ . Here, effective adiabatic exponent  $k(m)$  for each  $m$ , is coupled with compression in shock wave by known formula

$$\frac{k(m)+1}{k(m)-1} = \frac{\rho_s(m)}{\rho_0} + \frac{k_0+1}{k_0-1} \frac{\rho_0}{\rho_s(m)} = \frac{\rho_0}{\rho_s(m)} \quad (4.5)$$

In order to obtain distribution of parameters behind wave front by radius,

it is necessary to establish bond of

Lagrange coordinate of  $m$  with the

Euler of  $r$ . In the case of spherical

symmetry, these coordinates are coupled

with equation of inseparability

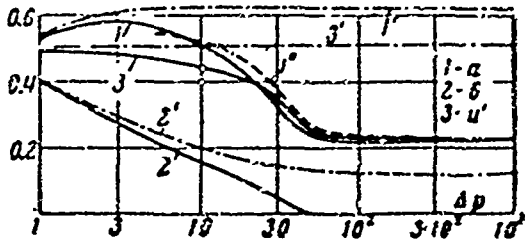


Fig. 7

$$\frac{\partial r^2}{\partial m} = \frac{3}{\mu} \quad (4.6)$$

Integrating and inserting boundary condition which at  $r = r_0$ ,  $m = M$  ( $\mu = 1$ ),

we obtain

$$r_0^2 = \xi - \frac{k-1}{k+1} \int \frac{d\mu}{\mu} \cdot r_0 = \frac{r_0^2}{\mu} \quad (4.7)$$

where magnitude of  $r_0$  is determined by

(4.3). As a result of numerical inte-

gration of expression (4.7), distribution

was obtained of main parameters of air,

by radius, behind front of shock wave.

In Figs. 8 and 9 is shown change of

pressure and air density up to contact surface ( $\mu = 0$ ). Figures on graphs desig-

nate position of front in radii of charge  $r_0$ . For comparison in Figs. 8 and 9

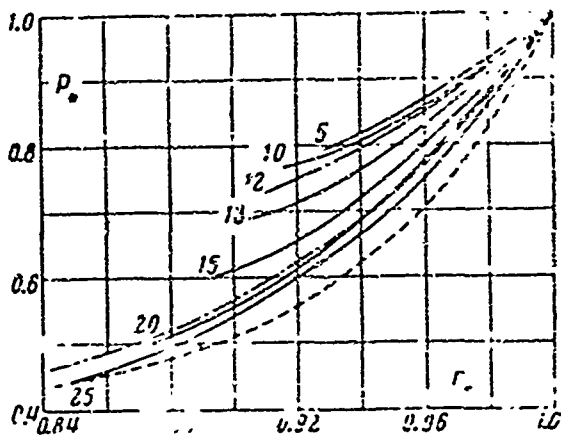


Fig. 8

by dotted line is represented distribution of corresponding magnitudes in case of strong point explosion [7], by dash-dotted line - from calculation of point explosion with regard to counterpressure [8] for wave with  $\Delta p_0 = 7.9 \text{ kg/cm}^2$  which corresponds, in our case, to position of front near  $25 r_0$ . We note, first, essential difference from case of strong explosion [7], and secondly, that distribution of pressure and density of air, in case of explosion of HE, becomes the same as and in case of point explosion, starting from 20 to  $25 r_0$ , where  $\Delta p_0 < 10 \text{ kg/cm}^2$ . We should note that distribution of density and magnitude of dynamic pressure  $\rho u^2$  in layer of air between wave front and PE, have practically the same form. For appraisal of dynamic pressure of air during explosion, it is possible to use magnitudes of  $u$ , presented as curve 2 in Fig. 5.

In conducted calculation, result was not used of experiment on position of boundary of PE - air and velocity of its motion. Therefore, determination of law of motion of contact surface from (4.7) at  $\mu = 0$ , and also calculation of magnitude of derivative of pressure on contact surface by speed of its motion, and comparison of it with value of derivative at front, can serve as control of applied approximation method of determination of parameters of air behind wave front. On the other hand, this will be additional confirmation of result of experiment on motion of contact surface, obtained, basically, with the help of optical observations of expanding cloud of PE. Indeed, at  $\mu = 0$   $r = r_k$ , i.e.,

$$r_{0k} = 1 - \frac{k-1}{k+1} \int_0^1 \frac{d\mu}{\rho_0}, \quad r_{0k} = \frac{r_k}{r_0} \quad (4.8)$$

Result of calculation of  $r_k$  is represented by dotted line 2' in graph of

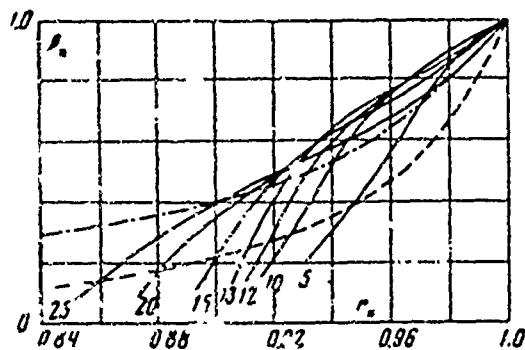


Fig. 9

Fig. 3, where curve 1 - front, 2 - boundary of PE - air from experiment. It is clear that there is good coincidence of calculated  $r_k$  with motion of edge of PE from experiment, in entire range where calculation of parameters

of air in shock wave was conducted.

Further, calculation was made of derivative of pressure at contact surface. From equation of motion

$$\frac{du_k}{dt} = -r_k^2 \frac{\partial p}{\partial r} \quad (4.9)$$

after certain conversions, we obtain

$$\frac{\partial p}{\partial t} \frac{M}{p_0} = - \frac{\rho_0 u D}{p_0} \frac{u_k}{r_k} \left( \frac{r_0}{r_k} \right)^2 \frac{d \ln u_k}{d \ln M}, \quad p_0 = \rho_0 u D + p_0 \quad (4.10)$$

Result of calculation of derivative at contact surface by (4.10) is represented in Fig. 7 by curve 1". It is clear that there is satisfactory coincidence with curve 1, the derivative of pressure at front of shock wave. Thus, profile of pressure, with sufficient degree of accuracy, is near to linear.

5. Form of shock wave in near zone of explosion. Fig. 8 shows that profile of pressure, in layer of air compressed by shock wave, changes comparatively slowly from one moment of time to another. Using this fact and including experimental dependence  $r = r(t)$  for wave front, on basis of obtained distribution of pressure by radius, were plotted curves of attenuation of pressure in time, in this perturbed layer of air, for certain fixed distances from center of explosion. Then, at those distances, where, with the help of piezo-probe, were obtained pressure recordings as functions of time [3], experimental curves of  $\Delta p = f(t)$  were augmented by those calculated. This allowed correctly to reproduce head portion of profile of shock wave heaped up by piezo-probes because of finite size and insufficiently high frequency responses of the data unit and electrical circuit. Result of such combination in regions near charge of HE, is presented in Fig. 10. On axis of abscissas is plotted time from moment of explosion  $t^0$  in  $\text{sec/kg}^{1/3}$ , near curves is designated distance from center of charge to point of measurement in radii of charge  $r_0$ . Shaded head portion of curve represents compressed air in wave behind which follows PE.

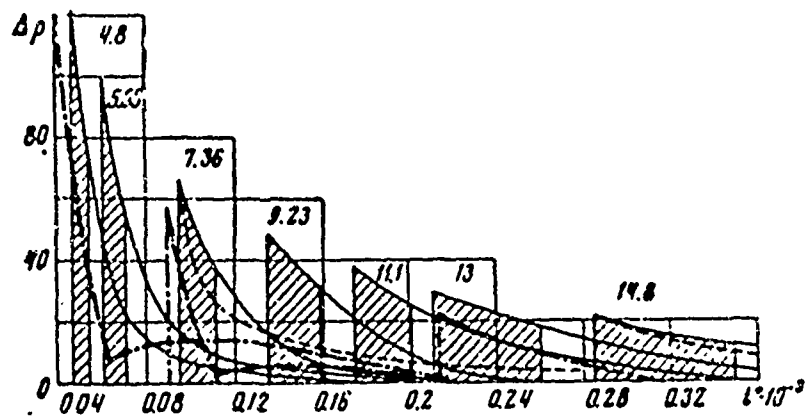


Fig. 10

Furthermore, degree of attenuation of pressure  $\Delta p$  in phase of compression, as proportion of passage by shock wave to point of measurement, is represented in table as function of time  $\tau$ , reckoned from moment of arrival of wave front. By solid line is designated boundary of PE - air. In first line, are values of pressures at wave front  $\Delta p_0$ . Magnitudes of excess pressures, given in Table 2, show process of forming of compression phase of shock wave. We note that piston action of PE is finished, when pressure at wave front becomes less than 20 kg/cm<sup>2</sup>. Wave length (compression phase), by then, is near 6  $r_0$ . PE is still present in compression phase, their volume attains 4000 volumes of charge of HE. Shock wave is gradually detached and is liberated from PE. However, approximately up to 30  $r_0$ , PE are expanded, being in compression phase of wave. Wave length, by then, is already 15  $r_0$ .

Analysis of form of shock wave in near zone of explosion showed that law of attenuation of pressure with time, behind wave front, is not exponential. However, near front, at  $\tau < 5 \cdot 10^{-5} \text{ sec/kg}^{1/3}$ , it can be represented in exponential form

$$\Delta p(\tau) = \Delta p_0 \exp(-\tau/\theta)$$

As functions of distance, quantities  $\theta$ , characterizing steepness of slump

of pressure behind wave front, can be represented by following empirical formula

$$\theta^* = 10^{-6} \left( \frac{r_s}{r_0} \right)^{1.6}, \quad \theta^* = - \frac{\Delta p}{dP/dt^2}, \quad 1 < \frac{r_s}{r_0} < 35 \quad (5.1)$$

For comparison, in Fig. 10 by dotted line is shown change of pressure in time by calculation of point explosion with counterpressure [8]. It is clear that in region where there are PE, there is a marked essential difference in character of pressure slump in wave of a trotyl explosion, as compared with wave of point explosion. Only for waves with intensity  $\Delta p_s < 10 - 20 \text{ kg/cm}^2$ , difference in profiles of these two types of explosion becomes immaterial.

Values of  $\Delta p$ ,  $\text{kg/cm}^2$  as Functions of  $r^* \times 10^6 \text{ sec/kg}^{-1/3}$

$r^*$	$\Delta p$					$r^*$	$\Delta p$		
0	122	100	67	49	38	0	30	22	12.5
3.9	96	80	58	45	35	9.7	25	19.5	11.3
7.8	75	65	52	41	33	19.4	21.5	17.5	10.3
11.6	45	50	46	38	31	29.2	18.5	16	9.2
15.5	30	38	40	35	30	39	17	14.5	8.5
19.4	23	30	35	32	28	97	8	7.5	5.2
29.2	14	18	22	26	25	194	2.5	3.7	2.6
39	9	12	13	20	22	292	1.2	1.9	1.5
58	4	6	7	10	16	390	0.8	1.3	0.9
77	2.5	4	3	3.5	12	486	0.5	0.8	0.5
97	1	2	1.5	1.5	8	580	0.2	0.5	0.3
116	0.5	1.0	0.5	0.5	5	680	0.2	0.2	0.15

By dash-dotted line in Fig. 10 are represented functions of  $\Delta p = f(t)$  by results of numerical calculation of shock wave from detonation of spherical charge of trotyl with density  $\rho = 1.5 \text{ g/cm}^3$  [6]. Comparison of above mentioned experimental data with results of work [6] showed that there are evident deviations in certain details of picture of development of explosion in region where there are PE. Thus, for example, according to [6], at pressure in shock wave near  $120 \text{ kg/cm}^2$ , pressure, after drop in "air plug," starts anew to increase behind contact surface, attaining maximum of near  $15 \text{ kg/cm}^2$  to a time three times longer than arrival time of wave front.

In present work, with such parameters, a front of similar peak was not observed, although piezo apparatus applied in investigations was able to register

this. Difference is observed also in width of layer of air between front and PF and in movement of contact surface. Thus, in [6], movement of contact surface from center ceases at a distance of 13 - 14 radii of charge. In our case, expansion of PE is observed to 30  $r_0$ . Cause of shown deviations can be that equation of state of PE used during calculation [12] insufficiently describes late stages of scattering of PE. Insufficient reliability of calculation of equation of state of explosives leads also to necessity of experimental investigation of the trotyl explosion.

6. Energy of air between wave front and products of explosion. By distribution of pressure and density in region front - PE and by magnitude of mass velocity of air behind wave front, energy acquired by disturbed layer of air from scattering PE was calculated. Magnitude of total energy of air in wave is composed of internal and kinetic energies. Taking expression  $(k-1)^{-1} p/\rho$ , for internal energy of a mass unit of air, we can calculate the increase of internal energy  $E_T$  of the layer of air compressed by a wave

$$E_T = M \int_0^1 \frac{p(\mu) d\mu}{\rho(\mu) [k(\mu) - 1]} - \frac{M p_0}{\rho_0 (k_0 - 1)} \quad (6.1)$$

Expression for kinetic energy  $E_k$  of air, brought to motion by shock wave, is written in the form

$$E_k = \frac{M u_0^2}{2} \int_0^1 [1 - b(1 - \mu)]^2 d\mu \quad (6.2)$$

Result of calculation of internal and kinetic energy of in reference to

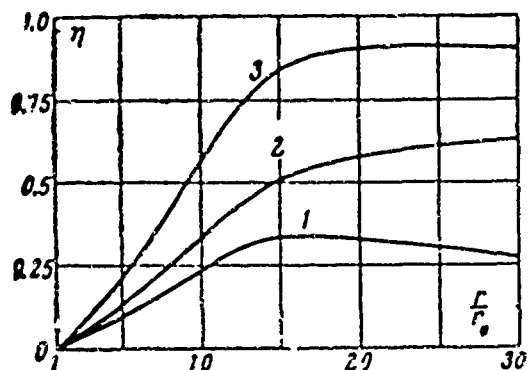


Fig. 11

total energy of explosion  $E = E_0$  is represented graphically in Fig. 11 as function of distance to wave front in radii of charge. Curve 1 shows change of kinetic energy of air in wave. It is interesting to note that at distance 13 - 15  $r_0$  is observed maximum of

kinetic energy which constitutes 30 - 35% the energy of explosion. Curve 2 presents rise of internal energy of turbulent air, and curve 3, the sum of kinetic and internal energies of layer of air in wave. From graphs, it is clear that PE intensely issue their own energy to the ambient air. Thus, when a mass of air equal to mass of charge of HE, set in motion which occurs at  $11 r_0$ , kinetic energy of turbulent air constitutes 25% of initial energy of explosion, internal - 40%, i.e., 65% of energy of explosion crossed to a narrow ( $1.2 r_0$ ) layer of air of compressed in the wave. When a mass of air, participating in motion, exceeds, by 2 to 3 times, the mass of charge of HE, which occurs when position of front is near  $15 r_0$ , almost 90% of the energy of explosion is transferred to layer of air between front and PE..

In conclusion, the author thanks I. V. Nemchinov for offered method of calculation of parameters of air behind front of shock wave and interest in the work.

Submitted  
9 November 1962

#### Literature

1. M. A. Sadovskiy. Mechanical action of air shock waves of explosion by given of experimental investigations, Coll. Physics of explosion, Izd. AN SSSR, 1952, No 1.
2. V. V. Adushkin, and I. V. Nemchinov. Approximate determination of parameters of gas behind front of shock wave according to law motion of front, PMTF, 1963, No 4.
3. G. G. Chernyy. Gas flows with great supersonic speed, Fizmatgiz, 1959.
4. G. G. Chernyy. Adiabatic motion of idea gas with shock waves of great intensity, Izv. AN SSSR, OTN, 1957, No 3.
5. V. V. Adushkin, and A. I. Korotkov. Parameters of shock wave near charge of explosive during explosion in air, PMTF, 1961, No 5.
6. H. L. Brode. Blast Wave from a Spherical Charge, the Physics of Fluids, March - April, 1959, vol. 2, No 2.
7. L. I. Sedov. Methods of similitude and dimensionality in mechanics, Gostekhteorizdat, 1954.
8. D. Ye. Okhotsimskiy, and others. Calculation of point explosion with regard to counterpressure, Tr. Matem. institute im. Steklov, 1957, vol. Leningrad.

9. Ya. B. Zel'dovich. Theory of shock waves and introduction to gas dynamics, Pub. House of Academy of Sciences of USSR, Moscow - Leningrad, 1946.
10. Ya. B. Zel'dovich, and Yu. P. Rayzer. Shock waves of great amplitude in gases, Progress of physical sciences, 1957, vol. XIII, issue 3.
11. R. Sauer. Flows of compressible liquid, IL, 1954.
12. H. Jones, and A. R. Miller. The detonation of solid explosives. Proc. Roy. Soc., 1948, vol. 194.

## COURSE OF REACTION IN DETONATION WAVE OF EXPLOSIVE MIXTURES

A. Ya. Apin, I. M. Voskoboynikov, and G. S. Sosnova

(Moscow)

Development of theory of explosives requires knowledge of kinetics of reactions at front of detonation wave. Complexity of study this question is caused by lack of direct methods of detection of composition of products of explosion in wave and by the impossibility to extrapolate, in region of such high temperatures  $T$  and pressures  $p$ , data on thermal decomposition of explosives at low  $T$  and  $p$ .

Certain information on the course of reactions under the conditions of detonation wave can be obtained, investigating dependence of velocity of detonation  $D$ , m/sec, on diameter of charge  $d$ , mm, of explosive mixture containing explosive constituents of various reaction ability. Due to various reaction times of decomposition of these constituents, growth of velocity of detonation, during increase of diameter of charge, will not be continuous, but occurs with fixation of certain values, corresponding to completion of intermediate stages of reaction. Analogous dependences of  $D(d)$  can also take place for mixtures of type oxidizer-fuel, if final reaction, after decomposition of explosive constituents, requires for its own completion a significant interval of time due to complexity of diffusion at detonation pressures of condensed explosives. Below are given experimental data on detonation velocities of various explosive mixtures, at front of wave of which is revealed the phasic character of course of reaction.

Initially investigated were mixtures consisting of explosive oxidizer and nonexplosive fuel; it was possible to judge the degree of progress of final-reaction, by increase of speed of detonation. In Fig. 1 are presented dependences of  $D = D(d)$  for suspension of lamp black with dimension of particles near one micron in tetranitromethane 10/90 (curve 1); mechanical mixtures of perchlorate of ammonium with paraffin 90/10, grain size 0.01 mm,  $\rho_s = 1.0 \text{ g/cm}^2$  (curve 2), and trotyl with colloidal boron 90/10,  $\rho_s = 0.65 \text{ g/cm}^2$  (curve 3). Common

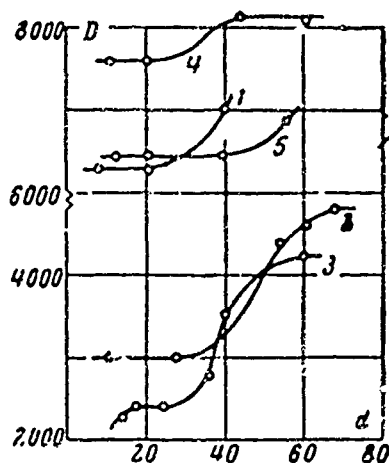


Fig. 1

to shown mixtures is constancy, within certain interval of diameters of charges of imperfect velocity of detonation ("pseudoideal" velocity), magnitude of which corresponds to energy of decomposition of oxidizer.

Increase of velocity of detonation of mixture of trotyl and colloidal boron, at diameters of charge greater than 40 mm, indicates that metals (in particular, boron) can burn in detonation wave of condensed explosives with emanation of additional quantity of heat, leading to increase of speed of detonation, - a fact which is frequently subject to doubt during investigation of powerful metallized explosives. Velocities of detonation were measured by the ionization and optical methods, error in both cases did not exceed 50 m/sec.

In Fig. 1 are also curves of  $D = D(d)$  for 58/42 mixture of hexogen and ammonium nitrate 58/42, grain size 0.1 mm (curve 4) and a suspension of macro-crystalline hexogen with particles size 1.0 to 1.6 mm in gelatinized, 2% plexiglas tetranitromethane 30/70 (curve 5). Magnitudes of pseudoideal velocities correspond to energies of decomposition of hexogen and tetranitromethane at wave front. In the latter, it is easy to check, measuring detonation velocity in

Table 1. Pseudoideal Detonation Velocities  $D_2$  of Explosive Mixtures, Corresponding to Decomposition of Only one Component

(a) Варивчатие вещества	$\rho$	$D_2$	$D_1$
58% $(\text{CH}_2\text{NNO}_2)_2 + 42\% \text{NH}_4\text{NO}_3$	1.73	7600	8100
58% $(\text{CH}_2\text{NNO}_2)_2 + 42\% \text{NaCl}$	1.89	—	7500
70% $\text{C}(\text{NO}_2)_4 + 30\% (\text{CH}_2\text{NNO}_2)_2$	—	6400	7500
70% $\text{C}(\text{NO}_2)_4 + 30\% \text{Na}_2\text{S}_2\text{O}_3$	—	—	6200
90% $\text{NH}_4\text{ClO}_4 + 10\%$ парафина (b)	1.00	3000	4800
$\text{NH}_4\text{ClO}_4$	1.00	—	2900
90% $\text{CH}_2\text{C}_6\text{H}_2(\text{NO}_2)_3 + 10\%$ B	0.65	2400	4200
$\text{CH}_2\text{C}_6\text{H}_2(\text{NO}_2)_3$	0.65	—	3800

Key: (a) Explosives; (b) paraffine.

mixtures, where constituent unable to decompose in wave (ammonium nitrate and macrocrystalline hexogen) is replaced by an inert substance. From values given in Table 1, it is clear that detonation velocity of mixture of hexogen and table salt and suspension of hyposulphite in tetranitromethane differs little from corresponding pseudoideal detonation velocities. In Table 1 are also values of ideal detonation velocities  $D_1$  of studied mixtures.

Pseudoideal detonation velocities are also observed for mixtures, the explosive constituents of which are decomposed in wave in short times. In Fig. 2, as an example, are presented curves of  $D(d)$  for suspensions of hexogen with dimension of particles 0.3-0.4 mm 30/70 and trotyl 20/80 in tetranitromethane (curves 1 and 2), and also for solution of dinitroethane in tetranitromethane

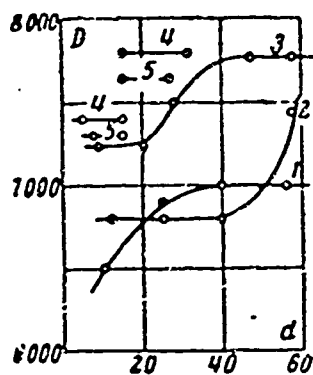


Fig. 2

76/24 (curve 3). Analysis of magnitudes of pseudoideal velocities in this case can be made with the help of calculation of parameters of detonation wave [1].

It is assumed that reaction in wave proceeds in the following manner: at first, explosive components completely decompose within their own volume, and

then, after the lapse of a certain interval of time, starts effective reaction

of final reaction between products of their decomposition. Coincidence of results of calculation of detonation velocities  $D_3$  corresponding to completion of first stage of reaction, with experimental values of pseudoideal detonation velocities  $D_2$  for series of explosive mixtures, serves as confirmation of such a diagram of the course of reaction.

Table 2. Pseudoideal Detonation Velocities of Explosive Mixtures Corresponding to Decomposition of two Constituents

(a) Выходные вещества	$\rho_0$ , (b) $g/cm^3$	$D_2$ , (c) $m/sec$	$D_3$ , (c) $m/sec$	$D_4$ , (c) $m/sec$
80% C(NO <sub>2</sub> ) <sub>4</sub> + 20% CH <sub>2</sub> C <sub>6</sub> H <sub>2</sub> (NO <sub>2</sub> ) <sub>4</sub>	1.64	6800	6800	7600
70% C(NO <sub>2</sub> ) <sub>4</sub> + 30% (CH <sub>2</sub> NNO <sub>2</sub> ) <sub>2</sub>	1.70	7000	7000	7500
78% CH <sub>2</sub> CH(NO <sub>2</sub> ) <sub>2</sub> + 24% C(NO <sub>2</sub> ) <sub>4</sub>	1.42	7250	7000	7800
50% C(CH <sub>2</sub> ONO <sub>2</sub> ) <sub>4</sub> + 50% CH <sub>2</sub> C <sub>6</sub> H <sub>2</sub> (NO <sub>2</sub> ) <sub>4</sub>	1.65	7450	7550	7450

Key: (a) Explosives; (b)  $\rho_0$  g/cm<sup>3</sup>; (c) m/sec.

During investigation of liquid explosive solutions, the authors discovered a strong dependence of detonation velocity on diameter of charge, although it is almost completely absent for individual liquids and single-crystal explosives. Sometimes this dependence has a very unique form: for example, for solutions of tetranitromethane with nitrobenzene (76/24) and kerosene (88/12) (curves 4 and 5, Fig. 2) it exists, at a certain diameter of charge, depending on thickness and material of shell, with equal probability for value of detonation velocity, differing by 400 m/sec. Temperatures of detonation fronts measured by electronic-optical method, differ by 500°K.

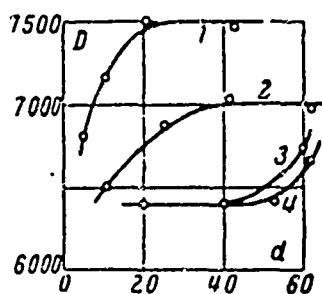


Fig. 3

Main cause of the observed phenomenon of pseudoideal detonation velocity is phasic course of reaction at front of detonation wave of the explosive mixture, caused by kinetics of decomposition the explosive constituents.

Velocity of energy release in wave is influenced by a whole series of factors (reaction capability of components, heat

of their explosive reaction, dispersity, and percentage of composition of mixture), action of each of which for concrete explosive mixture is frequently difficult to reveal. However, decrease of dispersity of components in a mixture always increases probability of observation of pseudoideal detonation velocity, since temporal difference between decomposition of components and subsequent final reaction increases. Thus, if for suspension of fine-crystalline hexogen with particles size near 0.1 mm in gelatinized tetranitromethane (curve 1, Fig. 3), build-up of detonation velocity, during increase of diameter of charge, is continuous, then, at particles size 0.3 - 0.4 mm (curve 2), at diameters of charges 20 - 50 mm, we are able to fix delay of final reaction between products of decomposition of tetranitromethane and hexogen. Increase of dimension of particles to 1.0 - 1.6 mm and 3 - 4 mm reveals that at small diameters of charges coarse metallic hexogen is not able to decompose in wave (curves 3 and 4).

Investigation of curves  $D(d)$  for suspension of hexogen in tetranitromethane (Fig. 3) shows that, during increase of dimension of particles above a certain magnitude (1.0 - 1.6 mm.), diameter of charge  $d_1$ , in which hexogen is decomposed, ceases to depend on its dispersity. Quantity  $d_1$  characterizes delay time of decomposition of hexogen by volume (for surface of reaction, it would be a function of dimension of particles) and decreases during increase of pressure in detonation wave.

Placing grain of macrocrystalline hexogen, by dimension 1.0 - 1.6 mm, in liquid explosives, pressure in detonation wave of which changes from 180 to 220

thousand atm, it was possible to trace decrease of diameter  $d_1$  with rise of pressure (Fig. 4). If it is considered that reaction progresses effectively as long as pressure does not decrease by a fixed fraction, delay times of reaction will be in first order of approximation

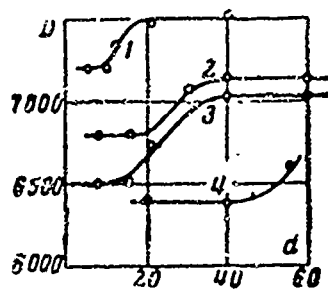


Fig. 4

proportional to diameters of charges  $d_1$ , and at pressures of 180, 190, and 205 thousand atm have ratio 8: 3: 2.

Curves 2 and 3 correspond to the same pressure  $p = 190$  thousand atm, but to various temperatures of products of explosion of liquid explosives: curve 2 -  $T = 3200^\circ\text{K}$ , curve 3 -  $T = 4200^\circ\text{K}$ , a difference of  $1000^\circ\text{K}$ . Grains of hexogen were decomposed at equal diameters of charge. Curve 1 corresponds to pressure  $p = 205$  thousand atm, and curve 4 -  $p = 180$  thousand atm. Liquid explosives had small critical diameters. For them was assumed comparatively short reaction time of decomposition in detonation wave.

Examination of curve D(d) for suspension of hexogen in liquid explosives indicates possibility of use of phenomenon of pseudoideal detonation velocities for estimation of times of decomposition of explosive components in wave.

Ideal detonation velocities correspond to composition of products of explosion, which depends only on contents of C - H - N - O and temperatures and pressures of detonations; all parameters of ideal detonation wave of explosive mixture can be calculated in exactly the same way as for individual explosives [1]. It is necessary only to consider peculiarities of course of reaction in detonation wave of explosive mixture, coupled with the fact that, at first, explosive components are decomposed in their own volume, and then final reaction occurs in products of explosion. When composition of products of explosion produces more energy in first stage than after the final reaction, the first stage of reaction is responsible for ideal detonation velocity (this refers to mixtures of pentolite type, Table 2).

Submitted  
25 May 1963

#### Literature

1. A. Ya. Apin and I. M. Voskoboynikov. Calculation of parameters of detonation wave of condensed explosives. PMTF, 1960, No 4.

INFLUENCE OF PRESSURE ON DISTURBANCE OF STABILITY OF COMBUSTION  
OF POROUS EXPLOSIVES

A. F. Belyayev, A. I. Korotkov, and A. A. Sulimov

(Moscow)

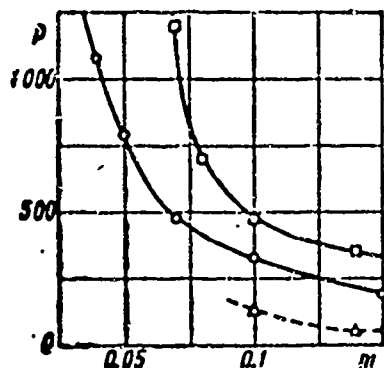
It was noted [1] that penetration of combustion to interior of a porous explosive, evoking sharp increase of surface of combustion and speed of gasification, can lead to explosion.

K. K. Andreyev [2] showed that triggering of explosion during combustion of porous explosives occurs with achievement, in process of burning, of sufficiently high pressure.

Below are given certain quantitative data on pressures at which stable combustion of pressed charges of hexogen, PETN, and trotyl (with particles of initial powders of similar dimension  $\sim 10$  to  $20\mu$  is disturbed. Charges were of various porosity  $m = 1 - \rho / \rho_{\max}$ , where  $\rho$ —density of charge and  $\rho_{\max}$ —density of single crystal. Quantity  $m$  gives fraction of volume, occupied by pores.

During conducting of experiments, elongated charges 10 mm in diameter of various porosity were ignited in a closed manometric bomb at considerable loading density with piezoelectric registration of rise of pressure. So long as a stable combustion layer was maintained, a smoothly accelerating build-up of pressure in time was observed. Sharp break  $p(t)$  (up to appearance of compression shock) attested to disturbance of layer combustion and to breakthrough of combustion to pores; pressure, at which this occurred, was directly indicated by recording  $p$ ).

Some of results obtained by us are given in figure, where on axis of abscissas is plotted porosity  $m$ , and on axis of ordinates—pressure  $p$  in bars (1 bar=1.02 kg/cm<sup>2</sup>) at which occurs breakthrough of combustion to pores. Squares indicate data for trotyl; circles, PETN, and triangles, hexogen.



Squares indicate data for trotyl; circles, PETN, and triangles, hexogen.

In rough approximation, it is possible to set  $pm = A$ , where constant  $A$  depends on properties of substance, character of porosity, and conditions of experiment. During a more detailed consideration of results, it is obvious that asymptote of curves on vertical is  $m \neq 0$ . For PETN,  $p(m - 0.02) = A_1$ , and for trotyl,  $p(m - 0.05) = A_2$ . Practically, this means that PETN, at  $m = 0.02$  ( $\rho = 1.735$ ) is able stably to burn at pressures measured in thousand atmospheres. This was established [3] also for PETN of somewhat less density. At identical porosity (for example, 0.1), the stablest combustion of trotyl (highest breakthrough pressure) and least stable combustion of hexogen occur.

By Taylor [4] it was noted that during combustion of PETN and hexogen (and all the more of trotyl) molten layer should be formed, stabilizing burning as long as its thickness (decreasing with pressure) is not less than dimension of pores. At identical pressure, the biggest layer should be for trotyl, the smallest—for hexogen.

For estimation of thickness of molten layer  $x$  for PETN\*, we have

$$x = \frac{\lambda}{\rho c u} \ln \frac{T_* - T_0}{T^0 - T_0} \quad (1)$$

Here  $\lambda$  - thermal capacity of liquid,  $c$  - heat capacity,  $u$  - mass combustion rate [5],  $T_*$  - stagnation temperature of PETN,  $T^0$  - melting temperature, and

---

\*For roughly tentative appraisals it is possible to limit ourselves to quantity  $\lambda/\rho c u$  - characteristic length of thermal wave - distance at which temperature dependence decreases by  $e$  times.

$T_0$  - initial temperature.

Under the conditions conducted experiments, at  $p = 330$  bar,  $m = 0.1$  for PETN

$$\frac{\lambda}{c} \sim 10^{-8} \frac{s}{cm^2 sec}, \quad \mu p \approx 6.4 \frac{s}{cm^2 sec}, \quad T_0 \sim 580^\circ, \quad T^* \sim 140^\circ, \quad T_c \sim 20^\circ C$$

Substituting these data in (1), we obtain that  $x$  is equal to several microns ( $\sim 2$  to  $3 \mu$ ). Let us assume that at limit, diameter of pores  $d$ , into which combustion is able to penetrate, is equal to thickness of molten layer  $d \approx x$  (if  $d > x$ , combustion will penetrate to interior; if  $d < x$ , there will be no penetration). Thus, we come to the conclusion that for PETN, at pressure  $p = 330$  bar, combustion is able to penetrate into pores with dimension of several microns.\* It is possible to estimate also the average hydraulic dimension of pores [6]  $D \sim \sqrt{k/m}$ , where  $k$  - gas-penetrability. For PETN at  $m = 0.1$ , we obtain  $D \sim 0.01 - 0.1 \mu$  which is 1 - 2 orders less than  $d$ . Difference obtained ( $d \gg D$ ) is explained naturally. Amount of gas-penetrability is determined by all including the small pores. Breakthrough of combustion in initial stage is to the biggest pores (possibly even to the biggest "pore"). Obviously, distribution of pores is by such dimension that the biggest pores  $d \sim x$  are 1 to 2 orders larger than average hydraulic dimension  $D$ .

During increase of pressure, velocity  $u$  increases ( $u \sim p$ ), thickness of molten layer  $x$  decreases, and combustion can penetrate to pores of increasingly smaller dimension

$$d \sim x \sim \frac{1}{u} \sim \frac{1}{p}, \quad \text{or } pd = c \approx \text{const}$$

The latter relationship is approximately satisfied. In any case, during increase of pressure, dimension of pores, gaps, into which combustion is able to penetrate, becomes increasingly smaller  $d \sim 1/p$ . For various substances, breakthrough of combustion to pores occurs at various pressures, but if stabilization is caused by molten layer and structure of charges is identical, thickness

---

\*If actual thickness of molten layer exceeds that calculated by formula (1), critical size of pores will be larger.

of molten layer should be similar. Calculation shows that for hexogen (at  $p = 130$  bar), thickness of molten layer (just as for PETN (at 330 bar)) will be several microns. For trotyl (at 430 bar), layer is thicker and breakthrough of combustion to pores should occur at pressure, approximately two times larger ( $\sim 800$  bar). It is obvious that at identical porosity ( $m = 0.1$ ) structure of charge of trotyl is quite distinct. By measurement of gas-penetrability it is directly established that average hydraulic dimension of pores of trotyl is 1.5 times greater than for PETN (at identical  $m = 0.1$ ). Apparently, dimension of the biggest pores for trotyl is twice as large. Incidentally, at less porosity (0.07 to 0.08), structures of charges of PETN and trotyl become more alike.

Given data are well coordinated with assumption of Taylor [4] about stabilizing action of molten layer. Andreyev [7] pointed out the opposite possibility of disturbance of stability of combustion of PETN due to self-turbulization of molten layer. This was not developed in an experiments (true, conditions in our experiments were considerably different).

Let us consider case of combustion of porous explosives not forming a molten layer. It would be incorrect to assume that for unmelting explosive, combustion will penetrate deeply at any (low) pressure. This penetration will be coupled with conditions of influx of products of combustion into pores and substances igniting them. Both these factors depend on conditions of combustion and on distance  $x'$  between surface of substance and zone of intense reaction in gas or smoke-gas phase; this distance

$$x' \approx \frac{\lambda'}{c'(\mu\rho)} \ln \frac{T^* - T_0}{T^0 - T_0} \quad \left( \frac{\lambda'}{c'} \sim 5 \cdot 10^{-4} \frac{\text{cm}}{\text{sec}} \right) \quad (2)$$

Here,  $\lambda'$  and  $c'$  - thermal conductivity and thermal capacity of gas phase,  $T^0$  - temperature of surface,  $T^*$  - temperature of intense reaction in gas phase (in majority of cases,  $T^*$  will not be maximum temperature of combustion). Remaining designations are the same as in (1). By tentative estimation,  $x'$  is somewhat less than thickness of molten layer  $x$ . Furthermore, viscosity of gas

is considerably less than viscosity of liquid which should facilitate flowing of gases into pores. Finally, in the absence of molten layer, deep penetration of combustion should be eased (at identical porosity, breakthrough of combustion to pores  $d'$  will be at pressures a few times lower; at identical pressure, several times lower). Roughly approximately also should be satisfied condition  $pd' = (\text{const})'$ , where  $(\text{const})' < \text{const}$ .

Test experiments with non-melting explosives showed that these conclusions, in general, are correct, and in particular, breakthrough of combustion to pores of unmelted explosives is easier than for those melted. It is necessary to note that break of curve  $p(t)$ , attests to passage of combustion to pores, for non-melting explosives which is somewhat blurred and is expressed less clearly.

Breakthrough of combustion to pores of mercury fulminate (triggering explosive) should be especially easy. This was noted in a work by author [8].\* Indeed, if for hexogen at  $p \approx 100$  bars, for penetration of combustion to depth of substance, the dimension of pores  $d$  must be several microns, then for fulminate of mercury with this same pressure, value of  $d$  must be estimated maximum by tenth fractions of a micron, and  $d$  should be still less for azide of lead. At one time, from certain indirect data, it was assumed [8] that combustion rate of azide was so great that it alone, without penetration of combustion to depth, caused very great jump of pressure and, consequently, detonation. In work of K. K. Andreyev and B. N. Kondrikov [9], is given a better grounded appraisal of combustion rate of azide of lead, which turned out to be higher than for mercury fulminate, but only by 2 - 3 times. In order to explain extremely sudden triggering of detonation of azide of lead (detonates upon ignition), with such a combustion rate, it is natural to assume that at moment of ignition (at any pressure) combustion immediately penetrates to depth and actual surface of combustion becomes quite large.

---

\*A. P. Belyayev. Mechanism of combustion of explosives, Doct. dissert., Institute of Chemical Physics of Academy of Sciences of USSR, 1946.

Here it is necessary to note that if mechanism of combustion of azide of lead is like that of mercury fulminate, then for azide of lead at low pressures, in particular at atmospheric pressure, combustion is able to penetrate into pores of order of one micron. Such gaps can be formed between particles of azide of lead even when pressed to high density. Moreover, for crystals of azide of lead of order of one micron, there can be intervals between crystallite (micropores and microcavities). To this, it is necessary to add that by direct observations of Bowden and collaborators [10], defects of crystals can be formed to grow in process of the actual combustion. At last, during combustion of azide of lead, dynamic increase of pressure should be very significant. All this shows that in case of azide of lead there are many possibilities for intensive penetration of combustion to depth, sharp increase of surface of combustion, i.e., for instantaneous explosion immediately transferred to detonation.

K. K. Andreyev [11], noting that for triggering explosives, the breakthrough of combustion into pores should be easier, as main cause points to the large completeness of reactions of explosive transformation and to higher temperature of combustion of triggering explosives. Value of temperature of combustion is absolutely essential (this is one of factors determining combustion rate), however main cause facilitating breakthrough of combustion to depth of triggering explosives, will be a short distance between surface of explosive and zone of intense reaction, which, other conditions being equal, for triggering explosives is considerably less than for secondary types. High temperatures of products undoubtedly promotes breakthrough of combustion into pores, but more important in this respect magnitude of temperature gradient  $dT/dx$  at the surface, which for triggering explosives is 2 - 3 orders higher than for secondary explosives, basically due to smaller extent of zone of heating up determined, in the final analysis, by character of reactions of combustion and by corresponding constants of the substance.

Returning to the investigated phenomenon in general plan, let us note that phenomenon breakthrough of combustion to pores. This very complicated phenomenon was considered here in simplified form. Breakthrough of combustion to pores and its character depend on physicochemical properties of the substance (our experiments were conducted with explosives reacting chiefly in gas phase [12]) on conditions of combustion, gas dynamics of inflowing products, and character of porous structure. If for example, we take an explosive consisting of larger crystals, its gas-penetrability will be increased, dimension of the largest pores will increase still more significantly; as a final result, breakthrough of combustion to depth of explosive will be eased. As was already noted, experiments were conducted in a manometric bomb under conditions of considerable  $dp/dt$  and fall of pressure  $dp/dx$ .

Under other conditions results could be different. Thus, for example, in bomb of constant pressure, stability of combustion increases: pores will be filled by inert compressed gas. Nevertheless, simplified investigation undertaken allowed to obtain useful results.

Institute of Chemical Physics  
of Academy of Sciences of USSR

Submitted  
25 April 1963

#### Literature

1. A. F. Belyayev. On conditions of stationary combustion of explosives. Reports of Academy of Sciences of USSR, 1940, vol. 28, page 715-718.
2. K. K. Andreyev. On combustion of explosives under increasing pressure. Reports of Academy of Sciences of USSR, 1940, 29, page 469-472.
3. A. F. Belyayev, A. I. Korotkov, A. K. Parfenov, and A. A. Sulimov. Combustion rate of certain explosives and mixtures at very high pressures, Zh. fiz. khim., 1963, vol. 37, page 150-157.
4. T. W. Taylor. A melting stage in the burning of solid secondary explosives, Comb. and Flame, 1962, vol. 6, No 2, p. 103-107.
5. A. P. Glazkova and I. A. Tereshkin. On function of combustion rate of explosives under pressure, Zh. fiz. khim., 1961, vol. 35, 1622-1628.
6. L. S. Leybenzon. Motion of natural liquids and gases in porous medium, Gestechnik, 1947.

7. K. K. Andreyev and P. P. Popov. On combustion of PETN, Zh. fiz. khim., 1961, vol. 35, 1979-1984.

8. A. F. Balyayev. On main cause of impossibility of stable combustion of explosive of lead nitride type. Coll. "Physics of explosions," 1952, No 1, page 185.

9. K. K. Andreyev and B. N. Kondrikov. On combustion of mixtures of lead nitride and liquid nitroesters. Report of Academy of Sciences of USSR, 1961, vol. 137, pages 130-133.

10. F. P. Bowden, B. L. Evans, and A. D. Ioffe. The combustion and Explosion of Crystals. 6-th Symp. (Intern.), Comb., p. 609.

11. K. K. Andreyev. On main causes of distinction between triggering and secondary explosives. Reports of Academy of Sciences of USSR, 1962, vol. 146, page 413-414.

12. A. F. Balyayev. On combustion of nitroglycol, Zh. fiz. khim., 1940, 14, page 1009-1925.

## ON INFLUENCE OF PRESSURE ON COMBUSTION RATE OF AMMONIUM PERCHLORATE

A. P. Glazkova

(Moscow)

To study of process of self-propagating intramolecular oxidation of ammonium perchlorate is devote a series of investigations.

Friedman, Nugent, and et al. [1] studied combustion of ammonium perchlorate (samples of square section 4 x 4 mm, unarmored) in range of pressures to 340 atm; under these conditions they established initially, the upper and lower limits of ability to burn according to pressure: perchlorate is able to burn, starting from ~ 40 atm; combustion ceases, if pressure exceeds ~ 270 atm.

Below is investigated function of combustion rate on pressure in a wider range (to 1000 atm). In work was applied photographic method of study of process of combustion, described in detail earlier [2]. Experiments were placed in vessels of constant pressure at 350 and 1000 atm in an atmosphere of nitrogen. For strengthening of glow of unarmored samples of ammonium perchlorate in realm of unstable combustion (160 - 350 atm), light conductor was applied: a rectangle of polished plexiglas touching, on one side, the window of vessel, on the other (protected by a thin glass plate), the specimen of perchlorate. Unsifted perchlorate (analytical grade) was used, dried to constant weight and pressed to density near to specific gravity (1.93 - 1.94 g/cm<sup>3</sup>). Diameter, shell, and form of samples were changed in various series of experiments.

1. On intensification of thermal loss during increase of pressure as possible cause of upper limit. It can be assumed that quenching of combustion at upper limit for American researchers was caused by thermal losses, all the more so since they used samples of small transverse dimension. Indeed, experiments with unarmored cylinders of perchlorate showed that at diameter of 5 mm,

combustion ceases at 270 atm, and at 7 mm, extinguishing of combustion at this pressure is no longer observed. Still more convincing were experiments with kernels in the form of a frustum of a cone (upper diameter of which was 7 mm, lower - 1 - 2 mm) igniting from large end. Combustion in all experiments was extinguished at 250 atm, up to a diameter of 4.7 - 5 mm.\* Inspection of unburned part of sample showed that front of combustion had a concave form, part of external lateral surface of kernel did not manage to burn and remained, after combustion, in the form of a thin border.

Lower limit, as one would expect under the same thermal considerations, also depends on diameter: at diameter of 5 mm, sample did not burn at 50 atm, at 7 mm, stable combustion was observed already at 30 atm.

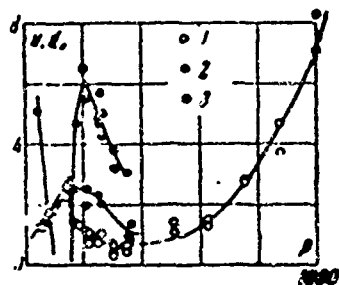


Fig. 1

Thus, both upper and lower limits of combustion are determined by pressure. This is due to the decrease of combustion rate, in other words, its duration. Thermal input is not able to compensate heat loss.

During explanation of upper limits ability to burn according to pressure, it was assumed that decrease of combustion rate occurs during increase of pressure and under conditions when thermal losses do not play an essential role. In Fig. 1 are given functions of combustion rate  $u$  (here and in the future  $u$  - mass combustion rate in  $\text{g}/\text{cm}^2 \text{ sec}$ , pressure  $p$  in  $\text{kg}/\text{cm}^2$ ) of perchlorate on pressure  $p$ . Points 1 and 2 for diameters of 7 and 12 mm of unarmored samples, point of 3 give values of critical diameter of combustion. From the figure it is clear that in interval of pressures to 150 atm, combustion rate is identical

---

\*In three analogous experiments, when air from vessel was not evacuated before experiment, combustion of kernels was complete. This is attributed to the influence of oxygen, remaining in vessel.

for thin and thick kernels from 200 to 400 atm. The latter burn rapidly, but their combustion rate also drops as for kernels of small diameter. In Fig. 1 are also presented oriented data on dependence of critical diameter of combustion (determined by extinguishing of bare conical kernels) of perchlorate on pressure. This dependence, up to pressure of 200 atm, in general, agrees well with curve  $u = f(p)$ . Decrease of critical diameter at pressures from 200 to 350 atm, in region where combustion rate remains constant, was not intelligible.

As can be seen from photographs (Fig. 2a), at pressure of 140 atm, combustion of unarmored samples of ammonium perchlorate is stable and differs from combustion of secondary explosives only by the presence of separate local flashes at front of flame. At pressures of 200 - 350 atm, character of combustion changes sharply: glow becomes weaker and combustion assumes a pulsating character - at front of combustion are stops when burning seems to cease and then starts again, and, as a rule, with the same rate as before the stop.

From photographs of combustion it follows also that in region of unstable combustion of perchlorate (see, for example, Fig. 2b, combustion at 247 atm), front of flame has striped structure and consists of alternating light and dark strips. At pressures of 200 - 500 atm, were observed cases of 7-millimeter samples not burning completely. In Fig. 1, region of unstable combustion is designated by dotted line.

GRAPHIC NOT  
REPRODUCIBLE

(a)

(b)

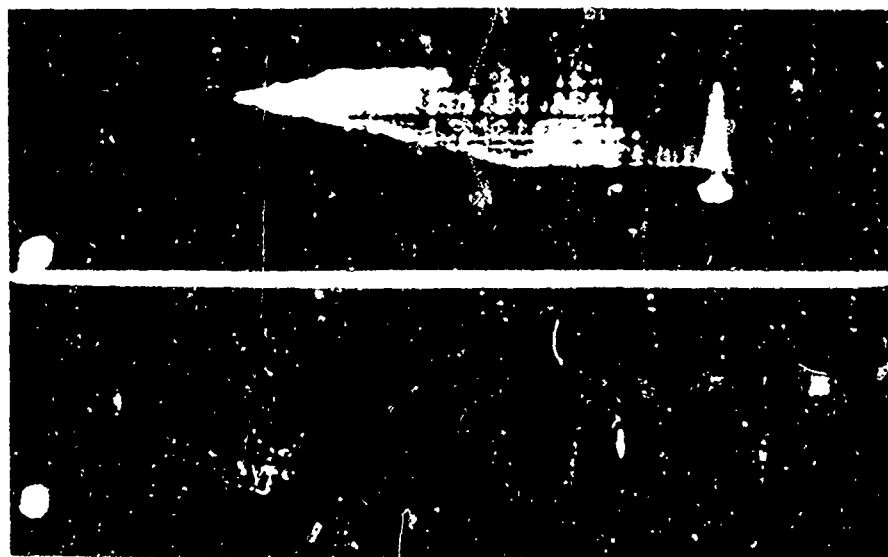


Fig. 2

Influence of thermal losses during combustion is lessened also, in addition to increase of diameter of sample, by application of shell of low thermal capacity (plexiglas). In Fig. 3 is given dependence of combustion rate on pressure for samples of perchlorate pressed in plexiglas pipes of diameter 5.7 and 10 mm, with wall thickness of 1 mm (points 1, 2 and 3 correspond to values of diameter,  $d = 7, 5, 10$  mm). As can be seen from Fig. 3,  $u = f(p)$  has basically the same character as that for unarmored kernels, and combustion rate does not depend on diameter of sample. It follows from this that drop of rate cannot be explained by thermal losses to the outside. Actual confirmation of this conclusion comes from following experiment: plexiglas tube of perchlorate (diameter 5 or 7 mm) was placed to half its height in water. If thermal loss had significant influence, combustion rate in that part of the tube located in the water, should have decreased. Experiments conducted at 200 atm, showed that combustion rate in both parts of tube were practically identical (1.44 - 1.39 for 7-millimeter diameter and 1.38 - 1.40  $\text{g/cm}^2 \text{ sec}$  for 5-millimeter).

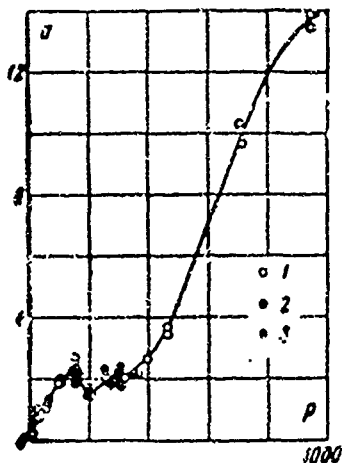


Fig. 3

Results of described experiments are subject to doubt in connection with the fact that combustion occurred in tubes of organic material - plexiglas, participation of which in combustion could accelerate it. This circumstance can be explained in two ways: either determine influence of plexiglas on combustion rate of perchlorate or take as material of

shell a low-reactive substance. In this work, both variant were applied.

Mixture with zero oxygen balance of perchlorate and plexiglas (particle size of components  $> 1 \mu < 250 \mu$ ) burns in significant range of pressures with slower rate, than perchlorate alone; at 50 atm, combustion rate of perchlorate

in plexiglas pipes was, on the average, 1.20, and combustion rate of mixture - 0.78 g/cm<sup>2</sup> sec. Thus, plexiglas does not accelerate, and even delays combustion of perchlorate in region of moderately increased pressures, and its application as a shell under these conditions does not evoke doubts. Incidentally, one should note that character of combustion of perchlorate changes somewhat depending upon conditions of conduction of experiments. In photograph of Fig. 4a, during combustion of perchlorate in pipe of diameter 10 mm at 156 atm, visible, adjacent to front, is a narrow luminescent strip of granular structure, as if front of combustion consisted of separate microflashes. Granularities of front, apparently, correspond to separate streams of burning gases, probably accompanied by particles giving flame a shaggy, striped, form. At pressure of 276 atm (Fig. 4b) velocity of gases was approximately 30 cm/sec.

**GRAPHIC NOT  
REPRODUCIBLE**

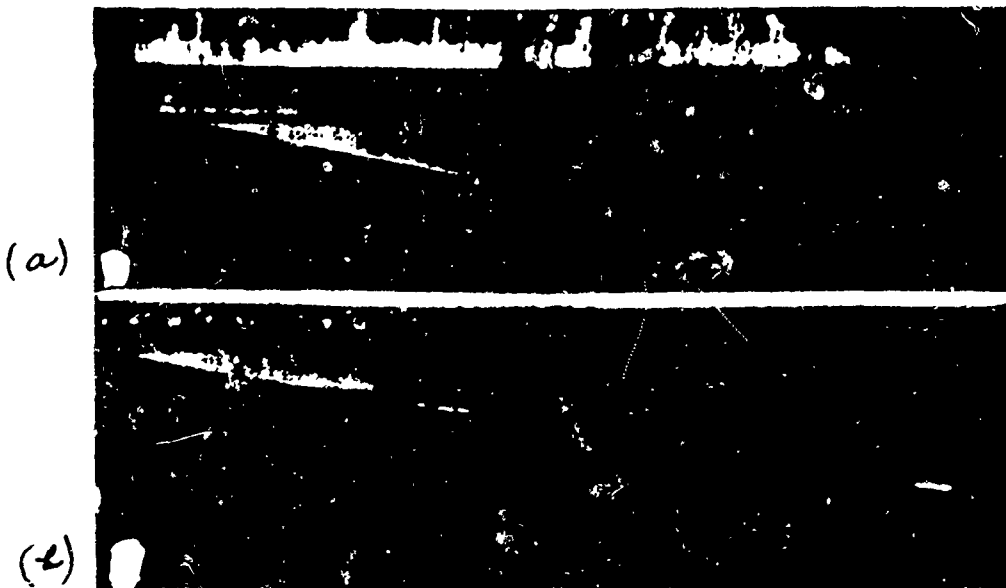


Fig. 4

In glass pipes, combustion of perchlorate proceeds otherwise. It goes by parallel layers, but glow on surfaces of combustion is weak and at separate points brighter flashes are observed. On walls of lower part of pipes, at height of 2 - 3 cm, after experiments there remains a layer of salt of noticeable

thickness externally baked and nonuniform with separate "burnt places" extending to wall of pipe. Comparing this picture with photographic prints of experiments, it may be concluded that combustion goes very nonuniformly; it is delayed at periphery; light points and spots on photographs correspond to approach of combustion at separate points, to walls of that part of pipe which is turned toward objective. Described process of combustion reminds us, in this respect, of combustion of catalyzed ammonium nitrate.

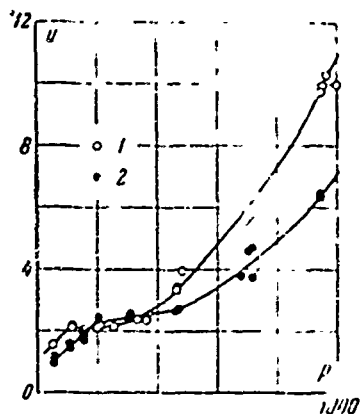


Fig. 5

Absence of these peculiarities on photographs of combustion in plexiglas pipes is probably explained by smaller thermal losses through walls of pipe and by a relatively high temperature of combustion. In general, these photographs graphically demonstrate nonuniform, local character of combustion of ammonium perchlorate.

bustion of ammonium perchlorate.

Experiments in low-reactive shell were run in following manner. Samples 15.3 mm in diameter were covered with varnish of vinyl-perchloride resin (content of Cl 60,-65%) dissolved in dichloroethane. Thickness of layer of varnish was 0.1 mm. In order to ensure uniformity of igniting with such diameter, ignition was triggered at high pressures by tablet of black powder, which led to sharp decrease of scattering of velocities in parallel experiments at 750 and 1000 atm. Furthermore, in order to explain influence of thickness of shell, a series of experiments was run in which 7-millimeter samples of perchlorate were covered by layer of varnish of thickness at 1 mm so that pipe was formed of vinyl-perchloride varnish.

At last, fluorinated lubricant was studied as shell. In Figs. 5 and 6 are presented obtained results.

Fig. 5 shows dependence of combustion rate on pressure for 15-millimeter

samples of perchlorate in shell of vinyl-perchloride varnish (0.1 mm, curve 1), and curve 2 for 7-millimeter samples in fluorinated lubricant.

In Fig. 6 are presented dependence of combustion rate on pressure for 7-millimeter samples of perchlorate in shell of vinyl-perchloride varnish of various thickness  $h$ : curve 1 for  $h = 0.1$  mm, curve 2 - for  $h = 1.0$  mm (scale on axis of ordinates is twice less).

Graphics show that on curves of dependence  $u = f(p)$  for samples in vinyl-perchloride varnish, section of velocity drop is preserved, although under these conditions it is expressed less distinctly than in plexiglas pipes.

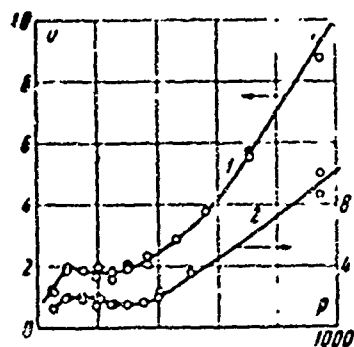


Fig. 6

combustion rate of perchlorate in various shells: 1 - without shell, 2 - in vinyl-perchloride varnish (0.1 mm), 3 - in vinyl-perchloride varnish (1 mm), 4 - in plexiglas pipes, 5 - in fluorinated lubricant.

Examination of graphs shows that for perchlorate, two regions of pressures are observed: first - up to pressures of approximately 400 atm where combustion rates of perchlorate in various shells are similar and drop of combustion rate with pressure is more sharply pronounced for unarmored samples and for perchlorate pressed in plexiglas pipes; second region from 500 to 1000 atm where magnitude of combustion rate is varied depending upon shell.

The question naturally arises of the physical meaning of this distinction and of which curve depicts, to the greatest degree, combustion of the perchlorate itself? The highest combustion rate at 1000 atm is shown by perchlorate in

## 2. Dependence of combustion rate

of ammonium perchlorate on presence of shell material at high (500 - 1000 atm)

pressures. In Fig. 7 are summed up data obtained in this work on combustion of samples of perchlorate of diameter

7 mm, and dependences are shown of

plexiglas pipes - 14 g/cm<sup>2</sup> sec. In pipes of perchlorvinyl (0.1mm), perchlorate burns with significantly less speed 9 g/cm<sup>2</sup> sec.

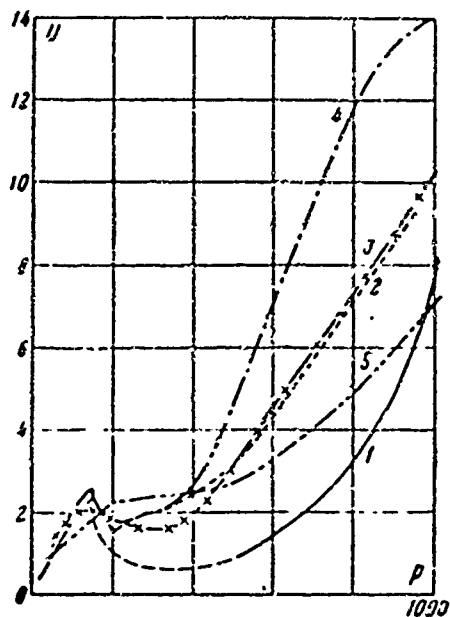


Fig. 7

During combustion in a thick shell of low thermal conducting material (plexiglas), thermal losses could be less than in a thin shell of vinyl-perchloride. Such explanation, however, could be checked. If thermal losses considerably affect rate, then the latter should depend on diameter. Therefore, at pressure of 950 atm were run experiments in a vinyl-perchloride their shell at various diameters; we list

obtained average rates of combustion  $u$  for various diameters of sample  $d$  in mm;

$d = 15$	$7$	$5$	$3$
$u = 10.0$	$9.06$	$8.98$	$8.33$

These data show that influence of thermal losses was slight, so that through it was possible to explain variations in combustion rates.

A still sharper influence of thermal losses should have shown up under these conditions for unarmored samples. However, experiments showed that combustion rate of 3-millimeter samples of perchlorate was even somewhat higher (7.4 g/cm<sup>2</sup> sec) than for 15-millimeter samples (6.0 g/cm<sup>2</sup> sec). Probably, here is manifested influence of combustion on lateral surface of oxygen contained in technical nitrogen.

A second possible explanation is that at high pressures, the plexiglas of the wall burns with perchlorate and this combustion in contact zone is faster than far from it and leads the process. Verification was possible, comparing combustion rate of mixtures of zero oxygen balance in plexiglas pipes and without

shell. Paraffin mixtures yield, in plexiglas and vinyl-perchloride shells identical rates -  $17 \text{ g/cm}^2 \text{ sec}$ . This rate applies also to combustion of a bare kernel of perchlorate with paraffin. This attests to the fact that such secondary factors as cooling, heat transfer in shell, washing by dense nitrogen, do not play an essential role, but difference in rates for perchlorate is actually caused by reaction of the substance with the wall. This interaction can not be considered completely excluded during combustion in vinyl-perchloride shell. Let us note that experiments with a bare kernel gave significantly lower rate -  $7 - 8 \text{ g/cm}^2 \text{ sec}$  which can be considered the combustion rate of the perchlorate itself.

Experiments with kernels covered with fluorinated lubricant gave still lower rate. We can assume that this latter shell in burning, partially volatilizing in proportion to rate of combustion, and mixing with products of combustion, decreases its rate somewhat, as compared with combustion rate of perchlorate without shell.

Thus, dependence of combustion rate on pressure for ammonium perchlorate, studied in wide range of pressures, differs considerably from that for other substances studied [2]. The most interesting of experimental facts is fall of combustion rate with pressure within its determined range, and also the pulsating, unstable character of combustion under these conditions. Fall of combustion rate with pressure, according to K. K. Andreyev, is connected with phase change which occurs during thermal decomposition of perchlorate at  $240^\circ\text{C}$ . This suggestion, however, requires experimental verification.

Author thanks K. K. Andreyev for valuable advice.

Institute of Chemical Physics  
of Academy of Sciences USSR.

Submitted  
7 February 1963

#### Literature

1. R. Friedman, R. G. Nugent, K. E. Rumbel, and Scurlock. Deflagration of Ammonium Perchlorate. VI Symposium (International) on Combustion, 1957, 612.

2. A. P. Glazkova and I. A. Tereshkin. On combustion rate of explosives as a function of pressure, Zh. Fiz. khim., 1961, 35, No 7, 1622.

ON HEAT EXCHANGE OF MICROTHERMOCOUPLES UNDER CONDITIONS OF  
COMBUSTION OF CONDENSED SUBSTANCES

A. A. Zenin

(Moscow)

For obtaining of temperature distribution during stable combustion of condensed substances, it is possible to apply thin thermocouples. Thermocouples sealed in kernels of burning condensed substance, with rate of its combustion, pass through a zone of variable temperature showing (during ideal heat exchange of thermocouple with the medium) temperature distribution. A similar method is widely used for study of combustion of powders (see [1, 2]), where encasing of thermocouples in kernels is done "by angle". The application of thermocouples of such form can be explained only as insufficient attention to the question of heat exchange of a thermocouple with gas and condensed medium in the process of combustion. It is natural to expect a significant lowering of temperature of thermojunction for thermocouples of such form owing to thermal losses to the ends, due to fact that coefficient of thermal conductance of a metallic thermocouple ( $\lambda_1$ ) exceeds by 2 - 3 order coefficient of thermal conductance of powder ( $\lambda_2$ ) and products of its decomposition ( $\lambda_3$ ). Possible also is distortion of temperature profile due to thermal inertness of thermocouples.

In present work are considered requirements which parameters of thermocouples must satisfy (form, thickness, etc.) to ensure minimum of distortion of obtained temperature profile. For that, initially we studied heat exchange of thermocouple with condensed and gas medium under conditions similar to conditions of measurements of temperature in wave of combustion; then, errors of thermocouple measurements are estimated. In work it will be shown that sealing of thermocouples "by angle" can indeed lead to large errors in temperature and serious distortion of form of temperature profile.

### Designations

$\lambda_1$ - coefficient of thermal conduction of gas phase, $\lambda_2$ - coefficient of thermal conduction of thermocouple. $\lambda_3$ - coefficient of thermal conduction of condensed phase $\alpha$ - coefficient of heat emission $c_2$ - specific thermal capacity of thermocouple $c_3$ - specific thermal capacity of powder $h$ - thickness of ribbon thermocouple $\underline{l}$ - size of shoulder of thermocouple $\rho_1$ - density of gas phase $\rho_2$ - density of thermocouples $\rho_3$ - density of powder $\tau_0$ - time constant of thermocouple in gas phase of burning, condensed substance $\tau_m$ - time constant during ideal heat exchange (very large $\alpha$ ) $a_1$ - coefficient of thermal diffusivity of gas phase $a_2$ - coefficient of thermal diffusivity of thermocouple $a_3$ - coefficient of thermal diffusivity of powder	$T_*$ - temperature of combustion $T_2$ - temperature of thermojunction $T_0$ - initial temperature of powder and thermocouple $T_3$ - surface temperature of burning powder $u_1$ - outflow velocity of gas from powder $u_2$ - rate of motion of thermocouple (combustion rate of powder) $H$ - deflection of mid portion of thermocouple shoulder $E$ - young modulus of thermocouple ribbon $I$ - moment of inertia of thermocouple ribbon $p$ - aerodynamic pressure $b$ - width of thermocouple ribbon $\mu_1$ - viscosity of gas $x$ - distance from temperature of combustion to measured temperature $y$ - distance through thickness of thermocouple from center of ribbon $B$ - Biot criterion $N$ - Nusselt number $R$ - Reynold's number
--	---

For obtaining of temperature profile is suggested (see also [3]) thermocouple  $\Pi$ -shaped. Presence of section, parallel to isotherms, called "shoulder," will decrease lowering of temperature of thermojunction from thermal loss to ends. Below will be shown that it is possible to select size of should  $\underline{l}$  so that error owing to heat transfer to ends will become small, and thermocouple will remain still rigid (deflection of middle part of shoulder will be slight). Investigation of heat exchange of thermocouples of  $\Pi$ -shaped form has sufficiently general character: at  $\underline{l} = 0$  we obtain a thermocouple "by angle," at  $\underline{l} = \infty$  - plane thermocouple (parallel to isotherms). Numerical calculations and quantitative results of experiments are given for ribbon thermocouples of alloys of tungsten and rhenium (95% W + 5% Re to 80% W + 20% Re) with thickness  $h = 7\mu$  and  $h = 3.5\mu$  and width  $b = 20 h$ .

At first, let us consider heat exchange of  $\Pi$ -shaped, ribbon thermocouples

in gas phase and calculate temperature errors owing to thermal inertness of thermocouples and thermal loss to their ends. We will also show that thermal inertness of thermocouples covered by a layer of melted borax is no higher than for those not covered by borax (the same total thickness). Then, let us consider heat exchange of a thermocouple with the condensed medium and determine understating of temperature owing to thermal inertness of thermocouple and thermal loss to its ends.

The problem of temperature distribution on length of thin H-shaped thermocouple during its passage with constant speed through front of flame with exponential growth of temperature was considered earlier [3]. In cited work, as in given, exponential rise of temperature was selected for simplicity, and also because actual zone of variable temperature is wider due to existence of several regions of heat release. Errors determined by us coupled with understating of temperature of thermojunction, will be maximum. In order to use obtained solution, we will experimentally determine coefficients of heat radiation  $\alpha$  of ribbon thermocouples. For a heated thermocouple moving with known speed, by rate of cooling we find its time constant  $\tau_c$  and then calculate  $\alpha$  by relationship which can be obtained from heat-conduction equation for a thin plate. If suddenly transfixed into a medium with different temperature (if criterion Biot  $B = \alpha h / 2\lambda_s \ll 1$ ; for our thermocouples  $B = 10^{-4}$  to  $10^{-5}$ )

$$\tau_c = \frac{c_2 \rho_2 h}{2\gamma_0}$$

Here  $c_2 \rho_2$  - volumetric heat capacity of thermocouple (for wire of radius  $r$  in this formula  $h$  is replaced by value of  $r$ ).

Diagram of experiment is shown in Fig. 1. Thermocouple 4 was braced on two rods welded to rings located on opposite sides of revolving disk 2, from which thermo emf is removed by brushes 3 and passes through preamplifier 6 to loop oscillograph 7. Thermocouple is heated while passing through a thin (diameter 1 to 2 cm) stream of hot air (temperature 500°C) and is cooled in air of room

temperature. Length of path of cooling 1 m. Blast velocities are high (5 to 15 m/sec), and therefore transition from hot gas to cold is practically instantaneous.

Results of experiments for flat, ribbon thermocouples are given in the form of dependence of Nusselt number  $N = \alpha h / \lambda_1$  on Reynolds criterion  $R = u_1 \rho_1 h / \mu_1$  in Fig. 2. Values of parameters entering into criteria were taken for air of room temperature ( $T_0 = 25^\circ \text{C}$ )

$$\rho_1 = 1.293 \cdot 10^{-3} \text{ g/cm}^3, \mu_1 = 1.81 \cdot 10^{-4} \text{ g/cm} \cdot \text{sec}, \lambda_1 = 0.6 \cdot 10^{-4} \text{ cal/cm} \cdot \text{sec} \cdot \text{deg}$$

For obtaining temperature profile, most expedient was the application  $\Pi$ -shaped and M-shaped thermocouples. Therefore, following series of experiments was conducted with them, and results are plotted in the same figure. Obviously, within limits of scattering of experimental data, form of thermocouple does not affect magnitude of  $\alpha$ .

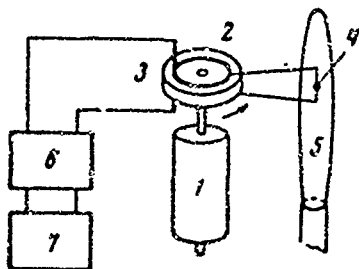


Fig. 1. Diagram of experiment for determination of coefficients of heat emission: 1 - electric motor, 2 - revolving disk, 3 - brushes, 4 - thermocouple, 5 - stream hot air, 6 - preamplifier, 7 - loop oscillograph.

Obtained criterial bond  $N = f(R)$  was used for calculation of coefficients of heat emission of mentioned thermocouples under conditions of burning of nitroglycerine powder H depending upon its combustion rate. Calculations were made for average temperature  $1000^\circ \text{C}$  values of parameters

$$\mu_1 = 4 \cdot 10^{-4} \text{ g/cm sec}, \lambda_1 = 3.5 \cdot 10^{-4} \text{ cal/cm} \cdot \text{sec} \cdot \text{deg}$$

As an example we point out that for thermocouple  $h = 3.5 \mu$  at pressure 20 atm (combustion rate of powder  $u_2 = 0.34 \text{ cm/sec}$ )  $\tau_0 = 0.6 \text{ millisecond}$ ,  $\alpha = 0.1114 \text{ cal/cm}^2 \times \text{sec} \times \text{deg}$  at pressure 150 atm ( $u_2 = 1.2 \text{ cm/sec}$ )  $\tau_0 = 0.22 \text{ millisecond}$ ,  $\alpha = 0.307 \text{ cal/cm}^2 \times \text{sec} \times \text{deg}$ .

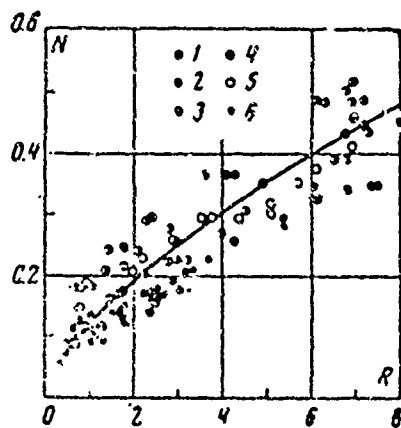


Fig. 2. Critical function  $N = f(R)$  for various ribbon thermocouples: 1 - flat thermocouple  $h = 7\mu$ ; 2 - flat thermocouple  $h = 3.5\mu$ ; 3 - flat thermocouple  $h = 7\mu$ , covered by borax layer  $\sim 7\mu$  (during processing of data, it was considered that  $h_{ef} = 10\mu$ ); 4 - flat thermocouple  $h = 3.5\mu$ , covered by borax layer  $\sim 3\mu$  (during processing of data, it was considered that  $h_{ef} = 5\mu$ ); 5 -  $\Pi$ -shaped thermocouple  $h = 7\mu$ ; 6 - M-shaped thermocouple  $h = 7\mu$ .

Table 1.

(a) $u_2$ , cm/sec.	0.2		0.5		1.0		1.5	
	a	b	a	b	a	b	a	b
$h = 7\mu, l = 1.2\text{ mm}$ $h = 3.5\mu, l = 0.4\text{ mm}$	4.5%	10%	19%	6.5%	43%	4.2%	58%	3%
	0.7%	6.8%	3.5%	3%	11.5%	1%	18%	0.4%

KEY: (a)  $u_2$  cm/sec; (b) Form of thermal losses.

Calculated values of  $a$  are used for calculation of relative understating of temperature by  $\Pi$ -shaped thermocouples in gas phase by the formula work [3].

Results of calculation are given in Table 1, where  $a$  - due to thermal inertness of thermocouples,  $b$  - from thermal loss to ends.

Increase of error due to thermal inertness of thermocouples with increase of combustion rate is obvious. Decrease of error due to heat losses to ends is coupled with decrease of time of stay of thermocouple in zone of variable temperature.

If one were to put  $\underline{l} = 0$  (thermocouple by angle), then by the formula of work [3] and calculated values of  $\alpha$  it is simple to receive that temperatures measured by thermocouple of temperature and temperature gradients for taken thermocouples and speed range will be approximately 10 times less than actual temperatures due to thermal loss to ends of thermocouples. Thus, thermocouple method, used in works [1, 2], cannot be considered acceptable, and results of measurements require check.

During use of thermocouples in zones of chemical reactions in gas phase, catalytic effect is possible on the surface of a metallic thermocouple. For its removal, thermocouple is covered by layer of melted borax. Investigation of thermoinertial properties of such thermocouples presents interest. Ribbon thermocouples  $h = 7\mu$  and  $h = 3.5\mu$  were covered by layer of melted borax: first layer with maximum thickness at center of ribbon  $\sim 7\mu$ , second  $\sim 3\mu$  (average thicknesses  $20\mu$  and  $10\mu$  accordingly) Results on heat radiation received by described method in criterial view are presented also in Fig. 2, and, in order to combine them with previously obtained dependence  $N = f(R)$  for bare thermocouples, it was assumed that first thermocouple has thickness  $10\mu$ , second  $5\mu$ . Thus, thermal inertness of thermocouples covered with borax turns out to be even less than thermal inertness of an uncovered thermocouple the same average thickness. This result is not strange, in spite of the fact that thermal conductance of borax is three orders less than thermal conductance of thermocouples. Actually, minimum time constant (during ideal heat exchange, internal problem of thermal conductance) our thermocouples is equal to

$$\tau_m = \frac{h^2}{\alpha \lambda^2} = 10^{-7} - 10^{-8} \text{ sec}$$

i.e., four orders less than  $\tau_{\infty}$ . This appraisal shows how strongly the thermal boundary layer on thermocouple determines thermal inertness of thin metallic thermocouples under the considered conditions. Its determining role is true also for poor conductors of heat (glass, borax) having dimensions of

taken thermocouples, since problem of thermal conductance remains external ( $B \sim 10^{-2}$ ). Thermal inertness of such bodies will be determined by their volumetric heat capacity  $c_p$  and not by thermal conductance. But  $c_p$  of borax is approximately 1.5 times less than for metal of thermocouple which explains, experimentally, the received decrease of inertness of thermocouples covered with borax as compared to inertness of bare thermocouples of the same average thickness. Another cause is the decrease of thickness of covering towards edge of ribbon.

We note also that calculation for accurate solution of problem of thermal conductance about temperature distribution by thickness of this flat thermocouple passing front of exponentially rising temperature, having form\*

$$\frac{T_1 - T_0}{(T_0 - T_0) e^{-u_1 x_1}} = \frac{\text{ch}(zy)}{\text{ch}(l/z \cdot h) + (\lambda_2 / \alpha) \text{sh}(l/z \cdot h)} \quad \left( z = \sqrt{\frac{u_1 u_2}{a_1 a_2}} \right)$$

shows practical independence of temperature change in time from coefficient of thermal conductance of thermocouple in wide range of change  $\lambda_2$  ( $\lambda_2 = 1$  to  $10^{-3}$  cal/cm · sec °C) under the conditions burning of powder H.

Appraisal of thermal losses by means of thermal conductance to ends of thermocouples and thermal inertness of thermocouples in condensed phase will be made by us separately, due to great complexity of problem.

At first, we will determine thermal inertness of flat thermocouples for which there are no losses of heat to ends, and then we will find lowering of temperature of thermojunction owing to thermal losses to ends under conditions when influence of thermal inertness of thermocouples is excluded. Estimates of understating of temperature of thermojunction obtained for each type of thermal loss can be integrated if these errors are small. This region of errors and conditions leading to small errors will also present interest.

In condensed phase, heat exchange with thermocouple is carried out by

---

\*A. A. Zenin. Study of temperature distribution during combustion of condensed substances. Dissertation, Moscow, 1962.

thermal conductance. Let us consider thermal inertness of thin, flat thermocouples. Difference in temperature of thermocouple and an adjacent condensed substance located in zone of heating can be caused only by large volumetric heat capacity of the thermocouple. Problem of heating of thermocouple in condensed phase under certain simplifying assumptions was considered earlier.\* Solution for maximum relative error has form

$$\frac{T_2 - T_0}{T_0 - T_0} = 1 - \frac{2}{1 - q} \frac{u_2 h q}{\sqrt{\pi a_2 a_3}} \left( 1 - \frac{c_2 \rho_2}{c_1 \rho_1} \right)$$

where

$$q = \frac{1 - \delta}{1 + \delta}, \quad \delta = \frac{\lambda_2}{\lambda_1} \sqrt{\frac{a_1}{a_2}}$$

In Table 2 are given magnitudes of maximum relative error in temperature owing to thermal inertness of thermocouples, calculated by this equation as

functions of burning rate of powder H.

Table 2.

h	u, cm/sec			
	0.2	0.5	1.0	1.5
7μ	0.8%	2%	4%	6%
3.5μ	0.3%	0.8%	1.6%	2.4%

Relative errors in temperature grow

proportionally to thickness of thermocouple

and burning rate. In absolute magnitude,

relative errors owing to thermal inertness in condensed phase are significantly less than in gas.

During appraisal of heat losses to ends of thermocouples, we will use thermal modeling. Average number of parameters determining heat exchange of thermocouple and condensed phase was six: thermal diffusivity of substance ( $a_3 \text{ cm}^2/\text{sec}$ ) and of thermocouple ( $a_2 \text{ cm}^2/\text{sec}$ ), their volumetric heat capacities ( $c_3 \rho_3, \text{ cal/cm}^3 \text{ }^\circ\text{C}$  and  $c_2 \rho_2, \text{ cal/cm}^3 \text{ }^\circ\text{C}$ ), thickness of thermocouple  $h$  cm and size of shoulder  $\underline{1}$  cm. Of these quantities, three are independent:  $c_3 \rho_3$ , (or  $c_2 \rho_2$ ),  $a_3$  (or  $a_2$ ) and  $\underline{1}$  (or  $h$ ).

According to II-theorem of theory, similar unknown function (in our case, dimensionless temperature of thermojunction) should depend on three dimensionless

\*A. A. Zenin. Study of temperature distribution during combustion of condensed substance. Dissertation, Moscow, 1962.

criteria

$$\frac{r_3 \rho_3}{c_3 \rho_3}, \frac{a_3}{a_2}, \frac{l}{h}$$

Since in model experiments substances with those some thermal coefficients were used. The aim was detecting of form of function F

$$\frac{T_2}{T_s} = F\left(\frac{l}{h}\right)$$

where  $T_2$  - temperature of junction,  $T_s$  - temperature of medium (surface).

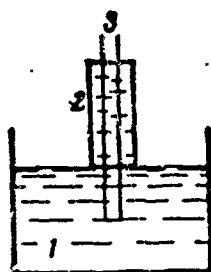


Fig. 3. Diagram of experiment for determination of thermal losses to ends of thermocouples in condensed phase: 1 - heated glycerine, 2 - glass, 3 - thermocouple.

To accurately reproduce conditions of heating of thermocouples in condensed substance during combustion is very difficult, therefore, for simplification it was considered that in heated zone is only the shoulder of thermocouple. Under actual conditions, part of ends directly adjacent to shoulder is in heated zone.

Therefore, model experiments will give a superficial appraisal of heat losses. This simplification leads to independence of results from regime of burning (for example, rate) and in essence was allowed for by us when rate in a number of determining parameters was not considered. Thus, is considered stationary part of the complicated problem of heat exchange (thermal inertness was considered earlier). Therefore, accepted scheme of experiments (constant temperature of heated medium) is permissible.

For experiments were used ribbon model thermocouples of copper-constantan of following dimensions:  $h = 0.05$  mm,  $0.5$  mm,  $0.7$  mm,  $2.0$  mm, and manganin-constantan  $h = 0.2$  mm,  $0.6$  mm,  $1.2$  mm. As medium was taken glycerine, similar in its thermal properties to many condensed substances (including powder H). Model thermocouple was sealed in plexiglas sleeve, in which there was glycerine at a temperature of  $50^\circ\text{C}$ , after which part of thermocouple protruding from bottom of sleeve was submerged in glycerine heated to  $250^\circ\text{C}$ . Thermocouples could

withdraw from bottom of sleeve. Process of heating of thermocouple was recorded on potentiometer EPP-09 (Fig. 3). Aim of measurements was determination of established temperatures of thermojunction. Temperature of fall everywhere was 300°C. Results of experiments are presented in Figs. 4 and 5, from which it is clear that there is a significant understating of temperature of medium at small sizes of shoulder, especially sharply developed for better heat-conducting thermocouple of copper-constantan.

Results can be described by formulas

$$\frac{T_1}{T_1 - T_0} = 0.008 \left(\frac{l}{h}\right)^2 \text{ for Fig. 4}$$

$$\frac{T_1}{T_1 - T_0} = 0.320 \left(\frac{l}{h}\right)^{1.5} \text{ for Fig. 5}$$

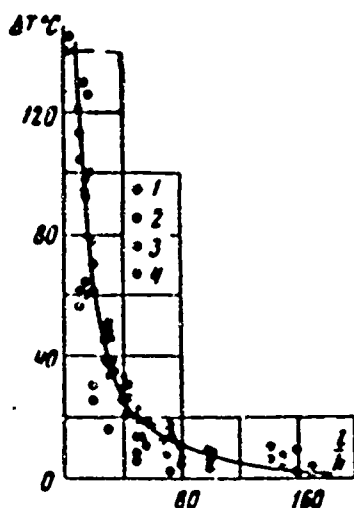


Fig. 4. Understating of temperature by thermocouple of copper-constantan due to thermal losses to end as a function of dimensionless depth of submersion: 1 -  $h = 0.05$  mm, 2 -  $h = 0.5$  mm, 3 -  $h = 0.7$  mm, 4 -  $h = 2.0$  mm.

Experiments with thermocouples of two indicated types differ by thermal conductance of thermocouples. Therefore, results can be combined if we consider coefficient of thermal conductance (true, it must be kept in mind that  $\lambda$  changed only at one electrode, and therefore the formula is tentative)

$$\frac{T_1 - T_0}{T_1 - T_0} = \frac{1}{1 + 135 \lambda_1^{1/2} (h/l)^2}$$

If we set relative error at 2%, we obtain following formula for size of shoulder of thermocouple.

$$l = 200 \sqrt{\lambda_1^2} \left( (c \mu, h \text{ cm}, \lambda_2 \text{ cal/cm} \cdot \text{sec} \cdot \text{deg}) \right)$$

As example we indicate that at  $h = 5 \mu$  for copper  $l/2 \underline{l} = 500 \mu$ , manganin and constantan  $l/2 \underline{l} = 80 \mu$ , for tungsten and rhenium  $l/2 \underline{l} = 200 \mu$ .

Thus, due to large losses of heat to ends, necessity of  $\Pi$ -shaped form of thermocouple is evident. However, for thermocouple of such form, there is

the possibility of deflection of central part of shoulder under action of gas flow, especially in first moment escape to gas phase. We will show that it is possible to select size of shoulder so that at its previously obtained dimensions (from considerations of smallness thermal losses to ends) deflection of shoulder is small.

Superficial estimate of dynamic deflection in center of shoulder, i.e., in place of thermojunction, assuming hinged joining of ends of shoulder with ends of thermocouple (obviously, rigid connection prevents deflection of shoulder), is possible by the formula (see [4])

$$H = \frac{5}{192} \frac{pb^3}{EI} \quad \left( p = \frac{64}{\pi R} \frac{\rho_1 u_1^2}{2}, R = \frac{\rho_1 u_1 l}{\mu_1} \right)$$

where H - amount of deflection, E - Young's modulus, I - moment of inertia, p - aerodynamic pressure [5], and R - Reynold's number for shoulder. Taking ratio  $b = 20 \underline{l}$ , we can find bond between h and  $\underline{l}$  during displacement of central part of thermocouple, equal to thickness of thermocouple ( $H = h$ ).

We obtain equation

$$\underline{l}^3 = 0.05 (\mu_1 / E) \mu_1^2,$$

where  $\mu_1$  - viscosity of gas, or for conditions of burning of powder H (pressure 5 to 150 atm [tech]),

$$\mu_1 = 10^{12} \text{ to } 10^{14} \text{ N}^2.$$

One is easily convinced that opposite requirements of small thermal loss to ends of thermocouple and its sufficient rigidity are compatible both for gas and for condensed phases which allows application of  $\Pi$  - shaped thermocouples.

Let us note that magnitudes of  $\underline{l}$

in Table 1 are selected in such a way as to satisfy requirements of rigidity

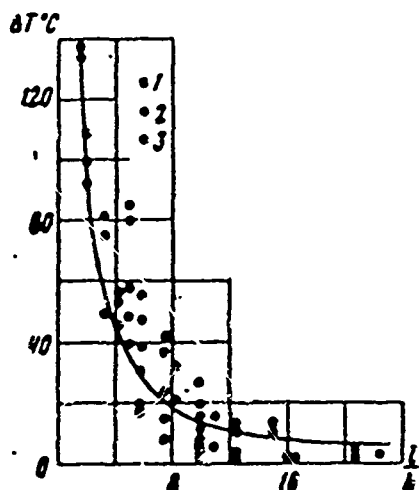


Fig. 5. Understating of temperature by thermocouple of manganin-constantan due to thermal loss to ends as function of dimensionless depth of submersion: 1 -  $h = 0.2$  mm, 2 -  $h = 0.6$  mm, 3 -  $h = 1.2$  mm.

and smallness of thermal losses to ends.

Comparing requirements presented to thermocouples for unerring recording of temperature distribution in gas and condensed phases, we arrive at conclusion that requirements in gas phase are more strict and if they are satisfied, temperature distributions in condensed phase will be also unerring.

Absence of influence of thermal losses to ends of thermocouples on their readings in condensed and gas phases for selected sizes of shoulder was checked experimentally with the help of M - shaped thermocouples for which thermal losses to ends change sign. Therefore, if thermal losses influence, then temperature profiles obtained by these thermocouples and usual  $\Pi$  - shaped must differ. Experiments showed that within limits usual scattering distinction is not observed.

Also observed experimentally was influence of absence of shoulder for a thermocouple by means of comparison of temperature profiles obtained by usual  $\Pi$  -shaped thermocouples and thermocouples with angle. In Fig. 6 are given typical recordings by these two forms of thermocouples (powder H, pressure 20 atm [tech], thermocouple  $\phi$  30  $\mu$ ) illustrating well the strong distortion of temperature distribution due to thermal loss to ends for thermocouples "by angle."

Approximately the same understating of temperature gradient can be obtained by calculating means presented in present work.

It is necessary to consider that distortion of temperature profile obtained by thermocouples sealed "by angle" will be connected also with disturbance of

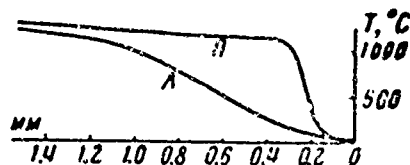


Fig. 6. Temperature profiles of H-powder at pressure of 20 atm [tech] obtained by thermocouples  $\phi$  30  $\mu$  of various form ( $\Pi$  -shaped and "by angle").

one-dimensionalness of process of burning of powder (in particular, with distending of surface of powder at output of thermocouple to gas phase, inasmuch as layer of condensed substance adjacent to thermojunction will

start to decompose only if temperature of thermojunction is near to temperature

of surface).

In conclusion we indicate the receipt of temperature profile with the help of thermocouples covered by thin borax layer. For nitroglycerine powder H, temperatures profiles received by these thermocouples ( $h = 3.5 \mu$ , layer of borax  $\sim 3 \mu$ ) to  $\sim 1400^\circ\text{C}$  (boiling point of borax) are within limits of usual scattering of experimental data which indicates absence of noticeable catalytic effect for our thermocouples.

The author thanks A. A. Koval'skiy for organization of the work and valuable remarks during discussion of results.

Submitted  
15 April 1963

#### Literature

1. R. Klein, M. Mentser, G. Elbe, and B. Lewis. Determination of the Thermal Structure of a Combustion Wave by Fine Thermocouples, *J. Phys. Chem.*, 1950, vol. 54, No 4, p. 877.
2. C. A. Heller and A. S. Gordon. Structure of the Gas Phase Combustion Region of a Solid Double Bas Propellant, *J. Phys. Chem.*, 1955, vol. 59, No 3, p. 773.
3. A. A. Zenin. On errors of thermocouples passing through flame. *Inzh, fiz. zh.*, 1962, No 5.
4. N. M. Belyayev. Resistance of materials, Fizmatgiz, 1962.
5. V. L. Aleksandrov. Technical hydrodynamics, Gostekhizdat, M. - L., 1946.

DISPERSION AND ACCIDENTAL ERROR OF MEASUREMENT OF TEMPERATURE OF  
LOCALLY ISOTROPIC TURBULENT FLOW

Yu. L. Rozenshmok

(Leningrad)

Process of measurement of temperature of nonisothermal flow of gas or liquid by contact method is accompanied by appearance of accidental error determined by statistical character of turbulent pulsation of temperature in flow and by dynamic characteristics of data unit. Appraisal of accidental error of measurement of temperature of air in turbulent atmosphere by linear thermal receiver was conducted in [1]. Here, resultant conclusion in [1] were based on approximations of transient response of thermometer of exponential function of time. Meanwhile, it is known that such approximation has very rough character and is valid only in case of equality of average temperature at surface of thermometer with its average volumetric temperature, which corresponds to application as thermometric body of material with infinite thermal conductivity. In general case this condition, obviously, does not have place, especially for high frequencies of energy spectrum of turbulence during intense heat radiation, and also for thermometers of low thermal conductance and not too small a radius.

Let us consider the problem of determination of accidental error of measurement of temperature of locally isotropic turbulent flow without essential

limitations.

Process of heat transfer in a thermometer is described by heat-conduction equation

$$\frac{\partial T^*}{\partial t} = a \nabla^2 T^* \quad (1)$$

with boundary conditions on surface of body

$$-\nabla T^*|_s + \frac{\alpha}{\lambda} (\theta - T^*) = 0 \quad (2)$$

and initial condition

$$T^*(x, y, z, 0) = 0 \quad (3)$$

Here  $T^*$  - temperature of body;  $\lambda$ ,  $a$  - coefficients of thermal conductance and thermal diffusivity of body;  $\alpha$  - coefficient of heat exchange;  $\theta$  - ambient temperature.

Applying operational calculus to problem, we obtain expression for sought temperature  $T^*(x, y, z, t)$  in the form of Duhamel integral

$$T^*(x, y, z, t) = \frac{\partial}{\partial t} \int_0^t u^*(x, y, z, \tau) \theta(t - \tau) d\tau \quad (4)$$

Here  $u^*(x, y, z, t)$  represents solution of problem when ambient temperature is described by the Heavyside function (of unit force).

Relationship (4) can be represented in following equivalent form with regard to (3)

$$T^*(x, y, z, t) = \int_0^t G^*(x, y, z, \tau) \theta(t - \tau) d\tau \quad (5)$$

where  $G^*(x, y, z, t)$  - local pulse transient function. For quasi-stationary regime, upper limit of integral can be taken as equal to infinity.

Since the majority of applied data units of temperature (thermocouples, thermometers of resistance etc.) will covert to a useful signal not local, but average volumetric value of temperature, it is necessary to average  $T^*(V)$  by volume of body.

$$T(t) = \frac{1}{V} \int_0^\infty \int_V G^*(V, \tau) \theta(t - \tau) d\tau dV = \int_0^\infty G(\tau) \theta(t - \tau) d\tau$$

$$\left[ G(\tau) = \frac{1}{V} \int_V G^*(V, \tau) dV \right] \quad (6)$$

Averaging both parts of (6) by time, when  $\theta(t)$  represents stationary random function of time, we find that mean value of temperature of medium and thermometer coincide in accuracy

$$\begin{aligned} \langle T(t) \rangle &= \langle \theta(t - \tau) \rangle \int_0^{\infty} G(\tau) d\tau = \\ &= \langle \theta(t) \rangle \frac{1}{V} \int_V (u^*(x, y, z, \infty) - u^*(x, y, z, 0)) dV = \langle \theta(t) \rangle \end{aligned} \quad (7)$$

since  $u^*(x, y, z, \infty) = 1$ ,  $u^*(x, y, z, 0) = 0$ . Thus, if we disregard systematic errors of measurement of temperature caused by pulsation of heat radiation with time [2], the systematic error of measurement of temperature of turbulent flow by linear thermometer is absent, in accordance with which mean square error is an accidental error of indications of instrument.

Considering

$$T(t) = T_0 + T'(t), \quad \theta(t) = \theta_0 + \theta'(t) \quad (8)$$

where  $T_0$  and  $\theta_0$  - constant constituents,  $T'$  and  $\theta'$  - pulsational parts, and considering that  $T_0 = \theta_0$ . we obtain formula for conversion of correlated function field of temperature  $K_0$  by linear thermal receiver

$$K_T(\tau) = \langle T'(t) T'(t + \tau) \rangle = \int_0^{\infty} \int_0^{\infty} G(\tau_1) G(\tau_2) K_0(\tau + \tau_2 - \tau_1) d\tau_1 d\tau_2 \quad (9)$$

Expressing correlated function through temporal structural function field of temperatures  $D_0$ . we obtain analogous formula for relationship structural functions  $D_0$  and  $D_T$  at entrance and output of thermometer

$$D_T(\tau) = 2(\sigma_T^2 - \sigma_0^2) + \int_0^{\infty} \int_0^{\infty} G(\tau_1) G(\tau_2) D_0(\tau + \tau_2 - \tau_1) d\tau_1 d\tau_2 \quad (10)$$

Here  $\sigma_T^2$  - dispersion of indications of thermometer,  $\sigma_0^2$  - average square of pulsation of temperature of flow

$$D_0(\tau) = \langle [\theta'(t + \tau) - \theta'(t)]^2 \rangle$$

From (9) or (10) at  $\tau = 0$  we find expression for dispersion and root mean square error of indications of thermometer through correlated or structural function of field of temperatures and pulse transient response of thermometer,

determined for bodies of simple form by analytic means

$$\sigma_T^2 = \sigma_\theta^2 - \frac{1}{2} \int_0^\infty \int_0^\infty G(\tau_1) G(\tau_2) D_\theta(\tau_2 - \tau_1) d\tau_1 d\tau_2 \quad (11)$$

Common integral of Fourier equation (1) with conditions (2) and (3) at  $\theta = 1$  in accordance with Boussinesq theorem [3] is expressed by formula

$$u^*(x, y, z, t) = 1 - \sum_{j=1}^{\infty} A_j U_j(x, y, z) e^{-\gamma_j t} \quad (12)$$

Here  $A_j$  - constants (initial thermal amplitudes),  $U_j$  - eigenfunctions of problem satisfying Helmholtz equation

$$\nabla^2 U_j + m_j U_j = 0 \quad (m_j = \gamma_j / a)$$

$m_j$  = eigenvalues. Eigenfunctions  $U_j$  satisfy boundary condition (2) of mixed type on surface  $S$  limiting considered body. Accordingly

$$G^*(x, y, z, t) = \sum_j A_j U_j \gamma_j e^{-\gamma_j t} \quad (13)$$

From (11) and (13) we obtain

$$\sigma_T^2 = \sigma_\theta^2 - \frac{1}{2} \sum_{j=1}^{\infty} \sum_{k=1}^{\infty} A_j A_k \gamma_j \gamma_k \Psi_j \Psi_{jk} \quad (14)$$

where

$$\begin{aligned} \Psi_j &= \frac{1}{V} \int_V U_j(V) dV, \quad \Psi_{jk} = \int_0^\infty \int_0^\infty \exp[-(\gamma_j \tau_1 + \gamma_k \tau_2)] D_\theta(\tau_2 - \tau_1) d\tau_1 d\tau_2 = \\ &= \frac{1}{\gamma_j + \gamma_k} \left[ \int_0^\infty e^{-\gamma_k \tau_1} D_\theta(\tau_1) d\tau_1 + \int_0^\infty e^{-\gamma_j \tau_2} D_\theta(\tau_2) d\tau_2 \right] \end{aligned} \quad (15)$$

In case of locally isotropic turbulence for temporal structural functions at small  $\tau$  can be taken exponential approximation of Kolmogorov - Obukhov [4-7]

$$D_\theta(\tau) = C\tau^\beta \quad (16)$$

where  $C$  and  $\beta$  - quantities independent of  $\tau$ . Hence

$$\Psi_{jk} = \frac{C\Gamma(1+\beta)}{(\gamma_j + \gamma_k)} (\gamma_j^{-(1+\beta)} + \gamma_k^{-(1+\beta)}) \quad (17)$$

Equivalent form of (17) during calculation of (16) is

$$\Psi_{jk} = \frac{\Gamma(1+\beta)}{(\gamma_j + \gamma_k)} [\gamma_j^{-1} D_0(\gamma_j^{-1}) + \gamma_k^{-1} D_0(\gamma_k^{-1})] \quad (18)$$

Putting (17) or (18) in (14) and changing indices of integration in resultant second double sum, will find

$$\sigma_T^2 = \sigma_e^2 - \Gamma(1+\beta) \sum_j \sum_k A_j A_k \frac{\gamma_j \gamma_k}{\gamma_j + \gamma_k} \varphi_j \varphi_k D_0(\gamma_j^{-1}) \quad (19)$$

We apply obtained expression (19) to determination of dispersion and accidental error of measurement of temperature of locally isotropic turbulent flow by thermometric bodies having plane, cylindrical, and spherical form (one-dimensional problem). Using certain results obtained in analytic theory of thermal conductance [9], for all three cases, after simple conversions, we obtain

$$\sigma_T^{(v)2} = \sigma_e^2 - v \Gamma(1+\beta) \sum_{j=1}^{\infty} F_j^{(v)} W_j^{(v)} D_0\left(\frac{1}{\gamma_j^{(v)}}\right) \quad (20)$$

Here  $v = 1, 2, 3$ , for plate, cylinder and sphere accordingly

$$\begin{aligned} \gamma_j^{(v)} &= \frac{\alpha \mu_j^{(v)2}}{R^2}, & F_j^{(1)} &= A_j^{(1)} \varphi_j^{(1)} = \frac{2B^2}{\mu_j^{(1)2} [B^2 + B + \mu_j^{(1)2}]} \\ F_j^{(2)} &= A_j^{(2)} \varphi_j^{(2)} = \frac{4B^2}{\mu_j^{(2)2} [B^2 + \mu_j^{(2)2}]}, & F_j^{(3)} &= A_j^{(3)} \varphi_j^{(3)} = \frac{6B^2}{\mu_j^{(3)2} [B^2 - B + \mu_j^{(3)2}]} \end{aligned} \quad (21)$$

where  $\mu_j^{(1)}, \mu_j^{(2)}$  and  $\mu_j^{(3)}$  - roots of characteristic equations:

$$\operatorname{ctg} \mu_j^{(1)} = \frac{\mu_j^{(1)}}{B}, \quad \frac{J_0(\mu_j^{(2)})}{J_1(\mu_j^{(2)})} = \frac{\mu_j^{(2)}}{B}, \quad \operatorname{tg} \mu_j^{(3)} = \frac{\mu_j^{(3)}}{1-B} \quad (22)$$

$$\begin{aligned} W_j^{(1)} &= \left(\frac{1}{\mu_j^{(1)}}\right)^2 \left(\frac{\operatorname{cth} \mu_j^{(1)}}{\mu_j^{(1)}} + \frac{1}{B}\right)^{-1}, & W_j^{(2)} &= \left(\frac{1}{\mu_j^{(2)}}\right)^2 \left(\frac{1}{\mu_j^{(2)}} \frac{I_0(\mu_j^{(2)})}{I_1(\mu_j^{(2)})} + \frac{1}{B}\right)^{-1} \\ W_j^{(3)} &= \left(\frac{1}{\mu_j^{(3)}}\right)^2 \left(\frac{1}{\mu_j^{(3)} \operatorname{cth} \mu_j^{(3)} - 1} + \frac{1}{B}\right)^{-1} \quad \left(B = \frac{\alpha R}{\lambda}\right) \end{aligned} \quad (23)$$

Here  $J_0$  and  $J_1$  - Bessel functions of first kind,  $I_0$  and  $I_1$  - modified Bessel functions of first kind,  $B$  - Biot criterion,  $R$  - characteristic dimension.

When there is accurate information on quantities  $C$  and  $\beta$ , it is expedient

to use for  $\Psi_{jt}$  expression (17). Here

$$\varepsilon_T^{(\nu)2} = \varepsilon_0^2 - CR^{2\beta} a^{-\beta} Q^{(\nu)}(B) \quad (24)$$

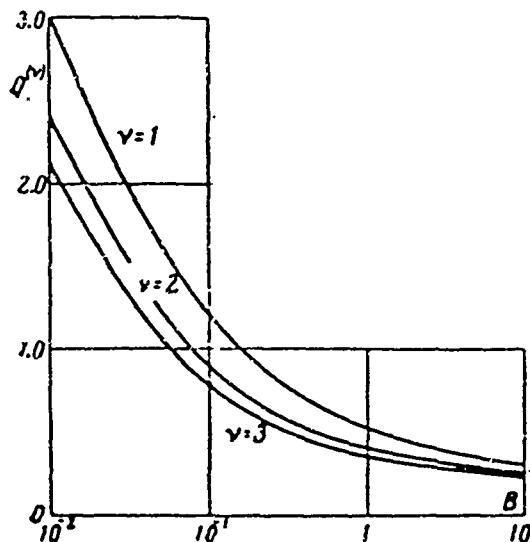
where

$$Q^{(\nu)}(B) = \nu \Gamma(1 + \beta) \sum_{j=1}^{\infty} (\mu_j^{(\nu)})^{-2\beta} F_j^{(\nu)} W_j^{(\nu)} \quad (25)$$

For conditions of atmospheric turbulence in surface layer  $\beta = 0.42$  [1, 8]. Graph of functions of  $Q^{(\nu)}$  for  $\nu = 1, 2, 3$  at  $\beta = 0.42$  is shown in figure.

Formulas (20) and (24) give possibility also to determine mean square error of indications of thermometer, and

$$\varepsilon^{(\nu)} = [\varepsilon_0^2 - \varepsilon_T^{(\nu)2}]^{1/2} = C^{1/2} R^{\beta} a^{-\beta/2} \sqrt{Q^{(\nu)}(B)} \quad (26)$$



representing, as was already indicated, accidental error of measurement of temperature of locally isotropic turbulent flow.

As follows from curves, optimum properties in the sense of minimum of accidental error belongs to the spherical thermal receiver, whereas thermometer-plate has worst properties in this sense. It is necessary to note the

presence of a finite, accidental error not vanishing to zero during infinite heat radiation. In this case pulsations of temperature on surface of thermometer coincide by phase and amplitude with pulsations of temperature in flow. However, as a result of presence of temperature drop through thickness of thermometer, accidental error does not turn into zero as would have occurred during formal application of condition  $B \rightarrow \infty$  to thermometer of infinite thermal conductance.

Function  $\sqrt{Q^{(n)}}(B)$ , and consequently, accidental error  $\epsilon^{(n)}$  change in range  $10^{-1} < B < 10$  by approximately three times. At  $B > 10$ , function  $\sqrt{Q^{(n)}}(B)$  remains constant and equals  $\approx 0.5$ .

Submitted  
26 April 1963.

#### Literature

1. A. M. Yaglom. On calculation of inertia of meteorological instruments. Tr. Geofiz. in-ta AN SSSR, 1954, issue 24.
2. M. A. Kaganov and Yu. L. Rozenshtok. On temperature of bodies in medium with pulsating heat radiation and temperature, PMTF, 1962, No 3.
3. T. V. Boussinesq. Theorie analitique de la chaleur, Paris, 1901.
4. A. N. Kolmogorov. Energy dissipation during locally isotropic turbulence, Reports of Academy of Sciences of USSR, 1941 vol. 32, 19.
5. A. M. Obukhov. On distribution of energy in spectrum of turbulent flow, News of Academy of Sciences of USSR, Ser. geogr. and geo phys., 1941, No. 4-5.
6. A. M. Obukhov. Structure of temperature field in turbulent flow, News of Academy of Sciences of USSR, Ser. geo phys., 1949, 13. No. 1.
7. A. M. Yaglom. On local structure field of temperatures in turbulent flow, Reports of Academy of Sciences of USSR, 1949, vol. 69, No. 6.
8. A. V. Perepelkin. Certain results of investigation of turbulent pulsations of temperature and vertical components of velocity of wind, Izv. AN SSSR, Ser. geofiz, 1957, No. 6.
9. A. V. Lykov. Theory of thermal conductance. Gostekhteorizdat, 1952.

ON ONE NONLINEAR PROBLEM OF THERMAL CONDUCTION

S. I. Anisimov and T. L. Perel'man (Minsk)

In theory of thermal explosion and in a number of questions of theory of thermal conductance [1, 2] is encountered nonlinear equation

$$\frac{\partial T}{\partial t} = \Delta T + q \exp\left(-\frac{E}{T}\right) \quad (1)$$

Source in right side of (1) approximately describes thermal divisions during chemical reaction, and constant E signifies activation energy of reaction.

Let us examine simplest one-dimensional boundary value problem for equation (1)

$$T(\pm l, t) = T_c, \quad T(x, 0) = T_0 \quad (-l < x < l) \quad (2)$$

or the same,

$$T(l, t) = T_c, \quad \frac{\partial T(0, t)}{\partial x} = 0, \quad T(x, 0) = T_0 \quad (3)$$

We will introduce dimensionless variables

$$\xi = \frac{x}{l}, \quad \tau = \frac{at}{l^2}, \quad \theta(\xi, \tau) = \frac{T(x, t) - T_c}{E}, \quad \theta_0 = \frac{T_0 - T_c}{E}, \quad \theta_c = \frac{T_c - T_c}{E}, \quad e = \frac{ql^2}{aE} \quad (4)$$

Let, further,  $G(\xi, \xi'; \tau - \tau')$  - Green's function of heat-conduction equation for unit section. Problem (1) - (3) will be reduced to integral equation

$$\theta(\xi, \tau) = \psi(\xi, \tau) + e \int_0^{\tau} \int_0^1 G(\xi, \xi'; \tau - \tau') \exp \frac{-1}{\theta(\xi', \tau')} d\xi' d\tau' \quad (5)$$

$$\psi(\xi, \tau) = \theta_c - \frac{2}{\pi} (\theta_c - \theta_0) \sum_{n=0}^{\infty} \frac{(-1)^n}{n + 1/2} \exp \left[ -\pi^2 \left( n + \frac{1}{2} \right)^2 \tau \right] \cos \left( n + \frac{1}{2} \right) \pi \xi \quad (6)$$

Green's function has form

$$G(\xi, \xi'; \tau - \tau') = 1/2 [\theta_1(1/2(\xi + \xi'); i\pi(\tau - \tau')) + \theta_2(1/2(\xi - \xi'); i\pi(\tau - \tau'))] \quad (7)$$

Theta functions in right side of (7) are determined by equality [3]

$$\vartheta_2(u, iv) = 2 \sum_{n=0}^{\infty} \exp \left[ -\pi \left( n + \frac{1}{2} \right)^2 v \right] \cos(2n+1)u$$

Let us note that Green's function (7) is symmetric about arguments  $\xi$  and  $\xi'$  and in considered region is nowhere negative.

Equation (5) can be solved by sequential approximations of form

$$\vartheta^{(0)}(\xi, \tau) = \psi(\xi, \tau), \quad \vartheta^{(n+1)}(\xi, \tau) = \psi(\xi, \tau) + \varepsilon \int_0^{\tau} \int_0^1 G(\xi, \xi'; \tau - \tau') \exp \frac{1}{\vartheta^{(n)}(\xi', \tau')} d\xi' d\tau' \quad (8)$$

During solution of boundary value problems analogous to (1) - (3), usually interesting are conditions of existence of such temperature distribution which when  $\tau \rightarrow \infty$  would change to stationary. It is not difficult to show that such distribution exists, if parameter  $\varepsilon$  is sufficiently small. Here, sequence of functions  $\vartheta^{(n)}(\xi, \tau)$  is evenly reduced to solution of integral equation (4). In order to show this, we will compose following expression

$$\begin{aligned} \vartheta^{(n+1)} - \vartheta^{(n)} &= \int_0^{\tau} \int_0^1 G(\xi, \xi'; \tau - \tau') \left( \exp \frac{-1}{\vartheta^{(n)}(\xi', \tau')} - \exp \frac{-1}{\vartheta^{(n+1)}(\xi', \tau')} \right) \times \\ &\times \frac{\vartheta^{(n)}(\xi', \tau') - \vartheta^{(n-1)}(\xi', \tau')}{\vartheta^{(n)}(\xi', \tau') - \vartheta^{(n-1)}(\xi', \tau')} d\xi' d\tau' \end{aligned} \quad (9)$$

Let us note that  $\vartheta^{(n)} - \vartheta^{(n-1)} \geq 0$ , since  $\psi(\xi, \tau) \geq 0$ ,  $G(\xi, \xi'; \tau - \tau') \geq 0$ . We will introduce designation

$$\max(\vartheta^{(n)} - \vartheta^{(n-1)}) = \Delta \lambda_n \geq 0$$

From (9), it follows that

$$M_{n+1} \leq A M_n, \quad A = \max \left\{ \varepsilon \int_0^{\tau} \int_0^1 \frac{G(\xi, \xi'; \tau - \tau')}{\vartheta^{(n)} - \vartheta^{(n-1)}} \left[ \exp \frac{1}{\vartheta^{(n)}} - \exp \frac{-1}{\vartheta^{(n-1)}} \right] \times d\xi' d\tau' \right\}$$

It is easy to check that  $A < 1$ , if  $\varepsilon < \frac{1}{\lambda_n}$ . In this case there exists limiting function of sequence (8), which will be solution of equation (5).

For chemical kinetics, case of  $\varepsilon \ll 1$  is of interest. It is easy to show that in this case inequality for  $\varepsilon$  has form

$$\varepsilon < \frac{1}{\vartheta_m^2} \exp \frac{-1}{\vartheta_m}$$

where  $\theta_m$  - the biggest value in considered region of  $\theta(\xi, \tau)$ .

Let us note that described method of successive approximations indicates the existence of a solution. Applying known theorems of theory of integral equations (see, for example [4]) it is easy to show that equation (5) has at least one solution at any values of parameter  $\varepsilon$ . Meaning of result is that in a certain interval of values, solution will be unique. We will return to this question below during investigation of the stationary problem.

Method of successive approximations allows to receive approximate solutions in certain simple extreme cases. Let us consider, at first, solution during rather long times.

1. We will consider that parameter  $\varepsilon$  is rather small, so that in all times there is a unique solution of equation (5) which can be obtained by iterations of (8). We will calculate  $\theta^{(n)}(\xi, \tau)$  taking, for zero approximation, stationary temperature distribution,  $\theta(\xi, \infty) \equiv \theta(\xi)$  satisfying relationships

$$\frac{d^2\theta(\xi)}{d\xi^2} + \varepsilon \exp\left(-\frac{1}{\theta(\xi)}\right) = 0, \quad \theta(1) = \theta_c, \quad \frac{d\theta(0)}{d\xi} = 0 \quad (10)$$

Solution of problem (10) has form

$$(1 - \xi) \sqrt{2\varepsilon} = \int_{\xi_c}^{\xi} \left[ \int_{\xi}^{\theta_m} \exp \frac{-1}{u} du \right]^{-1/2} d\xi \quad (11)$$

where  $\theta_m$  - the biggest value of function  $\theta(\xi)$  in section  $0 \leq \xi < 1$ , which due to symmetry is attained at  $\xi = 0$ .

Stationary solution of  $\theta(\xi)$  is unique if equation (11) at  $\xi = 0$  is unique for every  $\varepsilon$  value of constant  $\theta_m$ ; here integrals entering in (11) are not expressed in elementary functions. However, general character of dependence  $\theta_m(\varepsilon)$  can be investigated without resorting to numerical integration. It is easy to see, first of all, that equation (11) at  $\xi = 0$  has at least one solution for  $\theta_m$  at any values of  $\varepsilon$ ; indeed, takes place appraisal

$$\sqrt{2\varepsilon} \geq \int_{\xi_c}^{\theta_m} \left[ \int_{\xi}^{\theta_m} \exp \frac{-1}{u} du \right]^{-1/2} d\xi \geq \int_{\xi_c}^{\theta_m} \frac{\exp(1/2\theta_m) d\xi}{\sqrt{\theta_m - \theta_c}} = \sqrt{\theta_m - \theta_c} \exp \frac{1}{2\theta_m} \quad (12)$$

Consequently, values of  $\tau$  can be as large as desired. Let us note that after replacement in work [2]

$$\exp \frac{-1}{\theta} \exp \frac{-1}{\theta_c} \exp \frac{\Delta\theta}{\theta_c^2} \quad (13)$$

solution at sufficiently large  $\tau$  does not exist. This is intelligible because as a result of replacement of (13) in equation (10) instead of bounded function  $\exp(-1/\theta)$  there is an infinitely increasing function of  $\exp(\pi\theta)$ . and known conditions of existence of solution (see, for example, [5]) are unfulfilled.

Expansion of (13) is valid under two conditions;  $\theta_c \ll 1$  and  $\theta_m - \theta_c \ll \theta_c$ . Preserving the first of them and comparing result obtained in [2] with estimate of (12), it is simple to conclude that during fixed  $\theta_c$  function  $\theta(\theta_m)$  has at least two extremes among which is a region of ambiguity of solutions, where every value of  $\tau$  corresponds to more than one (in reality three) values of  $\theta_m$ . More detailed consideration shows that minimum of function  $\theta(\theta_m)$  lies in range of values  $\theta_m \sim 1$ , and also that there is such a critical value  $\theta_c^*$  so that  $\theta_c > \theta_c^*$  solution of stationary problem exists and is unique at all  $\tau$ . These remarks may be of interest in case of reactions with low activation energy.

Taking solution (11) for zero approximation, we obtain value of function  $\theta(\xi, \tau)$  similar to steady state. Result has form

$$\theta(\xi, \tau) = \theta(\xi) + \frac{4}{\pi} \exp\left(-\frac{\pi^2 \tau}{4}\right) \cos \frac{\pi \xi}{2} \left[ \theta_0 - \frac{\pi}{2} \int_0^1 \theta(\xi') \cos \pi \frac{\xi'}{2} d\xi' \right] \quad (15)$$

If in entire region  $\theta(\xi) \ll 1$ , it is possible, using method of steepest descents, to simplify initial integral equation. Omitting calculations, we obtain result

$$\theta(\xi, \tau) = \theta(\xi) - \frac{4}{\pi} \exp\left(-\frac{\pi^2 \tau}{4}\right) \cos \frac{\pi \xi}{2} \left[ \theta_c - \theta_0 + 2 \sqrt{\frac{2\xi}{\pi}} \theta_m \exp\left(-\frac{1}{2\theta_m}\right) \right] \quad (16)$$

Formulas (15) and (16) are true during condition  $\tau > 4/\pi^2$ .

2. Let us consider solution at brief times. In this case for zero approximation it is natural to take initial temperature  $\theta_0$ . Nucleus of integral equation (5) we simplify, using known relationship for Theta functions

$$\theta_1(u, iv) = v^{-1/2} \exp\left(-\frac{\pi u^2}{v}\right) \theta_0\left(\frac{u}{iv}, -\frac{i}{v}\right) \quad (17)$$

Leaving at  $\tau \rightarrow 0$  only main members of Green's function and executing integration we obtain in result

$$\begin{aligned} \theta(\xi, \tau) = & \theta_c + \varepsilon \exp \frac{-1}{\theta_0} \left\{ 1 - \xi^2 + \sqrt{\frac{\tau}{\pi}} \left[ (1 - \xi) \exp \left( -\frac{(1 - \xi)^2}{4\tau} \right) + \right. \right. \\ & \left. \left. + (1 + \xi) \exp \left( -\frac{(1 + \xi)^2}{4\tau} \right) - 2 \exp \frac{-1}{\tau} \right] \right\} + \left\{ \theta_0 - \theta_c + \varepsilon \left[ \frac{(1 - \xi)^2}{2} + \tau \right] \times \right. \\ & \left. \times \exp \frac{-1}{\theta_0} \operatorname{erf} \left( \frac{1 - \xi}{2\sqrt{\tau}} \right) \right\} + \left\{ \theta_0 - \theta_c + \varepsilon \left[ \frac{(1 + \xi)^2}{2} + \tau \right] \exp \frac{-1}{\theta_0} \operatorname{erf} \left( \frac{1 + \xi}{2\sqrt{\tau}} \right) \right\} - \\ & - \left\{ \theta_0 - \theta_c + \varepsilon \exp \frac{-1}{\theta_0} [2 + \tau] \operatorname{erf} \left( \frac{1}{\sqrt{\tau}} \right) \right\} \quad \left( \operatorname{erf}(x) = \frac{2}{\sqrt{\pi}} \int_0^x e^{-t^2} dt \right) \end{aligned} \quad (18)$$

3. Let us consider, at last, case when parameter  $\varepsilon$  is small. Solution in this case can be obtained in the form of series by degrees of  $\varepsilon$ , taking for zero approximation  $\Psi(\xi, \tau)$  (see (5)). Let us note that during  $\varepsilon \rightarrow 0$  difference  $\theta_m - \theta_c \rightarrow 0$ . This allows during sufficiently long times to disregard in (6) second member as compared with first. The same can be done for all times, if  $|\theta_c - \theta_0| \ll \theta_c$ .

In first order of approximation for  $\varepsilon$ , result has form

$$\begin{aligned} \theta(\xi, \tau) = & \Psi(\xi, \tau) + \varepsilon \exp \frac{-1}{\theta_c} \left[ \frac{1 - \xi^2}{2} - \frac{2}{\pi^2} \sum_{n=0}^{\infty} \frac{(-1)^n}{(n + \frac{1}{2})^2} \times \right. \\ & \left. \times \exp \left[ -\pi^2 \left( n + \frac{1}{2} \right)^2 \tau \right] \cos \left( n + \frac{1}{2} \right) \pi \xi \right] \end{aligned} \quad (19)$$

For receipt of highest approximation in corresponding calculations it is convenient to use method of steepest descents, applied above to calculation of expression (16).

4. We will show, in conclusion, that in process of establishment of stationary temperature distribution ( $\varepsilon < \tau_0$ ) temperature in any point monotonely strives during  $\tau \rightarrow \infty$  toward corresponding stationary temperature. Intuitively, this result is sufficiently obvious. For proof, we will formulate difference  $\Delta(\xi, \tau) = \theta(\xi, \tau) - \theta(\xi)$ .

The latter satisfies integral equation

$$\begin{aligned} \Delta(\xi, \tau) = & \Phi(\xi, \tau) + \varepsilon \int_0^{\tau} \int_0^1 G(\xi, \xi'; \tau - \tau') \left[ \exp \frac{1}{\theta(\xi') + \Delta(\xi', \tau')} - \exp \frac{1}{\theta(\xi')} \right] d\xi' d\tau' \quad (20) \\ \Phi = & 2 \sum_{n=0}^{\infty} \left\{ \int_0^1 [\theta_0 - \theta(\xi')] \cos \pi \left( n + \frac{1}{2} \right) \xi' d\xi' \right\} \exp \left[ \pi^2 \left( n + \frac{1}{2} \right)^2 \tau \right] \cos \left( n + \frac{1}{2} \right) \pi \xi \end{aligned}$$

tion,  
To equation (20) we apply method of successive approximations, considering

$$\Delta^{(0)}(\xi, \tau) = \Phi(\xi, \tau)$$

Considering that  $\Phi(\xi, \tau) \leq 0$  (in physically interesting case  $\theta_c > \theta_0$ , when medium is heated with time), and repeating reasonings conducted during proof of existence and singleness of solution of boundary value problem (1) - (2), we find that  $\Delta^{(n)} < 0$  at all  $\tau$  and difference  $\Delta^{(n)} - \Delta^{(n-1)} \rightarrow 0$  during  $\tau \rightarrow \infty$ .

Submitted  
1 June 1963

#### Literature

1. V. N. Kondrat'yev. Kinetics of chemical gas reactions, Pub. House of Academy of Sciences of USSR, 1958.
2. I. A. Frank-Kamenetskiy. Diffusion and heat transfer in chemical kinetics. Izd. AN SSSR, 1947.
3. F. Morse, and G. [Fishbach]. Methods of theoretical physics. II, Vol. 1, 1958.
4. N. S. Smirnov. Introduction to theory of nonlinear integral equations. M.-L., 1936.
5. D. Sansone. Ordinary differential equations, Vol. 2, Moscow, 1953.

ON HEAT EXCHANGE AT CRITICAL POINT OF A BLUNT  
BODY AT SMALL REYNOLDS NUMBERS

I. N. Murzinov

(Moscow)

On basis of analysis of flowing around spheres by hypersonic flow is revealed parameter determining heat exchange at critical point at small Reynolds numbers. Certain results of calculations are given which were approximated by analytic expression depending upon this parameter. Obtained function is compared with experimental data.

Using main assumptions of work [1], equations of momentum and energy in environment of critical point of sphere are written in the form

$$\begin{aligned} (\rho\mu/\sigma)' + 2f/f' - f'^2 + \frac{2b}{\rho} = 0, \quad \left(\frac{\rho\mu}{\sigma} i'\right)' - 2fi' = 0 \\ \left(u = x f'(\eta), \quad r = -\frac{2f(\eta)}{\rho \sqrt{R_\infty}}, \quad r_0 = \sqrt{R_\infty} \int_0^\eta \rho dy, \quad R_\infty = \frac{\rho_\infty V_\infty^2 r_0^2}{\mu_\infty}\right) \end{aligned} \quad (1)$$

Here  $x_{r_0}, y_{r_0}$  - distances along generatrix and on normal to body,  $r_0$  - radius of sphere,  $u V_\infty, v V_\infty, \rho \rho_\infty, \mu \mu_\infty, i V_\infty^2, p \rho_\infty V_\infty^2$  - accordingly constituent velocities on axes  $x$  and  $y$ , density, viscosity, enthalpy, and pressure of gas,  $\rho_\infty, \mu_\infty, V_\infty$  - density, viscosity, and approach stream velocity,  $\sigma$  - Prandtl number, dash signifies differentiation by variable  $\eta$ . Quantity  $b$  determines pressure gradient at critical point of body, so that

$$\frac{\partial p}{\partial x} = -2bx$$

Boundary conditions are condition on body and in shock wave:

$$\begin{aligned} i = i_w, \quad f = f' = 0 \quad \text{at } \eta = 0 \\ i \approx 0.5, \quad f = \frac{\sqrt{R_\infty}}{2}, \quad f' = \frac{1}{r_1} \quad \text{at } \eta = \eta_1 \end{aligned} \quad (2)$$

where  $r_1$  - radius of curvature of shock wave,  $\eta_1$  - unknown quantity characterizing position of shock wave.

At given  $b$  and  $r_1$  are six conditions (2) sufficient for solution of system (1) and determination of  $\eta_1$ .

Considering pressure distribution on sphere to be Newtonian, we can be obtained  $b = (1 - 1/2k)$ , where  $k$  - ratio of densities in direct shock wave. For spherical blunting at low wall temperature, thickness of displacement of boundary layer is small. Therefore, we will consider that magnitude of  $r_1$  will remain the same as during ambient flow around a sphere by inviscid gas. In calculations were used values of  $r_1$  determined by data of [2, 3] as functions of  $k$ .

Product of density by viscosity at constant pressure was considered power function of enthalpy

$$\rho\mu = cT^n \quad (3)$$

Constants  $c$  and  $n$  ( $n \sim 0.3$ ) were determined from results of [4]. Prandtl number in calculations was relied on as constant  $\sigma = 0.72$ .

Calculations showed that last member of first equation of system (1) weakly affects its solution at  $i_w \ll 1$ . Thus, during change of magnitude of  $b$  in interval  $b = 0.5$  to  $1.5$ , calculated heat flow changes by only 2 to 3%.

Therefore, density entering in last member of first equation was approximated by expression  $\rho = (2ki)^{-1}$ . This approximation, practically, is accurate in inviscid region of flow and very weakly affects amount of heat flow.

Equations of (1) and condition of (2) can be converted to form

$$\begin{aligned} (i^{-n}\varphi')' + 2q\varphi' - \varphi^2 + 4bki = 0 \\ \left(\frac{i^{-n}i'}{3}\right)' + 2\varphi i' = 0 \end{aligned} \quad (4)$$

$$\begin{aligned} i = i_w, \quad \varphi = \varphi' = 0 \quad \text{at } \zeta = 0 \\ i \approx 0.5, \quad \varphi = \frac{\sqrt{H_\infty}}{2\sqrt{c}}, \quad \varphi' = \frac{1}{r_1} \quad \text{at } \zeta = \zeta_1 \end{aligned} \quad (5)$$

???)

there

$$i = \sqrt{c} \varphi(\zeta), \quad i = i(\zeta), \quad \zeta = \frac{\eta}{\sqrt{c}}, \quad \zeta_1 = \frac{\eta_1}{\sqrt{c}}$$

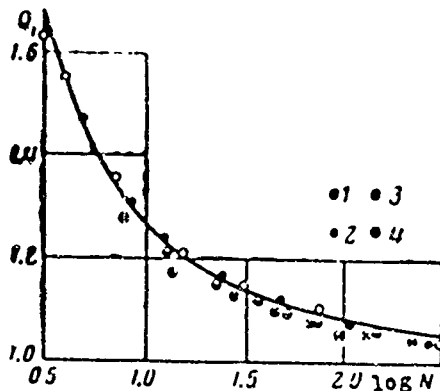


Fig. 1. 1 -  $V_\infty = 11,000$  m/sec,  $k = 0.06$ ; 2 -  $V_\infty = 8,000$  m/sec,  $k = 0.06$ ; 3 -  $V_\infty = 6,000$  m/sec,  $k = 0.07$ ; 4 -  $V_\infty = 4,000$  m/sec,  $k = 0.09$ .

Considering earlier state relationship of weak dependence of heat flow on member coupled with pressure gradient (see Lees [5]), and also fact that at hypersonic speeds  $r_1 \approx 1$  and for strongly cooled wall  $i_w \ll 1$ , from (4) and (5) it follows that unique quantity which determines influence of small Reynolds numbers on heat exchange is value of  $\varphi$  at  $\zeta = \zeta_1$ .

This value with aid of (3) we easily converted to form

$$\varphi = \frac{\sqrt{R_0 k^2} \sqrt{(0.5)^{-n}}}{2} \quad \left( R_0 = \frac{\rho_0 \sqrt{2i_0} r_0}{\mu_0} \right) \quad (6)$$

where  $R_0$  - Reynolds number calculated by parameters of deceleration behind the direct shock wave.

In such a manner, heat exchange in environment of critical point at wall Reynolds numbers will be determined by parameter  $N = R_0 k^2$ . Usually, results of investigations are presented as function of  $R_0$ , Mach number and adiabatic coefficient [6 - 8].

System of equations (1) was in numerical solved by Runge-Kutta method. Calculations conducted for sphere showed that heat flow normalized to its value without regard for interaction with shock wave, practically, depends only on parameter  $N$ . Quantities of heat flow for small Reynolds numbers without regard for interaction with shock wave were determined by results of calculations at large Reynolds numbers ( $R_\infty \sim 10^6$ ) on the assumption that heat flow  $q \sim \sqrt{R_\infty}$ . Heat flows thus normalized for various velocities depending upon parameter  $N$  are listed in Fig. 1. Results of calculation can be well approximated by dependence

$$Q_1 = 1 + \frac{2.14}{(\log N + 0.95)^2} \quad (7)$$

which is also shown in Fig. 1.

It is possible to expect, due to normalization of results of calculation, that use of a different kind of assumption will not strongly show up in (7).\*

Comparison of calculations by dependence (7) with experimental data of [6, 7] is shown in Fig. 2. It is clear that calculation satisfactorily agrees with experiment and parameter  $N$  is actually the determining parameter of the problem.

Investigations of influence of small Reynolds numbers on heat exchange are usually limited to the sphere. It is interesting to reveal influence of small Reynolds numbers on flowing around environment of stagnation point of bodies of other configurations. We will originate from assumption that, just as for sphere, for strongly cooled wall on such bodies, thickness of displacing of boundary layer is negligible as compared with departure of shock wave from blunting.

It was noted [10, 11] that for dimensionless departure of shock wave from body of rather general form can be obtained

$$\frac{b_1}{r_1} = \frac{k}{1 + \sqrt{2k}} \quad (8)$$

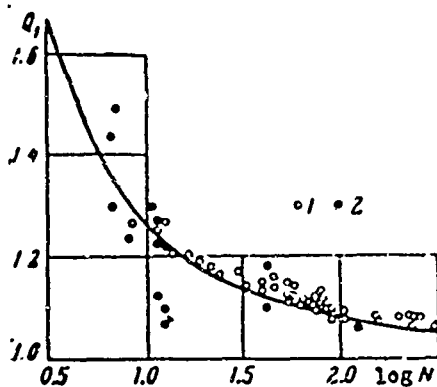


Fig. 2. 1 - experiment [6],  $k = 0.167$ ;  
2 - experiment [7],  $k = 0.07$  to  $0.09$ .

In [10] was indicated also that if radius of curvature of shock wave was used as characteristic dimension quantity  $b$  depends weakly on forms of body. This means that the same radius of curvature of shock wave, flow in environment of critical point of various bodies will be identical at identical incident parameters and conditions on body. From this ensues following approximate method of calculation of

\*At  $Re \sim 10^4$  results of calculation agree with data of [9] (when Lewis number  $L = 1$ ) with discrepancy not over 5%.

influence of small Reynolds numbers on characteristics of flow in environment of stagnation point of blunt bodies. We determine departure of shock wave (or its radius of curvature on axis) for given body as function of quantity  $k$ . By departure of shock wave we find radius of sphere  $r_{O*}$  which forms shock wave with that same departure and radius of curvature. By quantity  $r_{O*}$  and  $k$  we calculate parameter  $N$  and make correction for small Reynolds numbers according to (7).

Thus, for calculation of thermal flow at critical point of considered body, it is necessary to determine radius of sphere  $r_{O*}$  with that same departure and radius of curvature of shock wave and to find thermal flow at critical point of sphere. Departures of shock wave for considered body and sphere with  $r_0 = r_{O*}$  are equal, therefore, in environment of critical point radiation thermal flows from gas volume will be equal and heat exchange at critical point of sphere with  $r_0 = r_{O*}$  will completely model heat exchange at critical point of considered body.

Author thanks V. V. Lunev for discussion of work and remarks and N. G. Kas'yanov who made calculations.

Submitted  
7 March 1963

#### Literature

1. I. N. Murzinov. On influence of changeability of Prandtl number on flow in environment of critical point of blunt body at small Reynolds number, PMTF, 1962, No 2.
2. O. M. Belotserkovskiy. Calculation of flow around axisymmetric bodies with departing shock wave (calculating formulas and tables of flow fields, Calculation center Academy of Sciences of USSR, M., 1961.
3. M. D. Van Dyke, and H. Gordon. Supersonic flow past a family of blunt, axisymmetric bodies, NASA Technical Report R - 1, 1959.
4. A. S. Predvoditelev (ed.) Coll. Articles on Physical gas dynamics, Pub. House of Academy of Sciences of USSR, 1960.
5. L. Lees. Laminar heat transfer over blunt nosed bodies at hypersonic flight speeds, Jet Propulsion, 1956, No 4.
6. A. Ferry, V. Zakkay, and Ting Lu. Blunt body heat transfer at hypersonic speed and low Reynolds numbers. JASS, 1961, No 12.
7. S. E. Neise, R. W. Rutowski, and K. K. Chan. Stagnation point heat transfer measurements in hypersonic low-density flow. JASS, 1960, No 5.

8. A. Ferry and V. Zakkay. Measurements of stagnation point heat transfer at low Reynolds numbers. JASS, 1961, No 7.

9. Faye and Riddell. Theoretical analysis of heat exchange in frontal point washed by dissociated air, Coll. articles on Problems of motion of nose cone of long-range rockets. IL, 1959.

10. V. V. Lunev, and I. N. Murzinov. Influence of radiation on flow in environment of critical point of blunt body. PMTF, 1961, 2.

11. L. Lees. Contemporary state of aerodynamics of hypersonic flows. Collection of articles on "Problems of motion of nose cone of long-range rockets." IL, 1959.

DETERMINATION OF AVERAGE SECTION OF COLLISIONS OF ELECTRONS  
WITH NEUTRAL ATOMS OF WEAKLY-IONIZED GAS MIXTURE

E. P. Zimin and V. A. Popov

(Moscow)

Described are experiments on determination of average section of collisions of electrons with neutral atoms at temperatures of 1900 - 2300° K. Sections are determined by data on attenuation of radio waves in products of combustion of a methane-oxygen mixture with addition of potassium.

1. As was shown in [1, 2], under certain conditions, attenuation factor of radio waves in conducting gas is coupled with electrical conductivity of this medium by following relationship;

$$\alpha = 5.54 \cdot 10^6 \left(1 + \frac{\omega^2}{\nu^2}\right)^{\frac{1}{2}} \quad (1)$$

Here  $\sigma_0$  - electrical conductivity to direct current ( $\text{sec}^{-1}$ );  $\omega$  angular frequency radio emission;  $\nu$  - effective frequency of collisions of electrons with heavy particles of gas;  $\gamma$  - attenuation factor (db); and  $z$  - length of investigated object.

From equation (1) it follows that knowing the experimental values of  $\gamma$ , it is possible to calculate values of electrical conductivity to alternating current  $\sigma_0(1 + \omega^2/\nu^2)$  and further through known  $\nu$  to determine quantity  $\sigma_0$ . Unfortunately, quantity  $\nu$ , at low energies of electrons, i.e., at temperatures less than 5000°K, for majority of gases is not accurately known. Knowledge of it presents great practical interest.

However, from equation (1) it follows that by measurements of attenuation factor of radio waves on any two frequencies, one can determine both  $\sigma_e$  and  $v$ , here

$$\sigma_e = \frac{n_e e^2}{m v} \quad (2)$$

Here  $n_e$  - concentration of electrons,  $m$  and  $e$  - mass and charge of electron respectively.

Further, effective frequency of collisions of electrons with heavy particles of gas is expediently determined by following relationship:

$$v = v n_1 \left( Q_1 + Q_2 \frac{n_2}{n_1} + Q_i \frac{n_e}{n_1} \right) \quad (3)$$

which is a result of condition that resistance of gas can be represented as sum of resistances of weakly-ionized gas in which elastic collisions of electrons with neutral atoms predominate, and of strongly ionized gas in which Coulomb interactions of electrons with positive ions [3] predominate. In equation: (3)  $v$  - average thermal velocity of electrons;  $n_1$  - concentration of atoms of nonionizing component of mixture;  $n_2$  - concentration of atoms of ionizing component of mixture;  $Q_1$  and  $Q_2$  - average sections of collisions of electrons with atoms of corresponding components of mixture; and  $Q_i$  - apparent section of collisions of electrons with ions.

Above is assumed that: 1) mixture contains neutral atoms of only two gases - practically nonionized diluent ( $n_1, Q_1$ ) and slightly ionized admixture ( $n_2, Q_2$ ); 2) concentration of admixture is very small ( $n_2 \ll n_1$ ); 3) only single ionization takes place and 4) degree of ionization of admixture is small  $n_e / n_2 \ll 1$ .

Assuming form of function  $Q_i(n_e)$  given, it is expedient to use experimental measurements of attenuation of radio waves for determination of concentration of electrons and effective section of collisions of electrons with neutral atoms of mixture  $Q_e = Q_1 + Q_2 n_2 / n_1$ .

Problem reduces to solution of system of two algebraic equations

$$\frac{\alpha^2 z}{m v (Q_e + Q_{(z)})} = \beta_j \left[ 1 + \frac{\alpha^2 z}{v^2 n_1^2 (Q_e + Q_{(z)})^2} \right] \quad (i = 1, 2) \quad (4)$$

Here

$$\alpha = n_e / n_1, \quad \beta_j = 5.54 \cdot 10^4 T_j / z$$

It is necessary to note that since  $Q_0$  is linear function of relative concentration of admixture  $\alpha = n_2/n_1$ , knowing experimental dependence  $Q_0(\alpha)$ , one can determine average section of collisions of electrons with neutral atoms of diluent ( $Q_1$ ) and also of admixture ( $Q_2$ ).

Resolving system (4), we obtain ( $\omega_1 > \omega_2$ )

$$Q_0 = \frac{\alpha e^2}{2\beta_2 p n_1} + \left[ \left( \frac{\alpha e^2}{2\beta_2 p n_1} \right)^2 - \frac{\omega_1^2}{v^2 n_1^2} \right]^{1/2} - \alpha Q_1 \quad (5)$$

$$\alpha = \frac{m \omega_2 \beta_2}{e^2 n_1} \left( \frac{\omega_1^2}{\omega_2^2} - 1 \right) \left( \frac{\beta_2}{\beta_1} - 1 \right)^{-1/2} \left( \frac{\omega_1^2}{\omega_2^2} - \frac{\beta_2}{\beta_1} \right)^{-1/2} \quad (6)$$

or

$$Q_0 = \frac{1.87 \cdot 10^{23}}{\beta_2 \sqrt{T}} \left[ 1 + \left( 1 - 1.16 \cdot 10^{-20} \frac{T^2 \omega_2^2 \beta_2^2}{p^2 \alpha^2} \right)^{1/2} \right] - \alpha Q_1$$

$$\alpha = 5.38 \cdot 10^{21} \frac{T \omega_2 \beta_2}{p} \left( \frac{\omega_1^2}{\omega_2^2} - 1 \right) \left( \frac{\beta_2}{\beta_1} - 1 \right)^{-1/2} \left( \frac{\omega_1^2}{\omega_2^2} - \frac{\beta_2}{\beta_1} \right)^{-1/2}$$

Apparent section of collisions of electrons with ions is determined by expression (k - Boltzmann constant)

$$Q_i = 8.16^2 \ln \Lambda, \quad b = \frac{e^2}{3kT}, \quad \Lambda = \frac{3}{2} \frac{J}{\sqrt{2\pi}} \frac{k^3 T^3}{e^2 \sqrt{p_2}} \quad (7)$$

For simplification of calculations, expression (7) is conveniently converted to form

$$Q_i = \frac{2.9 \cdot 10^{-4}}{T^2} (\log T - \log p - \log \alpha - 14)$$

2. If  $n_2 \ll n_1$  and  $Q_2$  insignificantly differs from  $Q_1$ , determining parameter will be section of collisions  $Q_1$  which one can determine by the simpler graphic method [4]. Putting constants in equations (1) and (2), we obtain

$$\frac{1}{\gamma} = \frac{1}{\alpha} \frac{\omega^2}{v} + \frac{v}{\alpha} \quad (\alpha = n_2/2.16) \quad (8)$$

It is obvious that dependence plotted in system of coordinates  $(\gamma^{-1}, \omega^2)$ , has linear character and allows to determine, from angle of inclination of straight line to axis  $\omega^2$  and ordinate  $(\gamma^{-1})_{\omega=0}$  both  $n_2$  and  $v$ .

Of course this method cannot be used for determination of average sections of collisions of electron with neutral atoms of both diluent ( $Q_1$ ) and admixture ( $Q_2$ ).

3. Investigations were conducted on products of combustion methane-air and methane-oxygen mixtures. Mixture was burned on burner of torch type with formation of sufficiently uniform region of products of combustion. Temperature was modified by means of change of composition of mixture. Pressure was equal to 1 atm. Slightly ionized admixture was introduced into flow of oxidizer directly before preliminary mixing chamber of burner in the form of aqueous solution of  $K_2CO_3$  of various concentration. Temperature of products of combustion was measured by method of reversal of lines of Na. Method of use of waveguide lines  $\omega_1 = 10,000$  MC and  $\omega_2 = 40,000$  MC is analogous to that described in [1, 2].

T°K	$\nu \cdot 10^{-1} \text{ sec}^{-1}$	$Q_1 \cdot 10^{15} \text{ cm}^2$
1900	1.49	1.30
2000	1.64	1.47
2100	1.82	1.67
2200	2.39	2.24
2300	3.33	3.19

Experiments were conducted at three various values of concentration of solution of  $K_2CO_3$  fed into torch differing by  $10^2$  times.

Given results were obtained at various temperatures; error does not exceed 3 - 5%.

Submitted  
1 April 1963

#### Literature

1. E. P. Zimin and V. A. Popov. Investigation of electrical conductivity of flame by microwave method. *Inzh. fiz. zh.*, 1962, Vol. V. No 3.
2. E. P. Zimin and V. A. Popov. Research on the electrical conductivity of combustion products with potassium seeding. *Proc. of Symposium on magnetoplasma-dynamic electrical power generation, Newcastle, 1962.*
3. S. C. Lin, E. L. Resler, and A. Kantrowitz. Electrical conductivity of highly ionized argon produced by shock waves. *J. Appl. Phys.*, 1955, v. 26, p. 95
4. H. Belcher., and T. M. Sugden. Studies on the ionization produced by metallic salts in flames. *Proc. Roy. Soc. A*, 1950, 201, 480.

FLOW BETWEEN PARALLEL WALLS IN PERIODIC MAGNETIC FIELD

I. B. Chekmarev

(Leningrad)

S. A. Regirer [1] investigated flow between parallel plane walls in nonuniform field on the assumption that velocity of liquid does not change throughout flow. Recently, stationary flow of inviscid electrical conducting medium in a flat duct in the presence of a nonuniform external magnetic field was investigated in work of Sakurai and Naito [2]. Magnetohydrodynamic boundary layer in nonuniform fields was studied by Sherman [3] and Turcotte and Lyons [4].

Below is considered stationary flow of viscous electrical conducting liquid between parallel plates  $y = \pm a$  created by drop of pressure along axis  $x$ . Constituents of magnetic induction of external potential field are considered periodic functions of coordinate  $x$  and have following form:

$$B_x = -B_0 \sin \frac{2\pi x}{\lambda} \operatorname{sh} \frac{2\pi y}{\lambda}, \quad B_y = B_0 \frac{2\pi x}{\lambda} \operatorname{ch} \frac{2\pi y}{\lambda}, \quad B_z = 0 \quad (1)$$

Since in considered case all magnitudes are independent of coordinate  $z$ , confining ourselves to small magnetic Reynolds numbers, we have:

$$\begin{aligned} \rho u \frac{\partial u}{\partial x} + \rho v \frac{\partial u}{\partial y} &= -\frac{\partial p}{\partial x} - i_z B_y + \eta \left( \frac{\partial^2 u}{\partial x^2} + \frac{\partial^2 u}{\partial y^2} \right), \quad \frac{\partial u}{\partial x} + \frac{\partial v}{\partial y} = 0, \\ \rho u \frac{\partial v}{\partial x} + \rho v \frac{\partial v}{\partial y} &= -\frac{\partial p}{\partial y} + i_z B_x + \eta \left( \frac{\partial^2 v}{\partial x^2} + \frac{\partial^2 v}{\partial y^2} \right), \quad i_z = \sigma(uB_y - vB_x) \end{aligned} \quad (2)$$

Here  $B'_x$  and  $B'_y$  are determined by formulas of (1), and external electric field

is absent. We will introduce dimensionless variables

$$y^* = \frac{y}{a}, \quad x^* = \frac{x}{\lambda}, \quad u^* = \frac{u}{u_0}, \quad v^* = \frac{v}{\epsilon u_0}, \quad p^* = \frac{p}{p_0}, \quad \epsilon = \frac{a}{\lambda}, \quad u_0 = \frac{Q}{2a} \quad (3)$$

Here  $u_0$  - average velocity of medium;  $p_0$  - certain scale of pressure. System (2) in these variables has form (asterisks are omitted in the future)

$$\begin{aligned} \epsilon \left( u \frac{\partial u}{\partial x} + v \frac{\partial u}{\partial y} \right) &= -\epsilon E \frac{\partial p}{\partial x} - S \cos 2\pi x \operatorname{ch} 2\pi \epsilon y (u \cos 2\pi x \operatorname{ch} 2\pi \epsilon y + \\ &\quad + \epsilon v \sin 2\pi x \operatorname{sh} 2\pi \epsilon y) + \frac{1}{R} \left( \epsilon^2 \frac{\partial^2 u}{\partial x^2} + \frac{\partial^2 u}{\partial y^2} \right) \\ \epsilon^2 \left( u \frac{\partial v}{\partial x} + v \frac{\partial v}{\partial y} \right) &= -E \frac{\partial p}{\partial y} - S \sin 2\pi x \operatorname{sh} 2\pi \epsilon y (u \cos 2\pi x \operatorname{ch} 2\pi \epsilon y + \\ &\quad + \epsilon v \sin 2\pi x \operatorname{sh} 2\pi \epsilon y) + \frac{\epsilon}{R} \left( \epsilon^2 \frac{\partial^2 v}{\partial x^2} + \frac{\partial^2 v}{\partial y^2} \right) \\ \frac{\partial u}{\partial x} + \frac{\partial v}{\partial y} &= 0 \quad \left( E = \frac{p_0}{\rho u_0^2}, S = \frac{\sigma B_0^2 a}{\rho u_0}, R = \frac{\rho u_0 a}{\eta} \right) \end{aligned}$$

Let us consider case  $\lambda \gg a$ . Under this condition, magnetic field strength and velocity of liquid will change slightly along flow as compared with their lateral change in channel. We seek a solution of system (4) in the form of a series by degrees of small parameter  $\epsilon = a/\lambda \ll 1$ . Considering  $E = 1/\epsilon$ , we find for zero approximation of equation

$$\frac{1}{R} \frac{\partial^2 u}{\partial y^2} - S (\cos 2\pi x)^2 u = \frac{\partial p}{\partial x}, \quad \frac{\partial p}{\partial y} = 0, \quad \frac{\partial u}{\partial x} + \frac{\partial v}{\partial y} = 0 \quad (5)$$

Differentiating the first of equations (5) on  $y$ , we exclude pressure  $p$  and obtain equation for velocity

$$\frac{\partial^2 u}{\partial y^2} - (M \cos 2\pi x)^2 \frac{\partial u}{\partial y} = 0 \quad (M^2 = SR) \quad (6)$$

resolving which under condition:

$$u|_{y=\pm 1} = 0, \quad \int_{-1}^{+1} u \, dy = 2 \quad (7)$$

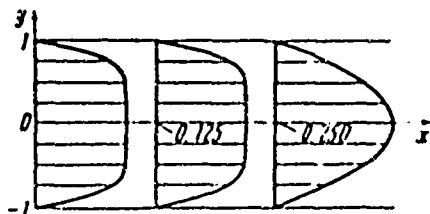
we find

$$u = \frac{\operatorname{ch}(M_y \cos 2\pi x) - \operatorname{ch}(M \cos 2\pi x)}{(M \cos 2\pi x)^{-1} \operatorname{sh}(M \cos 2\pi x) - \operatorname{ch}(M \cos 2\pi x)} \quad (8)$$

When  $\lambda \rightarrow \infty$  formula (8) changes to known solution of Hartmann problem for uniform magnetic field

$$u = \frac{\operatorname{ch} My - \operatorname{ch} M}{M^{-1} \operatorname{sh} M - \operatorname{ch} M} \quad (9)$$

It is curious to note that at points  $x = 1/2 n$ , where  $\cos 2\pi x = (-1)^n$ , we also obtain Hartmann profile. At points  $1/4 (2n + 1)$ , where  $\cos 2\pi x = 0$ , formula (8) gives usual Poiseuille profile  $u = 3/2 (1 - y^2)$ .



Thus, during motion of liquid in periodic external magnetic field, wave length of which is significantly longer than height of duct, distribution of velocities

is determined by formula (8) which is analogous formula (9) taken with certain effective Hartmann number  $M |\cos 2\pi x|$ . Here, velocity profile is periodically deformed from the Hartmann when  $|\cos 2\pi x| = 1$  to Poiseuille at  $\cos 2\pi x = 0$ .

Transverse velocity  $v$  can be found from last equation of (5) by known constituent  $u$ .

For determination of pressure distribution in duct, we have relationship

$$\frac{dp}{dx} = \frac{1}{R} \left[ \frac{\partial^2 u}{\partial y^2} - (M \cos 2\pi x)^2 u \right]$$

Calculating its right side with the help of (8), we find

$$\frac{dp}{dx} = \frac{(M \cos 2\pi x)^2}{R} \frac{\text{ch}(M \cos 2\pi x)}{(M \cos 2\pi x)^{-1} \text{sh}(M \cos 2\pi x) - \text{ch}(M \cos 2\pi x)} \quad (10)$$

In the figure is shown change of velocity profile as a function of longitudinal coordinate  $x$ .

Submitted  
13 June 1963

#### Literature

1. S. A. Regirer. On one accurate solution of equations in magnetohydrodynamics. PMM, 1960, vol. 24, No 2.
2. T. Sakurai, and M. Naito. Steady two-dimensional channel flow of an incompressible perfect fluid with small electric conductivity in the presence of nonuniform magnetic fields. J. Phys. Soc. Japan, 1962, vol. 17, No 4.
3. A. Sherman. Viscous magnetohydrodynamic boundary layer. Phys. of Fluids, 1961, vol. 4, No 5.
4. D. L. Turcotte. and J. M. Lyons. A periodic boundary-layer flow in magnetohydrodynamics. J. Fluid mech., 1962, vol. 13, Pt.

ABOUT MODELING OF MAGNETOHYDRODYNAMIC FLOW  
IN CHANNEL IN ELECTROLYTIC BATH

V. V. Nesterenko

(Moscow)

For flow of electrically conductive incompressible liquid in flat channel in presence of magnetic field at values of Reynolds magnetic number  $Re_m \ll 1$  it is possible to disregard influence of induced magnetic field on motion of liquid. Furthermore, in a number of cases, the hydrodynamic problem can be separated from the electrodynamic [1]. Velocity of liquid  $V$  can be determined from hydrodynamic equations, and distribution of current density  $j$  and electric potential  $\varphi$  in channel is found from Ohm's law and equation of inseparability for  $j$

$$j = \sigma \left( -\nabla\varphi + \frac{1}{c} V \times B \right), \text{div } j = 0 \quad (1)$$

Here,  $B$  - magnetic field strength,  $\sigma$  - electrical conductivity of liquid,  $c$  - velocity of light in a vacuum. Here,  $V$  and  $B$  are considered given functions of coordinates. Problem reduces to Poisson equation for function of  $\varphi$ .

If channel is composed of sections of conductors and dielectrics, boundary conditions will be constancy of potential of  $\varphi$  on conductors and absence of normal component of current density, on dielectrics  $j_n = 0$ .

For flow with variable velocity  $v(V(y), 0)$  in constant magnetic field ( $y$  - coordinate in transverse direction of axis of channel) problem also reduces to solution of Laplace equation for certain auxiliary function  $u$  determined by relationship

$$u = \varphi - \frac{1}{c} B \int_0^y v dy \quad (2)$$

Certain particular problems reducing to Laplace equation are considered in [2].

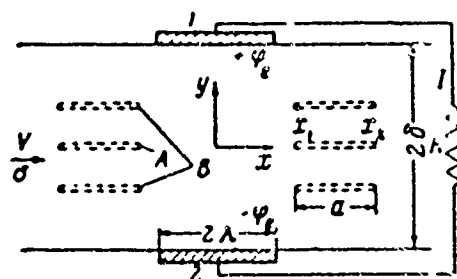


Fig. 1.

It is expedient, for solution of similar kind of problems in those cases when obtaining of analytic solution is difficult, to use methods of electric modeling, in particular - the electrolytic bath [4].

Lower are given certain results of investigation of flow of incompressible electric conductive liquid in flat channel with the help of electrolytic bath.

Flow was modelled in channel of width  $2\delta$ , walls of which were composed of sections of conductors and dielectrics (Fig. 1). Velocity of flow of liquid  $V$  was considered given, independent of  $x$ , and arbitrary even function of  $y$ . A pair of symmetrically located electrodes of length  $2\lambda$  was connected by a certain external load  $R$ . In entire extent of channel perpendicularly to its plane was applied constant magnetic field of intensity  $B \{0, 0, -B\}$ .

During motion of liquid in channel, on electrodes appears difference of potentials  $2\varphi_e$  and in external circuit flows electric current  $I$ . On external load  $R$  will be distinguished power  $N = 2\varphi_e I$ .

Under shown assumptions, function  $u$  determined by equation (2) satisfies Laplace equation [2]

$$\Delta u = 0 \quad (3)$$

with boundary conditions:

$$\begin{aligned} u = \pm u_1 & \text{ at } y = \pm \delta \text{ on electrodes} \\ \partial u / \partial y = 0 & \text{ at } y = \pm \delta \text{ on dielectrics} \end{aligned} \quad (4)$$

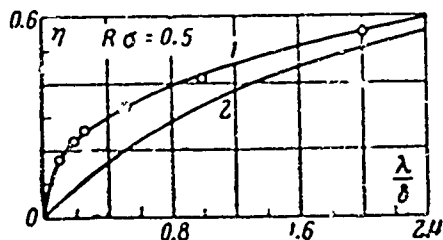


Fig. 2.

Values of function  $u$  on electrode is determined from following relationship

$$u_1 = \varphi_1 - \frac{B}{c} \int_0^{\delta} V dy \quad (\varphi_1 - \varphi_2 = 2\varphi_e > 0)$$

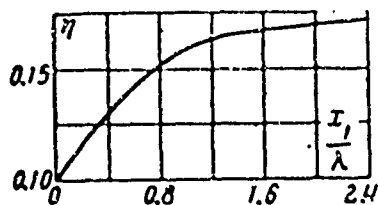


Fig. 3.

where  $\varphi_1$  meaning of potential on electrode 1.

Power separated on external load can be determined by following expression

$$N^* = \frac{N}{\sigma E^2} = \frac{1}{R\sigma} \left( \frac{2\varphi_e}{E} \right)^2 \left( E - \frac{R}{c} \int_{-\delta}^{\delta} V dy \right) \quad (5)$$

Expression for Joule dissipation  $Q$  in channel given in [3] in considered case has form

$$Q^* = \frac{Q}{\sigma E^2} = -\frac{1}{R\sigma} \left( \frac{2\varphi_e}{E} \right)^2 + \frac{\lambda}{\delta} \left( 1 - \frac{2\varphi_e}{E} \right) + \frac{2\varphi_e}{E} \int_{\lambda}^{\infty} \left[ \frac{E}{2\varphi_e} - 2 \left( \varphi^* - \frac{1}{2} \right) \right] dx, \quad (6)$$

$$\varphi^* = \frac{\varphi - \varphi_2}{2\varphi_e} \text{ when } y = \delta, x^* = \frac{x}{\delta}$$

Determining efficiency  $\eta$  as the ratio of power to sum of power and Joule dissipation, we have

$$\eta = \frac{N}{N+Q} = \frac{N^*}{N^*+Q^*} \quad (7)$$

Let us note that for determination of power, dissipation and efficiency it is sufficient to know quantity  $2\varphi_e$  and distribution of potential on dielectric wall of channel at given  $V$ ,  $B$ ,  $R$  and  $\sigma$ . Due to symmetry of problem it is sufficient to know value of  $\varphi$  (or  $\varphi^*$ ) in section  $\lambda < x < \infty$ ,  $y = \delta$ .

In electrolytic bath geometrically similar to considered channel, was modelled function of  $u$  determined by expression (2) with those same boundary conditions as in the channel. Here, value of  $u$  at corresponding points of channel and bath coincide. Using Ohm's law for electrolytic bath and external circuit of channel, we obtain following relationships between parameters of channel and bath

$$\frac{1}{\sigma} I = \frac{1}{\sigma_m} I_m, \quad \frac{2\varphi_e}{E} = \frac{\sigma R}{\sigma R + \sigma_m R_m} \quad (8)$$

$$u_1 - u_2 = 2\varphi_e - E$$

where  $\sigma_m$  and  $I_m$  - electrical conductivity of liquid and current intensity fo. bath, and  $R_m$  - resistance of electrolyte between electrodes of bath.

By values of  $u$  found experimentally is found distribution of potential  $\varphi$  in channel at given  $E$  (or  $R\sigma$ ).

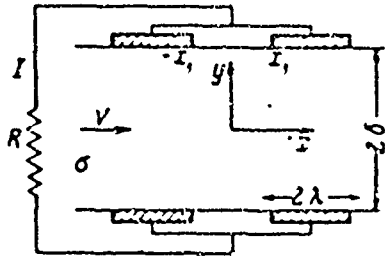


Fig. 4

$\eta$  as function of  $\lambda/\delta$  at  $Rs = 0.5$ .

In the same place is given an approximate solution for  $\eta$ , which is obtained on assumption that electric field is considered constant between electrodes and equal zero outside electrodes, i.e., a solution which disregards longitudinal edge effects "spreading" of current. In last case

$$\eta = \frac{Rs2\lambda/\delta}{2 + Rs2\lambda/\delta} \quad (9)$$

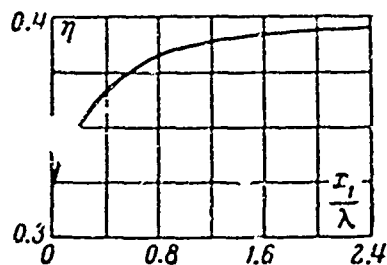


Fig. 5

conditions of (4) is added condition  $\frac{\partial u}{\partial y} = -\frac{\partial u}{\partial y} = 0$  on surface of baffles.

In determination of total Joule dissipation in this case, integration is performed also on surface of baffles, on which  $\eta$  endures a break.

Investigated were symmetric groups of plates A and B of various length  $a$  and at various distances on axis  $x$  between plates.

It was found that during closing of baffles there is a decrease of both electric current and power in channel and of efficiency all the more intense, the bigger the size of plates  $a$  and the more the plates in the group. In Fig. 3 is given dependence of  $\eta$  on distance  $x_1/\lambda$  between baffles for symmetric baffles of type B (Fig. 1) of dimension  $a/\delta = 1.0$  in channel with  $\lambda/\delta = 0.5$  at  $Rs = 0.5$ .

As experiment shows, application of dielectric baffles to obtain increase of power and efficiency takes from electrodes was found impractical. In addition, investigation was made of influence of distance between two pairs of symmetric electrodes with  $\lambda/\delta = 0.25$  coupled in parallel (Fig. 4) on power and efficiency in channel.

It was found that with increase of distance between electrodes, power and efficiency monotonely increase from theoretical values corresponding to a solid electrode of total extent  $\lambda/\delta = 0.5$  at  $Ro = 0.5$ . Function of  $\eta$  on distance between electrodes is shown in Fig. 5.

Submitted  
12 June 1963

#### Literature

1. A. B. Vatazhin, and S. A. Regirer. Approximate calculation of distribution of current during flow of conducting liquid through a channel in a magnetic field. PMM, 1962, vol. XXVI, issue 3.
2. A. B. Vatazhin. On solution of certain boundary value problems of magneto-hydrodynamics. PMM, 1961, vol. XXV, issue 5.
3. A. B. Vatazhin. Determination of Joule dissipation in channel of magneto-hydrodynamic generator, PMTF, 1962, No 5.
4. I. M. Tetel'baum. Electric modeling. Fizmatgiz, 1959.

VARIATIONAL METHODS OF SOLUTION OF PROBLEMS  
OF DEFORMATION AND STABILITY OF PLATES  
AND SHELLS UNDER CONDITIONS OF CREEP

G. V. Ivanov

(Novosibirsk)

Variational methods of solution of problems of deformation and stability of plates and shells under conditions of creep were considered in [1, 2]. In [1] is shown variational equation during condition of variation of speeds of stresses and speeds of shifts. In [2] is given variational equation during condition of variation of only speeds of shifts.

V. I. Rozenblyum [3] (see also [4]) by variational method solved problem of stability longitudinally compressed rods having initial (in undeformed state) deflection. Stress and displacements were modified, satisfying equations of equilibrium and boundary conditions. Below is derived an analogous equation for a mildly sloping, circular, cylindrical panel (figure). For plates and closed cylindrical shells it has the same form.

1. In fixed moment of time  $t$ , real stresses  $\sigma_x, \sigma_y, \tau$  and displacements  $u, v, w$  in panels are connected between themselves and with speeds of stresses and speeds of displacements by equations of [4, 5]:

$$\begin{aligned}
 \frac{\partial T_x}{\partial x} + \frac{\partial T_{xy}}{\partial y} &= 0, & \frac{\partial T_y}{\partial y} + \frac{\partial T_{xy}}{\partial x} &= 0 \\
 \frac{\partial M_x}{\partial x^2} + 2 \frac{\partial H}{\partial x \partial y} + \frac{\partial M_y}{\partial y^2} + T_x \frac{\partial^2 w}{\partial x^2} + T_y \left( \frac{1}{R} + \frac{\partial^2 w}{\partial y^2} \right) + 2T_{xy} \frac{\partial^2 w}{\partial x \partial y} + q &= 0 \\
 \frac{\partial \dot{T}_x}{\partial x} + \frac{\partial \dot{T}_{xy}}{\partial y} &= 0, & \frac{\partial \dot{T}_y}{\partial y} + \frac{\partial \dot{T}_{xy}}{\partial x} &= 0
 \end{aligned} \tag{1.1}$$

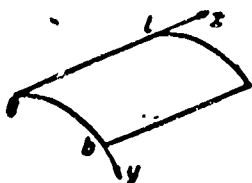
$$\frac{\partial M_x}{\partial x} + 2 \frac{\partial H}{\partial x \partial y} + \frac{\partial M_y}{\partial y} + T_x \frac{\partial w}{\partial x} + T_y \left( \frac{1}{R} + \frac{\partial w}{\partial y} \right) + 2T_{xy} \frac{\partial^2 w}{\partial x \partial y} + T_x \frac{\partial^2 w}{\partial x^2} + T_y \frac{\partial^2 w}{\partial y^2} + 2T_{xy} \frac{\partial^2 w}{\partial x \partial y} + \dot{q} = 0 \quad (1.2)$$

$$\dot{\epsilon}_x = \frac{\partial}{\partial x} \left( \Lambda + \frac{\partial \Pi}{\partial t} \right), \quad \dot{\epsilon}_y = \frac{\partial}{\partial y} \left( \Lambda + \frac{\partial \Pi}{\partial t} \right), \quad \dot{\gamma} = \frac{\partial}{\partial x} \left( \Lambda + \frac{\partial \Pi}{\partial t} \right)$$

$$\dot{\epsilon}_x = \frac{\partial \dot{u}}{\partial x} + \frac{\partial \dot{w}}{\partial x} \frac{\partial w}{\partial x} - z \frac{\partial^2 \dot{w}}{\partial x^2}, \quad \dot{\epsilon}_y = \frac{\partial \dot{v}}{\partial y} + \frac{\partial \dot{w}}{\partial y} \frac{\partial w}{\partial y} - z \frac{\partial^2 \dot{w}}{\partial y^2} - \frac{1}{R} \dot{w}$$

$$\dot{\gamma} = \frac{\partial \dot{u}}{\partial y} + \frac{\partial \dot{v}}{\partial x} + \frac{\partial \dot{w}}{\partial x} \frac{\partial w}{\partial y} + \frac{\partial \dot{w}}{\partial y} \frac{\partial w}{\partial x} - z \frac{\partial^2 \dot{w}}{\partial x \partial y} \quad (1.3)$$

Curvilinear system of coordinates for points of middle surface obtained here is shown in figure;  $T_x$ ,  $T_y$ ,  $T_{xy}$ ,  $M_x$ ,  $M_y$ ,  $H$  - forces and moments in middle surface,  $R$  - radius of panel,  $w$  - "full" deflection, i.e., sum of initial (in undeformed state) deflection and that appearing in process of deformation,  $q$  - intensity of surface load (point signifies differentiation by time)  $\Lambda$  - function of stresses and time,  $\Pi$  - function of stresses (energy of elastic deformations),  $z$  - coordinate of points of panel counted off from middle surface in the direction of internal normal.



Besides above-indicated equations, real stresses and displacements in panel satisfy given conditions on edges  $x = 0, \underline{l}, y = 0, b$  (figure). We assume that these conditions are given in forces, moments and zero displacements. For example, on edges

$x = 0, x = \underline{l}$  are given either

$$M_x, T_x, T_{xy}, T_x \frac{\partial w}{\partial x} + T_{xy} \frac{\partial w}{\partial y} + \frac{\partial M_x}{\partial x} + 2 \frac{\partial H}{\partial y}$$

or accordingly,

$$dw/dx = 0, \quad u = 0, \quad v = 0, \quad w = 0$$

Cases when on edges of panel instead of forces and moments are given non-zero speeds of displacements are not considered.

2. We will compare, in fixed moment of time  $t$ , the true stress and deformed

state with another characterized by the same speeds of stresses and speeds of displacements, but with different stresses and displacements, namely stresses  $\sigma_x + \delta\sigma_x$ ,  $\sigma_y + \delta\sigma_y$ ,  $\tau + \delta\tau$ , and displacements  $u + \delta u$ ,  $v + \delta v$ ,  $w + \delta w$ , infinitely near to real value satisfying equations of equilibrium, equations of equilibrium in speeds and given boundary conditions. These stresses and displacement will be called permissible.

Putting permissible stresses and displacements in equations

$$\begin{aligned} \frac{\partial}{\partial x} \delta T_x + \frac{\partial}{\partial y} \delta T_{xy} &= 0, & \frac{\partial}{\partial y} \delta T_y + \frac{\partial}{\partial x} \delta T_{xy} &= 0 \\ \frac{\partial^2}{\partial x^2} \delta M_x + 2 \frac{\partial^2}{\partial x \partial y} \delta H + \frac{\partial^2}{\partial y^2} \delta M_y + \delta T_x \frac{\partial^2 w}{\partial x^2} + \delta T_y \left( \frac{1}{R} + \frac{\partial^2 w}{\partial y^2} \right) + \\ + 2 \delta T_{xy} \frac{\partial^2 w}{\partial x \partial y} + T_x \delta \frac{\partial^2 w}{\partial x^2} + T_y \delta \frac{\partial^2 w}{\partial y^2} + 2 T_{xy} \delta \frac{\partial^2 w}{\partial x \partial y} &= 0 \end{aligned} \quad (2.1)$$

$$\delta T_x \frac{\partial^2 \dot{w}}{\partial x^2} + \delta T_y \frac{\partial^2 \dot{w}}{\partial y^2} + 2 \delta T_{xy} \frac{\partial^2 \dot{w}}{\partial x \partial y} + \dot{T}_x \delta \frac{\partial^2 w}{\partial x^2} + \dot{T}_y \delta \frac{\partial^2 w}{\partial y^2} + 2 \dot{T}_{xy} \delta \frac{\partial^2 w}{\partial x \partial y} = 0 \quad (2.2)$$

According to (1.3), variation of speeds of deformations depends on variation only of displacement  $w$

$$\delta \dot{e}_x = \frac{\partial \dot{w}}{\partial x} \delta \frac{\partial w}{\partial x}, \quad \delta \dot{e}_y = \frac{\partial \dot{w}}{\partial y} \delta \frac{\partial w}{\partial y}, \quad \delta \dot{\gamma} = \frac{\partial \dot{w}}{\partial x} \delta \frac{\partial w}{\partial y} + \frac{\partial \dot{w}}{\partial y} \delta \frac{\partial w}{\partial x} \quad (2.3)$$

3. Because real stresses and displacements satisfy equations of equilibrium and boundary conditions, it follows (see, for example, [5], section 7)

$$\int_V (\sigma_x \dot{e}_x + \sigma_y \dot{e}_y + \tau \dot{\gamma}) dV = A$$

where  $V$  - volume occupied by panel,  $A$  - power of external forces applied to panel. Permissible stresses and displacements also satisfy equations of equilibrium and given boundary conditions (let us remember that these conditions are considered given in forces, moments and zero displacements; cases, when on edges of panel, instead of efforts and moments, are given non-zero speeds of displacements, are not considered).

Therefore

$$\int_V [(\sigma_x + \delta\sigma_x)(\dot{e}_x + \delta\dot{e}_x) + (\sigma_y + \delta\sigma_y)(\dot{e}_y + \delta\dot{e}_y) + (\tau + \delta\tau)(\dot{\gamma} + \delta\dot{\gamma})] dV = A \quad (3.1)$$

i. e., power of deformations in class of permissible stresses and displacements is stationary. Omitting in (3.1) the product of variations as an infinitesimal quantities of the second order, we find

$$\int_V (\sigma_x \delta\dot{e}_x + \sigma_y \delta\dot{e}_y + \tau \delta\dot{\gamma}) dV + \int_V (\dot{e}_x \delta\sigma_x + \dot{e}_y \delta\sigma_y + \dot{\gamma} \delta\tau) dV = 0 \quad (3.2)$$

Validity of (3.2) is simple to prove and is directly integrated by parts with use of equations (2.1) and relationships of (2.3).

4. From equations of (1.2) it follows that second component in (3.2) is a variation of integral

$$\int_V \left( \Lambda + \frac{\partial \Pi}{\partial t} \right) dV$$

Under certain conditions, the first component in (3.2) is also a variation of certain expression.

Using the first two of equations of (2.1) and the first two equations of (1.1), we write (2.2) in the form

$$\begin{aligned} & \frac{\partial}{\partial x} \left( \delta T_x \frac{\partial w}{\partial x} \right) + \frac{\partial}{\partial y} \left( \delta T_y \frac{\partial w}{\partial y} \right) + \frac{\partial}{\partial x} \left( \delta T_{xy} \frac{\partial w}{\partial y} \right) + \frac{\partial}{\partial y} \left( \delta T_{xy} \frac{\partial w}{\partial x} \right) + \\ & + \frac{\partial}{\partial x} \left( \dot{T}_x \delta \frac{\partial w}{\partial x} \right) + \frac{\partial}{\partial y} \left( \dot{T}_y \delta \frac{\partial w}{\partial y} \right) + \frac{\partial}{\partial x} \left( \dot{T}_{xy} \delta \frac{\partial w}{\partial y} \right) + \frac{\partial}{\partial y} \left( \dot{T}_{xy} \delta \frac{\partial w}{\partial x} \right) = 0 \end{aligned} \quad (4.1)$$

Multiplying (4.1) by  $w$  and integrating by area of middle surface  $\Omega$ , we find

$$\begin{aligned} & \int_{\Omega} \left[ \delta T_x \frac{\partial w}{\partial x} \frac{\partial w}{\partial x} + \delta T_y \frac{\partial w}{\partial y} \frac{\partial w}{\partial y} + \delta T_{xy} \left( \frac{\partial w}{\partial y} \frac{\partial w}{\partial x} + \frac{\partial w}{\partial x} \frac{\partial w}{\partial y} \right) + \right. \\ & \left. + \dot{T}_x \frac{\partial w}{\partial x} \delta \frac{\partial w}{\partial x} + \dot{T}_y \frac{\partial w}{\partial y} \delta \frac{\partial w}{\partial y} + \dot{T}_{xy} \left( \frac{\partial w}{\partial x} \delta \frac{\partial w}{\partial y} + \frac{\partial w}{\partial y} \delta \frac{\partial w}{\partial x} \right) \right] d\Omega = \\ & = \int_0^b \left[ \kappa \delta \frac{d}{dt} \left( T_y \frac{\partial w}{\partial y} + T_{xy} \frac{\partial w}{\partial x} \right) \right]_{y=0}^{y=b} dx + \int_0^b \left[ \kappa \delta \frac{d}{dt} \left( T_x \frac{\partial w}{\partial x} + T_{xy} \frac{\partial w}{\partial y} \right) \right]_{x=0}^{x=l} dy \end{aligned} \quad (4.2)$$

Using (2.3) and (4.2), the first component in (3.2) can be written in the form

$$\int_V (\sigma_x \delta \epsilon_x + \sigma_y \delta \epsilon_y + \tau \delta \gamma) dv =$$

$$= \frac{1}{2} \delta \frac{d}{dt} \int_{\Omega} \left[ T_x \left( \frac{\partial w}{\partial x} \right)^2 + T_y \left( \frac{\partial w}{\partial y} \right)^2 + 2T_{xy} \frac{\partial w}{\partial x} \frac{\partial w}{\partial y} \right] d\Omega - \quad (4.3)$$

$$- \int_0^t w \delta \frac{d}{dt} \left( T_y \frac{\partial w}{\partial y} + T_{xy} \frac{\partial w}{\partial x} \right) \Big|_{y=0}^{y=b} dx - \int_0^b \left[ w \delta \frac{d}{dt} \left( T_x \frac{\partial w}{\partial x} + T_{xy} \frac{\partial w}{\partial y} \right) \right] \Big|_{x=0}^{x=l} dy$$

If boundary conditions are such that contour integral in (4.3) disappears (for example, in case, when on all edges of panel  $w = 0$ ), the first component in (3.2) is full variation and (3.2) takes form

$$\delta \Phi = \delta \left\{ \int_V \left( \Lambda + \frac{\partial \Pi}{\partial t} \right) dv + \frac{1}{2} \frac{d}{dt} \int_{\Omega} \left[ T_x \left( \frac{\partial w}{\partial x} \right)^2 + T_y \left( \frac{\partial w}{\partial y} \right)^2 + 2T_{xy} \frac{\partial w}{\partial x} \frac{\partial w}{\partial y} \right] d\Omega \right\} = 0 \quad (4.4)$$

Under these conditions, among all permissible stresses and displacements, true distribution of stresses and displacements is characterized by stationariness of functional  $\Phi$ .

It is not difficult to perceive that determination of deflection with the help of variational equation (4.4) reduces to integration of a system of resolved (relative to derivatives) nonlinear differential equations of the first order. Increase of number of parameters during assignment of class of permissible stresses and displacements shows only on increase of number of equations of system subjected to integration.

Submitted  
9 April 1963

#### Literature

1. J. L. Sanders, H. G. McComb, and F. R. Schlechte. A Variational Theorem for Creep with Applications to Plates and Columns. NACA Rep. 1342, 1958.
2. I. G. Teregulov. Variational methods of solution of problems of steady-state creep of plates and shells in case of finite dislocations. PMM, 1962, vol. XXVI, issue 3.
3. V. I. Rozenblyum. Stability of a compressed rod in state of creep. Inzh. sb., 1954, vol. 18.
4. L. M. Kachanov. Theory of creep. Fizmatgiz, 1960.
5. A. S. Vol'mir. Flexible plates and shells. Gostekhizdat, 1956.

APPROXIMATE METHOD OF CALCULATION  
FOR CREEP BUCKLING

S. A. Shesterikov

(Moscow)

Survey of solution of certain of the simplest particular problems on buckling of rods can be found, for example, in [1, 2]. Investigation of plates and shells was conducted, basically, in direction of development of criteria of stability for linearized formulation of problem of buckling. In works devoted to this problem [3-5], basically was studied behavior of thin-walled elements in initial phase after loading. Below is described a method for approximate calculation of buckling during creep.

1. The offered method is based on the assumption that for rods and thin-walled elements under the conditions of longitudinal compression the connection between stresses and deformations can be replaced by analogous functions for bending moments and warping.

A similar method was used earlier during investigation of other problems (see [6]). We emphasize that this assumption in certain cases can appear too coarse. Therefore, a critical appraisal of obtained results and indication of region where they are applicable is necessary each time. At the same time, such a hypothesis for a large class of problems considerably simplifies calculation without distorting the essence of the phenomenon.

For the uniaxial case, the taken hypothesis means that there is dependence

$$\Phi(x, \dot{x}, m, \dot{m}, T) = 0 \quad (1.1)$$

where  $\kappa$  - warping of element;  $m$  - bending moment of internal or external forces about the middle of section;  $T$  - average temperature by section; by dot is designated differentiation by time. For plates we assume that relationship (1.1) is executed for invariant characteristics  $M$  and  $H$

$$\Phi(H, \dot{H}, M, \dot{M}, T) = 0 \quad (1.2)$$

Here

$$M^2 = M_x^2 - M_x M_y + M_y^2 + 3M_{xy}^2$$

For  $H$ , two various determinations are possible

$$H^2 = \left(\frac{\partial^2 w}{\partial x^2}\right)^2 + \left(\frac{\partial^2 w}{\partial y^2}\right)^2 + 2\left(\frac{\partial^2 w}{\partial x \partial y}\right)^2 \quad (1.3)$$

or

$$\dot{H}^2 = \left(\frac{\partial^2 \dot{w}}{\partial x^2}\right)^2 + \left(\frac{\partial^2 \dot{w}}{\partial y^2}\right)^2 + 2\left(\frac{\partial^2 \dot{w}}{\partial x \partial y}\right)^2$$

In accordance with selected condition (1.3) will take either deformation relationships of form

$$\frac{\partial^2 w}{\partial x^2} = \lambda \frac{\partial M^2}{\partial M_x}, \dots \quad (1.4)$$

or relationship of flow type

$$\frac{\partial^2 \dot{w}}{\partial x^2} = \lambda \frac{\partial \dot{M}^2}{\partial \dot{M}_x}, \dots \quad (1.5)$$

We will take equations of equilibrium for a plate in the following form [7]:

$$\frac{\partial^2 M_x}{\partial x^2} - 2 \frac{\partial^2 M_{xy}}{\partial x \partial y} + \frac{\partial^2 M_y}{\partial y^2} = - \left( q + N_x \frac{\partial^2 w_n}{\partial x^2} + N_y \frac{\partial^2 w_n}{\partial y^2} + 2N_{xy} \frac{\partial^2 w_n}{\partial x \partial y} \right) \quad (1.6)$$

$w_n = w + w_{00}$

Here  $w_{00}$  - initial deflection;  $N_x$ ,  $N_y$ ,  $N_{xy}$  - forces acting on planes of plates which we consider known. System of equations (1.2) - (1.6) allows to determine deflection as a function of time.

2. Let us consider a rod compressed by longitudinal force  $P$ . Bending moment for the rod will be written in the form

$$m = \frac{Ph}{m_0} (u + u_{00}) \quad (2.1)$$

where  $h$  - thickness;  $u$  - dimensionless additional deflection;  $u_{00}$  - initial

dimensionless deflection. Relationship (1.1) is written in the form

$$-kx = \dot{f}(m) + \Psi(m) \quad (2.2)$$

First component in the right part corresponds instantaneous deformation, and second characterizes process of creep. Let us note that relationship (2.2) does not consider possible unloading in separate parts of section of rod. This naturally can lead to deviations during comparison with experimental data. Let us examine a hinged supported rod. We seek solution of equation (2.2) by method of combination. Then, assuming that deflections can be approximated by one half-wave of sinusoid, we obtain for amplitude of deflection  $u$  equation

$$k\dot{u} = f[p(u + u_0)] + \Psi[p(u + u_0)] \quad (k = \pi^2 h^2 / L^2, p = Ph / m_0) \quad (2.3)$$

Specifying functions  $f$  and  $\Psi$ . solution of number of concrete problems can be obtained.

Buckling of a rod under action of constant force  $P$ . Solution is divided into two stages. First stage corresponds to instantaneous application of force  $P$ , as a result of which rod receives deflection  $u_0$ . Value of  $u_0$  is determined from solution of equation corresponding to instantaneous deformation

$$ku_0 = f[p(u_0 + u_0)] \quad (2.4)$$

Further process corresponding to build-up of deflection in time is characterized by equation

$$\frac{k - f[p(u + u_0)]p}{\Psi[p(u + u_0)]} du = dt \quad (2.5)$$

It is obvious that when condition is fulfilled

$$k - f[p(u_1 + u_0)]p = 0 \quad (2.6)$$

speed of build-up of deflection will turn into infinity. Value of full deflection  $u_1 + u_0$  determined by condition (2.6) corresponds to value of critical deflection also for purely instantaneous deformation. Indeed, if in (2.4) condition  $\partial p / \partial u_0 = 0$  is used, it will lead to equation coinciding with (2.6). This property, during solution of problems of buckling with regard to creep; is analyzed in more detail in [2]. This phenomenon was first discovered by [Freiys de Vebek] [8]. It is necessary to note that independence of critical deflection from properties of creep follows

from monoparametric nature of considered system.

If accepted that functions of  $f$  and  $\psi$  can be presented in the form

$$f(x) \equiv Ax^n, \quad \psi(x) \equiv Bx^m \quad (2.7)$$

then solution of equation (2.5) will be written in form

$$\frac{k}{Bp^m(m-1)} \left\{ \frac{1}{(u_0 + u_{00})^{m-1}} - \frac{1}{(u + u_{00})^{m-1}} \right\} - \frac{Ap^{n-m}}{B(m-n)} \left\{ \frac{1}{(u_0 + u_{00})^{m-n}} - \frac{1}{(u + u_{00})^{m-n}} \right\} = t \quad (2.8)$$

Moment of destruction  $t_1$  is determined from (2.8) if instead of  $u$  we place  $u_1$  found from condition (2.6).

Of great interest is the case of slow change of applied force, starting from zero. We obtain solution of equation (2.3) by semi-inverse method. Let us assume that is satisfied relationship

$$p(u + u_{00}) = D(\sqrt{t_1} - \sqrt{t_1 - t}) \quad (2.9)$$

Then for case  $n = 2$  and  $m = 1$  we obtain

$$\frac{u}{u_{00}} = 2 - \tau - 2\sqrt{1-\tau} + \tau(1 - \sqrt{1-\tau})$$

$$p = \frac{c}{u_{00}} \frac{1 - \sqrt{1-\tau}}{3 - \tau - 2\sqrt{1-\tau} + \tau(1 - \sqrt{1-\tau})} \quad (2.10)$$

$$\left( \tau = \frac{2DCt_1}{3ku_{00}}, \frac{C^2 A}{k} = u_{00} + \frac{BCt_1}{3k}, C = D\sqrt{t_1}\tau = \frac{t}{t_1} \right)$$

Solution in final form can be obtained for any whole  $m$  and  $n$ , but here for simplicity we are limited by shown values. It is obvious that when  $\tau \rightarrow 1$   $u \rightarrow \infty$ , i.e.,  $\tau = 1$  corresponds to moment of destruction (at  $\tau > 1$  solution does not exist). As main given parameters we take initial deflection  $u_{00}$  and initial speed of loading  $p_0$ . Then  $t_1$  and  $C$  are determined through these parameters and

$$\tau = 2 \left\{ \frac{6Au_{00}p_0}{B} - 1 \right\}^{-1}, \quad t_1^2 = \frac{3k}{12Au_{00}p_0^2 - 2Bp_0}, \quad C = 2u_{00}p_0 t_1 \quad (2.11)$$

As illustration, in Figs. 1 and 2 are given graphs of  $u/u_{00}$  and  $p/p_0 t_1$  as functions of dimensionless time  $\tau$  for a number of values of parameter  $\gamma$ . At  $\gamma \ll 1$  there is almost proportional loading.

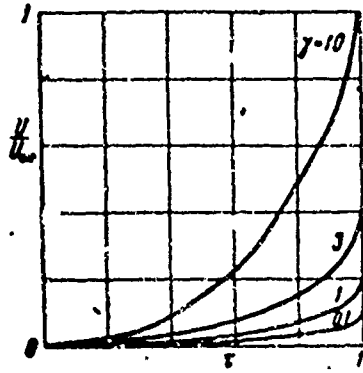


Fig. 1

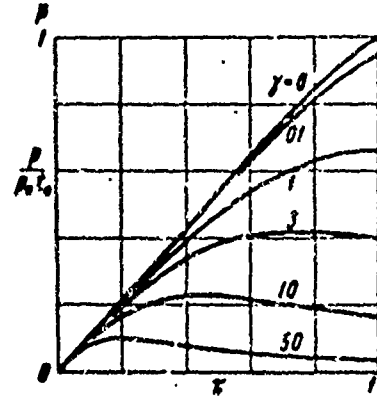


Fig. 2

3. Let us consider the simplest case of buckling of an evenly compressed, free-supported, square plate. We will take that

$$\begin{aligned}
 w &= u(t) \sin \frac{\pi x}{a} \sin \frac{\pi y}{a} & w_{00} &= u_{00} \sin \frac{\pi x}{a} \sin \frac{\pi y}{a} \\
 M_x = M_y &= m(t) \sin \frac{\pi x}{a} \sin \frac{\pi y}{a} & (M_{xy} &= 0 \text{ in the center})
 \end{aligned}
 \tag{3.1}$$

We satisfy equations of (1.2) in median point, then obtain dependence between  $m$  and  $u$  analogous to dependence for a rod (2.3)

$$k_1 \dot{u} = \dot{f}(k_2 m) + \Psi(k_2 m) \tag{3.2}$$

It is taken that for  $H$  and  $M$  there exists dependence analogous to connection between  $x$  and  $m$  for a rod. From (1.3) it is easy to obtain linear connection between  $m$  and  $(u + u_{00}) p$ , where  $p$  - uniform pressure on planes of plate. Consequently, for plate in considered case, equation connecting  $u$  and  $p$  coincided with equation (2.3) with accuracy up to constant factors characterizing geometry of considered element. Therefore investigation of solution conducted in part 2 is also valid in the present case. We note also that solution does not depend on which relationship - (1.4) or (1.5) is taken during investigation. It is obvious that this takes place in case when  $M$  is completely determined by one unknown parameter depending on time as it was in the considered case. When two or more parameters are preserved equation for plate during use of (1.5) does not reduce to first order equation and solution differs considerably from solution obtained for a rod.

Submitted  
22 March 1963

### Literature

1. N. J. Hoff. A survey of the theories of creep buckling. Proc. Third Nat. Congr. Appl. Mech., 1958, 29 - 49.
2. S. A. Shesterikov. Buckling during creep with regard for instantaneous plastic flows. PMTF, 1963, No 2.
3. Yu. N. Rabotnov and S. A. Shesterikov. Stability of rods and plates under the conditions creep. PMM, 1957, vol. 21, No 3.
4. L. M. Kurshin. Stability of plates under the conditions creep. PMTF, 1962, No 2.
5. G. Gerard. Theory of creep buckling of perfect plates and shells. J. Aerospace Sci., 1962, vol. 2, No 9.
6. V. Venkatraman, and P. G. Hodge. Approximate solutions of some problems in steady creep. Mem. Sympos. plast. sci. congr., Verona, 1956, Bologna, s. a., 138 - 165.
7. S. P. Timoshenko. Plates and shells. Ogiz. Gostekhizdat, 1948.
8. V. Freiys de Vebek. In coll.: "Influence of high temperatures on aviation designs", N. Khoff, ed., Oborongiz, 1961.

TORSION OF PRISMATIC RODS OF IDEALLY PLASTIC  
MATERIAL WITH CALCULATION OF MICROSTRESSES

I. A. Berezhnoy and D. D. Ivlev

(Voronezh)

Theory of torsion of rods of ideal rigidly-plastic material is presented in [1-4]. In [5] is considered torsion of prismatic rods of rigidly-plastic anisotropic reinforcing material under linearized condition of plasticity. In present work is considered torsion of rods polygonal cross section. Material of rods is assumed ideally plastic, where ideally plastic state is attained during transition through region strengthening [6]. In the material appear residual microstresses [7]. Similar material can be called material with terminal strengthening.

1. Let us consider problem of torsion of rods, material of which conforms to dependence between shear stresses and the nonreversible part of shear given in Fig. 1. We will select a coordinate system as shown in Fig. 2. In the future in designations of strains  $\tau_x, \tau_y$  and deformations  $\epsilon_x, \epsilon_y$  we will omit index z.

Initial relationships for problem of torsion of rods of anisotropic reinforcing, rigidly-plastic material with terminal strengthening have form

$$\frac{\partial \tau_x}{\partial x} \cdot \frac{\partial \tau_y}{\partial y} = 0 \quad (1.1)$$

$$(\tau_x - s_x)^2 + (\tau_y - s_y)^2 = k_1^2, \quad s_x^2 + s_y^2 < k_2^2, \quad k_1, k_2 = \text{const} \quad (1.2)$$

$$\frac{d\epsilon_x}{\tau_x - s_x} = \frac{d\epsilon_y}{\tau_y - s_y}, \quad \frac{dx_x}{s_x} = \frac{dx_y}{s_y} \quad (1.3)$$

$$s_x = c(\epsilon_x - x_x), \quad s_y = c(\epsilon_y - x_y), \quad c = \text{const} \quad (1.4)$$

If  $s_x^2 + s_y^2 < k_2^2$ , then  $x_x = x_y = 0$ .

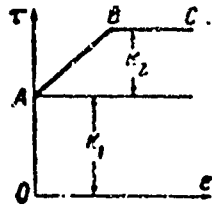


Fig. 1

Here  $s_x, s_y$  - components of micro-stresses,  $x_x, x_y$  - components of micro-deformations, and  $c$  - parameter of strengthening.

Condition of plasticity (1.2) in planes  $\tau_x, \tau_y$  represents a circle with coordinates of center  $s_x, s_y$ . In initial moment of plastic flow

$$s_x = s_y = 0, \quad \tau_x = \tau_x^0, \quad \tau_y = \tau_y^0 \quad (\tau_x^2 + \tau_y^2 = k_1^2)$$

Condition of plasticity (1.2) can be interpreted as rounding family of plasticity tangential to given condition. In the future, following [5], linearized condition of plasticity, considering that stress state at each point of the body corresponds to a tangent to circle of conditions of plasticity preserving its own direction in planes  $\tau_x, \tau_y$  in process of deformation of body,

$$\tau_x^0 (\tau_x - s_x) + \tau_y^0 (\tau_y - s_y) = k_1^2 \quad (1.5)$$

Similarly for microstresses we can assume that after attainment by them of limiting values  $s_x^0, s_y^0, (s_x^2 + s_y^2 = k_2^2)$  takes place linearized condition

$$s_x^0 s_x + s_y^0 s_y < k_2^2 \quad (1.6)$$

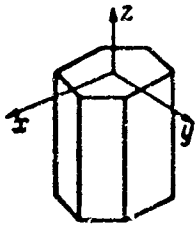


Fig. 2

Considering conditions (1.5) and (1.6) as plastic potentials, we obtain, instead of (1.3), relationships

$$\frac{ds_x}{\tau_x^0} = \frac{ds_y}{\tau_y^0}, \quad \frac{dx_x}{s_x^0} = \frac{dx_y}{s_y^0} \quad (1.7)$$

Since in process of plastic flow  $\tau_x^0, \tau_y^0$  and  $s_x^0, s_y^0$  do not depend on parameter of load, then integrating (1.7) we obtain

$$\frac{s_x}{\tau_x^0} = \frac{s_y}{\tau_y^0} + c_1(x, y), \quad \frac{x_x}{s_x^0} = \frac{x_y}{s_y^0} + c_2(x, y) \quad (1.8)$$

Assuming that at initial moment, rod was in rigid, undeformed state and microstresses was absent, we find that  $c_1 = c_2 = 0$ , and finally that relationships of

(1.8) take form

$$\tau_y^* e_x - \tau_x^* e_y = 0, \quad s_y^* x_x - s_x^* x_y = 0 \quad (1.9)$$

In the future it is necessary to exclude from initial relationships of quantities of microstresses and microdeformations. Using (1.4), we obtain (1.5) and (1.6) in the form

$$\tau_x^* [\tau_x - c(e_x - x_x)] + \tau_y^* [\tau_y - c(e_y - x_y)] = k_1^2 \quad (1.10)$$

$$s_x^* (e_x - x_x) + s_y^* (e_y - x_y) = \frac{k_2^2}{c} \quad (1.11)$$

Condition (1.11) can be written

$$x_x s_x^* + x_y s_y^* = q \quad \left( q = s_x^* e_x + s_y^* e_y - \frac{k_2^2}{c} \right) \quad (1.12)$$

Solving linear system of equations - relationship for microstrains of (1.9) and (1.12), we obtain expressions for micro-deformations

$$x_x = \frac{q s_x^*}{k_2^2}, \quad x_y = \frac{q s_y^*}{k_2^2} \quad (1.13)$$

Then, taking into account relationships of (1.13), condition (1.10) it assumes final form

$$\tau_x^* \left\{ \tau_x - c e_x + \left[ s_x^* \left( \frac{c s_x^* e_x + c s_y^* e_y}{k_2^2} - 1 \right) \right] \right\} + \tau_y^* \left\{ \tau_y - c e_y + \left[ s_y^* \left( \frac{c s_x^* e_x + c s_y^* e_y}{k_2^2} - 1 \right) \right] \right\} = k_1^2 \quad (1.14)$$

Components of deformations are determined by relationships

$$e_x = \frac{1}{2} \left( -\theta y + \frac{\partial w}{\partial x} \right), \quad e_y = \frac{1}{2} \left( \theta x + \frac{\partial w}{\partial y} \right) \quad (1.15)$$

where  $w(x, y)$  - warping of section,  $\theta$  - twist. Thus, for  $\tau_x, \tau_y$  and  $w$ , we have: equation of equilibrium (1.1), condition of plasticity (1.14), and law of plastic flow (first relationship of (1.9)).

2. Let us consider region oef of rod of polygonal cross section (Fig. 3a), where oe - line of break of strains. Equation of lines of break  $y = ax$  ( $a = \text{const}$ ). Here, axis  $x$  is perpendicular to free boundary of contour of rod ef.

From solution of theory of ideal plasticity [1-4] it follows

$$\tau_x^* = 0, \quad \tau_y^* = k_1 \quad (2.1)$$

As was noted in [5], warping of cross section of rod of reinforced material coincides with warping during ideally plastic flow of rod. Warping under the conditions of rigidly-plastic torsion is determined by expression  $w = n \theta d$ , where  $n$  - distance from point  $P(x, y)$  to line of break on normal to ef passing through point  $P$ . For considered region we have

$$\begin{aligned} w(x, y) &= \theta \left(x - \frac{y}{\alpha}\right) y \\ \varepsilon_x &= 0, \quad \varepsilon_y = \theta \left(x - \frac{y}{\alpha}\right) \end{aligned} \quad (2.2)$$

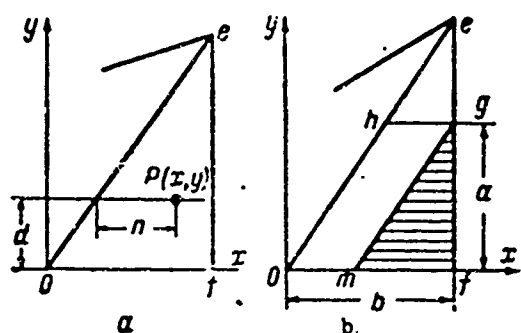


Fig. 3

Let us assume that in certain region mgf (Fig. 3b) material of rod reached yield point (BC in Fig. 1), then in considered region

$$\varepsilon_x^* = 0, \quad \varepsilon_y^* = k_2 \quad (2.3)$$

Linearized condition of fluidity (1.14),

taking into account (2.1) and (2.3), takes

form

$$\tau_y - \alpha \varepsilon_y + \left[ k_2 \left( \frac{\alpha \varepsilon_y}{k_2} - 1 \right) \right] = k_1 \quad (2.4)$$

It follows from this that in regions mgf

$$\tau_y = k_1 + k_2 \quad (2.5)$$

Putting expression (2.5) in equation of equilibrium (1.1), we find that

$\tau_x = \tau_x(y)$ . On counter ef always  $\tau_x' = 0$ , consequently,  $\tau_x = 0$  everywhere in region mgf.

In region oegm, state of material corresponds to section AB shown in Fig. 1. In this region  $\varepsilon_x^2 + \varepsilon_y^2 < k_2^2$  and  $\varepsilon_x = \varepsilon_y = 0$ . Then, in region oegm, condition of plasticity (2.4) takes form

$$\tau_y = k_1 + \alpha \varepsilon_y \quad (2.6)$$

Equation of equilibrium (1.1) under condition (2.6) will be satisfied in considered region if

$$\tau_y = k_1 + c\theta \left(x - \frac{y}{\alpha}\right), \quad \tau_x = \frac{c\theta}{\alpha} x + f(y) \quad (2.7)$$

On boundary of region of ideal plasticity mgf, we have  $\tau_y = k_1 + k_2, \tau_x = 0$ ,

whence, from expressions of (2.7) we find

$$c\theta \left(x - \frac{y}{\alpha}\right) = k_1 \quad \text{and} \quad f(y) = -\left(\frac{c\theta}{\alpha^2}\right)y.$$

In region ohgm we obtain

$$\tau_x = \frac{c\theta}{\alpha} \left(x - \frac{y}{\alpha}\right) - \frac{k_1}{\alpha} \quad (2.8)$$

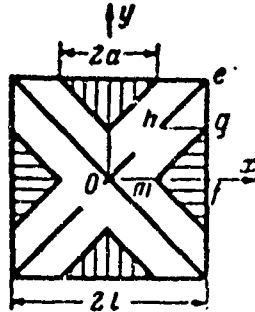


Fig. 4

In region heg satisfying condition  $\tau_x = 0$  on contour eg, we obtain

$$\tau_x = \frac{c\theta}{\alpha} (x - b) \quad (2.9)$$

On boundary hg, component of stress  $\tau_x$  endures break. Break of component of stress  $\tau_x$  we assume static, since contacting stresses  $\tau_y$  during transition through hg are continuous. Appearance of break is caused by use of limiting circuit. We will designate length of region of ideal plasticity along free contour ef through  $s/\alpha = a$ . then from (2.7) we have

$$a = \left(b - \frac{k_2}{c\theta}\right)\alpha \quad (a = 0 \quad \text{when} \quad \theta < k_2/cb) \quad (2.10)$$

3. Let us consider concrete examples.

1) In case of a rod of square section (Fig. 4) with length of  $2l$  in region oef, equation of line of break oe has form  $y = x, \alpha = 1$ . From (2.5), (2.7), (2.8), and (2.9) we find

$$\begin{aligned} \tau_y &= k_1 + k_2, & \tau_x &= 0 \quad (\text{in } \underline{mgf}) \\ \tau_y &= k_1 + c\theta(x - y), & \tau_x &= c\theta(x - y) - k_2 \quad (\text{in } \underline{ohgm}) \\ \tau_y &= k_1 + c\theta(x - y), & \tau_x &= c\theta(x - l) \quad (\text{in } \underline{heg}) \end{aligned} \quad (3.1)$$

Torque for entire section will be

$$M = 4(k_1 + k_2) \left( la^2 - \frac{a^3}{3} \right) + \frac{8}{3} k_1 \left( l^3 - \frac{3}{2} a^2 l + \frac{a^3}{3} \right) + 2k_2(la^2 - a^3) + \frac{4}{3} c\theta (l^4 + 4l^2 a - 24l^2 a^2 + 32la^3 - 13a^4) \quad (3.2)$$

where

$$a = 0 \quad \text{at} \quad \theta < \frac{k_2}{c\theta}, \quad a = l - \frac{k_2}{c\theta} \quad \text{at} \quad \theta > \frac{k_2}{c\theta} \quad (3.3)$$

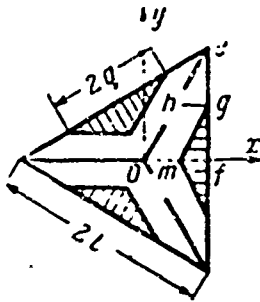


Fig. 5

Regions of plasticity corresponding to state of ideal plasticity of material (BC in Fig. 1) here and everywhere are shaded.

2) Considering region cef of rod of triangular section (Fig. 5) with side  $2l$ , we obtain equation of line of break oe in

the form  $y = 3x/\sqrt{3}$ ,  $a = 3/\sqrt{3}$ .

Then from (2.5), (2.7), (2.8), and (2.9) we find components of stresses

$$\tau_y = k_1 + k_2, \quad \tau_x = 0 \quad (\text{in } \underline{mrf})$$

$$\tau_y = k_1 + c\theta \left( x - \frac{\sqrt{3}}{3} y \right), \quad \tau_x = c\theta \frac{\sqrt{3}}{3} \left( x - \frac{\sqrt{3}}{3} y \right) - k_2 \frac{\sqrt{3}}{3} \quad (\text{in } \underline{ohgm})$$

$$\tau_y = k_1 + c\theta \left( x - \frac{\sqrt{3}}{3} y \right), \quad \tau_x = c\theta \frac{\sqrt{3}}{3} \left( x - \frac{\sqrt{3}}{3} l \right) \quad (\text{in } \underline{heg}) \quad (3.4)$$

Torque for entire section will be equal to

$$M = (k_1 + k_2) \left( \frac{13}{3} a^2 l - 2a^3 - \frac{5}{3} a^3 \right) + k_1 \left( \frac{2}{3} l^3 - a^2 l + \frac{a^3}{3} \right) + k_2(la^2 - a^3) + c\theta \frac{\sqrt{3}}{9} (l^4 - 2l^2 a - 3l^2 a^2 + 5la^3 - a^4) \quad (3.5)$$

where

$$a = 0 \quad \text{at} \quad \theta < \frac{3k_2}{\sqrt{3}c\theta}, \quad a = l - \frac{3k_2}{\sqrt{3}c\theta} \quad \text{at} \quad \theta > \frac{3k_2}{\sqrt{3}c\theta} \quad (3.6)$$

3) Solution for rod of rectangular section with sides  $2h$  and  $2l$  (Fig. 6) in region cef is determined is analogous to rod of square section.

In region  $o_1 o m m_1$ , gradient of line of break  $\alpha = \infty$ , then from (2.5), (2.7), (2.8), and (2.9) components of stresses will be determined

$$\tau_y = k_1 + k_2, \quad \tau_x = 0 \quad (\text{in } m_1 m f f_1) \quad (3.7)$$

$$\tau_w = c\theta x + k_1, \quad \tau_x = 0 \quad (\text{in } o_1 o m m_1)$$

Torque for entire section will be equal to

$$M = M^* + 4(h-l) [(k_1 + k_2)al + k_1(l^2 - al) + k_2(la - a^2) + 1/3 c\theta(l - a)^3] \quad (3.8)$$

where  $M^*$  - torque for rod of square section determined by formula (3.2). Let us note that dependence  $M = M(\theta)$  for rods of rigidly-plastic material with terminal strengthening at values of twist within limits

$$0 < \theta < \frac{k_2}{cb} = \frac{k_2}{cd} \alpha$$

coincides with dependence  $M = M(\theta)$  for ideally plastic material with linear strengthening [5]. In interval of values of twist

$$\frac{k_1}{cl} \alpha < \theta < \infty$$

dependence  $M = M(\theta)$  becomes nonlinear and by measure of growth of twist is asymptotically similar to solution for ideally plastic material with yield point  $(k_1 + k_2)$ . This circumstance is shown in Fig. 7.

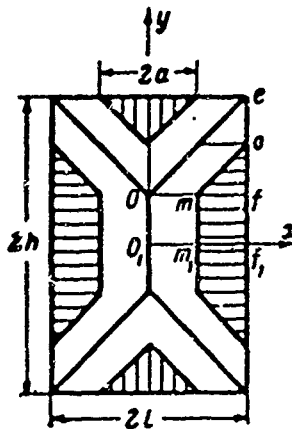


Fig. 6.

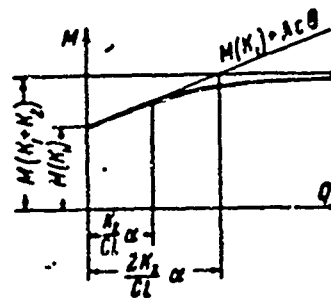


Fig. 7.

Submitted  
26 March 1963

#### Literature

1. V. V. Sokolovskiy. Theory of plasticity. Izd. AN SSSR, 1946; Gostekhtheoretizdat, 1950.

2. R. Khill. Mathematical theory of plasticity. Gostekhtheoretizdat, 1956.
3. V. Prager and F. Hodge. Theory of ideally plastic bodies, II, 1956.
4. L. M. Kachanov. Bases of theory of plasticity, Gostekhtheoretizdat, 1956.
5. V. V. Dudukalenko, and D. D. Ivlev. On torsion of prismatic rods of reinforcing material under linearized condition of plasticity, Pub. House of Academy of Sciences of USSR, OTN, Mechanics and machine building, 1963, No. 3.
6. D. D. Ivlev. On ideally plastic flow of material with regard to residual microstresses. PMM, 1962 vol. XXVI, No. 4.
7. Yu. I. Kadeshevich and V. V. Novozhilov. Theory of plasticity, considering microstresses.

THEORY OF STRAIGHT LINES OF DISCONTINUITY OF  
STRESSES FOR TRUE PLANE FLOW OF A  
RIGIDLY-PLASTIC BODY

O. D. Grigor'yev (Novosibirsk)

Considered is connection between the condition of positiveness of dispersion power and the picture of true plane flow near a straight line break. Kinematic characteristic of existence of straight line of break of stresses is established.

We will prove the following kinematic characteristic of existence of straight line of break. So that a certain straight line of break of stresses for true plane flow of a rigidly-plastic body, it is necessary and sufficient, so that the indicated straight line:

a) does not coincide with slip line;

b) after exclusion of translational motion of plastic region it is orthogonal to flow lines, and divides trajectories orthogonal to flow lines of various concavity (convexity); here line of break does not coincide with inflection points of flow lines.

Necessity. Let there be a straight line of break of stresses. Obviously it does not coincide with slip line. Excluding translational motion of plastic region, we find what line of break is orthogonal to field of speeds. Since speeds are continuous near straight line of break, the curvilinear grid in the form of flow

lines and trajectories orthogonal to them has here a continuous tangential.

Lengthwise along shown orthogonal grid take place relationships [1, 2]

$$\left. \begin{aligned} \sigma_{11} \\ \sigma_{22} \end{aligned} \right\} = \sigma \pm k \cos 2\beta, \quad \sigma = \frac{1}{2}(\sigma_{11} + \sigma_{22}), \quad \sigma_{12} = k \sin 2\beta \\ \xi_{11} = -\xi_{22} = \frac{1}{H_1} \frac{\partial v}{\partial q_1} = \frac{v}{R_2}, \quad \xi_{12} = \frac{H_1}{H_2} \frac{\partial v}{\partial q_2} \frac{1}{H_1} = 2 \operatorname{tg} 2\beta \frac{v}{R_2} \end{aligned} \quad (1)$$

Here  $\sigma_{ij}$ ,  $\xi_{ij}$  - physical components of stress tensors and rates of deformations;  $H_1$ ,  $H_2$  - Lamé coefficients;  $\beta$  - angle between direction of large main stress and speed vector;  $v$  - modulus of speed vector;  $R_2$  - radius of curvature of trajectories orthogonal to flow lines.

According to (1), from both sides of straight line of break (after exclusion of translational motion) we have

$$\sin 2\beta^+ = \sin 2\beta^-, \quad \beta^- = 90^\circ - \beta^+ \quad (2)$$

Here values from various sides of line of break differ by plus and minus indices.

Let us consider condition of positiveness of dispersion power near line of break, expressing the latter in the form [2]

$$\begin{aligned} R_2 > 0 & \text{ for } 45^\circ < \beta < 135^\circ \text{ or } 135^\circ < \beta < 225^\circ \\ R_2 < 0 & \text{ for } 45^\circ < \beta < 135^\circ \text{ or } 225^\circ < \beta < 315^\circ \end{aligned} \quad (3)$$

Here, radius of curvature is considered positive if it is directed toward the side of rise of parameter  $q_1$ .

From (3)- (2) it follows that straight line of break splits orthogonal trajectories of various concavity (convexity).

Sufficiency. Let there be true plane flow. Field of flow lines, after exclusion of translational motion of plastic region, contains straight line orthogonal to flow lines which does not coincide with slip line and divides orthogonal trajectories of various concavity. By condition along indicated straight line

$$R_2 = \infty \quad (4)$$

Therefore, tensor of rates of deformation turns along it into zero. On the other hand, due to various concavity of orthogonal trajectories, function  $\beta$ , during transition through straight line endures a break (3). Thus, considered straight can only be a line of break of stresses for true plane flow [3]. Let us note that from investigation there was a case of straight flow lines, i.e., when medium moves as a solid body. We will show in conclusion that line of break does not coincide with inflection points of orthogonal trajectories. In view of (1), we have

$$\xi_{11}^+ = \xi_{11}^-, \quad v^+ = v^-, \quad \left[ \frac{\partial \ln v}{\partial s_2} - \frac{\partial x}{\partial s_1} \right]^+ = \left[ \frac{\partial \ln v}{\partial s_2} - \frac{\partial x}{\partial s_1} \right]^- = 0 \quad (5)$$

where  $\partial x / \partial s_1$  - curvature of flow lines;  $\partial / \partial s_2$  - derivative along line of break.

Since translational motion is excluded, then

$$\frac{\partial \ln v^+}{\partial s_2} = \frac{\partial \ln v^-}{\partial s_2} \neq 0, \quad \frac{\partial x^+}{\partial s_1} = \frac{\partial x^-}{\partial s_1} \neq 0 \quad (6)$$

Hence, due to the lemma about preservation of a continuous function in environments of a point, where its own sign, is, other than zero, we find that curvature of flow lines does not change sign during transition through line of break. Consequently, straight line of break is not locus of inflection of flow lines. In Figs. 1 and 2 are depicted possible views of plane flow near straight line of break.

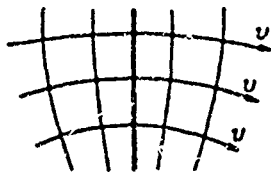


Fig. 1.

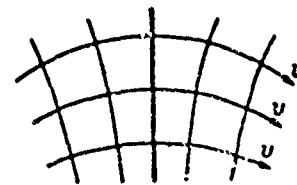


Fig. 2.

Submitted  
22 November 1962.

#### Literature

1. O. D. Grigor'yev. On theory of flat deformation of a rigidly-plastic body. PMM, 1961, vol. 25, issue 5.
2. O. D. Grigor'yev. On condition of positiveness of dispersion power in plane flow of a rigidly-plastic body. PMTF, 1962, No. 1.
3. L. M. Kachanov. Bases of theory of plasticity, Gostekhizdat, 1956.

## RELAXATION OF STRESSES IN THIN-WALLED PIPE

V. S. Namestnikov (Novosibirsk)

In work [1] during the investigation of relaxation of thin-walled pipe twisted and stretched simultaneously it was assumed that elastic instantaneous components of deformation satisfy condition of incompressibility. Let us consider this problem disregarding requirement of incompressibility.

We dispose axes  $x$  and  $y$  in tangent plane, heading axis  $x$  parallel with axis of pipe. Stress tensor in considered case leads to

$$\sigma_x = \sigma, \quad \tau_{xy} = \tau, \quad \sigma_y = \sigma_z = \tau_{xz} = \tau_{yz} = 0 \quad (1)$$

Tensor of elastic deformations is expressed

$$\epsilon_x = \sigma/E, \quad \epsilon_y = \epsilon_z = -\nu\sigma/E, \quad \epsilon_{xy} = (1+\nu)\tau/E, \quad \epsilon_{xz} = \epsilon_{yz} = 0 \quad (2)$$

(E-Young's modulus,  $\nu$ -Poisson coefficient)

Expressions for creep have form

$$\dot{p}_x = \frac{\dot{p}}{\sigma_1} \sigma, \quad \dot{p}_y = \dot{p}_z = \frac{-\dot{p}}{2\sigma_1} \sigma, \quad \dot{p}_{xy} = \frac{3}{2} \frac{\dot{p}}{\sigma_1} \tau, \quad \dot{p}_{xz} = \dot{p}_{yz} = 0 \quad (3)$$

$p$  and  $\sigma_1$  are connected by dependence

$$\dot{p} p^{\alpha} = \kappa \exp \left\{ \frac{\sigma_1}{A} + \frac{|\tau_{\max}|}{A_0} \right\} \quad \left( \dot{p}^2 = \frac{2}{3} \dot{p}_i \dot{p}_{ij}, \sigma_1^2 = \frac{3}{2} \sigma_{ij} \sigma_{ij} \right) \quad (4)$$

In considered case

$$\sigma_1 = \sqrt{\sigma^2 + 3\tau^2}, \quad \tau_{\max} = \sqrt{(3/2)\sigma^2 + \tau^2} \quad (5)$$

Lengthening and angle of rotation of pipe are kept constant. Therefore, condition of relaxation reduces to

$$\epsilon_x = \epsilon_x + P_x = \text{const}, \quad \epsilon_{xy} = \epsilon_{xy} + P_{xy} = \text{const} \quad (6)$$

From (2), (3), and (6) we obtain

$$\dot{\sigma} + \frac{E\dot{p}}{\sigma_0} \sigma = 0, \quad \dot{\tau} + \frac{E\dot{p}}{m\sigma_0} \tau = 0 \quad \left(m = \frac{2(1+\nu)}{3}\right) \quad (7)$$

Hence

$$\frac{\dot{\sigma}}{\sigma} = m \frac{\dot{\tau}}{\tau} \text{ OR } \frac{\tau^m}{\sigma} = \frac{\tau_0^m}{\sigma_0} \quad (8)$$

Here  $\sigma_0$  and  $\tau_0$  - initial values of stresses. Putting (8) in (5), we obtain

$$\sigma_1 = \tau (c^2 \tau^{2m-2} + 3)^{1/2}, \quad \tau_{\text{max}} = 1/3 \tau (c^2 \tau^{2m-2} + 4)^{1/2} \quad (c = \sigma_0^2 / \tau_0^{2m}) \quad (9)$$

Hence from second equation of (7) we have

$$m (c^2 \tau^{2m-2} + 3)^{1/2} \dot{\tau} + E\dot{p} = 0 \quad (10)$$

From (4) and (9) we obtain

$$\dot{p} p^2 = \kappa \exp \left\{ \frac{\tau}{A} (c^2 \tau^{2m-2} + 3)^{1/2} + \frac{\tau}{2A_0} (c^2 \tau^{2m-2} + 4)^{1/2} \right\} \quad (11)$$

Thus, problem was reduced to solution of systems (10) and (11) with initial conditions

$$\tau = \tau_0, \quad p = 0 \quad \text{at} \quad t = 0 \quad (12)$$

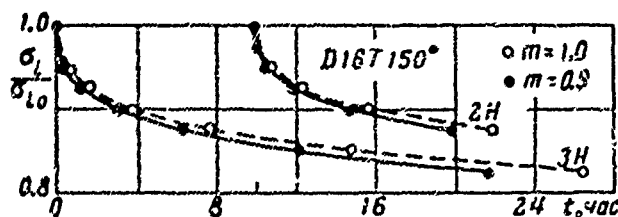
Solution of systems (10) and (11) has form

$$t = \frac{1}{\kappa} \left(\frac{m}{E}\right)^{m+1} \int_{\tau_0}^{\tau} \left\{ (c^2 \eta^{2m-2} + 3)^{1/2} \left[ \int_{\eta}^{\tau_0} (c^2 \xi^{2m-2} + 3)^{1/2} d\xi \right]^2 \times \right. \\ \left. \times \exp \left[ -\frac{\eta}{A} (c^2 \eta^{2m-2} + 3)^{1/2} - \frac{\eta}{2A_0} (c^2 \eta^{2m-2} + 4)^{1/2} \right] \right\} d\eta \quad (13)$$

Relationship (8) is result of hypothesis of proportionality deviators which for elastically incompressible material ( $\nu = 0.5$ ,  $m = 1$ ) reduces to

$$\tau / \sigma = \tau_0 / \sigma_0, \text{ OR } \lambda = \lambda^0 \quad (14)$$

(relationship (6) of work [1]). In [1] by experimental data on duralumin and copper it was shown that in majority of cases divergence of left part from right in (14) does not exceed 14%.



We assume that  $\nu = 0.35$  ( $m = 0.9$ ).

In this case we obtain somewhat better conformity of left and right sides in (8).

If for example, in first case of divergence were compiled, - 14 + 4, - 16.7, - 4.1, - 10.7%, then in second they are equal respectively to - 8.3, + 7.5, - 15, + 2.6, - 6.7%.

In the figure are given examples of comparison of relaxation curves, calculated by (13) taking into account ( $m = 0.9$ ) and without calculation of ( $m = 1$ ) of compressibility of material. As can be seen, curves turned out to be quite similar in both cases, difference in time at the same level of stress is near 20%. As one should have been led to expect, relaxation curves with respect to compressibility of material are lower than curves without calculation of compressibility, i.e., calculation of compressibility improves conformity of computed relaxation curves with experiments, so long as the latter are always lower than computed curves [1].

The fact that computed relaxation curves turned out to be above those of experiments is partly caused by the fact that elastic modulus obtained on the usual testing machine is understated due to influence of creep. Error in determination of  $E$  (equals  $k\%$ ) changes relaxation time during the same stress by not less than  $(\alpha + 1) k\%$ .

Calculations of relationship (13) were performed by S. N. Savchenko to whom the author expresses gratitude.

Submitted  
28 May 1963

#### Literature

1. V. S. Namestnikov. Relaxation under complex strain state. PMTF, 1962, No 6.